The geochemical cycling and paleoceanographic application of combined oceanic Nd-Hf isotopes

Tianyu Chen

Dissertation

The geochemical cycling and paleoceanographic application of combined oceanic Nd-Hf isotopes

Dissertation
zur Erlangung des Doktorgrades

Dr. rer. nat.

der Mathematisch-Naturwissenschaftlichen Fakultät

der Christian-Albrechts-Universität zu Kiel

vorgelegt von

Tianyu Chen

Kiel, 2013

1. Gutacher und Betreuer: Prof. Dr. Martin Frank

2. Gutachter: Prof. Dr. Anton Eisenhauer

Eingereicht am:

Datum der Disputation: 26.11.2013

Zum Druck genehmigt: 26.11.2013

Gez. (Prof. Dr. Wolfgang J. Duschl, Dekan):

Erklärung

Hiermit versichere ich an Eides statt, dass ich diese Dissertation selbständig und nur mit Hilfe der angegebenen Quellen und Hilfsmittel erstellt habe. Diese Arbeit ist unter Einhaltung der Regeln guter wissenschaftlicher Praxis der Deutschen Forschungsgemeinschaft entstanden und wurde weder ganz, noch in Teilen an anderer Stelle im Rahmen eines Prüfungsverfahrens eingereicht.

Teile dieser Arbeit sind bereits veröffentlicht oder sind in Vorbereitung eingereicht zu werden.

Kiel, den 23.10.2013

Tianyu Chen

Contents

Chapter 7

Late Quaternary Nd-Hf isotope evolution of seawater at the Weddell Sea margin and in the abyssal Southern Ocean

Abstract

Combined oceanic hafnium (Hf) and neodymium (Nd) isotope compositions are a geochemical tool developed over the past 15 years to study the present and past ocean circulation and continental weathering regimes. Since Hf isotopes are a relatively new proxy in marine research, a number of issues regarding the geochemistry of oceanic Hf have previously not been investigated or are still controversial. This thesis presents Hf and Nd concentration/isotope data from a variety of archives, such as marine sediments, dust deposits, as well as seawater and river water in order to better understand the sources and cycling of oceanic Nd and Hf isotopes and to apply them in paleoceanographic studies.

The distribution of neodymium concentrations in open ocean surface waters (0-100 m) was generally assumed to be controlled by lateral mixing and advection of Nd via coastal surface currents and by removal through reversible particle scavenging. In Chapter 3 of this study, it is found that more stratified regions of the world ocean are generally associated with lower surface water Nd concentrations, implying that upper ocean stratification is a previously neglected primary factor in determining the basin scale variations of surface water Nd concentrations. Similar to the mechanism of nutrient supply, it is likely that stratification inhibits vertical supply of Nd from the subsurface thermocline waters and thus the magnitude of Nd flux to the surface layer. These findings have been corroborated by modeling applying the Bern3D ocean model of intermediate complexity and also have important implications for understanding of the cycling of many other trace metals, including micronutrients.

To investigate the mechanisms controlling the systematic offset of seawater radiogenic Nd-Hf isotope compositions from those of the upper continental crust (UCC) rocks, leaching experiments on Chinese desert and loess samples of different size groups were conducted in this thesis (Chapter 4). The motivation was to investigate if the above offset already occurs as a consequence of continental weathering or only later during marine processes. The dust and loess samples were recovered from deserts and arid areas

distributed over an area extending 600 km from north to south and 4,000 km from east to west in northern China. Since these samples have a wide spectrum of Nd isotope compositions, they are suggested to be representative to address Hf isotope fractionation during weathering of large scale averaged UCC. Overall, the leaching data either plot along or slightly above the Nd-Hf isotope seawater array, providing strong direct support that seawater Nd-Hf isotope relationship is predominantly generated by weathering of UCC.

Nevertheless, the cycling of oceanic Nd and its radiogenic isotopes is much better understood than of oceanic Hf isotopes. Fortunately, analytical techniques have been available for about 5 years now that enable direct and accurate measurements of dissolved seawater Hf isotope compositions, despite the fact that very low Hf concentrations and the requirement of large volumes of seawater per sample (60-140 liters).

In this thesis these techniques were for the first time applied to seawater from the central Baltic Sea, which is a marginal brackish basin with periodically euxinic bottom waters (anoxic and sulfidic) and source terrains of very different ages at its northern and southern boundaries. This allows the application of radiogenic Nd and Hf isotopes and concentratios for tracing water mass mixing, as well as to investigate their geochemical cycling across the redox boundaries in the water column (Chapter 5). In addition, their signatures in two rivers flowing into Baltic Sea (Kalix and Schwentine) are reported. In general, the distribution of the Nd isotopes can be explained by mixing of local inputs and Atlantic-derived more radiogenic source waters demonstrating the effectiveness of Nd isotopes as a water mass tracer in the central Baltic Sea. Hafnium isotopes, however, show an unexpectedly large variability and do not follow the water mass mixing trends. Hafnium is thus suggested to have a shorter residence time than Nd in seawater and to be more strongly influenced by local inputs. The results obtained from the Kalix river waters support previous assumptions that the Hf isotope signature released during incipient weathering of glacial tills is highly radiogenic due to the dissolution of easily alterable accessory minerals.

Based on the above understanding, Hf isotopes can be applied with more confidence in paleocenographic studies on marine sediments. Chapter 6 represents pioneering work that applied combined Hf-Nd isotopes of authigenic Fe-Mn fractions of marine sediments (IODP Leg 302, ACEX) to reconstruct changes in seawater composition in the central Arctic Ocean over the past 14 million years. The results show that deep water Hf isotope signatures can be reliably extracted from marine sediments and that their evolution in Arctic intermediate Water has been closely associated with Nd isotopes. The results therefore suggest that the evolution of Hf isotope compositions in central Arctic intermediate water has primarily been controlled by changes in ocean circulation and provenance of weathering inputs, rather than changes in continental weathering regimes.

In contrast, investigations of two Southern Ocean sediment cores (PS2082-1 and PS1388-3) reveal different relationships between Hf and Nd isotopes (Chapter 7). Consistent with previous studies, the deep water signatures obtained from bulk sediment leachates and planktic foraminifera record show systematically more radiogenic Nd isotope compositions of deep waters during glacial times than during interglacial times in the abyssal Agulhas Basin (Core PS2082-1). Unlike atmospheric CO_2 concentration or temperature recorded in Antarctic ice cores, there is no early interglacial maximum of unradiogenic Nd isotope signatures (MIS 5e or early MIS 7) which most likely reflects the decoupling of sea surface gas exchange and deep circulation during glacial-interglacial transitions. The Hf isotope signatures of Core PS2082-1 show relatively little variation, implying very small variations in chemical weathering intensity over the last two glacial-interglacial cycles affecting Southern Ocean deep water. Moreover, the Nd isotope record of deep water at the site of Core PS1388-3 (Weddell Sea margin) has been controlled by local weathering inputs suggesting that exchange with continental shelves play an important role close to the Antarctic continental margin. In comparison, preferential release of Hf from fresh surfaces of minerals with high Lu/Hf is the most likely explanation for pronounced radiogenic Hf isotope peaks at the very beginning of interglacial stages 7, 5, and 1, possibly implying a retreat of the peripheral ice sheets inland to some extent during these times.

Zusammenfassung

Die kombinierte Hafnium (Hf) und Neodymium (Nd) Isotopenzusammensetzung des Meerwassers wurde in den vergangenen 15 Jahren zu einem geochemischen Werkzeug entwickelt um die heutige und vergangene Ozeanzirkulation und die kontinentalen Verwitterungsbedingungen zu rekonstruieren. Da es sich um einen relativ neuen Proxy-Iddikator in den Meereswissenschaften handelt, gibt es eine Vielzahl von Fragen zur marinen Hf-Geochemie, die bisher noch nicht untersucht werden konnten oder diskutiert werden. Die vorliegende Arbeit präsentiert neue Hf und Nd Konzentrations-/Isotopendaten aus einer Reihe von Archiven, wie zum Beispiel marinen Sedimenten, äolischen kontinentalen Ablagerungen, aber auch Meer- und Flusswasser, mit dem Ziel die Quellen und die biogeochemischen Kreisläufe von Nd und Hf Isotopen im Meerwasser besser zu verstehen und diese in der Paläo-Ozeanographie anwenden zu können.

Es wurde allgemein angenommen, dass die Streuung von Neodym-Konzentrationen im Oberflächenwasser (0-100 m) des offenen Ozeans durch die laterale Durchmischung, Advektion von Nd durch küstennahe Oberflächenströmungen und durch den Verlust durch reversible Anhaftung an Partikel kontrolliert wird. In Kapitel 3 dieser Studie wird nachgewiesen, dass stratifiziertere Regionen der Meere allgemein mit niedrigeren Oberflächenwasser Nd Konzentrationen übereinstimmen. Dies impliziert, dass die Stratifizierung des oberen Ozeans ein bislang vernachlässigter, primärer Faktor ist, der die beckenweite Verteilung von Oberflächenwasser-Nd-Konzentrationen bestimmt. Ähnlich wie die Mechanismen der Nährstoffbereitstellung ist es wahrscheinlich, dass die Stratifizierung den vertikalen Eintrag von Nd aus den tiefer gelegenen Wasserschichten der Thermokline hemmt und somit auch die Nd-Zufuhr in das Oberflächenwasser. Diese Erkenntnisse wurden durch Modellierungen auf Grundlage des Bern3D-Ozean Modells mittlerer Komplexität bestätigt und haben auch eine große Bedeutung für das Verständnis der Kreisläufe von vielen anderen Spurenmetallen.

Um die Mechanismen zu untersuchen, die den systematischen Unterschied der radiogenen Nd-Hf Isotopenzusammensetzungen des Meerwassers zu denen der Gesteine

der oberen kontinentalen Kruste kontrollieren, wurden im Rahmen dieser Arbeit Laugungs-Experimente an Staub- und Löss-Proben verschiedener Größenfraktionen aus der chinesischen Wüste durchgeführt (Kapitel 4). Die Absicht dabei war es, zu untersuchen, ob der oben genannte Unterschied zwischen Meerwasser und Kruste bereits als Konsequenz der kontinentalen Verwitterung auftritt oder erst später durch marine Prozesse. Die Staub- und Löss-Proben wurden aus Wüsten und Aariden Regionen im nördlichen China, verteilt über eine Fläche, die sich über 600 km von Nord nach Süd und 4.000 km von Ost nach West erstreckt, entnommen. Da die Proben ein weites Spektrum an Nd-Isotopenzusammensetzungen aufweisen, kann davon ausgegangen werden, dass sie die Hf-Isotopenfraktionierung während der Verwitterung der durchschnittlichen oberen kontinentalen Kruste repräsentieren. Die Laugungs-Daten stimmen entweder mit dem Nd-Hf Isotopen-Bereich des Meerwassers überein oder sind leicht radiogener in ihrer Hf-Isotopie , was die Hypothese stützt, dass das Nd-Hf Isotopenverhältnis des Meerwassers vorwiegend durch kontinentale Verwitterung generiert wird.

Nichtsdestotrotz ist das Verständnis des Kreislaufes von Nd und seinen radiogenen Isotopen im Ozean weitaus besser als das der Hf-Isotope. Seit etwa 5 Jahren sind jedoch analytische Methoden verfügbar, die direkte und präzise Messungen von im Meerwasser gelösten Hf-Isotopenverhältnissen erlauben, obwohl nur sehr geringe Hf Konzentrationen im Meerwasser vorliegen und deshalb große Proben (60-140 Liter) entnommen werden müssen.

In der vorliegenden Arbeit wurden diese Methoden zum ersten Mal an Meerwasser aus der zentralen Ostsee, einem Brackwasser-Randmeer mit periodisch euxinischem Tiefenwasser (anoxisch und sulfidisch) und mit kontinentalen Liefergebieten von Hf und Nd verschiedenster Alter an den nördlichen und südlichen Rändern, angewandt. Dies erlaubt es, radiogene Nd und Hf Isotopensignaturen und Konzentrationen als Wassermassen-Tracer zu benutzen, sowie deren geochemische Kreisläufe in der Wassersäule über die Redox-Grenzen hinweg zu untersuchen (Kapitel 5). Zusätzlich wurden die Signaturen zweier in die Ostsee mündender Flüsse (Kalix und Schwentine) ermittelt. Im Allgemeinen kann die Verteilung der Nd-Isotope durch die Mischung von lokalen Einflüssen und atlantischen, radiogeneren Wassermassen erklärt werden, was die

Eignung von Nd Isotopen als Wassermassen-Tracer in der zentralen Ostsee zeigt. Die Hafnium-Isotopensignaturen hingegen weisen eine unerwartet hohe Variabilität auf und folgen nicht den Wassermassen-Mischungstrends. Daher wird angenommen, dass Hf eine kürzere Verweildauer als Nd im Meerwasser hat und stärker von lokalen Einflüssen geprägt wird. Die Ergebnisse aus dem Flusswasser des Kalix unterstützen vorherige Annahmen, dass die Hf-Isotopensignatur, die während der beginnenden Verwitterung von glazialem Moränenmaterial freigesetzt wird, sehr radiogen ist, da leicht verwitterbare Minerale aufgelöst werden.

Basierend auf den zuvor genannten Erkenntnissen können Hf Isotope nun mit höherer Zuverlässigkeit in Paläo-Ozeanographischen Studien mariner Sedimente angewandt werden. Kapitel 6 beschreibt die erstmalige Anwendung von kombinierten Hf-Nd Isotopen aus authigenen, frühdiagentischen Fe-Mn-Beschichtungen mariner Sedimente vom Lomonosovrücken (IODP Leg 302, ACEX) um die Veränderungen der Meerwasserzusammensetzung im zentralen Arktischen Ozean in den letzten 14 Millionen Jahren zu rekonstruieren. Die Ergebnisse zeigen, dass Hf-Isotopensignaturen zuverlässig aus marinen Sedimenten extrahiert werden können und dass deren Evolution im zentralen Arktischen Zwischenwasser mit der von Nd Isotopen eng gekoppelt war. Die Ergebnisse lassen deshalb zu die Schlussfolgerung zu, dass die Evolution der Hf-Isotopenzusammensetzungen des zentralen Arktischen Zwischenwassers hauptsächlich von Veränderungen der Ozeanzirkulation und der Herkunft der Verwitterungseinträge geprägt wurde und nicht von Veränderungen in den Verwitterungsbedigungen auf den Kontinenten.

Im Gegensatz dazu zeigen Untersuchungen von zwei Sedimentkernen (PS2082-1 und PS1388-3) aus dem Südozean unterschiedliche Zusammenhänge zwischen Hf- und Nd-Isotopen (Kapitel 7). Im Einklang mit vorangegangen Studien zeigen die Tiefenwasser-Signaturen aus den Gesamtsediment-Laugungen und Daten von ungereinigten planktonischen Foraminiferen systematisch radiogenere Nd-Isotopenzusammensetzungen während Glazialphasen als während Interglazialen im abyssalen Agulhas Becken (Kern PS2082-1). Im Gegensatz zur Entwicklung der atmosphärischen CO_2-Konzentrationen oder den Temperaturaufzeichnungen aus Eisbohrkernen der Antarktis, wird kein

Maximum der unradiogenen Nd Isotopensignaturen am Beginn der Interglazialstadien (MIS 5e oder frühes MIS 7) beobachtet, was höchstwahrscheinlich den eingeschränkten Gasaustausch an der Meeresoberfläche in den Kaltzeiten und die Verstärkung der Tiefenzirkulation während Glazial-Interglazial-Übergängen reflektiert, die dann aber in den folgenden Interglazialen konstant bleibt. Die Hf-Isotopensignaturen des Kerns PS2082-1 weisen relativ geringe Variationen auf, was auf sehr geringe Schwankungen der Intensität der chemischen Verwitterung auf dem antarktischen Kontinent im Laufe der letzten zwei Glazial-Interglazial-Zyklen hindeutet, die sich im Tiefenwasser des Südozeans widerspiegeln. Desweiteren wurde eine Veränderungen der Nd-Isotopenzusammensetzung des Tiefenwassers an der Lokalität von Kern PS1388-3 am Rand des Weddell-Meeres als Funktion von lokalen Verwitterungseinträgen gefunden, was die Vermutung nahe legt, dass der Austausch mit Kontinentalschelfs in der Nähe des Antarktischen Kontinentalrands eine wichtige Rolle spielen. Im Vergleich dazu ist die bevorzugte Freisetzung von Hf aus frisch erodierten Mineraloberflächen mit hohem Lu/Hf die wahrscheinlichste Erklärung für ausgeprägt radiogene Maxima der Hf Isotopensignaturen am Anfang der Interglazialstadien 7, 5, und 1, was vermutlich auf einen temporären Rückzug des Inlandeises auf dem antarktischen Kontinent zurückzuführen ist.

Chapter 1

Introduction

1.1 Background

On glacial-interglacial and millennial time scales, deep ocean circulation has regulated global climate mainly through heat distribution and carbon cycling (e.g., Broecker, 1998; Rahmstorf, 2002; Sigman et al., 2010; Robinson and Siddall, 2012; Adkins, 2013). The deep ocean holds the largest carbon reservoir of the Earth's surficial systems and thus atmospheric CO_2 concentrations are sensitive to changes in the partitioning of CO_2 between the ocean and the atmosphere. To understand past carbon cycling and its control on global climate variability, it is thus essential to have an accurate knowledge on past changes in deep water sources and their mixing, which is based on proxies recorded in marine archives. An ideal tracer of past water mass sources and mixing should (a) behave conservatively during water mass mixing and (b) have clearly distinguishable and well constrained endmember compositions that did not change over time. Classical tools such as stable carbon isotope (e.g., Duplessy et al., 2008; Curry and Oppo, 2005) and Cd/Ca ratios (Boyle 1988, 1992) of benthic foraminiferal tests have been widely used in paleoceanographic studies for this purpose. However, these nutrient-based proxies are tightly linked to nutrient dynamics and/or atmospheric-sea gas exchange and this non-conservative component makes is difficult to unambiguously and quantitatively constrain past water mass endmember compositions and their mixing (e.g., Piotrowski et al., 2005; 2008). A potentially ideal proxy to reconstruct past water mass mixing are radiogenic Nd isotopes (e.g. Frank, 2002), which will be introduced in detail below.

On tectonic time scales, the chemical weathering of continental silicate rocks represents the most important sink of atmospheric CO_2, which has strongly affected the Earth's past climate (e.g., Berner et al., 1983; Raymo et al.,1988; Raymo and Ruddiman, 1992; Wallmann, 2001). One critical component of continental silicate weathering is the intensity of weathering in different climatic different environments, which determines the sensitivity of feedbacks between weathering and climate, as well as the rates of element (e.g., nutrient) transfer from the continents to the ocean (e.g., West et al., 2005; Willenbring et al., 2013). Nevertheless, the direct investigation and reconstruction of the response of chemical weathering to past climate is challenging because records of past continental weathering on the continents are rarely preserved, but such information has

been recorded continuously by the marine sediments. The distribution and changes of radiogenic Hf isotopes in space and time are one of the potential oceanic proxies to study changes continental weathering regimes given that rock forming minerals with distinct Hf isotope compositions are differently susceptible to weathering (e.g., van de Flierdt et al., 2002; Bayon et al., 2006; 2009). Since Hf isotopes are a relatively new proxy in paleoceanographic and paleoclimate research, there is still considerable lack of knowledge on the marine cycling of Hf. Compared to other proxies of continental weathering with long residence times in the ocean, such as radiogenic Sr or Os isotopes, the relatively short residence time of Hf isotopes allows to record short term changes in chemical weathering signatures on the continents and it is thus worthy to be studied systematically.

1.2 Sm-Nd and Lu-Hf isotope systematics of the terrestrial rocks, marine sediments and seawater

Neodymium is a rare earth element with 7 naturally occurring stable isotopes (^{142}Nd, ^{143}Nd, ^{144}Nd, ^{145}Nd, ^{146}Nd, ^{148}Nd, and ^{150}Nd). Among these isotopes, a fraction of the ^{143}Nd is the product of α decay of ^{147}Sm. Due to the long half-life of ^{147}Sm (1.06×10^{11} y), the variations of ^{143}Nd abundances in the natural samples are measurable but very small. For convenience, the radiogenic Nd isotopic composition is often reported in the ϵ_{Nd} notation, which is the deviation from the Chondritic Uniform Reservoir (CHUR) in parts per 10,000:

$$\epsilon_{Nd} = (\frac{(^{143Nd}/_{144Nd})_{sample}}{(^{143Nd}/_{144Nd})_{CHUR}} - 1) \times 10^4 \ ,$$

whereby (^{143}Nd/^{144}Nd)$_{CHUR}$ has a modern value of 0.512638 (Jacobsen and Wasserburg, 1980).

Hafnium has 6 naturally occurring stable isotopes (^{174}Hf, ^{176}Hf, ^{177}Hf, ^{178}Hf, ^{179}Hf, and ^{180}Hf), of which a fraction of the ^{176}Hf is the radiogenic product of radioactive ^{176}Lu through β^- emission (half-life = 3.6×10^{10} y). Similar to Nd isotopes, the radiogenic Hf isotopic composition is also expressed in ϵ_{Hf} units:

$$\epsilon_{Hf} = \left(\frac{\left(^{176}Hf/^{177}Hf\right)_{sample}}{\left(^{176}Hf/^{177}Hf\right)_{CHUR}} - 1\right) \times 10^4 \, ,$$

whereby $(^{176}Hf/^{177}Hf)_{CHUR}$ has a modern value of 0.282769 (Nowell et al., 1998).

During Earth's magmatic processes (i.e., crystallization differentiation and partial melting), the fractionation behavior of Sm-Nd is similar to that of Lu-Hf, in that Nd and Hf are more incompatible than Sm and Lu, respectively. This results in lower Sm/Nd and Lu/Hf ratios in the magma than in the residual fraction. Therefore, Hf and Nd isotopic compositions of most terrestrial rocks display a strong positive correlation, which has previously been defined as the terrestrial array (Vervoort et al., 1999, $\epsilon_{Hf} = 1.35\epsilon_{Nd} + 2.82$, Figure 1.1).
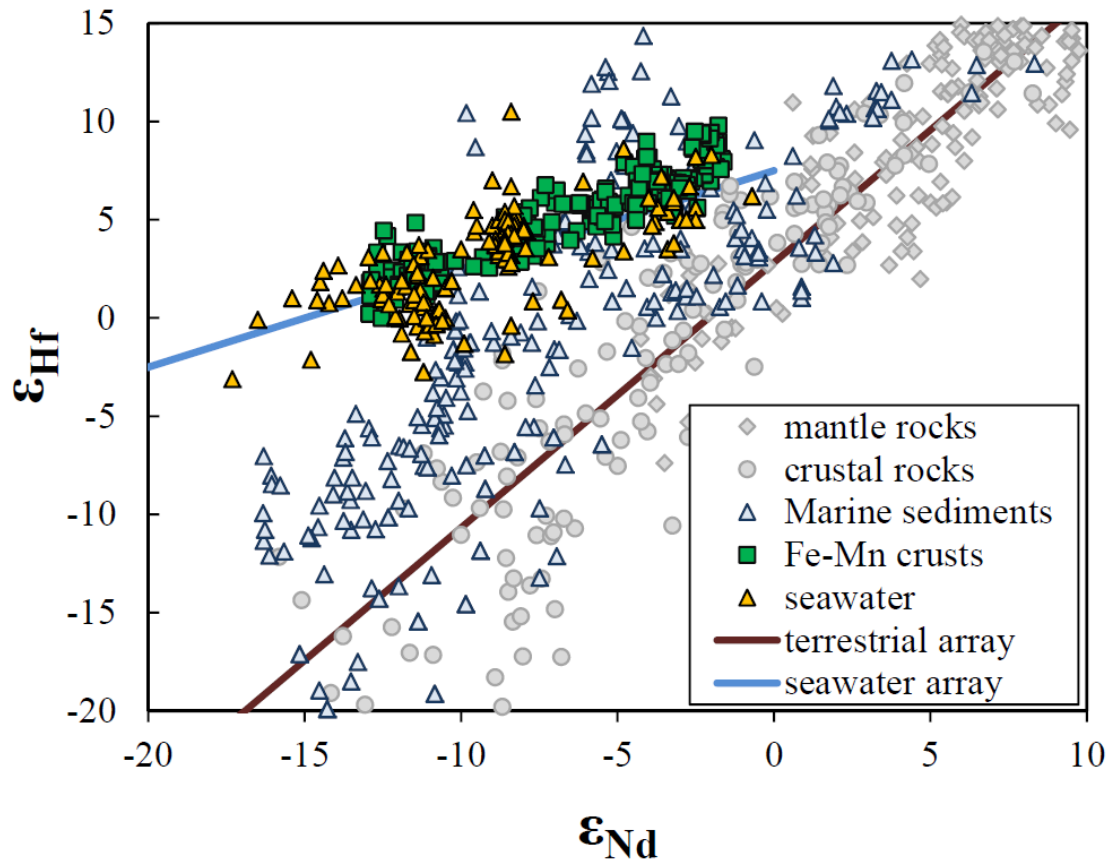
Figure 1.1 Hafnium–neodymium isotope systematics of seawater, Fe-Mn crusts/nodules, and terrestrial rocks. The terrestrial array (Vervoort et al., 1999) and seawater array (Albarède et al., 1998) are regressions of Hf-Nd isotope compositions of the terrestrial rocks and Fe-Mn crusts/nodules, respectively. Data sources: Marine sediments, mantle and crustal rocks (Vervoort et al., 1999; 2011), hydrogenetic Fe-Mn

crusts/nodules (Lee et al., 1999; Piotrowski et al., 2000; David et al., 2001; van de Flierdt et al., 2004) and dissolved seawater data (<0.45 µm, Rickli et al., 2009, 2010; Zimmermann et al., 2009a, b; Stichel et al., 2012a, b).
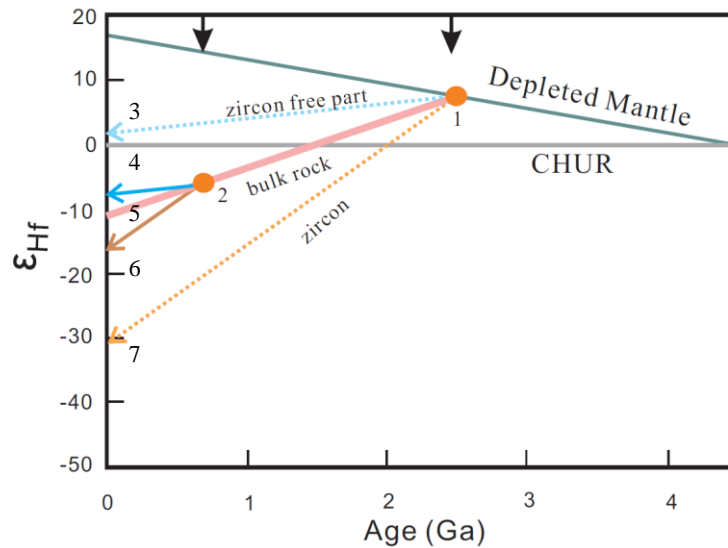
Figure 1.2 Schematic Hf isotopic evolution of zircon, its corresponding bulk parent rock, and the zircon free part of the bulk rock. Thick black arrows indicate two hypothesized main stages of melting events of the mantle. 1: Extraction of the primitive continental rocks from the depleted mantle. 2: Formation of the upper continental crust by remelting of the primitive continental crust. At this stage, the zircons reached isotopic re-equilibrium with the corresponding zircon free part. 3,7: The present ideal $\varepsilon_{Hf(0)}$ values of the zircon-free part and the zircons (which do not include the influence of further re-melting events). 4, 6. Actual $\varepsilon_{Hf(0)}$ values of the zircon-free part and zircon. 5. The present $\varepsilon_{Hf(0)}$ value of the bulk rock.

However, unlike Sm/Nd ratios in different minerals which are generally similar to each other, Lu/Hf ratios vary considerably among different minerals. Zircon as a heavy and refractory mineral hosts much of the Hf present in the rocks, while it does not incorporate significant amounts of Lu. Consequently, zircons become distinctively less radiogenic than the corresponding bulk rocks over time (see the illustration in Figure 1.2). During weathering and subsequent sediment transport, Hf isotope signatures may thus be fractionated from the terrestrial rocks due to the mineral sorting effect (e.g., Carpentier et

al. 2008). Besides, because of the zircons' very high resistivity to weathering, Hf isotope signatures released to the weathering solutions are expected to be more radiogenic than those of the bulk rocks (van de Flierdt et al., 2002, 2007). The Hf isotope fractionation related to zircon during mineral sorting and to its resistivity to weathering has previously been termed as the "zircon effect" (van de Flierdt et al., 2007).

As a consequence of these fractionation processes, the reported dissolved Nd-Hf isotope compositions of seawater as well as of authigenic sedimentary Fe-Mn oxihydroxides precipitated from seawater show a unique correlation in the ε_{Nd}- ε_{Hf} space (Figure 1.1). For a given ε_{Nd} value, the Hf isotope composition of seawater is characterized by more radiogenic signatures ($\varepsilon_{Hf} = 0.5\varepsilon_{Nd} + 7.5$, Albarède et al., 1998). The mechanism of the formation of Nd-Hf seawater array most likely involves the incongruent release of Hf isotopes from the bulk rock during weathering, especially the zircon effect mentioned above, and/or the hydrothermal contribution of radiogenic Hf (Bau et al., 2006). It is also possible that Hf has a longer residence time than Nd in the ocean resulting in more homogenized signatures. However, these processes controlling the behavior of Hf isotopes and the oceanic Hf budget are still not well resolved.

In contrast, the oceanic cycling of Nd isotopes is much better understood than Hf owing to a large number of dedicated studies over the last more than three decades. It is well known that seawater dissolved Nd isotopes are not notably affected by hydrothermal sources (German et al., 1990; Halliday et al., 1992). Thus in general and independent of the location, seawater Nd is ultimately and exclusively derived from continental inputs. Its sources include particulate and dissolved riverine inputs, dissolution of eolian dust, and the "boundary exchange" flux (e.g., Lacan and Jeandel., 2005; Arsouze et al., 2007, 2009, Rempfer et al., 2011, Wilson et al., 2012), a process leading to the exchange and release of Nd to seawater by leaching and mobilization from continental slope sediments.

The vertical distribution of Nd in the water column is characterized by reversible scavenging of Nd by particles. This is supported by low Nd concentrations in surface waters and increasing Nd concentrations with increasing depth (c.f., Siddall et al., 2008; Oka et al., 2009). Reversible scavenging describes the physical process of Nd adsorption onto particles and subsequent desorption due to particle dissolution and remineralisation

or as a consequence of aggregation and disaggregation. Hf also shows slightly enriched concentration with depth in the water column, but with much less variability (Rickli et al., 2009; Zimmermann et al., 2009b; Stichel et al., 2012).

1.3 The acquisition of past seawater Nd-Hf isotope compositions

The dissolved concentrations of Nd and Hf in the modern seawater are generally very low, amounting to less than 100 pmol/kg of Nd and less than 2 pmol/kg of Hf. In order to measure accurate and precise isotope compositions of dissolved Nd and Hf in seawater, generally 10-20 liters and 60-140 liters of seawater are needed, respectively, depending on the concentrations. Because of the analytical difficulties involved in direct seawater Hf isotope measurements, there have up to now only been few studies that have focused on seawater dissolved Hf isotope compositions and all of them were published in the last 5 years. The ε_{Hf} of modern open ocean water ranges from -2.8 to +10.5, which agrees very well with data obtained from the Fe-Mn crusts, though with larger variability reported for the modern seawater (Figure 1.1).

Initially, the reconstruction of the Nd-Hf isotope evolution of seawater in the past almost entirely depended on records obtained from marine Fe-Mn crusts (e.g. Frank, 2002). Fe-Mn crusts are direct authigenic precipitates from ambient seawater, which only grow at rates of a few mm per Myr on submarine seamounts or other locations protected from pelagic or hemipelagic sedimentation by bottom currents. Thus Fe-Mn crust can serve as a reliable archive of past seawater Nd and Hf isotope composition. However, with the very low time resolution achievable from Fe-Mn crust time series, it is difficult or impossible to extract isotopic information on glacial-interglacial or shorter time scales, which are of fundamental interest for paleoceanographic reconstructions.

In the past decade, amorphous authigenic Fe-Mn oxihydroxide coatings formed at the sediment water interface and supplied by the pore waters of the sediments during early diagenesis (Haley et al., 2004) were explored as a high resolution paleoceanographic archive to reconstruct seawater Nd isotope fluctuations (100-1000 years) (e.g. Rutberg et al., 2000; Bayon et al., 2002; Piotrowski et al., 2005). Nevertheless, the reliability of the leaching procedure may be variable as a function of the type and location of the

sediments due to the potential contamination by preformed oxides and/or by the detrital fractions, in particular by volcanic material (e.g., Elmore et al., 2011; Wilson et al., 2013). Therefore it is necessary to critically evaluate the reliability of the leaching procedure (e.g., core-top calibration) for each location studied.

The first attempts to obtain seawater Nd isotope signatures from Fe-Mn oxihydroxide coatings of foraminifera shells were made in the 1980s (Palmer and Elderfield, 1985; 1986). There is currently still debate, which water depth of the Nd isotopes signature extracted from cleaned planktonic foraminifera may reflect (e.g., for the latest studies, see Roberts et al., 2012; Pena et al., 2013; Kraft et al., 2013). For example, Pena et al., (2013) tried to reconstruct the surface seawater Nd isotope composition by removing the Fe-Mn coatings of the sedimentary planktonic foraminifera shells using reductive/oxidative cleaning and measuring the pure calcite carbonate similar to the initial attempts by e.g., Burton and Vance, (2000). Other studies, however, indicate that such cleaning is not complete and that bottom water Nd is incorporated diagenetically into the Mn-rich layer of planktonic foraminiferal shells and thus both reductively cleaned and uncleaned forams will essentially reflect the bottom water Nd isotope composition (e.g., Roberts et al., 2012; Kraft et al., 2013).

1.4 Principles and application of radiogenic Nd and Hf isotopes as tracers of ocean circulation and continental weathering

Nd isotopes have been demonstrated to be a reliable water mass tracer both for modern and past times due to the fact that: (1) Nd isotopes are controlled by input from the continents while hydrothermal contributions are negligible. (2) Different oceanic basins are surrounded by geological formations with significantly different Nd isotope compositions allowing water masses to acquire systematically different isotope compositions. For example, the two major deep water end-members in the Atlantic Ocean (i.e., North Atlantic Deep Water, $\varepsilon_{Nd} = -13.5 \pm 0.5$ Piepgras and Wasserberg 1987; and deep waters in the North Pacific, $\varepsilon_{Nd} = \sim -3$ to -4, Amakawa et al., 2009) have pronouncedly different radiogenic Nd isotope signatures. (3) The residence time of Nd in the ocean allows long distance transport of deep water mass signatures and prevents complete

isotopic homogenization (e.g. Figure 1.3, von Blanckenburg, 1999). (4) The radiogenic Nd isotopes in seawater are not fractionated by biological and adsorption-desorption processes. As a result, changes in their deep water isotope compositions are only related to the mixing of water masses and to a much lesser extent the release of Nd from particles sinking from the overlying upper ocean, at least in the open Atlantic Ocean and the Southern Ocean. Therefore, in contrast to traditional water mass tracers of the past ocean, such as $\delta^{13}C$ or Cd/Ca, the radiogenic Nd isotope signatures provide independent information on past deep water circulation and water mass mixing.
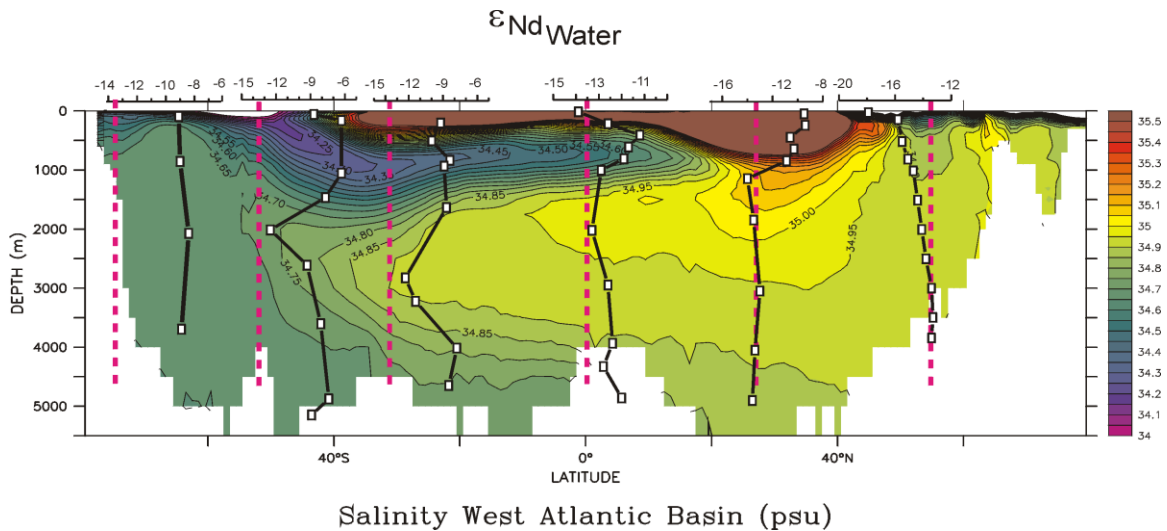
Figure 1.3 Illustration of the reliability of Nd isotopes as a water mass tracer in the deep Atlantic. The contour lines show the present day salinity distribution of the western Atlantic section, onto which is the seawater Nd isotope compositions is superimposed (adapted from von Blanckenburg, 1999).

In the case of Hf isotopes, however, their application in paleoceanographic studies has still not been pursued very often. The main reason is the poor understanding of the present day marine Hf isotope geochemistry, the improvement of which is the subject of this Ph.D. thesis.

1.5 An introduction of the major research questions of this thesis

1.5.1 The surface ocean cycling of Nd

Despite that the first studies on the distribution of dissolved Rare Earth Elements (REEs) in seawater were undertaken several decades ago, the factors controlling Nd concentrations in open ocean surface waters are still not well understood. Such knowledge is, however, important for interpreting seawater Nd isotope compositions in both modern and paleoceanographic studies. Due to a number of recent geochemical studies on Nd concentrations along important oceanic sections such as in the Southern Ocean (in particular south of 30°S as proposed by Lacan et al. (2012)), a more complete picture of the basin scale variations of surface water Nd concentrations has now become available for the first time. Based on these global distributions, this thesis aims to evaluate the role of different factors controlling variations of Nd concentrations in open ocean surface waters (0-100 m).

1.5.2 The formation of the Nd-Hf isotope seawater array

Early studies proposed that contributions of radiogenic Hf from hydrothermal sources may be important for the seawater budget of Hf (White et al., 1986; Godfrey et al., 1997; Bau and Koschinsky, 2006). However, recent dissolved seawater Hf isotope and concentration data have not favored such a scenario (Rickli et al., 2009; Firdaus et al., 2011; Stichel et al., 2012). Nevertheless, an unambiguous conclusion has still not been achieved. Instead it has been proposed that incongruent weathering of the the Upper Continental Crust (UCC) alone may be responsible for the seawater Hf isotope compositions. To resolve this issue, the weathering signal of UCC was investigated by leaching Asian dust and loess samples recovered from North China.

1.5.3 The oceanic cycling and residence time of Hf and Nd

The oceanic residence time of Hf and its input mechanisms are important for determining how to use Hf isotopes in paleoceanographic and paleoclimate studies. Direct seawater studies are of highest priority to increase the so far small globally available data set.

Despite seawater Hf concentrationy are extremely low (<2 pmol/kg), current analytical and mass spectrometric techniques now enable the measurement of seawater dissolved Hf isotope compositions albeit with large volume of seawater (60-140 liters, e.g., Zimmerman et al., 2009a, b, Rickli et al., 2009). In this thesis, the distribution of Nd and Hf concentrations and their isotopic compositions of 6 profiles and 3 surface sites were obtained during a cruise in the central Baltic Sea onboard the RV Oceania in the frame of the international GEOTRACES program in order to better understand sources and sinks, as well as their biogeochemical cycling.

1.5.4 The combined Hf-Nd isotope evolution of seawater on glacial-interglacial time scales

So far, millennial scale resolution reconstructions of weathering regimes and water mass mixing applying past Hf isotopes have been hampered by the lack of suitable analytical methods to extract seawater Hf isotope compositions from marine sediments. The leaching methods routinely applied for extracting seawater Nd and Pb isotope compositions do not work for Hf isotopes due to the re-adsorption of the seawater-derived Hf to the detrital phases during the leaching procedure.

Here the first combined seawater Hf and Nd isotope compositions of past Arctic Intermediate Water extracted from the authigenic Fe-Mn oxyhydroxide fraction of two sediment cores recovered near the North Pole are presented applying a leaching method avoiding re-adsorption of Hf by adding Na-EDTA (Gutjahr, 2006) to reconstruct changes in contributions from glacial brines of the Eurasian shelf and past inflow of Atlantic waters.

The Southern Ocean has been increasingly recognized to be a critical region in controlling glacial-interglacial (G-I) variability of atmospheric CO_2 concentrations. However, the reconstruction of deep Southern Ocean circulation on orbital time scale is still lacking, limiting our understanding in the role of deep Southern Ocean circulation in the late Quaternary climate variability. Therefore, the studies of Nd-Hf isotopes of Southern Ocean sediments have also been carried out to reconstruct changes in Southern Ocean circulation as well as weathering input over the last 250 ky.

1.6 Outline of the thesis and declaration of my contribution to the following chapters

Chapter 1 introduces the Nd and Hf isotope systematics of crustal rocks, marine sediments and seawater, and also their previous applications in paleocenographic studies. The major research questions including the sources, cycling and the possible application of combined seawater Nd-Hf isotopes in high time resolution paleoceanographic studies are discussed.

Chapter 2 presents the chemical procedures applied to extract and purify the Nd-Hf fractions of leachates and detrital fractions from marine sediments, dust deposits, and waters. The mass spectrometric measurements of Nd and Hf isotopes are also described in detail.

The following chapters (Chapter 3, 4, 5, 6, and 7) address the questions discussed in section 1.3 following different approaches.

Chapter 3 (published in *JGR-oceans*, 118, 3887–3894, 2013) suggests that that vertical supply of Nd from subsurface waters to shallower depths, itself limited by upper ocean stratification, provides an important contribution to the Nd budget of open ocean surface waters. These ideas are based on published near surface Nd concentration data and ^{228}Ra activities.

<u>Chapter 3 Declaration</u>: I have proposed the study, compiled the data from literature, and written the manuscript. J. Rempfer, University of Berne, carried out a 3-D modeling experiment and wrote the model description as part of the Appendix of this manuscript. M. Molina-Kescher provided surface Nd concentration data of the South Pacific. All co-authors and 2 external reviewers helped improving and revising the manuscript.

Chapter 4 (published in *GRL*, 40, 916-920, 2013) presents leaching experiments on Chinese desert and loess samples of different size fractions. From the results of these experiments it is inferred that the seawater array is directly generated by incongruent weathering of upper continental rocks.

<u>Chapter 4 Declaration</u>: I have proposed the study, carried out the experiment, and written the manuscript. G. Li discussed the samples to be analyzed and also provided the

samples. All co-authors and 2 external reviewers helped improving and revising the manuscript.

Chapter 5 (published in *GCA*, 123, 166-180) investigates the Hf and Nd geochemical cycling in the central Baltic Sea.

<u>Chapter 5 Declaration</u>: M. Frank proposed the study. All co-authors were involved in planning of the sampling. The samples were taken by R. Stumpf and myself during the cruise on RV Oceania. R. Stumpf assisted in the subsequent analyses and the calculation of Nd and Hf concentrations applying an isotope spiking technique. I have carried out the analyses and written the manuscript. All co-authors, the *GCA* editor D. Vance, J. Rickli and other 2 external reviewers helped improving and revising the manuscript.

Chapters 6 (published in *EPSL*, 353–354, 82-92, 2012) & 7 (to be submitted) present the extraction of Hf isotopes from authigenic Fe-Mn fractions of marine sediments from the Arctic and Southern Oceans, respectively, for high time resolution reconstructions of past bottom waters and their mixing. The results demonstrate that seawater Hf isotope compositions can be reliably extracted from marine sediments and provide complementary and unique information on weathering inputs from the continents and deep circulation on glacial-interglacial time scales.

<u>Chapter 6 Declaration:</u> M. Frank proposed the study locations and discussed the samples to be analyzed, as well as the leaching procedures. M. Gutjahr provided valuable suggestions for my analyses. R. Spielhagen provided the samples for analyses. I carried the analyses and wrote the manuscript. All co-authors, J. D. Gleason and an external reviewer helped improving and revising the manuscript.

<u>Chapter 7 Declaration</u>: M. Frank proposed the study locations and discussed the samples to be analyzed, as well as the leaching procedures. A. Osborne and S. Kraft helped picking the foraminifera samples and with the redox-cleaning. I performed the analyses of the data and wrote the chapter. M. Frank improved and revised this chapter.

The last chapter (Chapter 8) presents a brief summary of this thesis and an outlook to future studies.

References

Adkins, J. F. (2013) The role of deep ocean circulation in setting glacial climates. *Paleoceanography*, in press, doi: 10.1002/palo.20046.

Albarede, F., Simonetti, A., Vervoort, J. D., Blichert-Toft, J., and Abouchami, W. (1998) A Hf-Nd isotopic correlation in ferromanganese nodules. *Geophysical Research Letters* **25**, 3895-3898.

Amakawa, H., Sasaki, K., and Ebihara, M. (2009) Nd isotopic composition in the central North Pacific. *Geochimica et Cosmochimica Acta* **73**, 4705-4719.

Arsouze, T., Dutay, J. C., Lacan, F., and Jeandel, C. (2007) Modeling the neodymium isotopic composition with a global ocean circulation model. *Chemical Geology* **239**, 165-177.

Arsouze, T., Dutay, J. C., Lacan, F., and Jeandel, C. (2009) Reconstructing the Nd oceanic cycle using a coupled dynamical - biogeochemical model. *Biogeosciences* **6**, 2829-2846.

Bau, M. and Koschinsky, A. (2006) Hafnium and neodymium isotopes in seawater and in ferromanganese crusts: The "element perspective". *Earth and Planetary Science Letters* **241**, 952-961.

Bayon, G., German, C. R., Boella, R. M., Milton, J. A., Taylor, R. N., and Nesbitt, R. W. (2002) An improved method for extracting marine sediment fractions and its application to Sr and Nd isotopic analysis. *Chemical Geology* **187**, 179-199.

Bayon, G., Burton, K. W., Soulet, G., Vigier, N., Dennielou, B., Etoubleau, J., Ponzevera, E., German, C. R., and Nesbitt, R. W. (2009) Hf and Nd isotopes in marine sediments: Constraints on global silicate weathering. *Earth and Planetary Science Letters* **277**, 318-326.

Bayon, G., Vigier, N., Burton, K. W., Brenot, A., Carignan, J., Etoubleau, J., and Chu, N. C. (2006) The control of weathering processes on riverine and seawater hafnium isotope ratios. *Geology* **34**, 433-436.

Berner, R. A., Lasaga, A. C., and Garrels, R. M. (1983) The Carbonate-Silicate Geochemical Cycle and Its Effect on Atmospheric Carbon-Dioxide over the Past 100 Million Years. *American Journal of Science* **283**, 641-683.

Boyle, E. A. (1988) Cadmium: Chemical tracer of deepwater paleoceanography. *Paleoceanography* **3**, 471-489.

Boyle, E. A. (1992) Cadmium and Delta-C-13 Paleochemical Ocean Distributions during the Stage-2 Glacial Maximum. *Annual Review of Earth and Planetary Sciences* **20**, 245-287.

Broecker, W. S. (1998) Paleocean circulation during the last deglaciation: A bipolar seesaw? *Paleoceanography* **13**, 119-121.

Burton, K. W. and Vance, D. (2000) Glacial-interglacial variations in the neodymium isotope composition of seawater in the Bay of Bengal recorded by planktonic foraminifera. *Earth and Planetary Science Letters* **176**, 425-441.

Carpentier, M., Chauvel, C., Maury, R. C., and Mattielli, N. (2009) The "zircon effect" as recorded by the chemical and Hf isotopic compositions of Lesser Antilles forearc sediments. *Earth and Planetary Science Letters* **287**, 86-99.

Curry, W. B. and Oppo, D. W. (2005) Glacial water mass geometry and the distribution of delta C-13 of Sigma CO2 in the western Atlantic Ocean. *Paleoceanography* **20**, PA1017, doi: 10.1029/2004PA001021.

David, K., Frank, M., O'Nions, R. K., Belshaw, N. S., and Arden, J. W. (2001) The Hf isotope composition of global seawater and the evolution of Hf isotopes in the deep Pacific Ocean from Fe-Mn crusts. *Chemical Geology* **178**, 23-42.

Duplessy, J. C., Shackleton, N. J., Fairbanks, R. G., Labeyrie, L., Oppo, D., and Kallel, N. (1988) Deepwater source variations during the last climatic cycle and their impact on the global deepwater circulation. *Paleoceanography* **3**, 343-360.

Elmore, A. C., Piotrowski, A. M., Wright, J. D., and Scrivner, A. E. (2011) Testing the extraction of past seawater Nd isotopic composition from North Atlantic deep sea sediments and foraminifera. *Geochemistry Geophysics Geosystems* **12**, Q09008, doi: 10.1029/2011gc003741.

Firdaus, M. L., Minami, T., Norisuye, K., and Sohrin, Y. (2011) Strong elemental fractionation of Zr-Hf and Nb-Ta across the Pacific Ocean. *Nature Geoscience* **4**, 227-230.

Frank, M. (2002) Radiogenic isotopes: Tracers of past ocean circulation and erosional input. *Review of Geophysics* **40**, 1001, doi: 10.1029/2000RG000094.

German, C. R., Klinkhammer, G. P., Edmond, J. M., Mitra, A., and Elderfield, H. (1990) Hydrothermal Scavenging of Rare-Earth Elements in the Ocean. *Nature* **345**, 516-518.

Godfrey, L. V., Lee, D. C., Sangrey, W. F., Halliday, A. N., Salters, V. J. M., Hein, J. R., and White, W. M. (1997) The Hf isotopic composition of ferromanganese nodules and crusts and hydrothermal manganese deposits: Implications for seawater Hf. *Earth and Planetary Science Letters* **151**, 91-105.

Haley, B. A., Klinkhammer, G. P., and McManus, J. (2004) Rare earth elements in pore waters of marine sediments. *Geochimica et Cosmochimica Acta* **68**, 1265-1279.

Halliday, A. N., Davidson, J. P., Holden, P., Owen, R. M., and Olivarez, A. M. (1992) Metalliferous Sediments and the Scavenging Residence Time of Nd near Hydrothermal Vents. *Geophysical Research Letters* **19**, 761-764.

Jacobsen, S. B. and Wasserburg, G. J. (1980) Sm-Nd Isotopic Evolution of Chondrites. *Earth and Planetary Science Letters* **50**, 139-155.

Kraft, S., Frank, M., Hathorne, E. C., and Weldeab, S. (2013) Assessment of seawater Nd isotope signatures extracted from foraminiferal shells and authigenic phases of Gulf of Guinea sediments. *Geochimica et Cosmochimica Acta* **121**, 414-435.

Lacan, F. and Jeandel, C. (2005) Neodymium isotopes as a new tool for quantifying exchange fluxes at the continent-ocean interface. *Earth and Planetary Science Letters* **232**, 245-257.

Lacan, F., Tachikawa, K., and Jeandel, C. (2012) Neodymium isotopic composition of the oceans: A compilation of seawater data. *Chemical Geology* **300–301**, 177-184.

Lee, D. C., Halliday, A. N., Hein, J. R., Burton, K. W., Christensen, J. N., and Gunther, D. (1999) Hafnium isotope stratigraphy of ferromanganese crusts. *Science* **285**, 1052-1054.

Nowell, G. M., Kempton, P. D., Noble, S. R., Fitton, J. G., Saunders, A. D., Mahoney, J. J., and Taylor, R. N. (1998) High precision Hf isotope measurements of MORB and OIB by thermal ionisation mass spectrometry: insights into the depleted mantle. *Chemical Geology* **149**, 211-233.

Oka, A., Hasumi, H., Obata, H., Gamo, T., and Yamanaka, Y. (2009) Study on vertical profiles of rare earth elements by using an ocean general circulation model. *Global Biogeochemical Cycles* **23**, GB4025, doi: 10.1029/2008gb003353.

Palmer, M. R. and Elderfield, H. (1985) Variations in the Nd isotopic composition of foraminifera from Atlantic Ocean sediments. *Earth and Planetary Science Letters* **73**, 299-305.

Palmer, M. R., and Elderfield H. (1986) Rare earth elements and neodymium isotopes in ferromanganese oxide coatings of Cenozoic foraminifera from the Atlantic Ocean, *Geochimica et Cosmochimica Acta* **50**, 409-417.

Pena, L. D., Goldstein, S. L., Hemming, S. R., Jones, K. M., Calvo, E., Pelejero, C., and Cacho, I. (2013) Rapid changes in meridional advection of Southern Ocean intermediate waters to the tropical Pacific during the last 30 kyr. *Earth and Planetary Science Letters* **368**, 20-32.

Piepgras, D. J. and Wasserburg, G. J. (1987) Rare-Earth Element Transport in the Western North-Atlantic Inferred from Nd Isotopic Observations. *Geochimica et Cosmochimica Acta* **51**, 1257-1271.

Piotrowski, A. M., Lee, D. C., Christensen, J. N., Burton, K. W., Halliday, A. N., Hein, J. R., and Gunther, D. (2000) Changes in erosion and ocean circulation recorded in the Hf isotopic compositions of North Atlantic and Indian Ocean ferromanganese crusts. *Earth and Planetary Science Letters* **181**, 315-325.

Piotrowski, A. M., Goldstein, S. L., Hemming, S. R., and Fairbanks, R. G. (2005) Temporal Relationships of Carbon Cycling and Ocean Circulation at Glacial Boundaries. *Science* **307**, 1933-1938.

Piotrowski, A. M., Goldstein, S. L., R, H. S., Fairbanks, R. G., and Zylberberg, D. R. (2008) Oscillating glacial northern and southern deep water formation from combined neodymium and carbon isotopes. *Earth and Planetary Science Letters* **272**, 394-405.

Rahmstorf, S. (2002) Ocean circulation and climate during the past 120,000 years. *Nature* **419**, 207-214.

Raymo, M. E., Ruddiman, W. F., and Froelich, P. N. (1988) Influence of Late Cenozoic Mountain Building on Ocean Geochemical Cycles. *Geology* **16**, 649-653.

Raymo, M. E. and Ruddiman, W. F. (1992) Tectonic Forcing of Late Cenozoic Climate. *Nature* **359**, 117-122.

Rickli, J., Frank, M., and Halliday, A. N. (2009) The hafnium-neodymium isotopic composition of Atlantic seawater. *Earth and Planetary Science Letters* **280**, 118-127.

Roberts, N. L., Piotrowski, A. M., Elderfield, H., Eglinton, T. I., and Lomas, M. W. (2012) Rare earth element association with foraminifera. *Geochimica et Cosmochimica Acta* **94**, 57-71.

Robinson, L. F. and Siddall, M. (2012) Palaeoceanography: motivations and challenges for the future. *Philos T R Soc A* **370**, 5540-5566.

Rutberg, R. L., Hemming, S. R., and Goldstein, S. L. (2000) Reduced North Atlantic Deep Water flux to the glacial Southern Ocean inferred from neodymium isotope ratios. *Nature* **405**, 935-938.

Siddall, M., Khatiwala, S., van de Flierdt, T., Jones, K., Goldstein, S. L., Hemming, S., and Anderson, R. F. (2008) Towards explaining the Nd paradox using reversible scavenging in an ocean general circulation model. *Earth and Planetary Science Letters* **274**, 448-461.

Sigman, D. M., Hain, M. P., and Haug, G. H. (2010) The polar ocean and glacial cycles in atmospheric CO2 concentration. *Nature* **466**, 47-55.

Stichel, T., Frank, M., Rickli, J., and Haley, B. A. (2012) The hafnium and neodymium isotope composition of seawater in the Atlantic sector of the Southern Ocean. *Earth and Planetary Science Letters* **317–318**, 282-294.

van de Flierdt, T., Frank, M., Lee, D. C., and Halliday, A. N. (2002) Glacial weathering and the hafnium isotope composition of seawater. *Earth and Planetary Science Letters* **198**, 167-175.

van de Flierdt, T., Frank, M., Lee, D. C., Halliday, A. N., Reynolds, B. C., and Hein, J. R. (2004) New constraints on the sources and behavior of neodymium and hafnium in seawater from Pacific Ocean ferromanganese crusts. *Geochimica et Cosmochimica Acta* **68**, 3827-3843.

van de Flierdt, T., Goldstein, S. L., Hemming, S. R., Roy, M., Frank, M., and Halliday, A. N. (2007) Global neodymium-hafnium isotope systematics - revisited. *Earth and Planetary Science Letters* **259**, 432-441.

Vervoort, J. D., Patchett, P. J., Blichert-Toft, J., and Albarede, F. (1999) Relationships between Lu-Hf and Sm-Nd isotopic systems in the global sedimentary system. *Earth and Planetary Science Letters* **168**, 79-99.

Vervoort, J. D., Plank, T., and Prytulak, J. (2011) The Hf-Nd isotopic composition of marine sediments. *Geochimica et Cosmochimica Acta* **75**, 5903-5926.

von Blanckenburg, F. (1999) Perspectives: Paleoceanography - Tracing past ocean circulation? *Science* **286**, 1862-1863.

Wallmann, K. (2001) Controls on the Cretaceous and Cenozoic evolution of seawater composition, atmospheric CO2 and climate. *Geochimica et Cosmochimica Acta* **65**, 3005-3025.

West, A. J., Galy, A., and Bickle, M. (2005) Tectonic and climatic controls on silicate weathering. *Earth and Planetary Science Letters* **235**, 211-228.

White, W. M., Patchett, J., and Benothman, D. (1986) Hf Isotope Ratios of Marine-Sediments and Mn Nodules - Evidence for a Mantle Source of Hf in Seawater. *Earth and Planetary Science Letters* **79**, 46-54.

Wilson, D. J., Piotrowski, A. M., Galy, A., and McCave, I. N. (2012) A boundary exchange influence on deglacial neodymium isotope records from the deep western Indian Ocean. *Earth and Planetary Science Letters* **341–344**, 35-47.

Wilson, D. J., Piotrowski, A. M., Galy, A., and Clegg, J. A. (2013) Reactivity of neodymium carriers in deep sea sediments: Implications for boundary exchange and paleoceanography. *Geochimica et Cosmochimica Acta* **109**, 197-221.

Willenbring, J. K., Codilean, A. T., and McElroy, B. (2013) Earth is (mostly) flat: Apportionment of the flux of continental sediment over millennial time scales. *Geology* **41**, 343-346.

Zimmermann, B., Porcelli, D., Frank, M., Andersson, P. S., Baskaran, M., Lee, D. C., and Halliday, A. N. (2009a) Hafnium isotopes in Arctic Ocean water. *Geochimica et Cosmochimica Acta* **73**, 3218-3233.

Zimmermann, B., Porcelli, D., Frank, M., Rickli, J., Lee, D. C., and Halliday, A. N. (2009b) The hafnium isotope composition of Pacific Ocean water. *Geochimica et Cosmochimica Acta* **73**, 91-101.

Chapter 2

Materials and Methods

The contents of the methods and materials Chapter below have been described similarly (but only briefly) in the following chapters. Detailed information on reagents used in this study is provided in Table A1.

2.1 Seawater and river water samples

2.1.1 Sampling and pre-concentration

Seawater samples were collected in the central Baltic Sea at 6 depth profile stations and 3 surface water sites during the GEOTRACES cruise on RV Oceania in November 2011. Sixty liters of deep water sample were taken from a standard rosette equipped with Niskin bottles, while surface water samples were taken from a surface pump, using 3 acid-cleaned 20 L LDPE-collapsible cubitainers for each sample. Immediately after collection, samples were filtered through 0.45 μm nitro-cellulose acetate filters. After filtration, all samples were acidified to pH = ~2 using distilled concentrated HCl (for precise laboratory-based concentration measurements of Hf and Nd, 2 L aliquots of the filtered and acidified samples were kept separately in clean PE-bottles). Then about 0.5 ml pre-cleaned Fe-chloride solution (~200 mg Fe per ml) waere added to each cubitainer. After equilibration for about 6-12 hours, suprapure ammonia solution (25%) was added to adjust the pH of the filtered seawater to 8~9. In this way, Nd, Hf and other trace metals co-precipitated with FeOOH for about 1~2 days. After settling of the precipitate the supernatant was siphoned off and discarded while the FeOOH precipitate was transferred into the PE-bottles on board. To further reduce the amount of major elements (e.g., Mg and other cations), the precipitates for the isotope measurement were redissolved in the laboratory and reprecipitated at lower pH (7.0 - 8.0) prior to purification and separation of Nd and Hf.

Two river water samples were taken from the Kalix river, Sweden, in June 2012 and the Schwentine river, Germany in July 2012, respectively. Both samples were very rich in particles. While the Schwentine river sample was filtered immediately, the filtration of Kalix river water was delayed for about two months until the sample reached the laboratory in Kiel. After filtration, the procedure was identical to the treatment of the

seawater samples. However, probably due to the very high amount of dissolved organic matter of both rivers, the precipitation did not happen at a pH of 7.0-8.0, even after waiting for one week. The pH was then adjusted to about 9.0 by adding ammonia solution and 10 ml of suprapure hydrogen peroxide (30%) were added to facilitate co-precipitation. The co-precipitation of the river water samples thus took about 2 weeks.

2.1.2 Chemical procedures prior to ion chromatographic purification of the samples

To further reduce the amount of major elements (e.g., Mg), the precipitates of the seawater samples for the isotope measurement were re-dissolved by adding HCl (the pH was adjusted to about 2) and put into the oven at a temperature of 40~50 ℃ for about 1 hour. After the precipitate had dissolved, the co-precipitation was repeated at lower pH (7.0 - 8.0). The precipitates were then centrifuged and rinsed with Milli-Q water three times, and finally transferred into 60 ml teflon vials using 3 ml 6 M HCl. After drying, the samples were refluxed with 8 ml of aqua regia at 120 ℃ overnight in order to oxidize the organics. Then the samples were dried again and transferred into Cl$^-$ using 10 ml 6 M HCl. Due to the large amounts of Fe contained in the samples, a back-extraction method to seperate the Fe (see details in Stichel, 2010) was applied to avoid overloading the columns. For our samples, 5 ml × 3 times of pre-cleaned diethylether were added to the samples and the Fe was extracted from the acid phase, in which Nd and Hf remained.

Even after the the aqua regia step the samples still contained notable amounts of organics. Thus the sample was treated with 1 ml H_2O_2 (30%) and left for one day to oxidize the remaining organics. Then the samples were dried and refluxed in 2 ml 6 M HCl. After centrifugation, any jelly-like residues were separated from the supernatant. The residues were then dissolved in 2 M HF. Subsequently, the 2 M HF solutions were dried at 120 ℃ in order to remove of the excess silica in the residues. Afterwards, the residues were refluxed and recombined with the supernatant, which was then evaporated to dryness again to be taken up in the loading solutions for cation column chemistry.

2.1.3 Isotope dilution measurements of concentrations and blanks

For Hf and Nd concentration analyses, about 500 g of water was taken from the 2 L aliquot samples and weighed. Pre-weighed ^{178}Hf single spike and ^{150}Nd spike solutions were added to each sample and the blanks (e.g., Rickli et al., 2009). After 4 – 5 days of isotopic equilibration, the samples were co-precipitated with Fe-hydroxide at pH 7 to 8. Normally the co-precipitation only took 2 to 3 days, while the samples were shaken once after the first 24 hours of co-precipitation. After the samples were ready (when the water turned clear in color and the brownish precipitate settled at the bottom of the bottles). The precipitates were then transferred into 7 ml teflon vials and were treated with aqua regia to be evaporated to dryness. The samples were then refluxed with 6 M HCl to transfer them into Cl$^-$. Finally they were dried down and re-dissolved in the loading solutions for cation column chemistry.

2.2 Sediment and dust deposits

2.2.1 Sediment cores

Four sediment cores from the Arctic and Southern Ocean have been investigated for Hf-Nd isotope compositions. The signatures of past seawater and of the detrital fraction were extracted covering the late Cenozoic and Late Quaternary, respectively.

Arctic Cores

The Late Quaternary samples of the central Arctic Ocean were obtained from combined box/kastenlot core PS2185-6 (87° 31.9' N; 144° 22.9' E; 1,051 m water depth, recovered during RV Polarstern Cruise ARCTIC'91) with a total length of 7.7m from the Lomonosov Ridge. X-ray photographs support that the sediments were deposited continuously throughout the core (Spielhagen et al., 1997). The age model of PS2185 was mainly constrained by magnetostratigraphy as well as a few ^{14}C data (Spielhagen et al., 1997). The sediment composition of PS2185-6 is dominated by terrigenous silty clays with four distinct sandy layers almost barren of planktic foraminifera.

Integrated Ocean Drilling Program (IODP) Leg 302 (a composite record of holes M0002A and M0004A, 87°5' N, 137° 0' E; 1,250 m water depth, recovered during the "ACEX" expedition in 2004) was obtained near the site of core PS2185-6. The total length of the drilled cores reached 339.1 m with 68% recovery. Among the drilled sites (Backman et al., 2005), Hole M0002A yielded a somewhat higher recovery of 78.5% between the surface and 272 mbsf (middle Eocene) and thus was used for this study. This depth interval is mainly composed of soft terrigenous silty clays with occasional occurrences of biogenic carbonates in the upper 15–18 m.

In addition, a number of core-top sediments mainly consisting of terrigenous detrital silts (obtained during RV Polarstern ARCTIC'91 and during a Kara Sea cruise with RV Akademik Boris Petrov in 1997) were also investigated.

Southern Ocean sediment cores

Core PS2082-1 (gravity core, 43°13.21' S, 11° 44.30' E, water depth 4610 m, recovered during RV Polarstern Cruise ANT IX-4) was recovered in the Agulhas Basin in the subantarctic zone of the Southern Ocean. Calcareous mud layers (with occationally more than 60% of carbonate) representing interglacial periods alternate with diatomaceous muds (c.f., Frank, 1996). Core PS1388-3 (gravity core, 69°2.0' S, 5° 55.0' W, water depth 2526 m, recovered during RV Polarstern Cruise ANT-IV/3) was recovered on the mid-slope of the Antarctic continent of the eastern Weddell Sea. This core is mainly composed of detrital silts and sands, with small to negligible amounts of biogenic carbonates, except during MIS 5 and 7 over the last 250 ky (up to 12% of carbonate, Grobe and Mackensen, 1992).

2.2.2 Asian dust samples

All the loess and desert samples were collected by the Institute of Surficial Geochemistry at Nanjing University. The samples are from different tectonic environment with distinctly different radiogenic isotope compositions (Chen et al., 2007). The particle sizes of Chinese loess are mostly less than 75 µm, while Asian dust deposited in the North Pacific is characterized by an even smaller grain size, usually less than 5 µm. For

consistency, the desert and loess samples were divided into two size groups: <5 μm and <75 μm applying the method described in Chen et al. (2007).

2.2.3 Leaching and total dissolution procedures of different fractions of the marine and terrestrial sediments

Approximately two grams of bulk sediment per sample were used for the leaching and extracting Nd and Hf from Fe-Mn hydroxide fractions of marine sediments and Asian dust samples and similar procedures were applied:

(a) Decarbonation

In order to remove the often abundant detrital carbonates contained in the dust samples, they were treated with 0.5 M acetic acid for 8 hours at room temperature and were then centrifuged (Chen et al., 2007). Some of the marine sediment samples were also decarbonated before leaching in order to compare the isotopic results to those obtained using the non-decarbonated leachates. These samples were decarbonated with 7 M acetic acid (buffered to pH = 4 with sodium acetate; 25 ml×2 times) for a day on a shaker.

(b) Leaching

After washing samples three times with de-ionized (Milli-Q) water, Nd and Hf contained in the Fe-Mn oxyhydroxide fraction were extracted by leaching for about one hour in a single step using 25 ml of a dilute reducing and complexing solution consisting of 0.005 M hydroxylamine hydrochloride, 1.5% acetic acid, and 0.03 M EDTA-2Na, buffered to pH = 4 with suprapure NaOH.

To keep the extracted Hf in solution, 0.03M Na-EDTA were added to the leaching solution for complexing the Hf following Gutjahr (2006), which yielded 50-100 ng of authigenic, seawater derived Hf per gram of carbonate barren sediments from the central Arctic, and 10-25 ng per gram of carbonate-rich sediments from the Southern Ocean.

(c) Total dissolution

The above sediment samples were leached again with a stronger leaching solution (0.05 M hydroxylamine hydrochloride, 15% acetic acid, 0.05 M Na-EDTA), in order to completely remove the remaining authigenic Fe-Mn hydroxides. Then the samples were dried and ground carefully to homogenize the material and 100 mg sediment per sample was totally dissolved for isotope measurement (Table 2.1). These samples were first treated with 12 ml 5% H_2O_2 at room temperature over the weekend to preliminarily oxidize organics, and then dried down. Afterwards 4 ml of aqua regia was added to further oxidize the organics. After evaporation to dryness, the mixed acids of HF, HNO_3, and $HClO_4$ were added to remove Si (in the form of SF_4 vapor) and organics, as well as destroy the heavy minerals, following the steps given in Table 2.1. Since zircon is very resistant to dissolution, bomb dissolution is necessary to completely dissolve zircon. Thus the samples were further dissolved in bombs at 190-200°C for 4 days. After the high pressure dissolution, normally there would be white precipitates at the bottom of the vials, presumably being the calcium fluorides (which were destroyed by adding 1 ml perchloric acid and 2 ml concentrated HNO_3 to each sample). Subsequently, the samples need to be dried down at relatively high temperature (190°C) overnight to fully remove the perchloric acid (until no white fume can be seen). After all the above-mentioned steps, the samples should be easily dissolved in 1 ml mixed acid of 1 M HCl and 0.05 M HF.

Table 2.1 the procedure for total dissolution of detrital marine sediments (modified after Bayon et al., 2002).

Step	Remark
2 ml H_2O_2 (30%), 10 ml MQ, room temperature loose lids, over weekend dry down at 100°C	oxidize organics
3 ml conc. HCl, 1ml conc. HNO_3 (aqua regia) close vials, at 140°C overnight dry down at 140°C	oxidize organics
1ml conc. HNO_3, 2ml conc. HF close vials, at 140° overnight dry down at 140°	dissolve silicate remove Si
2 ml conc. HNO_3, 1 ml conc. HF, 0.5 ml $HClO_4$	dissolve refractory minerals and organics

dry down at 180-190°C overnight	
2 ml conc. HNO$_3$, 4ml conc. HF	
to high pressure digestion at 190-200°C for	
4 days	dissolve refractory minerals
dry down at 140°C	
1 ml perchloric acid +2 ml HNO$_3$ conc	destroy fluorides
dry down at 180-190°C	remove perchloric acid
2 ml conc. HNO$_3$	
dry down at 180-190°C	remove perchloric acid
0.5 ml conc. HNO$_3$	
dry down at 180-190°C	remove perchloric acid
1 ml conc. HCl	change to Cl$^-$ form
dry down at 100°C	
reflux overnight with loading solution	

2.2.4 Foraminifera samples

Recent studies suggest that authigenic Fe-Mn hydroxide coatings of foraminifera are a more reliable archive to record past bottom water Nd isotope signatures (Elmore et al., 2011). In order to compare the results of Nd isotopes extracted from bulk sediment leachates and foraminifera samples, foraminifera were picked for Nd isotope analysis.

The bulk sediment samples were first freeze dried and the fine minerals (<64 μm) were then thoroughly washed out through a sieve. After drying the samples, they were further sieved into different size groups (64-150 μm, 150-250 μm, 250-355 μm, > 355 μm). Then about 100 mg of mixed planktic and benthic foraminifera were carefully picked, crushed between two glass slides whilst viewed through a microscope, and then transferred into 15 ml centrifuge tubes for subsequent cleaning processes (Vance and Burton, 1999):

(a) Removal of fine clay particles

About 10 ml MilliQ water were added to the foraminifera, and were ultrasonicated for one minute. Afterwards the suspended particles were pipetted out. This step was repeated twice and then repeated again with methanol. The samples were washed again with MilliQ water until the water containing the calcite shells was clear (i.e., no more clay attached to the foram shells).

Some of the samples did not go through the redox cleaning procedures and were dissolved in about 0.3 M HNO_3 overnight, in order to compare the results of redox cleaned and non-redox cleaned foraminifera samples.

(b) Reductive cleaning to remove Fe-Mn oxyhydroxide coatings from the foraminifera

The reducing solution consists of 2.4 ml part 100% aqueous hydrazine, 30 ml 30% ammonia, 18 ml citric acid. About 10 ml of reducing solution was added to each sample and was then kept in a water bath at 80° for 30 minutes. For every 2 minutes (starting after 5 minutes) the samples were put in an ultrasonic bath for about 10-15 seconds. Finally the samples were rinsed with MQ water.

(c) Oxidative removal of organic material

The oxidizing solution contains 99 parts 0.2 M NaOH and 1 part 30% H_2O_2. About 10 ml of oxidizing solution was added to each sample and kept in a water bath at 80° for 30 minutes. Every 10 minutes, the samples were put in an ultrasonic bath for about 30 seconds and were finally rinsed with MQ water.

The foraminifera samples were then dissolved in diluted HNO_3 overnight.

2.3 Column Chemistry

The cation exchange resin AG 50W-X8 is used to separate High Field Strength Elements (HFSEs) from REEs. It has a capacity of 1.7 meq/ml of resin. For reference, seawater has high ion contents with a concentration of about 605 meq/ liter (salinity 35). This is very large compared to the ion exchange capacity of AG 50W-X8 resin. The processes of ion-exchange are as follow:

$$x RSO_3^- H^+ + M^{x+} \rightleftharpoons (RSO_3^-)_x M^{x+} + xH^+$$

resin   solution   resin   solution
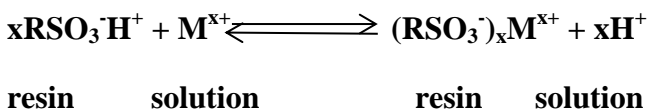
The sulfonic acid groups (—SO3-H+) which are attached to the polymeric matrix will release protons while trace metals are absorbed during the elution processes. Since different trace metals have different exchange coefficients with the resin under different pH, it is possible to separate trace metals by acid elution.

For example, Hf has very low affinity to the AG 50WX8 resin and can be directly eluted out when loading the samples. This contrasts with REEs which have higher affinity to the resin and need to be eluted out using 6M HNO_3. Table 2.2 shows the detailed procedure to separate REEs and HFSEs. The Nd and Hf cuts were further separated with Ln-spec resin. Table 2.3 and 2.4 shows the procedure to purify Nd from other REEs for leachates/detrital fractions and foraminifera samples, respectively (after Pin and Zalduegui, 1997). Table 2.5 shows the procedure to further separate Hf from the matrix (after Münker et al., 2001).

Table 2.2 AG50W-X8 (1.4ml, 200-400μm) column chemistry

volume	acid	stage
8 ml	6M HNO_3 / 0.5M HF	pre-clean
2×1ml	MQ	change acid
0.5ml	1M HCl / 0.05M HF	pre-clean
1ml	1M HCl / 0.05M HF	pre-condition
0.5ml	1M HCl / 0.05M HF	load and collect Hf
2 ml	1M HCl / 0.05M HF	collect Hf
5ml	3M HCl	elute Fe
2×1ml	MQ	change acid
12ml	2M HNO_3	elute Ba
6ml	6M HNO_3	collect Ac/REE
6ml	6M HNO_3 / 0.5M HF	clean
1ml	MQ	pass and store

Table 2.3 Eichrom®LN-Spec (2ml, 50-100μm) column chemistry for leachate and seawater samples

volume	acid	stage
8 ml	6M HCl	pre-clean
0.5 ml	0.1M HCl	pre-condition
1 ml	0.1M HCl	pre-condition

volume	acid	stage
0.5 ml	0.1M HCl	load sample
0.5 ml	0.1M HCl	wash-in/elute Ba
7.5 ml	0.25M HCl	elute LREE
5 ml	0.25M HCl	collect Nd
8 ml	6M HCl	Clean
1+1 ml	0.3M HCl	pass and store

Table 2.4 Eichrom®LN-Spec (~3.14 ml, 50-100um) column chemistry for foraminifera samples

volume	acid	stage
8 ml	6M HCl	pre-clean
0.5 ml	0.1M HCl	pre-condition
1 ml	0.1M HCl	pre-condition
0.5 ml	0.1M HCl	load sample
0.5 ml	0.1M HCl	wash-in
10 ml	0.25M HCl	elute LREE
2 ml	0.3M HCl	elute
6 ml	0.3M HCl	collect Nd
8 ml	6M HCl	clean
1 + 1 ml	0.3M HCl	pass and store

Table 2.5 Eichrom®LN-Spec (1ml, 100-150μm) for leachate and seawater samples

volume	acid	stage
15ml	6M HCl	pre-clean
15ml	2M HF	pre-clean
2ml	MQ	wash HF
2×3ml	3M HCl	pre-condition
4ml+0.8ml	3M HCl + 0.4M ascorbic acid[a]	load
50ml	6M HCl	elute matrix, REE
2×3ml	MQ	change acid
30ml	0.45M HNO3/0.09M Citric/1wt% H_2O_2[a]	elute Ti, W
2×3ml	MQ	change acid
5ml	2M HCl / 0.1M HF	elute Zr
6ml	3M HCl / 0.2M HF	collect Hf
25ml	6M HCl	clean
25ml	2M HF	clean

| 2×3ml | 1M HCl | pass and store |

a. ascorbic acid and H_2O_2 should be added on the day of column chemistry.

2.4 Mass spectrometry

All the isotope measurements were performed on a Nu Plasma HR MC-ICP-MS at GEOAR, Kiel at low mass resolution in static mode. Gain calibration for the Faraday cup efficiency was carried out on a daily basis. Samples which were introduced into the mass spectrometer were dissolved in 2% (v/v) HNO_3 for Nd isotopes and 0.5 M HNO3/ 0.1 M HF for Hf isotopes. Except for the isotope spiked samples, the concentrations of all purified samples were tested, and required sample amounts were calculated accordingly to get similar beam for both the samples and the standards during the later isotope batch run.

2.4.1 Isotope dilution

In the GEOMAR laboratory Sm-Nd and Hf spikes (Table 2.6) enriched in ^{149}Sm, ^{150}Nd and ^{178}Hf, respectively, are used for the determination of seawater Nd and Hf concentrations. The principle, error estimation and calculations of the isotope dilution method have been presented in details in Stichel 2010 (see also Heumann, 1992 for a review). Briefly, the Nd and Hf masses in the samples were calculated using the following equations, respectively:

$Nd\_mass_{sample} = (mass_{SPIKEsolution} \times conc_{SPIKEsolution} \times NdMass_{sample}/NdMass_{spike}) \times [^{150}Nd_{spike} - R_{mix} \times {}^{144}Nd_{spike}/(R_{mix} \times {}^{144}Nd_{natural} - {}^{150}Nd_{natural})]$;

$Hf\_mass_{sample} = (mass_{SPIKEsolution} \times conc_{SPIKEsolution} \times HfMass_{sample}/HfMass_{spike}) \times [^{179}Hf_{spike} - R_{mix} \times {}^{178}Hf_{spike}/(R_{mix} \times {}^{178}Hf_{natural} - {}^{179}Hf_{natural})]$

$NdMass_{sample}$ and $NdMass_{spike}$ are the atomic weights of Nd in the sample (without spiking) and the spike solution, respectively. $HfMass_{sample}$ and $HfMass_{spike}$ are the atomic weights of Hf in the sample (without spike) and the spike solution, respectively. R_{mix} is

the measured abundance ratio of spiked isotope (m_1) and one stable/long-lived isotope (m_2) in the spiked samples.

An important concept of the isotope dilution technique is the optimum abundance ratio (R_{opt}). R_{opt} is reached when $R_{mix} = (R_n \times R_s)^{0.5}$, while R_n is m_1/m_2 of the natural unspiked sample and R_s is m_1/m_2 of the spike solution. With known R_n and R_s, it is possible to calculate the optimum ratio. For example, R_s ($^{150}Nd/^{144}Nd$) in our lab is 199.6356 while R_n ($^{150}Nd/^{144}Nd$) of natural samples is 0.235837, resulting in R_{opt} of $(199.6356 \times 0.235837)^{0.5} = 6.86$. Similarly, for Hf, the R_{opt} ($^{178}Hf/^{179}Hf$) with the spike solution in our lab is 10.16. See Table 2.6 for information of the spike solution.

Table 2.6 The compositions of Sm-Nd and Hf spike.

Sm mass	conc. Spike (ug/g)	abund. Spike (%)	abund. Natural (%)
146.91489	0.0022522	0.38%	14.99%
148.91718	**0.5948497**	**99.23%**	**13.82%**
151.91973	0.0023946	0.39%	26.75%

		unit
conc. Nd spike stock solution	1.967183212	ug/g
conc. Nd spike diluted for use	**0.015853843**	ug/g
av. Nd atomic mass (spike)	**149.8063725**	amu
av. Nd atomic mass (natural)	**144.2825186**	amu

Nd mass	conc. Spike (ug/g)	abund. Spike (%)	abund. Natural (%)
141.90773	0.007559033	0.41	27.16
142.90982	0.004526674	0.24	12.18
143.9101	**0.009261732**	**0.49**	**23.86**
144.91258	0.004079658	0.21	8.3
145.91313	0.008362157	0.44	17.17
147.9169	0.007195243	0.37	5.74
149.9209	**1.926198715**	**97.84**	**5.62**

		unit

33

	Hf mass	conc. Spike (ug/g)	abund. Spike (%)	abund. Natural (%)
conc. Hf spike stock solution	33.71529944	pg/g		
conc. Hf spike diluted for use	**33.71529944**	pg/g		
av. Hf atomic mass (spike)	**177.9453182**	amu		
av. Hf atomic mass (natural)	**178.4851349**	amu		

Hf mass	conc. Spike (ug/g)	abund. Spike (%)	abund. Natural (%)
173.94007	0	0	0.16
175.94142	0.00073472	0	5.26
176.94323	0.51726392	1.54	18.6
177.94371	**32.0298678**	**94.9**	**27.28**
178.94583	**0.62502604**	**1.84**	**13.62**
179.94656	0.57728083	1.69	35.08

For all Sm-Nd isotopes in the spiked samples (Table 2.7), there are no known ratios between each of these isotopes. Thus the initial exponential fractionation must be guessed. Iterations are then carried out until the exponential fractionation factor meets certain condition (Table 2.8). For Hf spike (Table 2.9), the calculation is much simpler. There is no mass interference on ^{179}Hf and ^{177}Hf. The fractionation factor is determined by measuring ^{182}W/^{183}W. Thus ^{179}Hf/^{177}Hf in the spiked sample could be easily known.

Table 2.7 Cup configuration for Nd concentration measurements using the isotope dilution technique.

H5	H4	H3	H2	H1	Ax	L1	L2	L3	L4	L5
^{152}Nd	^{150}Nd		^{148}Nd		^{146}Nd	^{145}Nd	^{144}Nd	^{142}Nd	^{140}Ce	^{138}Ba
^{152}Sm	^{150}Sm	^{149}Sm	^{148}Sm	^{147}Sm			^{144}Sm			

Table 2.8 The procedure to calculate the exact ^{150}Nd/^{144}Nd ratio in the spiked sample.

(mixture: spiked sample; sample: sample before spiking; spike: the spike solution)

step	calculated quantities (mass fractionation corrected)	
1	assume an initial exponential fractionation factor (β_0)	
2	(^{147}Sm/^{149}Sm)$_{mixture}$	from 1

2'	^{149}Beam/^{150}Beam	from 1
2"	^{146}Beam/^{150}Beam	from 1
2'''	^{149}Beam/^{144}Beam	from 1
2''''	^{150}Beam/^{144}Beam	from 1
3	$(^{149}$Sm$)_{sample}$/$(^{149}$Sm$)_{spike}$	from 2
4	$(^{150}$Sm/^{149}Sm$)_{mixture}$	from 2' 3
5	$(^{146}$Nd/^{150}Nd$)_{mixture}$	from 4, 2"
6	$(^{146}$Nd$)_{sample}$/$(^{150}$Nd$)_{spike}$	from 5
7	$(^{146}$Nd/^{145}Nd$)_{mixture}$	from 6
8	calculate exponential fractionation factor (β)	from 7
9	iteration from 1 to 8 until Abs(β-β$_0$) is sufficiently small	
10	$(^{148}$Sm$)_{sample}$/$(^{149}$Sm$)_{spike}$	from 3
11	$(^{148}$Sm/^{149}Sm$)_{mixture}$	from 10, 3
12	$(^{148}$Sm$)_{mixture}$/$(^{144}$Beam$)$	from 2''', 11
13	$(^{144}$Sm$)_{mixture}$/$(^{144}$Beam$)$	similar to 10-12
14	$(^{150}$Sm$)_{mixture}$/$(^{144}$Beam$)$	similar to 10-12
15	$(^{150}$Nd/^{144}Nd$)_{mixture}$	from 2'''', 13, 14

For 15: $(^{150}$Nd/^{144}Nd$)_{mixture}$ = [^{150}Beam/^{144}Beam - $(^{150}$Sm$)_{mixture}$/$(^{144}$Beam$)$] / [1 - $(^{144}$Sm$)_{mixture}$/$(^{144}$Beam$)$]

Table 2.9 Cup configuration for Hf concentration measurements using isotope dilution technique.

H5	H4	H3	H2	H1	Ax	L1	L2	L3	L4	L5
	^{183}W	^{182}W			^{179}Hf	^{178}Hf	^{177}Hf			

2.4.2 Isotope composition measurement

Table 2.10 Cup configuration for Nd isotope measurements.

H5	H4	H3	H2	H1	Ax	L1	L2	L3	L4	L5
^{150}Nd	^{148}Nd		^{146}Nd	^{145}Nd	^{144}Nd	^{143}Nd	^{142}Nd			
^{150}Sm	^{148}Sm	^{147}Sm			^{144}Sm		^{142}Ce	^{140}Ce	^{138}Ba	

To monitor the external reproducibility and system drift, generally 3 to 5 samples were bracketed by analyses of the standards with beam intensities similar to the samples.

The cup configuration for Nd isotope measurements is displayed in Table 2.10. The calculation first subtracts ^{144}Sm beam from 144beam (so ^{144}Nd beam is known), and then applies a mass fractionation law using ^{146}Nd/^{144}Nd = 0.7219 to calculate ^{143}Nd/^{144}Nd. The reliability of this method critically depends on the amount of Sm present in the sample, since ^{144}Sm beam is only roughly calculated from ^{147}Sm beam without applying a mass fractionation law. ^{138}Ba is monitored as an index of the matrix. For example, the presence of ^{130}Ba^{16}O could interfere with the beam of ^{146}Nd, which will then affect the mass fractionation calculation.

Our method above only applies a rough correction for ^{147}Sm and therefore it is important to keep in mind that Sm/Nd in the purified sample should be as small as possible to reduce the mass interference. JNdi-1 and an internal laboratory standard (SPEX) were measured as standards for Nd isotopes sessions. ^{143}Nd/^{144}Nd results were normalized to JNdi-1 = 0.512115 (Tanaka et al., 2000).

Table 2.11 Cup configuration for Hf isotope measurements.

H5	H4	H3	H2	H1	Ax	L1	L2	L3	L4	L5
	^{180}Hf	^{179}Hf	^{178}Hf	^{177}Hf	^{176}Hf	^{175}Lu	^{174}Hf			
^{182}W	^{180}W				^{176}Yb		^{174}Yb	^{172}Yb		

The cup configuration for Hf isotope measurements is displayed in Table 2.11. The mass fractionation was calculated using ^{179}Hf/^{177}Hf = 0.7325. The ^{176}Yb beam is calculated from ^{172}Yb beam applying the mass fractionation law. Some seawater samples still contained a considerable amount of Yb, which cannot be adequately corrected by applying the exponential mass fractionation factor derived from ^{179}Hf/^{177}Hf and the commonly accepted Yb isotope ratios (Chu et al., 2002). Therefore, we adopted a Yb-doped JMC475 standard calibration method for all of the seawater samples, in order to precisely correct for the Yb contribution (Stichel et al., 2012). Given that the changes of the Hf isotope compositions of the differently doped JMC475 standards were linearly correlated with the Yb contribution, this additional correction method is considered to

provide reliable results. JMC 475 and an internal laboratory standard solution (CertiPUR) were measured as standards for Hf isotopes. ^{176}Hf/^{177}Hf results were normalized to JMC475 = 0.282160 (Nowell et al., 1998).

The precision of the measurements, blank, and standard reproducibility will be reported separately in the following chapters.

References

Backman, J., Moran, K., McInroy, D., and the IODP Expedition 302 Scientists. (2005) IODP Expedition 302, Arctic Coring Expedition (ACEX): A First Look at the Cenozoic Paleoceanography of the Central Arctic Ocean. *Scientific Drilling* **1**, 12-17.

Bayon, G., German, C. R., Boella, R. M., Milton, J. A., Taylor, R. N., and Nesbitt, R. W. (2002) An improved method for extracting marine sediment fractions and its application to Sr and Nd isotopic analysis. *Chemical Geology* **187**, 179-199.

Chen, J., Li, G. J., Yang, J. D., Rao, W. B., Lu, H. Y., Balsam, W., Sun, Y. B., and Ji, J. F. (2007) Nd and Sr isotopic characteristics of Chinese deserts: Implications for the provenances of Asian dust. *Geochimica et Cosmochimica Acta* **71**, 3904-3914.

Chu, N.-C., Taylor, R. N., Chavagnac, V., Nesbitt, R. W., Boella, R. M., Milton, J. A., German, C. R., Bayon, G., and Burton, K. (2002) Hf isotope ratio analysis using multi-collector inductively coupled plasma mass spectrometry: an evaluation of isobaric interference corrections. *J Anal Atom Spectrom* **17**, 1567-1574.

Frank, M. (1996) Reconstruction of Late Quaternary environmental conditions applying the natural radionuclides [23]Th, ^{10}Be, [231]Pa and [23]U: A study of deep-sea sediments from the eastern sector of the Antarctic Circumpolar Current System. Berichete zur Polarforschung. 186.

Grobe, H, Mackensen, A (1992): Sedimentology of core PS1388-3. doi:10.1594/PANGAEA.51609.

Heumann, K. G. (1992) Isotope dilution mass spectrometry (IDMS) of the elements. *Mass Spectrometry Reviews* **11**, 41-67.

Münker, C., Weyer, S., Scherer, E., and Mezger, K. (2001) Separation of high field strength elements (Nb, Ta, Zr, Hf) and Lu from rock samples for MC-ICPMS measurements. *Geochemistry Geophysics Geosystems* **2**, doi: 10.1029/2001GC000183.

Nowell, G. M., Kempton, P. D., Noble, S. R., Fitton, J. G., Saunders, A. D., Mahoney, J. J., and Taylor, R. N. (1998) High precision Hf isotope measurements of MORB and OIB by thermal ionisation mass spectrometry: insights into the depleted mantle. *Chemical Geology* **149**, 211-233.

Pin, C. and Zalduegui, J. F. S. (1997) Sequential separation of light rare-earth elements, thorium and uranium by miniaturized extraction chromatography: Application to isotopic analyses of silicate rocks. *Anal Chim Acta* **339**, 79-89.

Rickli, J., Frank, M., and Halliday, A. N. (2009) The hafnium-neodymium isotopic composition of Atlantic seawater. *Earth and Planetary Science Letters* **280**, 118-127.

Spielhagen, R. F., Bonani, G., Eisenhauer, A., Frank, M., Frederichs, T., Kassens, H., Kubik, P. W., Mangini, A., NorgaardPedersen, N., Nowaczyk, N. R., Schaper, S., Stein, R., Thiede, J., Tiedemann, R., and Wahsner, M. (1997) Arctic Ocean evidence for late Quaternary initiation of northern Eurasian ice sheets. *Geology* **25**, 783-786.

Stichel, T. (2010) Tracing water masses and continental weathering by neodymium and hafnium isotopes in the Atlantic sector of the Southern Ocean, University of Kiel.

Tanaka, T., Togashi, S., Kamioka, H., Amakawa, H., Kagami, H., Hamamoto, T., Yuhara, M., Orihashi, Y., Yoneda, S., Shimizu, H., Kunimaru, T., Takahashi, K., Yanagi, T., Nakano, T., Fujimaki, H., Shinjo, R., Asahara, Y., Tanimizu, M., and Dragusanu, C. (2000) JNdi-1: a neodymium isotopic reference in consistency with LaJolla neodymium. *Chemical Geology* **168**, 279-281.

Vance, D. and Burton, K. (1999) Neodymium isotopes in planktonic foraminifera: a record of the response of continental weathering and ocean circulation rates to climate change. *Earth and Planetary Science Letters* **173**, 365-379.

Chapter 3

Upper ocean vertical supply: a neglected primary factor controlling the distribution of neodymium concentrations of open ocean surface waters?

Abstract

Neodymium (Nd) isotopes are an important geochemical tool to trace the present and past water mass mixing as well as continental inputs. The distribution of Nd concentrations in open ocean surface waters (0-100 m) is generally assumed to be controlled by lateral mixing of Nd from coastal surface currents and by removal through reversible particle scavenging. However, using [228]Ra activity as an indicator of coastal water mass influence, surface water Nd concentration data available on key oceanic transects as a whole do not support the above scenario. From a global compilation of available data, we find that more stratified regions are generally associated with low surface Nd concentrations. This implies that upper ocean vertical supply may be an as yet neglected primary factor in determining the basin scale variations of surface water Nd concentrations. Similar to the mechanism of nutrients supply, it is likely that stratification inhibits vertical supply of Nd from the subsurface thermocline waters and thus the magnitude of Nd flux to the surface layer. Consistently, the estimated required input flux of Nd to the surface layer to maintain the observed concentrations could be nearly two orders of magnitudes larger than riverine/dust flux, and also larger than the model-based estimation on shelf-derived coastal flux. In addition, preliminary results from modeling experiments reveal that the input from shallow boundary sources, riverine input, and release from dust are actually not the primary factors controlling Nd concentrations most notably in the Pacific and Southern Ocean surface waters.

3.1 Introduction

The quasi-conservative isotopic composition of the rare earth element (REE) Nd in seawater is being widely used as a powerful tracer for modern and past water-mass mixing, as well as for continental inputs [e.g., von Blanckenburg 1999; Goldstein et al., 2003; Peucker-Ehrenbrink et al., 2010]. Although considerable efforts and progress have been made in the understanding of the modern marine Nd cycle in recent years [e.g., Lacan and Jeandel, 2005; Arsouze et al., 2007, 2009, Siddall et al., 2008; Andersson et al., 2008; Porcelli et al., 2009; Oka et al., 2009; Amakawa et al., 2009; Rickli et al., 2010; Rempfer et al., 2011; Carter et al., 2012; Grasse et al., 2012; Stichel et al., 2012; Singh et

al., 2012; Grenier et al., 2013], some important issues, such as the nature and magnitude of Nd sources and the scavenging behavior of Nd by different particle-types, remain unresolved. In addition, although both Nd-concentrations and Nd isotopic composition have recently been simulated in reasonable agreement with observations using three dimensional ocean models, Nd concentrations at shallow depths of the open ocean are underestimated by these models [Arsouze et al., 2009; Rempfer et al., 2011]. The limited understanding of the Nd cycle at the ocean surface in turn complicates the reliable use of the Nd isotopic composition (ε_{Nd}) as a (paleo)circulation proxy [e.g., Rempfer et al., 2012a, b].

With recent geochemical studies on Nd along important oceanic transects such as in the Southern Ocean (in particular south of 30°S as proposed by Lacan et al. [2012]), a more complete picture of the basin scale variations of surface Nd concentrations has now become available for the first time. Based on these global distributions compiled in our study, we aim to evaluate the role of different factors that control variations of Nd concentration in open ocean surface waters (0-100 m, with bottom depth >500 m).

Neodymium concentrations in the surface ocean (0-100 m) are highly variable, with reported data ranging from 2.72 to 101.5 pmol/kg [Lacan et al., 2004; Zhang and Nozaki, 1996]. High values (>30 pmol/kg) are usually observed in oceanic regions close to continents such as in the Nordic seas [Lacan and Jeandel, 2004] and in the Mediterranean Sea [Tachikawa et al., 2004]. Input of Nd from rivers, release of Nd from shelf sediments, as well as dissolution of Nd from dust have been shown to be important sources and input pathways to surface waters, particularly at the ocean margins [e.g., Tachikawa et al., 2004; Porcelli et al., 2009; Rickli et al., 2010; Singh et al., 2012]. These areas, however, only account for a small fraction of the total surface area of the global ocean.

In general and independent of the location, Nd is ultimately and exclusively derived from continental inputs. Its sources include riverine inputs, dissolution of eolian dust, and the flux across the sediment water interface [e.g., Lacan and Jeandel., 2005; Arsouze et al., 2007, 2009, Rempfer et al., 2011, Wilson et al., 2012; Grenier et al., 2013]. The vertical distribution of Nd in the water column is characterized by reversible scavenging by

particles [c.f., Siddall et al., 2008; Oka et al., 2009]. Surface water Nd concentrations are therefore expected to be partly controlled by the intensity of particle scavenging. Open ocean surface water Nd concentrations have been considered to primarily reflect coastal supplies and contributions from atmospheric dust and subsequent mixing processes via surface currents coupled with removal through particle scavenging [e.g., Bertram and Elderfield, 1993; Nozaki, 2001; Amakawa et al., 2000; Arsouze et al, 2009].

It is well known that the resupply of nutrients (e.g., iron, de Baar et al. [1995]) from subsurface to surface waters is the major mechanism to maintain productivity in open ocean surface waters [Sarmiento et al., 2004, Palter et al., 2010]. Processes contributing to the flux of nutrients to the euphotic zone are for example, diapycnal diffusion from the thermocline, Ekman pumping and upwelling [Williams and Follows, 1998], isopycnal perturbation by mesoscale eddies [McGillicuddy et al., 2007], and transport from the thermocline into the mixed layer during winter convection [Williams et al., 2006]. In this respect, Nd (and the REEs) and nutrients share some similarities. They are removed by biogenic particles and released at depth through particle dissolution and remineralization. Therefore it is likely that underlying mechanisms of exchange fluxes of Nd and nutrients between the subsurface and shallower depths are analogous.

In this study we argue that surface water Nd concentrations are influenced by all the above mentioned external and subsurface fluxes. In order to identify the most influential factor that drives the variations of surface water Nd concentrations, we will separately evaluate the potential influences of the fluxes mentioned above.

3.2 Methods

To estimate the potential influence of coastal advection versus scavenging, we refer to a well-established tracer for surface coastal water mass mixing. [228]Radium with a half-life of 5.75 years has been applied in many studies for tracing coastal supply and lateral mixing processes of the upper ocean [e.g., Kaufman et al., 1973; Nozaki et al., 1998; Nozaki et al., 1990]. [228]Radium mainly originates from the α-decay of [232]Th in estuarine, coastal, and shelf sediments, and is released into the water column via diffusion from

porewaters or submarine groundwaters [e.g., Moore, 1969]. It is then transported to the open ocean by lateral surface advection and mixing with an average decay residence time of about 8 years. Because of its radioactive decay along the transport path, it exhibits sharp gradients between the coast and the open ocean [e.g. Kaufman et al., 1973; Nozaki et al., 1990]. It is thus assumed that the surficial distribution of ^{228}Ra provides the actual pattern of coastal water mass influence on open ocean surface waters [e.g., Nozaki et al., 1990]. However, when ^{228}Ra has already decayed away, it cannot be a sensitive tracer for coastal water mass influence anymore. Fortunately, ^{228}Ra has a residence time (removed through radioactive decay) of about 8 years which is comparable with surface layer Nd scavenging residence time (1-4 years in the upper 100 m, [Amakawa et al., 2000; Rickli et al., 2010]). Consequently, if ^{228}Ra originating from coastal sources has decayed away, the Nd flux from the same coastal sources will have been removed by scavenging and the Nd concentrations will have been diminished to negligible levels in the surface layer.

Similar to nutrients, the vertical supply of Nd from subsurface water may also depend on upper ocean stratification. A measure of upper ocean stratification is the "buoyancy frequency" [e.g., Jenkins 2003] which is a function of fluid density and vertical density gradient. However, this approach needs complex data processing, and is beyond the scope of our study. Instead, for simplicity we tentatively use the potential density anomaly at the base of the euphotic layer (~200m, Figure 3.1) as an index of upper ocean stratification (200-1000 m, assuming 1000 m water depth is the lower boundary of the upper ocean mixing regime, e.g, Wunsch and Ferrari, 2004). Since the global oceans have more similar potential densities in the deep waters at a given water depth (e.g., 1000 m) than the surface layers, it is reasonable to assume that the lower the potential density anomaly near the surface layer, the larger the potential density range of the upper ocean (i.e., more stratified). A similar approach to define ocean stratification as potential density differences between the upper and lower boundaries of the studied waters can be found for example in Capotondi et al. [2012]. As an additional index for upper ocean stratification we introduce the potential density difference between 200 and 1000 m water depth ($\Delta\sigma_0$). $\Delta\sigma_0$ is thus a more direct measure of the density gradient in the upper ocean.

For example, a larger $\Delta\sigma_0$ would indicate higher potential density contrast in the upper ocean (200 to 1000 m water depth) and thus stronger stratification.

Our main assumption is that if a specific flux or mechanism cannot cause geographical variations of Nd concentration similar to what we observe in the ocean (Figure 3.1), it cannot be considered as a primary controlling factor. Besides, we will estimate the Nd fluxes to the surface waters required to achieve the observed concentrations to constrain our assumption. Finally, we will apply a three dimensional model approach [Rempfer et al., 2011, 2012b] to further test our arguments (see a brief description of the model in Supplementary Materials).
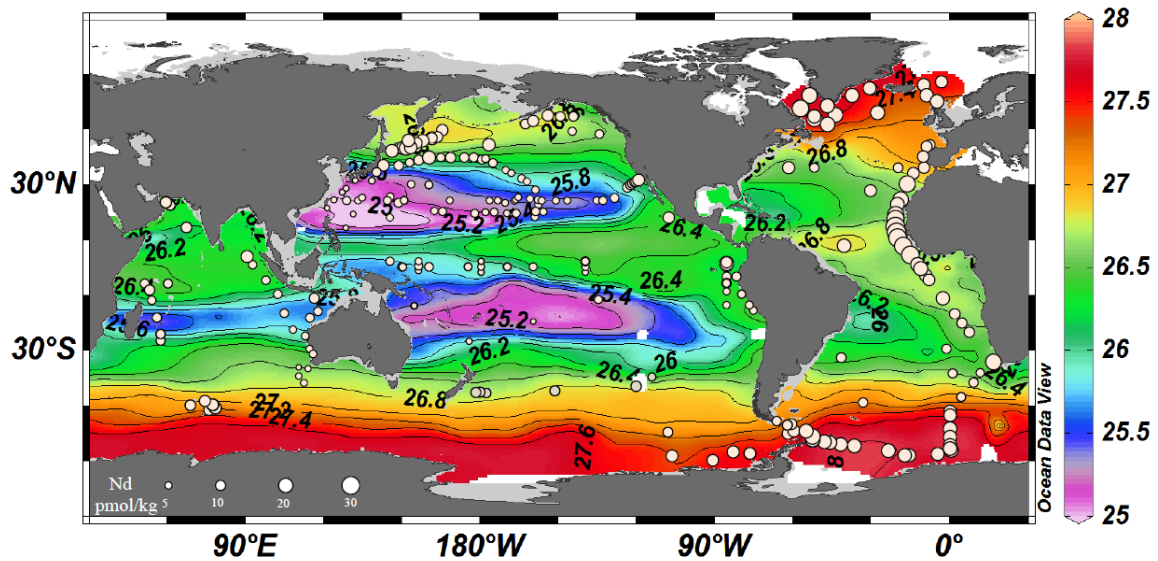
Figure 3.1 The distribution of Nd concentrations (circles) in the open ocean surface layer (shallower than 100m). Also shown for comparison is the potential density anomaly σ_0 (contours) at the water depth of 200 m. The semi-enclosed basins or marginal seas (e.g., the Arctic [Andersson et al., 2008; Porcelli et al., 2009], the Bengal Bay [Singh et al., 2012], the Nordic seas [Lacan and Jeandel, 2004], and the Mediterranean Sea [Tachikawa et al., 2004]) are not compiled here. Some new data from the South Pacific reported in this study are marked by gray circles. See Supplementary Table A2 for data collection.

3.3 Discussion

3.3.1 The influence of coastal/dust flux and particle scavenging on Nd concentrations in the surface layer

Although Nd released from atmospheric dust is one of the important sources of the oceanic surface waters, previous studies have revealed that the distribution of Nd concentrations can hardly be explained by dust transport through the prevailing wind system [Nozaki, 2001]. Therefore atmospheric dust deposition cannot be the dominant source of Nd for most of the global surface ocean with the exception of areas directly downwind of major dust plumes such as the eastern tropical North Atlantic [Rickli et al., 2010].
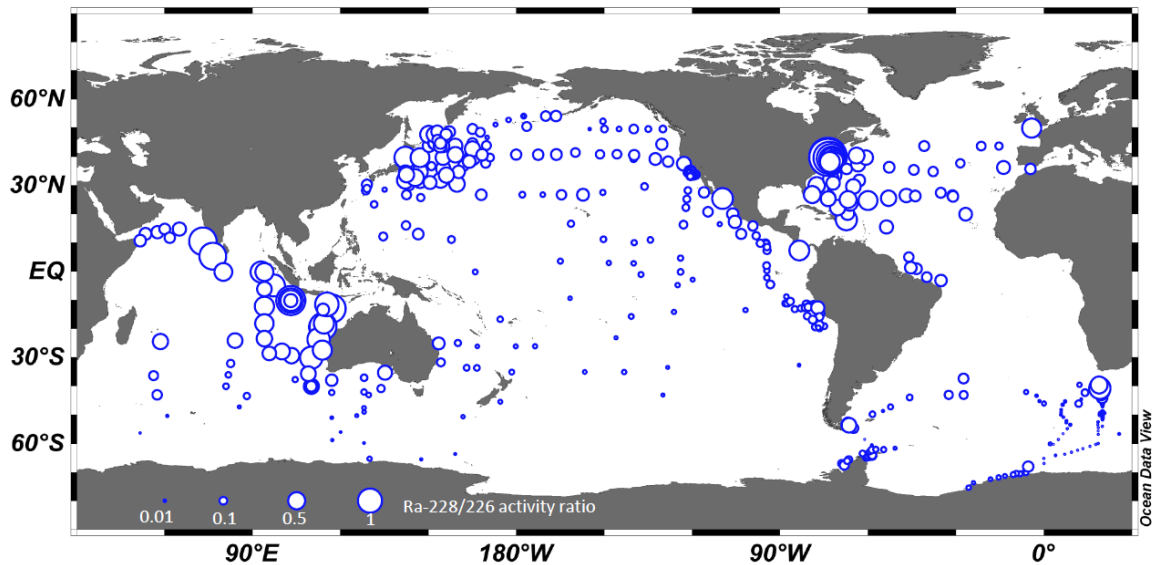
Figure 3.2 Compilation of ^{228}Ra/^{226}Ra activity ratios of the surface ocean. To account for the potential particle scavenging effect, ^{226}Ra activity was normalized by ^{226}Ra (e.g., Nozaki et al., [1990]). Data sources: Moore, [1969]; Knauss et al., [1978]; Kaufman et al., [1973]; Nozaki et al., [1990]; Nozaki et al., [1998]; Nozaki and Yamamoto, [2001]; Hanfland, [2002]; Kawakami et al., [2008].

To constrain the coastal water mass influence, we compiled the global surface seawater ^{228}Ra activities (Figure 3.2). ^{228}Radium is enriched in the continental margins and major surface currents e.g., Kuroshio and its extension (Northwest and mid-North Pacific), or the Gulf stream (Northwest Atlantic), but strongly depleted in the southern Hemisphere oceans due to their remoteness from coastal influences. In contrast, high Nd concentrations are observed in high latitude oceans of both hemispheres, while low Nd concentrations generally occur in subtropical gyres. In particular, in the Southern Ocean where ^{228}Ra activities are relatively low, Nd concentrations are higher than in the middle and low latitudes of the North Pacific (Figure 3.1). Nevertheless, there are also areas showing comparatively high ^{228}Ra activities in the Southern Ocean (e.g., Western Australia, off the tip of South America, South Africa). Given these sites are mostly close to continents, it is likely that they have been considerably influenced by coastal fluxes, for which it is well known that they are characterized by high ^{228}Ra activities. These fundamental and systematic differences between Nd concentrations and ^{228}Ra activities indicate that surface water Nd concentrations must also be influenced by processes other than the coastal influence. It is noteworthy that Nd concentrations in high latitude surface waters of both hemispheres [Siddall et al., 2008] are actually not lower than in subtropical areas where particle export fluxes are lower. This characteristic challenges the role of particle concentration as the major controlling factor of the global distribution of surface water Nd concentrations. Instead, we suggest that flux of Nd from the subsurface waters is an important source of Nd to surface waters and thus an important mechanism for driving basin scale variations of Nd concentrations in the surface ocean.
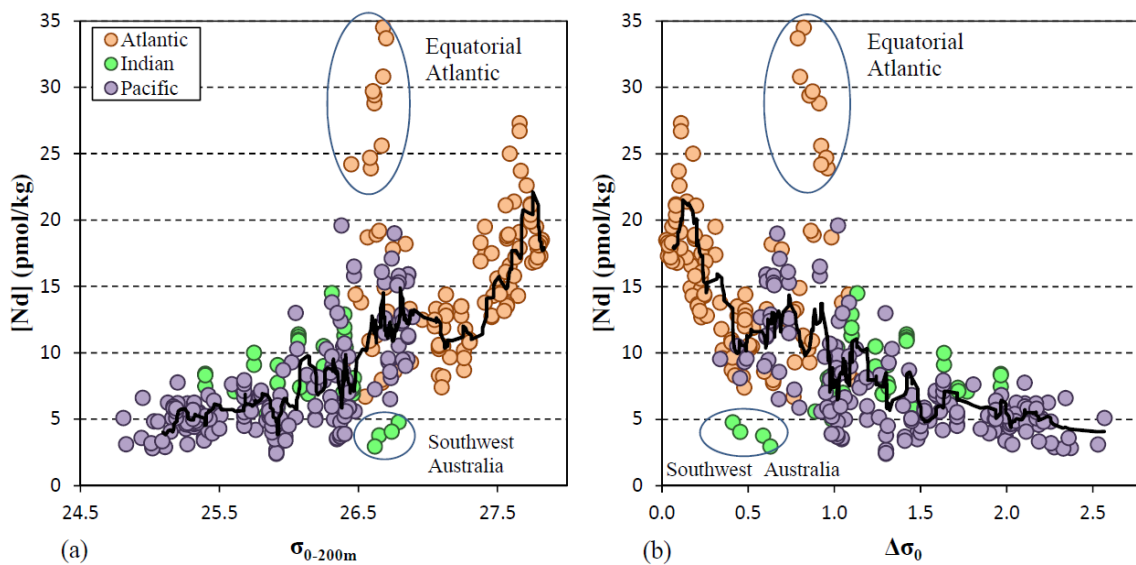
Figure 3.3 Surface water Nd concentrations ([Nd], 0-100 m water depth) versus potential density anomaly $\sigma_{0\text{-}200m}$ at 200 m water depth (a), and density differences $\Delta\sigma_0$ (between 200 m and 1000 m water depth) (b). The data of $\sigma_{0\text{-}200m}$ and $\sigma_{0\text{-}1000m}$ have been extracted from the Electronic Atlas of WOCE (http://www.ewoce.org/). A depth of 200 m (which corresponds to the bottom of the euphotic layer) is chosen because such depth does not greatly suffer from seasonal disturbances, variability of particle concentrations as well as hydrographic changes, but still tracks the overall stratification status of the upper ocean as a first approximation. The lower boundary of the upper ocean mixing regime is taken as 1000 m depth in all ocean basins (e.g, Wunsch and Ferrari, 2004). Deviations from the general trend are marked by ovals. Solid lines are the 10 points moving average of these data which have a (linear) correlation coefficient (R^2) of 0.65 between [Nd] and $\sigma_{0\text{-}200m}$, and of 0.59 between [Nd] and $\Delta\sigma_0$ (excluding the circled outlier data).

3.3.2 The supply of Nd from subsurface thermocline waters to the surface layer

Because Nd behaves similar to nutrients as introduced in section 3.1, a potentially important issue is the mechanism by which nutrients are transferred from the subsurface thermocline waters to the euphotic layer at different latitudes, which is still subject of considerable biogeochemical debate both in observational and modeling studies [e.g., Oschlies and Garcon, 1998; McGillicuddy et al., 2007, Sarmiento et al., 2004, Palter et al., 2010].

In high latitudes where the surface ocean is generally less stratified than in low latitudes, nutrients are transferred from thermocline waters into the overlying deepened mixed layer by a combination of vertical and lateral advection [e.g., nutrient streams, Williams et al., 2006; Marshall and Speer, 2012]. Pronounced vertical mixing and upwelling of nutrient rich waters in the Southern Ocean sustains export fluxes in large parts of the global ocean [Sarmiento et al., 2004, Palter et al., 2010]. The mixed layer depths become deeper towards high latitudes, and this is where increased supply occurs. In contrast, at low latitudes, water is preferentially subducted to the permanent thermocline (i.e. formation of mode waters, Qiu and Huang [1995]). In this case, shallow Ekman advection most likely brings the major part of marginal nutrients to the gyre interior. In addition, there is growing evidence for mesoscale eddies driving the thermocline nutrients to the surface and a number of studies [Oschlies and Garcon, 1998; McGillicuddy et al., 2007] have suggested that this mechanism may be important for maintaining primary surface water productivity of the subtropical ocean, although the quantitative significance of mesoscale eddies is still under debate. To summarize, exchange between thermocline and surface waters at different latitudes is controlled by different mechanisms. Overall, stratification inhibits vertical mixing within the water column and thus limits the magnitude of the flux of nutrients and probably also of Nd from subsurface to surface waters.

The Pacific subtropical gyres which correspond to lowest surface concentrations of Nd, are significantly more stratified than the high latitudes where higher Nd concentrations prevail (Figure 3.1). Interestingly, a positive (negative) correlation between $\sigma_{0\text{-}200m}$ ($\Delta\sigma_0$) and surface water Nd concentrations is also observed (Figure 3.3). In contrast, there is virtually no relation between the ^{228}Ra/^{226}Ra ratio and $\sigma_{0\text{-}200m}$ (Figure 4). Note however that the majority of observations for surface water ^{228}Ra concentrations available in the literature have been obtained from locations close to continental margins. Such a bias may result in the fact that Figure 3.4 is not fully representative of the global surface ocean. Given the already poor correlation presented in Figure 3.4, it seems rather unlikely that more data from the oceanic interior (expected to show low ^{228}Ra/^{226}Ra ratios) would improve the correlation between the ^{228}Ra/^{226}Ra ratios and the $\sigma_{0\text{-}200m}$. Moreover, the

observation that Nd concentrations are generally lower in subtropical gyres than at high latitudes is robust (e.g., see Pacific data in Figure 3.1), despite Nd concentration data are sparse in most of the subtropical gyres compared to other locations.
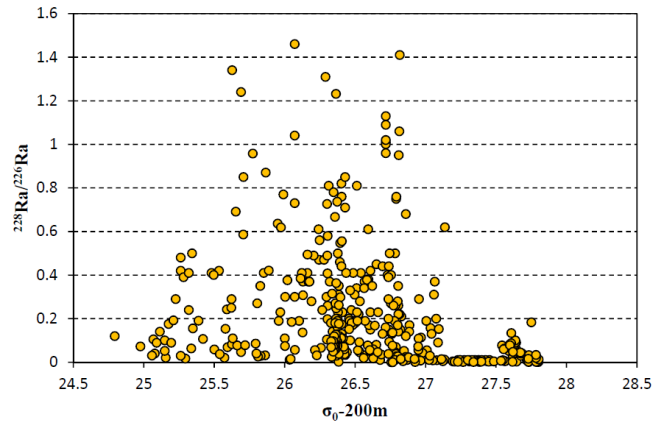
Figure 3.4 Surface water ^{228}Ra/^{226}Ra activity ratio versus potential density anomaly σ_0 at 200 m water depth. The data of σ_0-200m are from Electronic Atlas of WOCE, while data of ^{228}Ra/^{226}Ra are the same as in Figure 3.2.

This leads us to hypothesize that upper ocean vertical supply, itself limited by density stratification, is an important factor in controlling variations of open ocean surface Nd concentrations. As mentioned above the magnitude of Nd concentrations is modified by a number of processes at any location (e.g., dust dissolution, lateral advection, and scavenging/remineralization), thus complicating the quantitative interpretation of variations of surface Nd concentrations. In particular, lateral advection (e.g., within the ACC) has the potential to effectively transport thermocline-derived Nd over long distances within surface currents. Moreover, efficient remineralization of sinking particles within subsurface layers may rapidly release the adsorbed Nd flux back to the water column. The magnitude of Nd flux being released this way at shallower depths may not only depend on the stratification of the upper ocean but also on the nature of the particles. Finally, in some local open ocean areas like the eastern equatorial Atlantic, dust and/or coastal sources may in fact be the major sources for Nd in the surface waters (Rickli et al. [2010], marked outliers in Figure 3.3). In the Southern Ocean southwest of

Australia, Nd concentrations are unexpectedly low, and more observational studies are needed to evaluate the main controlling processes in this area. All the above factors contribute to the scatter of observations in Figure 3.3. In addition, the scatter could also simply be related to the uncertainties in estimating potential density anomalies for each sampling location.

3.3.3 Surface Nd flux estimation and modeling

The inventory of Nd in the uppermost 100 m of the global ocean excluding the Arctic is about 5.9×10^{10} g (based on the compilation of Tachikawa et al. [2003]). To be consistent with a scavenging residence time of 1~4 yr [Amakawa et al., 2000; Rickli et al., 2010], an influx between $\sim1.48\times10^{10}$ and 5.90×10^{10} g/yr is needed. This is about two orders of magnitude larger than the riverine and dust fluxes of Nd (about 3.4×10^{8} g Nd/yr and 2.6×10^{8} g Nd/yr, respectively, Rempfer et al. [2011]). Clearly, large additional influxes of Nd to the surface layer are required, as also noted in earlier studies [e.g., Amakawa et al., 2000]. It has been proposed that the supply of Nd from the ocean margins via dissolution of and exchange with marine sediments [e.g., Jeandel et al, 1998; Amakawa et al., 2000; Tachikawa et al., 2003; Lacan and Jeandel., 2005; Arsouze et al., 2009; Rempfer et al., 2011, 2012b] is an important, even overwhelming source of Nd to the global ocean. Since the exact nature of the boundary Nd source is still largely unknown, a precise estimation of shallow coastal Nd flux to the surface layer is difficult. Even if we assume that all the Nd from the boundary source (5.5×10^{9} g Nd/yr following Rempfer et al. [2011]) is supplied to the ocean via the surface layer, the total external flux from dust, river, and boundary source (summing up to 6.1×10^{9} g Nd/yr) only accounts for up to 37% of the required surface flux. Moreover, it is important to keep in mind that extremely high oceanic surface productivity normally occurs in the continental shelf areas [Falkowski et al., 1998]. It is thus likely that, due to the high particle concentration and associated scavenging on or near the shelves, a large fraction of shelf Nd cannot escape the shelf area to the open ocean via surface currents [Grasse et al., 2012]. Thus, the shallow coastal Nd flux reaching open ocean surface waters is further reduced. The argument above is consistent with the study of von Blanckenburg and Igel, [1999]. Using an idealized two-dimensional model, these authors showed that the distribution of particle reactive tracers

(such as Be, Pb) would have high concentration gradients from the continental margin to the gyre interior, when only considering lateral advection and scavenging of the coastal inputs.

Using a 3-dimensional modeling approach [Rempfer et al., 2011, 2012b], we examine the potential influence of shallow coastal/dust supply on surface Nd concentrations (see a brief description of the model in Supplementary Materials). Figure 3.5a, b show the Nd concentrations and ε_{Nd}, respectively, as obtained with the CTRL experiment of Rempfer et al. [2012a]. In an additional simulation, Nd inputs by dust and riverine discharge are omitted and the Nd boundary source is confined to depths between about 200 and 3000 m depth while keeping its magnitude unchanged (EXP1, Figure 3.5c for concentrations, Figure 3.5d for ε_{Nd}). In this experiment, no sources are applied at depths shallower than 200 m. The difference (CTRL-EXP1) between the two simulations is indicated in Figures 3.5e (concentrations) and 5f (ε_{Nd}).

Interestingly, the simulated ε_{Nd} of CRTL experiment is broadly consistent with observations (Figure 3.5b) and is similar to those of EXP1 (Figure 3.5d). In most of the Pacific and Southern Ocean, the differences between CTRL and EXP1 are less than 0.5-1.0 ε_{Nd} units. Exceptions are the tropical and subtropical Atlantic, where CRTL-EXP1 is larger than 2 ε_{Nd} units, implying riverine and dust inputs might have exerted a notable influence on the Nd isotope compositions of ocean surface waters in these areas. On the other hand, the simulated surface water Nd concentrations in CTRL (Figure 3.5a, Appendix Figure A1) are 1-2 pmol/kg in most of the open Pacific, 2-10 pmol/kg in the open Atlantic, and 4-8 pmol/kg in the ACC which is lower than available observations (e.g., 4-15 pmol/kg in the open Pacific, 10-30 pmol/kg in the open Atlantic, and 10-20 pmol/kg in the Antarctic circumpolar current, see also Figure 3.1). Nevertheless, the CTRL experiment initially presented Rempfer et al. [2012a] is an optimal parameterization designed for the simulation of both Nd concentration and ε_{Nd} in the global ocean in agreement with available observations. First order characteristics of distributions of Nd concentrations in the surface ocean are clearly captured by the model. For example, simulated Nd concentrations are lower in the Pacific than in the Atlantic and the ACC. Nd concentrations are also lower in subtropical gyres than in high latitudes

51

where Nd concentrations become higher towards the polar regions. Given that the vertical transport of Nd was simulated by the model, we can obtain information on the relative importance of this vertical supply in different oceanic areas relative to the contributions from the boundary sources, rivers and dust.
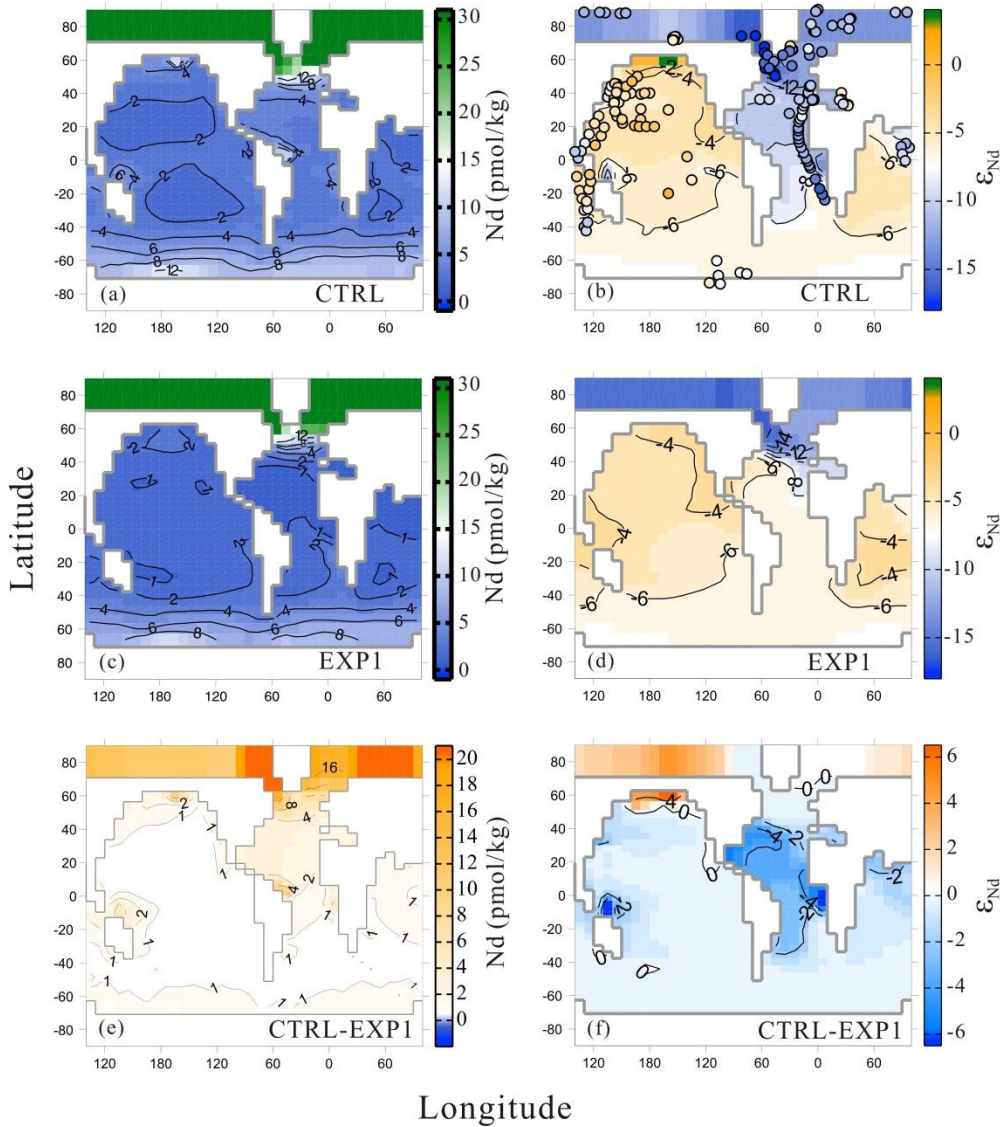
Figure 3.5 Surface Nd concentration (pmol/kg) (a) and ε_{Nd} (b) obtained with the CTRL of Rempfer et al. [2012a]. Observations (circles) are superimposed using the same color coding [Rempfer et al., 2012a]. Nd concentration (pmol/kg) (c) and ε_{Nd} (d) from a simulation (EXP1) where all Nd sources at depths shallower than 200m have been omitted. Note, in EXP1 the boundary source is confined to depths between 200 and 3000 m. The concentration (e) and ε_{Nd} (f) differences between the two simulations (CTRL-EXP1).

Overall, the effect of cutting off external Nd-input into the upper 200 m on Nd concentrations is larger in regions close to the margins than in regions far away from the continents. The results in Figures 3.5e, and 5f imply that input from shallow boundary sources, riverine supply, and release from dust might not be of primary importance notably in the Southern Ocean and the Pacific, which supports our case made in section 3.1. Unfortunately, the low simulated Nd concentrations compared to observations complicate the estimation of the quantitative importance of internal Nd sources (i.e., subsurface Nd fluxes) on a global scale. Improving the ability of models to simulate surface Nd concentrations in agreement with observations is beyond the scope of this study. Nevertheless, it has become apparent from our discussion that such improvement cannot simply be achieved by increasing the shallow coastal Nd input. A recent study [Akagi, 2013] proposed that incorporation of Nd into diatoms and subsequent diatom dissolution in deep water (thus irreversible intake and release) is the dominant mechanism in explaining the non-zero surface seawater REE (including Nd) concentrations as well as enrichment of REE at depth. While a close link of Nd with silicic cycling (or other nutrient elements) is not surprising, as discussed in Section 3.3.2, our modeling above clearly shows that non-zero surface Nd concentrations and first order surface Nd concentration distribution can be produced using a reversible scavenging model. Moreover, given that reversible scavenging of Nd is required to successfully simulate both Nd concentrations and isotope compositions of the deep water profiles [e.g., Bertram and Elderfield, 1993; Siddall et al., 2008; Arsouze et a.., 2009; Oka et al., 2009; Rempfer et al., 2011], it appears that future modeling studies should aim at resolving the surface concentration issue by focusing on the fluxes related to vertical supply and reversible scavenging parameters of Nd in the upper ocean.

3.4 Conclusions

The knowledge on Nd cycling in surface waters is important for interpreting oceanic Nd isotope records in terms of oceanic environmental changes, such as ocean circulation versus local shallow weathering supply [e.g., Rempfer et al., 2012b]. Our study implies that open ocean surface Nd concentrations are influenced by processes other than shallow

coastal/dust input and subsequent surface current mixing and scavenging. We propose that vertical supply of Nd from subsurface waters to shallower depths, itself limited by upper ocean stratification, may represent an important contribution to the Nd budget of open ocean surface waters. This is supported by (1) the systematic differences of global distribution of Nd concentrations and ^{228}Ra activities; (2) the positive correlation between Nd concentrations and the potential density anomaly at 200 m water depth (i.e., the base of euphotic layer); (3) the estimation of the magnitude of required Nd input flux to maintain the observed surface ocean Nd concentrations, and (4) results from a 3-dimensional modeling experiment. Future field and modeling studies focusing on the scavenging of Nd and stratification-related Nd flux in the surface layer are thus of high priority in order to precisely understand the surface water Nd cycle as well as to better constrain the use of Nd isotopes as a (paleo)circulation proxy.

References

Akagi, T. (2013), Rare earth element (REE)–silicic acid complexes in seawater to explain the incorporation of REEs in opal and the "leftover" REEs in surface water: New interpretation of dissolved REE distribution profiles, *Geochim. Cosmochim. Acta*, *113*(0), 174-192.

Amakawa, H., D. S. Alibo, and Y. Nozaki (2000), Nd isotopic composition and REE pattern in the surface waters of the eastern Indian Ocean and its adjacent seas, *Geochim. Cosmochim. Acta*, *64*(10), 1715-1727.

Amakawa, H., K. Sasaki, and M. Ebihara (2009), Nd isotopic composition in the central North Pacific, *Geochim. Cosmochim. Acta*, *73*(16), 4705-4719.

Andersson, P. S., D. Porcelli, M. Frank, G. Bjork, R. Dahlqvist, and O. Gustafsson (2008), Neodymium isotopes in seawater from the Barents Sea and Fram Strait Arctic-Atlantic gateways, *Geochim. Cosmochim. Acta*, *72*(12), 2854-2867.

Arsouze, T., J. C. Dutay, F. Lacan, and C. Jeandel (2007), Modeling the neodymium isotopic composition with a global ocean circulation model, *Chem. Geol.*, *239*(1-2), 165-177.

Arsouze, T., J. C. Dutay, F. Lacan, and C. Jeandel (2009), Reconstructing the Nd oceanic cycle using a coupled dynamical - biogeochemical model, *Biogeosciences*, *6*(12), 2829-2846.

Bertram, C. J., and H. Elderfield (1993), The Geochemical Balance of the Rare-Earth Elements and Neodymium Isotopes in the Oceans, *Geochim. Cosmochim. Acta*, *57*(9), 1957-1986.

Carter, P., D. Vance, C. D. Hillenbrand, J. A. Smith, and D. R. Shoosmith (2012), The neodymium isotopic composition of waters masses in the eastern Pacific sector of the Southern Ocean, *Geochim. Cosmochim. Acta*, *79*, 41-59.

Capotondi, A., M. A. Alexander, N. A. Bond, E. N. Curchitser, and J. D. Scott (2012), Enhanced upper ocean stratification with climate change in the CMIP3 models, *J. Geophys. Res., 117*, C04031, doi:10.1029/2011JC007409.

de Baar, H. J. W., J. T. M. de Jong, D. C. E. Bakker, B. M. Loscher, C. Veth, U. Bathmann, and V. Smetacek (1995), Importance of iron for plankton blooms and carbon dioxide drawdown in the Southern Ocean, *Nature*, *373*(6513), 412-415.

Falkowski, P. G., R. T. Barber, and V. Smetacek (1998), Biogeochemical controls and feedbacks on ocean primary production, *Science*, *281*(5374), 200-206.

Goldstein, S. J., and S. B. Jacobsen (1987), The Nd and Sr Isotopic Systematics of River-Water Dissolved Material - Implications for the Sources of Nd and Sr in Seawater, *Chem. Geol.*, *66*(3-4), 245-272.

Grasse, P., T. Stichel, R. Stumpf, L. Stramma, and M. Frank (2012), The distribution of neodymium isotopes and concentrations in the Eastern Equatorial Pacific: Water mass advection versus particle exchange, *Earth Planet. Sci. Lett.*, *353–354*(0), 198-207.

Grenier, M., C. Jeandel, F. Lacan, D. Vance, C. Venchiarutti, A. Cros, and S. Cravatte (2013), From the subtropics to the central equatorial Pacific Ocean: Neodymium isotopic composition and rare earth element concentration variations, *J. Geophys. Res. 118*, doi: 10.1029/2012JC008239.

Hanfland, C., (2002). Radium-226 and Radium-228 in the Atlantic sector of the Southern Ocean: Reports on Polar and Marine Research, Bremerhaven, Alfred Wegener Institute for Polar and Marine Research, 431, 135 p.

Jeandel, C., D. Thouron, and M. Fieux (1998), Concentrations and isotopic compositions of neodymium in the eastern Indian Ocean and Indonesian straits, *Geochim. Cosmochim. Acta*, *62*(15), 2597-2607.

Jenkins, W. J. (2003), Tracers of Ocean Mixing, in *Treatise on Geochemistry*, edited by D. H. Editors-in-Chief: Heinrich and K. T. Karl, pp. 223-246, Pergamon, Oxford.

Knauss, K. G., T. L. Ku, and W. S. Moore (1978), Radium and Thorium Isotopes in Surface Waters of East Pacific and Coastal Southern-California, *Earth Planet. Sci. Lett.*, *39*(2), 235-249.

Kaufman, A., R. M. Trier, W. S. Broecker, and H. W. Feely (1973), Distribution of Ra-228 in World Ocean, *J. Geophys. Res.*, *78*(36), 8827-8848.

Kawakami, H., and M. Kusakabe (2008), Surface water mixing estimated from 228Ra and 226Ra in the northwestern North Pacific, *J Environ. Radioactiv.*, *99*(8), 1335-1340.

Lacan, F., and C. Jeandel (2004), Denmark Strait water circulation traced by heterogeneity in neodymium isotopic compositions, *Deep Sea Res., Part I*, *51*(1), 71-82.

Lacan, F., and C. Jeandel (2005), Neodymium isotopes as a new tool for quantifying exchange fluxes at the continent-ocean interface, *Earth Planet. Sci. Lett.*, *232*(3-4), 245-257.

Lacan, F., K. Tachikawa, and C. Jeandel (2012), Neodymium isotopic composition of the oceans: A compilation of seawater data, *Chem. Geol.*, *300–301*(0), 177-184.

Marshall, J., and K. Speer (2012), Closure of the meridional overturning circulation through Southern Ocean upwelling, *Nature Geosci.*, *5*(3), 171-180.

McGillicuddy, D. J., et al. (2007), Eddy/wind interactions stimulate extraordinary mid-ocean plankton blooms, *Science*, *316*(5827), 1021-1026.

Moore, W. S. (1969), Oceanic Concentrations of [228]radium, *Earth Planet. Sci. Lett.*, *6*(6), 437-446.

Nozaki, Y. (2001), Rare earth elements and their isotopes, *Encyclopedia of Ocean Sciences*, *4*, 2354–2366.

Nozaki, Y., and Y. Yamamoto (2001), Radium 228 based nitrate fluxes in the eastern Indian Ocean and the South China Sea and a silicon-induced "alkalinity pump" hypothesis, *Global Biogeochem. Cycles*, *15*(3), 555-567.

Nozaki, Y., V. Kasemsupaya, and H. Tsubota (1990), The Distribution of Ra-228 and Ra-226 in the Surface Waters of the Northern North Pacific, *Geochem. J.*, *24*(1), 1-6.

Nozaki, Y., F. Dobashi, Y. Kato, and Y. Yamamoto (1998), Distribution of Ra isotopes and the Pb-210 and Po-210 balance in surface seawaters of the mid Northern Hemisphere, *Deep Sea Res., Part I*, *45*(8), 1263-1284.

Oka, A., H. Hasumi, H. Obata, T. Gamo, and Y. Yamanaka (2009), Study on vertical profiles of rare earth elements by using an ocean general circulation model, *Global Biogeochem. Cycles*, *23*, GB4025, doi: 10.1029/2008GB003353.

Oschlies, A., and V. Garcon (1998), Eddy-induced enhancement of primary production in a model of the north Atlantic Ocean, *Nature*, *394*(6690), 266-269.

Palter, J. B., J. L. Sarmiento, A. Gnanadesikan, J. Simeon, and R. D. Slater (2010), Fueling export production: nutrient return pathways from the deep ocean and their dependence on the Meridional Overturning Circulation, *Biogeosciences*, *7*(11), 3549-3568.

Peucker-Ehrenbrink, B., M. W. Miller, T. Arsouze, and C. Jeandel (2010), Continental bedrock and riverine fluxes of strontium and neodymium isotopes to the oceans, *Geochemistry, Geophysics, Geosystems*, *11*(3), Q03016, 10.1029/2009gc002869.

Porcelli, D., P. S. Andersson, M. Baskaran, M. Frank, G. Bjork, and I. Semiletov (2009), The distribution of neodymium isotopes in Arctic Ocean basins, *Geochim. Cosmochim. Acta*, *73*(9), 2645-2659.

Qiu, B., and R. X. Huang (1995), Ventilation of the North Atlantic and North Pacific: subduction versus obduction, *J. Phys. Oceanogr.*, *25*(10), 2374-2390.

Rempfer, J., T. F. Stocker, F. Joos, and J.-C. Dutay (2012a), Sensitivity of Nd isotopic composition in seawater to changes in Nd sources and paleoceanographic implications, *J. Geophys. Res.*, *117*(C12), doi: 10.1029/2012jc008161.

Rempfer, J., T. F. Stocker, F. Joos, and J. C. Dutay (2012b), On the relationship between Nd isotopic composition and ocean overturning circulation in idealized freshwater discharge events, *Paleoceanography*, *27*, Pa3211, doi 10.1029/2012pa002312.

Rempfer, J., T. F. Stocker, F. Joos, J. C. Dutay, and M. Siddall (2011), Modelling Nd-isotopes with a coarse resolution ocean circulation model: Sensitivities to model parameters and source/sink distributions, *Geochim. Cosmochim. Acta*, *75*(20), 5927-5950.

Rickli, J., M. Frank, A. R. Baker, S. Aciego, G. de Souza, R. B. Georg, and A. N. Halliday (2010), Hafnium and neodymium isotopes in surface waters of the eastern Atlantic Ocean: Implications for sources and inputs of trace metals to the ocean, *Geochim. Cosmochim. Acta*, *74*(2), 540-557.

Sarmiento, J. L., N. Gruber, M. A. Brzezinski, and J. P. Dunne (2004), High-latitude controls of thermocline nutrients and low latitude biological productivity, *Nature*, *427*(6969), 56-60.

Siddall, M., S. Khatiwala, T. van de Flierdt, K. Jones, S. L. Goldstein, S. Hemming, and R. F. Anderson (2008), Towards explaining the Nd paradox using reversible scavenging in an ocean general circulation model, *Earth Planet. Sci. Lett.*, *274*(3-4), 448-461.

Singh, S. P., S. K. Singh, V. Goswami, R. Bhushan, and V. K. Rai (2012), Spatial distribution of dissolved neodymium and εNd in the Bay of Bengal: Role of particulate matter and mixing of water masses, *Geochim. Cosmochim. Acta*, *94*(0), 38-56.

Stichel, T., M. Frank, J. Rickli, and B. A. Haley (2012), The hafnium and neodymium isotope composition of seawater in the Atlantic sector of the Southern Ocean, *Earth Planet. Sci. Lett.*, *317–318*(0), 282-294.

Tachikawa, K., V. Athias, and C. Jeandel (2003), Neodymium budget in the modern ocean and paleo-oceanographic implications, *J. Geophys. Res.*, *108*(C8), 3254, doi 10.1029/1999jc000285.

Tachikawa, K., M. Roy-Barman, A. Michard, D. Thouron, D. Yeghicheyan, and C. Jeandel (2004), Neodymium isotopes in the Mediterranean Sea: Comparison

between seawater and sediment signals, *Geochim. Cosmochim. Acta*, *68*(14), 3095-3106.

von Blanckenburg, F. (1999), Perspectives: Paleoceanography - Tracing past ocean circulation? *Science*, *286*(5446), 1862-1863.

von Blanckenburg, F., and H. Igel (1999), Lateral mixing and advection of reactive isotope tracers in ocean basins: observations and mechanisms, *Earth and Planetary Science Letters*, *169*(1-2), 113-128.

Williams, R. G., and M. J. Follows (1998), The Ekman transfer of nutrients and maintenance of new production over the North Atlantic, *Deep Sea Res. Part I*, *45*(2-3), 461-489.

Williams, R. G., V. Roussenov, and M. J. Follows (2006), Nutrient streams and their induction into the mixed layer, *Global Biogeochem. Cycles*, *20*(1), GB1016, doi: 10.1029/2005gb002586.

Wilson, D. J., A. M. Piotrowski, A. Galy, and I. N. McCave (2012), A boundary exchange influence on deglacial neodymium isotope records from the deep western Indian Ocean, *Earth Planet. Sci. Lett.*, *341–344*(0), 35-47.

Wunsch, C., and R. Ferrari (2004), Vertical mixing, energy and the general circulation of the oceans, *Annu Rev Fluid Mech*, *36*, 281-314.

Zhang, J., and Y. Nozaki (1996), Rare earth elements and yttrium in seawater: ICP-MS determinations in the East Caroline, Coral Sea, and South Fiji basins of the western South Pacific Ocean, *Geochim. Cosmochim. Acta*, *60*(23), 4631-4644.

Chapter 4

Hafnium isotope fractionation during continental weathering: implications for the generation of the seawater Nd-Hf isotope relationships

Abstract

To investigate the mechanisms of the offset of seawater radiogenic Nd-Hf isotope compositions from those of the upper continental crust (UCC) rocks, combined Nd-Hf isotope compositions of desert and loess samples from northern China (which integrate a wide range of lithologies and ages of continental rocks) are presented in this study. The results show significant and systematic fractionation of Hf isotopes between fine-grained detritals/leachates (<5 μm) and coarser fractions (<75 μm) of the same samples. A small but systematic difference of Nd isotope compositions between leachates and detrital silicates is also revealed. Overall, the leaching data either plot along or slightly above the Nd-Hf seawater array, providing strong direct support that the seawater Nd-Hf isotope relationship is predominantly generated by weathering of UCC. Our study supports the application of dissolved Hf isotopes as a proxy for different modes of weathering regimes rather than for continental source provenances.

4.1 Introduction

Since the finding of a strong Hf-rare earth element (REE) fractionation in the Earth's sedimentary system in the 1980s [Patchett et al., 1984; White et al., 1986], a number of studies have contributed to the understanding of Hf isotope geochemistry during sediment transport and oceanic cycling [c.f. van de Flierdt et al., 2007; Vervoort et al., 2011]. With more radiogenic Hf isotopes for a given Nd isotope composition, seawater and ferromanganese crusts show a unique correlation (seawater array, Figure 4.2) which is oblique to the terrestrial array in ε_{Nd}-ε_{Hf} space [Albarède et al., 1998]. Despite earlier studies proposing that contributions of radiogenic Hf from hydrothermal sources may be important for the seawater budget of Hf [White et al., 1986; Godfrey et al., 1997; Bau and Koschinsky, 2006], recent dissolved seawater Hf isotope and concentration data have not favored such a scenario [Rickli et al., 2009; Firdaus et al., 2011; Stichel et al., 2012]. However, an unambiguous conclusion has not been achieved due to the fact that hydrothermal contributions of Hf have so far not been measured and also because there are still no isotopic measurements of truly dissolved versus colloidal Hf isotopes in

seawater [e.g., Bau and Koschinsky, 2006]. In addition, Hf isotope data on rivers that directly supply the world's ocean are very scarce. Available data on rivers such as the Hudson ($\varepsilon_{Hf} > +30$, Godfrey et al., [2009]) and Moselle basin rivers ($\varepsilon_{Hf} < -3$, Bayon et al., [2006]) are actually not consistent with the seawater array (Figure 4.2), whereas a recent study of four Swiss rivers [Rickli et al., 2013] suggested that the Hf-Nd isotope compositions of the rivers are broadly consistent with the seawater array but also that the lithologies and even runoff may exert a large influence. It is still possible, however, that the drainage areas of all these rivers are too small to realistically represent the mean UCC trend. In this study, we aim to obtain a broader picture of the UCC weathering signal and clarify whether UCC weathering can produce combined Hf-Nd isotope signatures that are consistent with the seawater array.

The Chinese continent was formed through multiple stages of collision and aggregation of many continental blocks [e.g., Ren, 1996]. Thus it provides an opportunity to constrain the averaged Nd-Hf isotope signatures of the exchangeable component of upper continental crustal rocks. The dust samples of our study recovered from deserts and other arid areas that distributed over area extending 600 km from North to South and 4,000 km from East to West in northern China are ideal for investigating continental Hf isotope fractionation. The extent of the Chinese deserts and arid areas have been tectonically controlled by the major orogenic belts in East Asia and have been associated with Asian aridification over the late Cenozoic [Chen et al., 2007; Chen and Li, 2011]. Despite that the exact source areas of Chinese deserts and loess deposits are still a matter of debate, these eolian materials always integrate a large range of lithologies (including recycled sedimentary rocks) exposed at the Earth's surface. Dust particles are commonly coated with Fe-Mn oxyhydroxides (the so-called desert varnish, e.g., Bayon et al., [2004]) and trace metal evidence indicated that the desert varnish components are largely formed through natural aqueous leaching of the dust materials [Thiagarajan and Lee, 2004]. Therefore, leaching experiments conducted on these dust samples are assumed to be representative of the Nd-Hf isotopic composition of the labile component of UCC rocks ultimately released by chemical weathering, which provides valuable information on the formation mechanism of the seawater Nd-Hf isotopic array.

4.2 Materials and Methods

The desert and loess samples of this study were collected through the efforts of Institute of Surficial Geochemistry at Nanjing University, and have been described in detail elsewhere (Chen et al., [2007], Li et al., [2009]; see Figure 4.1 and Table 4.1).
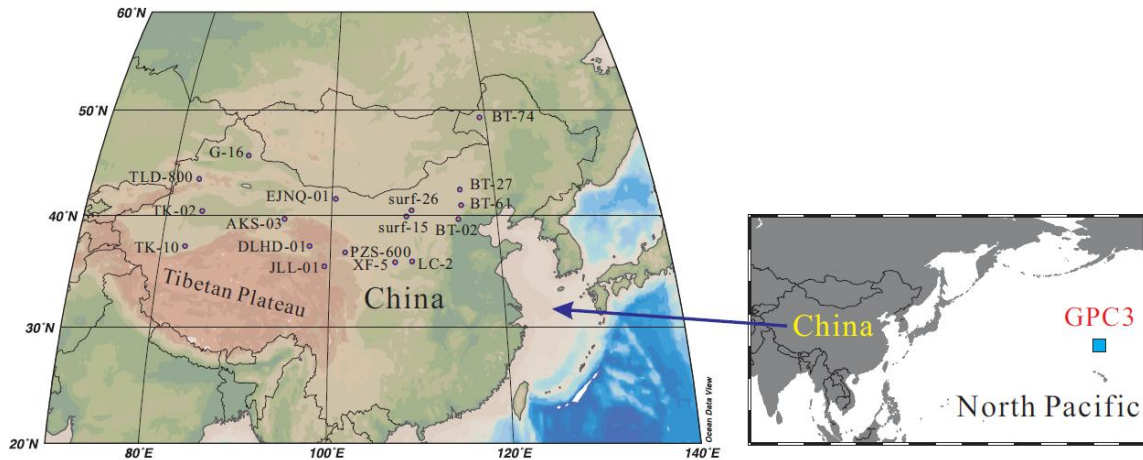
Figure 4.1 Sample location map showing the distribution of northern China loess and desert samples as well as the North Pacific dust core LL44-GPC3.

Before leaching, a de-carbonation step was carried out using excess 0.5 M acetic acid for 8 hours. This is expected to remove the detrital and secondary carbonates while leaving the labile Fe-Mn oxyhydroxide fraction of the silicate grains untouched. Then a dilute reducing and complexing solution consisting of 0.005 M hydroxylamine hydrochloride, 1.5% acetic acid, and 0.03 M EDTA-2Na, buffered to pH about 4 with superpure NaOH was used to extract the mobile component of the dust for about 2 hours [Chen et al., 2012]. After complete removal of Fe-Mn oxides, the silicate residues, of which paired leachate data (<75 um and <5 um size fractions) have been obtained, were totally dissolved in steel jacketed autoclaves at ~180-200°C for 4 days. Subsequent purification and measurement of the Nd and Hf isotopes followed Chen et al. [2012] (see Table 4.1 for more details).

Table 4.1 Nd-Hf isotopes from leachates of the desert and loess sample from North China

Region	sample name	Longitude (°E)	Latitude (°N)	size	^{143}Nd/^{144}Nd (2σ) leachate	leachate ε_{Nd}[a]	^{176}Hf/^{177}Hf (2σ) leachate	leachate ε_{Hf}[b]	^{143}Nd/^{144}Nd (2σ) detrital	detrital ε_{Nd}	^{176}Hf/^{177}Hf (2σ) detrital	detrital ε_{Hf}
Taklimakan Desert	TK-10	82.79	37.23	<75 um	0.512242±5	-7.7	0.283253±3	17.1				
Loess, West China	TLD-800	83.27	43.41	<5 um	0.512289±6	-6.8	0.282780±2	0.4				
Taklimakan Desert	TK-02	84.25	40.43	<75 um	0.512264±5	-7.3	0.283179±3	14.5				
Gurbantunggut Desert	G-16	89.11	45.60	<75 um	0.512463±5	-3.4	0.282936±2	5.9	0.512439±3	-3.9	0.282708±3	-2.2
	duplicate run										0.282694±2	-2.7
Gurbantunggut Desert	G-16	89.11	45.60	<5 um	0.512445±4	-3.8	0.282909±2	5.0	0.512377±4	-5.1	0.282859±3	3.2
	duplicate sample[c]						0.282916±4	5.2	0.512386±4	-4.9	0.282872±2	3.6
Kumtag Desert	AKS-03	94.35	39.69	<5 um	0.512138±5	-9.8	0.282886±4	4.2				
Qaidam Desert	DLHD-01	97.52	37.23	<75 um	0.512056±3	-11.4	0.282927±4	5.6	0.511997±3	-12.5	0.282192±2	-20.4
Qaidam Desert	DLHD-01	97.52	37.23	<5 um	0.512012±4	-12.2	0.282796±3	1.0	0.512050±4	-11.5	0.282635±2	-4.8
Loess, West China	JLL-01	99.33	35.40	bulk	0.512267±4	-7.2	0.282966±3	7.0	0.512159±3	-9.3	0.282432±3	-11.9
	duplicate run										0.282424±2	-12.2
Loess, West China	JLL-01	99.33	35.40	<5 um	0.512254±3	-7.5	0.282875±3	3.7	0.512189±3	-8.8	0.282718±3	-1.8
Badain Jaran Desert	EJNQ-01	100.46	41.55	<5 um	0.512222±4	-8.1	0.283002±4	8.3	0.512114±4	-10.2	0.282520±2	-8.8
Badain Jaran Desert	EJNQ-01	100.46	41.55	<5 um	0.512175±3	-9.0	0.282881±3	4.0	0.512096±4	-10.6	0.282687±2	-2.9
Loess, West China	PZS-600	101.74	36.65	<5 um	0.512165±5	-9.2	0.282746±2	-0.8				
Loess, Loess Plateau	XF-5	107.60	35.78	<5um	0.512188±5	-8.8	0.282822±3	1.9				
Mu Us Desert	surf-15	109.05	39.92	<75 um	0.511905±4	-14.3	0.283046±9	9.8	0.511773±4	-16.9	0.282107±2	-23.4
	duplicate run										0.282101±2	-23.6
Mu Us Desert	surf-15	109.05	39.92	<5um	0.511908±5	-14.2	0.282914±4	5.1	0.511784±5	-16.7	0.282699±2	-2.5
	duplicate run				0.511913±5	-14.1						
Loess, Loess Plateau	LC-2	109.60	35.85	bulk	0.512236±6	-7.8	0.282916±3	5.2	0.512086±4	-10.8	0.282439±2	-11.7
	duplicate run								0.512098±3	-10.5		

Location	Sample				$^{143}Nd/^{144}Nd$	ε_{Nd}	$^{176}Hf/^{177}Hf$	ε_{Hf}	$^{143}Nd/^{144}Nd$	ε_{Nd}	$^{176}Hf/^{177}Hf$	ε_{Hf}
Loess, Loess Plateau	LC-2	109.60	35.85	<5 um	0.512200±3	-8.5	0.282833±3	2.3	0.512094±3	-10.6	0.282710±3	-2.1
Hobq Desert	surf-26	109.70	40.47	<75 um	0.511902±6	-14.3	0.283026±3	9.1	0.511840±5	-15.6	0.282161±2	-21.5
	duplicate run				0.512213±5	-8.3					0.282169±3	-21.2
	duplicate sample								0.511844±4	-15.5	0.282165±3	-21.4
Hobq Desert	surf-26	109.70	40.47	<5um	0.511854±4	-15.3	0.282921±3	5.4	0.511735±4	-17.6	0.282719±2	-1.8
Loess, East China	BT-02	115.32	39.68	<5 um	0.512209±5	-8.4	0.282816±2	1.6				
	duplicate run				0.512323±5	-6.1						
Loess, East China	BT-27	115.77	42.40	bulk	0.512344±3	-5.7	0.282874±2	3.7	0.512208±4	-8.4	0.282536±3	-8.2
Loess, East China	BT-27	115.77	42.40	<5 um	0.512334±5	-5.9	0.282835±2	2.4	0.512199±4	-8.6	0.282755±3	-0.5
	duplicate run											
Loess, East China	BT-61	115.78	40.97	<5um	0.512256±3	-7.4	0.282838±2	2.4				
Hunlun Buir Sandy Land	BT-74	119.27	49.27	bulk	0.512436±4	-3.9	0.282877±2	3.8	0.512398±3	-4.7	0.282670±2	-3.5
Hunlun Buir Sandy Land	BT-74	119.27	49.27	<5 um	0.512445±5	-3.8	0.282874±2	3.7	0.512388±5	-4.9	0.282805±2	1.3
	duplicate run						0.282879±2	3.9				
Central North Pacific	dust core GPC3-55703	-157.83	30.3	bulk	*0.512445±5*	*-3.8*	*0.282954±2*	*6.6*		*-10.7[c]*	*0.282683±6[d]*	*-3.0*
	duplicate run				*0.512440±3*	*-3.9*						

a. $\varepsilon_{Nd} = [(^{143}Nd/^{144}Nd)_{sample}/(^{143}Nd/^{144}Nd)_{CHUR} - 1]*10^4$; where $(^{143}Nd/^{144}Nd)_{CHUR} = 0.512638$ (Jacobsen and Wasserburg, 1980).

b. $\varepsilon_{Hf} = [(^{176}Hf/^{177}Hf)_{sample}/(^{176}Hf/^{177}Hf)_{CHUR})-1]*10^4$; where $(^{176}Hf/^{177}Hf)_{CHUR}=0.282769$ (Nowell et al., 1998).

c. duplicate samples were taken from the same sample powder.

d. from Pettke et al., 2002 (GPC3-55704).

4.3 Results

The Hf and Nd isotope data of dust leachates and detrital fractions are shown in Table 4.1 and Figure 4.2.

There is virtually no difference between the Nd isotope composition of coarse and fine grained dust leachates (Figure 4.3a). In addition, the total dissolution data of the fine and coarse-grained silicate fraction further reveal that their Nd isotope compositions are also distributed very close to the 1:1 line (Figure 4.3b). Interestingly, a small but detectable and systematic difference between the Nd isotope compositions of the leachates and detrital silicate fractions (about 1.4 epsilon units) is remarkable (Figure 4.3c).
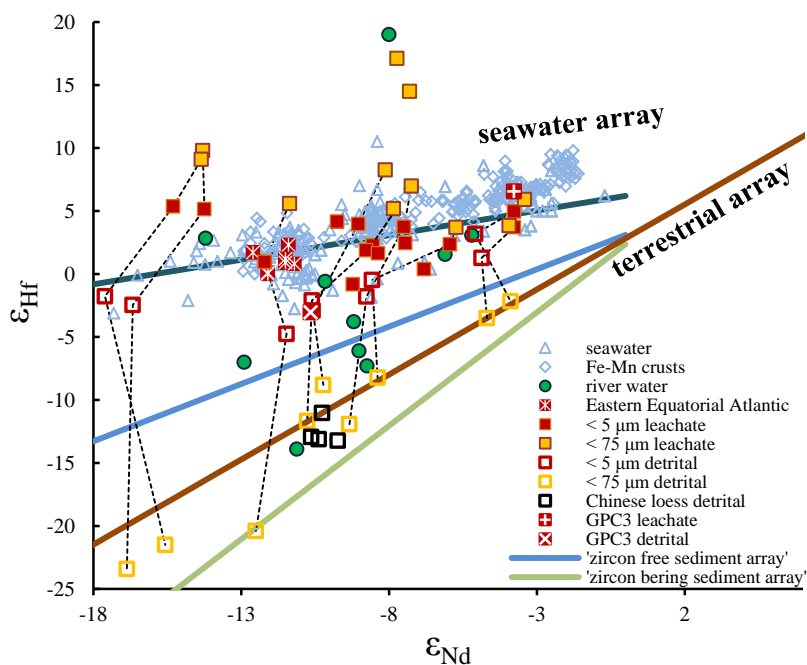
Figure 4.2 Combined hafnium–neodymium isotope compositions of dust leachates and detrital fractions (<5 μm and <75 μm), compared with seawater and river water signatures [van de Flierdt et al., 2004 and references therein; Bayon et al., 2006; Godfrey et al., 2009; Zimmermann et al., 2009; Stichel et al., 2012 and references therein]. The seawater array reflects the Nd-Hf isotopes of ferromanganese precipitates and dissolved seawater, while crustal array reflects the isotopic trend of upper continental rocks [Vervoort et al., 1999] e.g., see also the data of <75 μm detrital fractions and bulk Chinese loess [Vervoort et al., 2011]. The

dashed lines link the leachates and detrital fraction of the same samples. For comparison, the zircon free and zircon rich sediment arrays (defined by regression of the marine fine-grained and coarse-grained sediment data, respectively [Bayon et al., 2009]. 2σ errors of the data presented in this study are similar to the size of the symbols.

With the exception of Taklimakan leachates which have highly radiogenic Hf isotope signatures (ε_{Hf}: +14.5, +17.0), most of the ε_{Hf} values of the leachates are in the range of -0.8 to +9.9, while their corresponding ε_{Nd} signatures vary from -15.4 to -3.4. The most striking feature of the leaching data is that they all fall along or slightly above the seawater array (Figure 4.2). And the hafnium isotope compositions are more radiogenic in leachates of the coarser size fraction (<75 um) than the corresponding finer grain size leachates (<5 um) (Figure 4.2, 4.2d).

As expected, the detrital silicates of the <75 um size fraction has Nd and Hf isotope signatures consistent with the crustal array in ε_{Hf}-ε_{Nd} space, while the <5 um fraction is more radiogenic in its Hf isotope composition (Figure 4.2, 4.3e). Moreover, the leachate Hf isotope data of the fine and coarse size groups deviate notably from such a 1:1 line (Figure 4.3d). Also, the Hf isotope compositions of the leachates are fractionated significantly from those of the silicates (Figure 4.3f).

4.4 UCC weathering could fully produce the seawater array

Interestingly, the leachate of a typical Asian dust sample GPC3 recovered from the North Pacific [Table 4.1, Pettke et al., 2002] shows ε_{Nd} and ε_{Hf} signatures of -3.8 and +6.6, respectively (Figure 4.2), which are entirely consistent with central North Pacific deep water compositions [Amakawa et al., 2009]. Thus the Nd-Hf isotopic signal of the leaching experiments of GPC3 supports that the leaching protocol is robust in extracting the exchangeable component (e.g., Fe-Mn coatings) of the Asian dust (Figure 4.2).

Supporting evidence for the agreement of the dust leaching signal with seawater array comes from the eastern equatorial Atlantic which receives high loads of Saharan dust input. The Nd-Hf isotopes of eastern equatorial Atlantic surface waters (5°N-15°N, Figure 4.2) were suggested to be dominated by dissolution of Saharan dust [Rickli et al.,

2010]. The consistency of leached Nd-Hf isotope trend between the fine-grained dust of this study and the Saharan dust implies that over a wide range of source rock compositions and ages, as well as geographical locations, aquatic Hf isotope fractionation of dust particles can provide Hf isotope signatures radiogenic enough to match the seawater array. Note that the leachates reflect Hf isotope signatures released during weathering of large-scale averaged upper continental crust (in our case represented by the dust materials). Therefore it is reasonable to assume that Hf isotope signatures released from (large-scale averaged) rivers or shelf sediments are similar to the dust leachates. Our study thus cannot quantitatively distinguish the specific delivery mechanism of Hf-Nd isotopes to the ocean.

For the samples with ε_{Nd} signatures below -13, the Hf isotope compositions of the leachates are more radiogenic than the corresponding value of the seawater array (Figure 4.2). Since the largest difference between the seawater and crustal arrays (least radiogenic Nd isotope compositions, Figure 4.2) also indicates the largest degree of incongruent weathering, it is not surprising that actual leaching of Hf isotope signatures from older continental rocks shows more scatter. Given that the least radiogenic Hf isotope signatures of seawater have been found in the Labrador Sea [Rickli et al., 2009] which is surrounded by cold and glacial weathering input, it may be that weathering in such an environment is more congruent [van de Flierdt et al., 2002]. It is also likely that the rocks of Northern Canada surrounding the Labrador Sea region had an evolution history different from the old cratons in North China, resulting in different mineralogical composition and thus a different degree of aquatic Hf isotope fractionation in these two regions.

The leachate data clearly and robustly indicate that no "extra" radiogenic Hf is necessary to produce the observed seawater array. Thus, contributions from hydrothermal Hf sources are probably negligible for the global seawater Hf budget.

4.5 Implications for Nd and Hf isotopes as oceanographic and provenance tracers

The exchangeable fractions of continental particles or their preformed coatings either enter seawater via eolian or riverine transport. On the continental shelf, such a preformed leachable component may become the source of "boundary exchange", a process proposed in previous studies [Lacan and Jeandel, 2005].
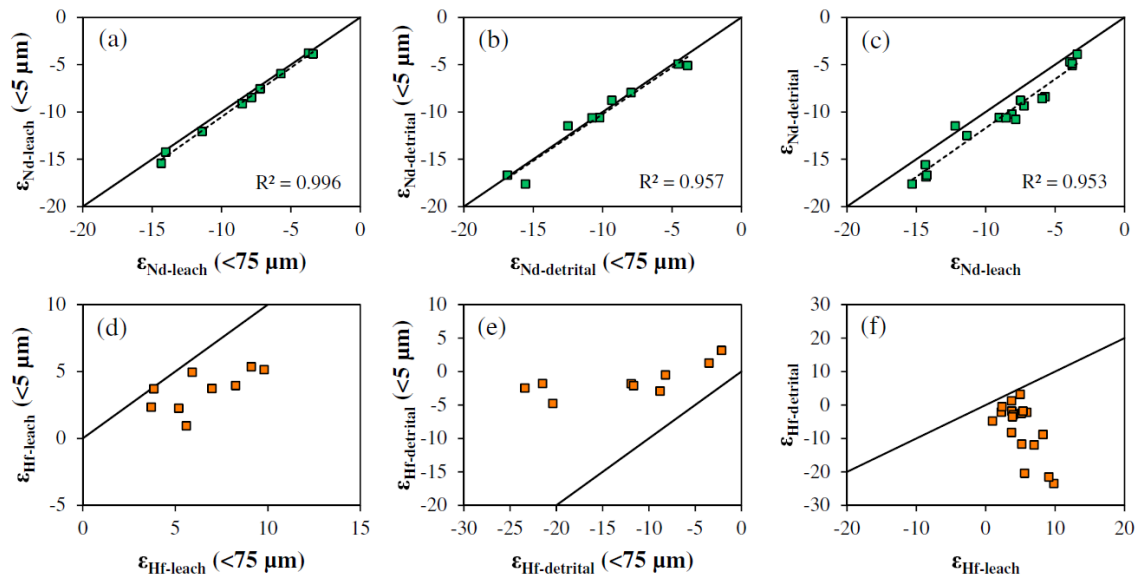
Figure 4.3 Hafnium and Nd isotope relationships in the dust leachates and corresponding detrital fractions of different grain sizes. (a) ε_{Nd} of <75 μm leachates versus <5 μm leachates; (b) ε_{Nd} of <75 μm detritals versus <5 μm detritals; (c) ε_{Nd} of leachates versus detritals; (d) ε_{Hf} of <75 μm leachates versus <5 μm leachates; (e) ε_{Hf} of <75 μm detritals versus <5 μm detritals; and (f) ε_{Hf} of leachates versus detritals. The solid lines represent 1 to 1 relationships.

Due to the small Sm/Nd fractionation in different minerals [Bayon et al., 2006], the negligible fractionation of Nd isotopes between coarse and fine grain sizes of the detrital material (Figure 4.3b) is not surprising. Leaching of the dust particles, in contrast, appears to produce small but systematically more radiogenic Nd isotope signatures than the corresponding silicate dust fractions (Figure 4.3c) although no fractionation is observed between the fine and corresponding coarse grain size leachates (Figure 4.3a).

Given that stable isotope fractionation cannot cause such a difference and that the good correlation in Figure 4.3c precludes external sources, our preferred explanation is that this pattern reflects the time integrated effect of slightly higher Sm/Nd in the leachable component during past weathering/sedimentary cycles. For example, the typical MREE enrichments during aquatic natural leaching of dust [Thiagarajan and Lee, 2004] would lead to a higher Sm/Nd ratio of the mobile component (e.g., preformed Fe-Mn coatings) than that of the silicate residue. Nevertheless, it is possible that the slightly more radiogenic leaching Nd signal only represents mean state upper continental crust weathering especially in the mid to low latitudes, while recently glacially eroded rocks/till may yield less radiogenic Nd isotope compositions of the leachates than the bulk silicates in a cold climate [Andersson et al., 2001].

Hafnium isotope fractionation during mineral sorting and leaching is significantly larger than that of Nd isotopes. Overall, the Hf isotope fractionation between leachates and corresponding detrital material is larger the older the source rocks are (i.e., less radiogenic Nd isotopes, Figure 4.2), reflecting time integrated effect of Hf isotopic differences between different minerals. The Hf isotope signatures of the <5 μm silicate (Figure 4.2) are close to the seawater array (though still not radiogenic enough). Interestingly, in marine settings, essentially all detrital sediments fall below the seawater array [Bayon et al., 2009; Vervoort et al., 1999, 2011, Figure 4.2]. Given that the <5 μm size samples in this study are already close to the lowest size range observable in natural sediments and are also expected to have experienced maximum heavy mineral loss during weathering and transport (including zircon), we propose that the <5 μm size fraction reflects the upper limit of Hf isotope fractionation due to zircon loss. Furthermore, the <5μm fractions (Figure 4.2) are close but still systematically more radiogenic in Hf isotope composition than the 'zircon-free sediment array' [Bayon et al., 2009]. This implies that the marine fine-grained sediments on average, though clearly depleted in zircons, may not be completely "zircon-free".

Surprisingly, Hf isotopes are systematically more radiogenic in the leachates of the coarse grain size fraction than of their fine counterparts (Figure 4.3b). Given that the leachable component is not necessarily the product of current weathering in the arid

deserts, one explanation is that the <5 um particles may mainly come from a more deeply weathered environment than the large particles (<75 um). These <5 um particles would thus have the potential of receiving somewhat higher contributions from zircon weathering. However, such an explanation is unlikely since Nd isotope compositions of the fine and coarse particles are essentially identical. Therefore, our data imply that incongruent weathering of minerals other than zircon are also important for Hf isotope fractionation during aquatic leaching of UCC rocks and consequently in the formation of Nd-Hf seawater array, which is consistent with recent studies [Bayon et al., 2006, 2009; Rickli et al., 2009; Chen et al., 2011]. Unfortunately, the exact contribution of different minerals to the Hf isotope fractionation is unknown and remains to be studied in detail before an unequivocal explanation for this grain size effect on Hf isotopes can be provided.

Recent direct water mass studies on dissolved Hf isotopes have indicated that Hf isotopes are not a sensitive water mass tracer due to their limited isotopic variability in the oceanic water column [Stichel et al., 2012]. Early studies on Fe-Mn crusts [van de Flierdt et al., 2004] and a recent study on authigenic sediment fractions form the Arctic Ocean [Chen et al., 2012], however, still showed a broad positive correlation between evolution of Hf isotopes and Nd isotopes in seawater, which is also reflected by the well constrained seawater array. As shown in Figure 4.2, it is evident that there is a large range in the leached Hf isotope compositions from the same rocks which essentially prevents clear identification of source rocks from the dissolved Hf isotope composition of seawater. Consequently dissolved seawater Hf isotope signatures and their records in authigenic sediment fractions will be most useful in distinguishing different modes of weathering regimes on land or even changes in runoff [Rickli et al., 2013].

References

Albarède, F., A. Simonetti, J. D. Vervoort, J. Blichert-Toft, and W. Abouchami (1998), A Hf-Nd isotopic correlation in ferromanganese nodules, *Geophys. Res. Lett.*, *25*(20), 3895-3898.

Amakawa, H., K. Sasaki, and M. Ebihara (2009), Nd isotopic composition in the central North Pacific, *Geochim. Cosmochim. Acta.*, *73*(16), 4705-4719.

Andersson, P. S., R. Dahlqvist, J. Ingri, and O. Gustafsson (2001), The isotopic composition of Nd in a boreal river: A reflection of selective weathering and colloidal transport, *Geochim. Cosmochim. Acta.*, *65*(4), 521-527.

Bau, M., and A. Koschinsky (2006), Hafnium and neodymium isotopes in seawater and in ferromanganese crusts: The "element perspective", *Earth Planet. Sci. Lett.*, *241*(3-4), 952-961.

Bayon, G., C. R. German, K. W. Burton, R. W. Nesbitt, and N. Rogers (2004), Sedimentary Fe–Mn oxyhydroxides as paleoceanographic archives and the role of aeolian flux in regulating oceanic dissolved REE, *Earth Planet. Sci. Lett.*, *224*(3–4), 477-492.

Bayon, G., N. Vigier, K. W. Burton, A. Brenot, J. Carignan, J. Etoubleau, and N. C. Chu (2006), The control of weathering processes on riverine and seawater hafnium isotope ratios, *Geology*, *34*(6), 433-436.

Bayon, G., K. W. Burton, G. Soulet, N. Vigier, B. Dennielou, J. Etoubleau, E. Ponzevera, C. R. German, and R. W. Nesbitt (2009), Hf and Nd isotopes in marine sediments: Constraints on global silicate weathering, *Earth Planet. Sci. Lett.*, *277*(3-4), 318-326.

Chen, J., and G. J. Li (2011), Geochemical studies on the source region of Asian dust, *Sci. China Earth Sci.*, *54*(9), 1279-1301.

Chen, J., G. J. Li, J. D. Yang, W. B. Rao, H. Y. Lu, W. Balsam, Y. B. Sun, and J. F. Ji (2007), Nd and Sr isotopic characteristics of Chinese deserts: Implications for the provenances of Asian dust, *Geochim. Cosmochim. Acta.*, *71*(15), 3904-3914.

Chen, T.-Y., H.-F. Ling, M. Frank, K.-D. Zhao, and S.-Y. Jiang (2011), Zircon effect alone insufficient to generate seawater Nd-Hf isotope relationships, *Geochem. Geophys. Geosyst.*, *12*(5), Q05003, doi: 10.1029/2010gc003363.

Chen, T.-Y., M. Frank, B. A. Haley, M. Gutjahr, and R. F. Spielhagen (2012), Variations of North Atlantic inflow to the central Arctic Ocean over the last 14 million years inferred from hafnium and neodymium isotopes, *Earth Planet. Sci. Lett.*, *353–354*(0), 82-92.

Firdaus, M. L., T. Minami, K. Norisuye, and Y. Sohrin (2011), Strong elemental fractionation of Zr-Hf and Nb-Ta across the Pacific Ocean, *Nat. Geosci.*, *4*(4), 227-230.

Godfrey, L. V., D. C. Lee, W. F. Sangrey, A. N. Halliday, V. J. M. Salters, J. R. Hein, and W. M. White (1997), The Hf isotopic composition of ferromanganese nodules and crusts and hydrothermal manganese deposits: Implications for seawater Hf, *Earth Planet. Sci. Lett.*, *151*(1-2), 91-105.

Godfrey, L. V., B. Zimmermann, D. C. Lee, R. L. King, J. D. Vervoort, R. M. Sherrell, and A. N. Halliday (2009), Hafnium and neodymium isotope variations in NE Atlantic seawater, *Geochem. Geophys. Geosyst.*, *10,* doi: 10.1029/2009GC002508.

Lacan, F., and C. Jeandel (2005), Neodymium isotopes as a new tool for quantifying exchange fluxes at the continent-ocean interface, *Earth Planet. Sci. Lett.*, *232*(3-4), 245-257.

Li, G. J., J. Chen, J. F. Ji, J. D. Yang, and T. M. Conway (2009), Natural and anthropogenic sources of East Asian dust, *Geology*, *37*(8), 727-730, doi: 10.1130/G30031a.1.

Patchett, P. J., W. M. White, H. Feldmann, S. Kielinczuk, and A. W. Hofmann (1984), Hafnium Rare-Earth Element Fractionation in the Sedimentary System and Crustal Recycling into the Earths Mantle, *Earth Planet. Sci. Lett.*, *69*(2), 365-378.

Pettke, T., A. N. Halliday, and D. K. Rea (2002), Cenozoic evolution of Asian climate and sources of Pacific seawater Pb and Nd derived from eolian dust of sediment core LL44-GPC3, *Paleoceanography*, *17*(3), doi: 10.1029/2001PA000673.

Ren, J. (1996), The continental tectonics of China, *J. Southeast Asian Earth Sci.*, *13*(3–5), 197-204.

Rickli, J., M. Frank, and A. N. Halliday (2009), The hafnium-neodymium isotopic composition of Atlantic seawater, *Earth Planet. Sci. Lett.*, *280*(1-4), 118-127.

Rickli, J., M. Frank, A. R. Baker, S. Aciego, G. de Souza, et al. (2010), Hafnium and neodymium isotopes in surface waters of the eastern Atlantic Ocean: Implications for sources and inputs of trace metals to the ocean, *Geochim. Cosmochim. Acta.*, *74*(2), 540-557.

Rickli, J., M. Frank, T. Stichel, R. B. Georg, D. Vance, and A. N. Halliday (2013), Controls on the incongruent release of hafnium during weathering of metamorphic and sedimentary catchments, *Geochim. Cosmochim. Acta.*, *101*(0), 263-284.

Stichel, T., M. Frank, J. Rickli, and B. A. Haley (2012), The hafnium and neodymium isotope composition of seawater in the Atlantic sector of the Southern Ocean, *Earth Planet. Sci. Lett.*, *317–318*(0), 282-294.

Thiagarajan, N., and C. T. A. Lee (2004), Trace-element evidence for the origin of desert varnish by direct aqueous atmospheric deposition, *Earth Planet. Sci. Lett.*, *224*(1-2), 131-141.

van de Flierdt, T., M. Frank, D. C. Lee, and A. N. Halliday (2002), Glacial weathering and the hafnium isotope composition of seawater, *Earth Planet. Sci. Lett.*, *198*(1-2), 167-175.

van de Flierdt, T., M. Frank, D. C. Lee, A. N. Halliday, B. C. Reynolds, and J. R. Hein (2004), New constraints on the sources and behavior of neodymium and hafnium in seawater from Pacific Ocean ferromanganese crusts, *Geochim. Cosmochim. Acta.*, *68*(19), 3827-3843.

van de Flierdt, T., S. L. Goldstein, S. R. Hemming, M. Roy, M. Frank, and A. N. Halliday (2007), Global neodymium-hafnium isotope systematics - revisited, *Earth Planet. Sci. Lett.*, *259*(3-4), 432-441.

Vervoort, J. D., T. Plank, and J. Prytulak (2011), The Hf-Nd isotopic composition of marine sediments, *Geochim. Cosmochim. Acta.*, *75*(20), 5903-5926.

Vervoort, J. D., P. J. Patchett, J. Blichert-Toft, and F. Albarede (1999), Relationships between Lu-Hf and Sm-Nd isotopic systems in the global sedimentary system, *Earth Planet. Sci. Lett.*, *168*(1-2), 79-99.

White, W. M., J. Patchett, and D. Benothman (1986), Hf Isotope ratios of marine-sediments and Mn Nodules - evidence for a mantle source of Hf in seawater, *Earth Planet. Sci. Lett.*, *79*(1-2), 46-54.

Zimmermann, B., D. Porcelli, M. Frank, P. S. Andersson, M. Baskaran, et al. (2009), Hafnium isotopes in Arctic Ocean water, *Geochim. Cosmochim. Acta.*, *73*(11), 3218-3233.

Chapter 5

Contrasting geochemical cycling of hafnium and neodymium in the central Baltic Sea

Abstract

The central Baltic Sea is a marginal brackish basin which comprises anoxic bottom waters and is surrounded by geological source terrains with a wide variety of compositions and ages. This allows the investigation of water mass mixing using radiogenic isotope compositions of Nd and Hf as well as their geochemical cycling across varying redox conditions in the water column. In this study, we present the distribution of Nd and Hf concentrations and their isotopic compositions for 6 depth profiles and 3 surface water sites obtained during a cruise in the central Baltic Sea onboard the RV Oceania as a part of the international GEOTRACES program.

The results obtained indicate that Nd isotopes effectively trace the mixing between more radiogenic saline waters from the south and unradiogenic fresh waters from the north, which helps to understand the reliability of Nd isotopes as water mass tracer in the open ocean. In surface waters, Nd shows higher concentrations and less radiogenic isotope compositions at the northern stations, which are progressively diluted and become more radiogenic to the south, consistent with the counterclockwise circulation pattern of central Baltic Sea surface waters. In contrast to the variable Nd concentrations, Hf shows much less variability. At the Gotland Deep station, the Nd concentrations of the euxinic waters are higher by a factor >10 than those of the overlying oxygen-depleted waters, whereas Hf only shows small concentration variations, which indicates faster removal of Hf from the water column than of Nd. Moreover, the dissolved Hf isotope signatures document great variability but no consistent mixing trends. Our explanation is that Hf has a lower residence time than Nd, and also that the Hf isotope signatures of the sources are highly heterogenous, which is attributed to their differing magmatic and tectonic histories and incongruent post-glacial weathering around the central Baltic Sea.

5.1 Introduction

Combined Nd and Hf isotope compositions of seawater have been used for tracing present and past ocean circulation, as well as continental weathering inputs (e.g., Lee et al., 1999; Piotrowski et al., 2000; David et al., 2001; van de Flierdt et al., 2002). With a mean oceanic residence time of several hundred years (Arsouze et al., 2009; Rempfer et

al., 2011), Nd is considered a quasi-conservative tracer for water mass mixing (e.g. von Blanckenburg, 1999; Frank, 2002, Goldstein et al., 2003). Seawater Nd is supplied via boundary exchange with shelf sediments (Amakawa et al., 2000; Lacan and Jeandel, 2001, 2005; Tachikawa et al., 2003), dust dissolution and riverine inputs, whereas hydrothermal contributions have been suggested to be negligible (German et al., 1990; Halliday et al., 1992). In the oceanic water column, Nd undergoes reversible scavenging by particles (Bertram and Elderfield, 1993; Sholkovitz et al., 1994; Nozaki and Alibo, 2003) resulting in a progressive increase of dissolved Nd concentrations with depth (Siddall et al., 2008; Arsouze et al., 2009; Oka et al., 2009; Rempfer et al., 2011). In contrast, the marine geochemistry of Hf is much less well constrained, and only a few Hf isotopic data of dissolved continental inputs are available (Bayon et al., 2006; Godfrey et al., 2009; Zimmermann et al., 2009a; Rickli et al., 2013). Estimates of the present day mean residence time of Hf in the global ocean range from a few hundred years (comparable to or shorter than that of Nd) to several thousand years (and thus longer than the global ocean mixing time) (Godfrey et al., 1996, 2008, 2009; Rickli et al., 2009, 2010; Zimmermann et al., 2009a, 2009b; Firdaus et al., 2011). Moreover, Hf cycling in the water column is also poorly understood. Open ocean Hf has been reported to have slightly higher concentrations in deep waters than in the surface mixed layer (Rickli et al., 2009; Zimmermann et al., 2009b; Stichel et al., 2012a), indicating that Hf experiences biogeochemical cycling similar to Nd. However, a previous study also hypothesized that Hf in seawater may be dominantly associated with colloidal Fe oxides rather than Mn oxides or truly dissolved species ($Hf(OH)_5^{-1}$) (Bruland, 1983; Byrne, 2002). In contrast, dissolved Nd speciation in the open ocean is dominated by $NdCO_3+$, $Nd(CO_3)_2-$, and a fraction bound to colloids (both negatively and positively charged, Byrne 2002; Dahlqvist et al., 2005; Bau and Koschinsky, 2006).

The central Baltic Sea is a strongly stratified shallow brackish basin with a number of areas where bottom waters are permanently anoxic (e.g., Hansson et al., 2009), and where intense cycling of organic material and redox sensitive elements such as Fe and Mn occurs. Since the sink of both Nd and Hf from seawater is most likely closely related to Fe/Mn hydroxides and organic species (e.g., Ingri et al., 2000; Bau and Koschinsky, 2006), the central Baltic Sea is ideal to investigate Nd-Hf geochemical cycling in the

water column. In addition, as a semi-enclosed basin dominated by continental inputs (i.e., no hydrothermal contributions), combined dissolved Nd-Hf isotope compositions from the Baltic Sea provide direct weathering signatures from the continent and thus will contribute to understanding how the seawater Nd-Hf isotope relation (e.g., Albarède et al., 1998) is generated.

In an early study (with one reported station in the central Baltic Sea), Andersson et al. (1992) showed that Nd isotopes in the Gulf of Bothnia are significantly less radiogenic than Atlantic-derived waters from the southern Baltic Sea. In addition, Nd concentrations were found to be enriched in anoxic bottom waters, consistent with other studies on REE distributions in anoxic water bodies (e.g., German et al., 1991). In this study, we analyzed Hf and Nd isotopic compositions and concentrations of 6 depth profiles and 3 surface sites in the central Baltic Sea (Figure 5.1). In particular, a high resolution profile (20-30 m sampling interval across the redoxcline) of the Gotland Deep is presented to investigate Nd and Hf cycling at the oxic-anoxic interface. These data represent the first systematic investigation of the distribution of combined Hf-Nd concentrations and isotope compositions in a marginal ocean basin.

5.2 Hydrographic and geological background

The semi-enclosed central Baltic Sea is characterized by salinities ranging between 5 to 8 psu at the surface and 10 to 14 psu in bottom waters (mostly shallower than 250 m), with a counterclockwise circulation (Figure 5.1) (Meier, 2007). It is one of the largest brackish water bodies on Earth. Saline and dense inflow from the Atlantic (about 16,100 m^3/s) spills over the shallow sills of the Kattegat and then largely transforms into bottom waters when enters the central Baltic Sea (Meier, 2007; Reissmann et al. 2009). Freshwater is supplied by rivers and precipitation to the surface mixed layer. This estuarine circulation system promotes stable stratification of the water column and widespread anoxia in bottom waters (e.g., Hansson et al., 2009; Reissmann et al. 2009). In the central Baltic Sea, the halocline is at 40-80 m depth, coinciding with a sharp decrease in oxygen content. The ventilation of the major central Baltic anoxic bottom water bodies (i.e. the Gotland Deep, the Landsort Deep) only occurs episodically, via strong and fast intrusions

of oxygen-rich and saline North Sea-derived water, i.e. once per several years. The latest major ventilation event occurred in 2003 (Feistel et al., 2003). Northward advection of saline deep water into the Gulf of Bothnia is prevented by a sill between the central Baltic Sea and the Aland Sea, resulting in the restriction of water mass exchange between these two basins.
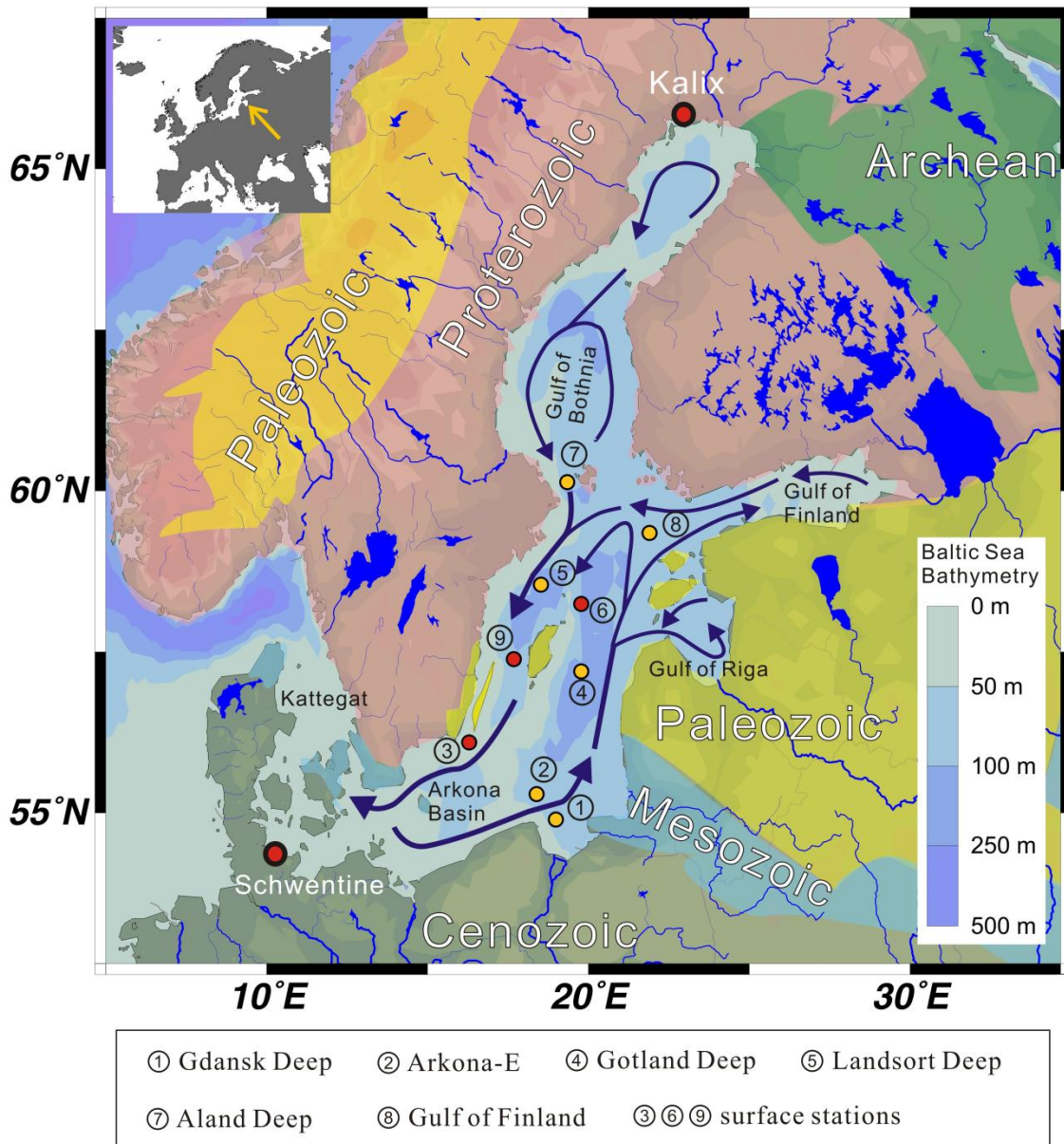
Figure 5.1 Map illustrating the sampling locations of the GEOTRACES cruise on R/V Oceania in the central Baltic Sea in November 2011, as well as the river water sampling locations (generated using Ocean Data View, Schlitzer, 2012). Red dots represent surface water stations whereas yellow dots represent depth profile stations. Also shown is the simplified geology of the continental area surrounding the Baltic Sea (after Kuhlmann et al., 2004).

The modern catchment area of the Baltic Sea (Figure 5.1) includes a wide range of geological source terrains from Cenozoic sedimentary rocks in the south to the very old Proterozoic and Archean rocks of northern Scandinavia (e.g., Gaál and Gorbatschev, 1987; Mansfeld, 2001; Kuhlmann et al., 2004; Bock et al., 2005). The rivers that drain the Paleozoic, Proterozoic, and Archean terrains mostly flow into the Gulf of Bothnia or the Gulf of Finland, while rivers draining younger terrains are restricted to the southern Baltic Sea (Figure 5.1). Neodymium and hafnium concentrations as well as isotope compositions of two rivers (Schwentine and Kalix) were measured for reference in this study. The Schwentine river is a small river in northern Germany with a length of only about 62 kilometres. Its catchment area (Schwentine basin) is part of the lowlands of northern Germany, which have been affected by the active land-based Scandinavian glaciers during the Middle and Late Pleistocene (Piotrowski, 1997). The topmost layer of the Schwentine basin consists of sediments deposited during the Holocene and the last glacial stage, while the unconsolidated subsurface layers largely consist of glaciolacustrine or lacustrine sands and clays deposited during earlier glacial stages (e.g., Marine Isotope Stages 6 and 12, Piotrowski, 1997). In contrast, the major part of the basement of the Kalix river system consists of Precambrian intermediate and basic volcanic rocks and granitoids (Gaál and Gorbatschev, 1987). However, bedrock exposure represents less than 1% of this area, which is mainly covered by coniferous forests and peatlands. The soils are dominated by podosols developed on tills, which likely formed after the retreat of the last glaciers from this area during the early Holocene (i.e., around 9 ky before present, Lundqvist, 1986).

5.3 Sampling and methods

Water samples were collected in the central Baltic Sea at 6 depth profiles and 3 surface water sites during the GEOTRACES cruise on RV Oceania in November 2011. Stichel et al. (2012a, b) provided a detailed description of the sampling procedures, REE/Hf pre-concentration, chromatography, and mass spectrometric measurements. We will therefore only briefly describe these here given that we basically followed the same protocols in the same laboratory at GEOMAR, Kiel, which are identical to the agreed GEOTRACES protocols (http://www.obs-vlfr.fr/GEOTRACES/libraries/documents/Intercalibration/

Cookbook.pdf). Sixty liters of seawater were taken using 3 acid-cleaned 20 L LDPE-collapsible cubitainers for each sample. Immediately after collection, samples were filtered through 0.45 μm nitro-cellulose acetate filters. The two river water samples were taken from the Kalix river, Sweden, in June 2012 and the Schwentine river, Germany in July 2012. Both samples were very rich in particles. The Kalix river is characterized by low concentrations of suspended detrital particles but relatively high concentrations of organic and Fe-oxyhydroxide particles (Ingri et al., 2000). While the Schwentine sample was filtered immediately, the filtration of Kalix river water was delayed for about two months after collection. Thus, the measured concentrations are likely to be lower than directly after sampling due to adsorption processes. After filtration, all the samples were acidified to pH = ~2 using distilled concentrated HCl. For precise laboratory-based concentration measurements of Hf and Nd, 2 L aliquots of the filtered and acidified samples were kept separately in clean PE-bottles. Hafnium and neodymium of large volume seawater samples for isotopic measurement were pre-concentrated on board by co-precipitation with Fe-hydroxide (see details in Stichel et al., 2012a) at a pH of 8 to 9 through addition of super-pure ammonia.

To further reduce the amount of major elements (e.g., Mg), the precipitates for the isotope measurement were re-dissolved and precipitated at lower pH (7.0 - 8.0) prior to element purification in the laboratory. The precipitates were then centrifuged and rinsed with deionised water (MilliQ system), and finally transferred into teflon vials. Subsequently, the samples were treated with aqua regia to destroy organic matter and were then dissolved in 6 M HCl. A back extraction method using a diethyl ether phase

was applied to remove the large amounts of Fe while keeping Hf and Nd dissolved in an acidic phase. Hafnium and Nd were then separated and purified following the established methods of Stichel et al. (2012a, b). Procedural blanks for Nd and Hf isotopes were less than 1% of the sample amounts.

For Hf and Nd concentration analyses, about 0.5 L of water was taken from the 2 L aliquot samples. Pre-weighed ^{178}Hf single spike and ^{150}Nd spike solutions were added to each sample (e.g., Rickli et al., 2009). After 4 – 5 days of isotopic equilibration, the samples were co-precipitated with Fe-hydroxide at pH 7 to 8. Further separation of Hf and Nd was carried out by cation chromatography (1.4 ml resin bed, BIORAD® AG50W-X8, 200–400 mesh-size). Duplicate samples for Nd concentrations of subsurface water were processed about one month later than the first batch of measurements, and yielded an external reproducibility of better than 1%. Due to the limited amount of Hf spike available in our laboratory, no duplicate samples for Hf concentrations were analyzed. The reproducibility of Hf concentration measurements reported by Stichel et al. (2012a, b) from the same laboratory was 3%-10% depending on concentrations. Procedural blanks for concentration measurements were 14-23 pg for Nd and 6-8 pg for Hf (n=2), which has been applied to the sample concentration corrections.

Hafnium and Nd isotope ratios were measured on a Nu instruments MC-ICP-MS at GEOMAR, Kiel. Instrumental mass bias was corrected using a ^{146}Nd/^{144}Nd ratio of 0.7219 and a ^{179}Hf/^{177}Hf ratio of 0.7325, applying an exponential mass fractionation law. Concentrations of the Nd and Hf standards measured during each session were adjusted to be similar to those of the samples. All ^{176}Hf/^{177}Hf results were normalized to JMC475=0.282160 (Nowell et al., 1998) while all ^{143}Nd/^{144}Nd results were normalized to JNdi-1=0.512115 (Tanaka et al., 2000). The 2σ external reproducibility deduced from repeated measurements of the Hf and Nd isotope standards at concentrations similar to those of the samples was ±1.30 and ±0.30 epsilon units, respectively. Some seawater samples still contained a considerable amount of Yb (i.e., up to 1.98% contribution on mass 176), which cannot be adequately corrected by applying the exponential mass fractionation factor derived from ^{179}Hf/^{177}Hf and the commonly accepted Yb isotope ratios (Chu et al., 2002). Therefore, we adopted a Yb-doped JMC475 standard calibration

method for all of the seawater samples, in order to precisely correct the Yb contribution (Stichel et al., 2012a). The extra corrections (i.e., after the standard internal mass fractionation correction using $^{179}Hf/^{177}Hf$) of the seawater samples based on Yb-doping never exceeds 3.2 ε_{Hf} units. Given that the changes of the Hf isotope compositions of the differently doped JMC475 standards were linearly correlated (R^2=0.97) with the Yb contribution, this additional correction method is considered to provide reliable results.
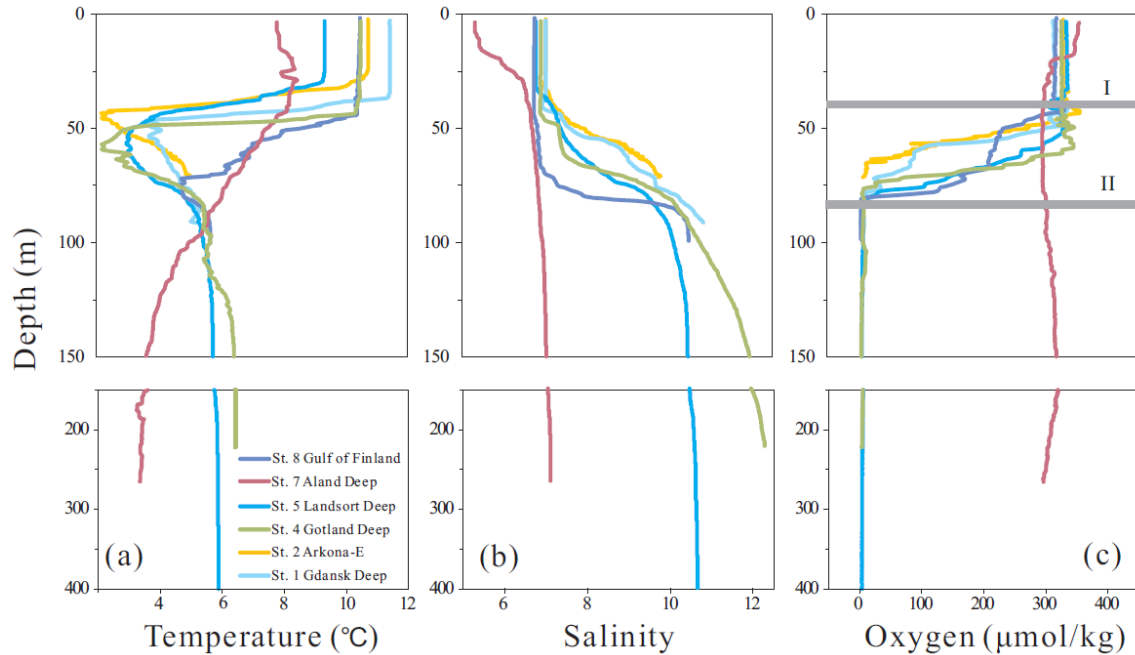
Figure 5.2 Temperature (a), salinity (b), and oxygen concentration (c) of the studied depth profiles. (I): boundary between the mixed layer and the subsurface halocline layer (~40 m water depth); (II) boundary between the subsurface halocline layer and the anoxic layer (~80 m water depth).

5.4 Results

5.4.1 Hydrography and concentrations of Hf and Nd

The hydrographic data of the 6 studied depth profiles obtained during the RV Oceania cruise are presented in Figure 5.2. The cold temperatures near 50 m water depth (Figure 5.2a) correspond to the seasonal thermoclines (stations 1, 2, 4, 5) which are shallower than the corresponding haloclines (Figure 5.2b). From south to north (Figure 5.1), the

deep water salinities become progressively lower (Figure 5.2b). The rapid decreases in oxygen concentrations observed at the other depth profiles roughly coincide with the haloclines, with the only exception of the Aland Deep where strong vertical mixing prevails. (Figure 5.2b, c).

Due to the lack of sulfide concentration data from our cruise, it is difficult to define the exact depth of the euxinia for each depth profile, despite that widespread euxinia in bottom waters of the central Baltic Sea during periods of prolonged stagnation have been reported (Matthäus et al., 2008). In addition, we only have 2 or 3 samples for most of the depth profiles (except the Gotland Deep). Any further subdivision of the anoxic layers has thus not been attempted for most stations and would also not substantially contribute to the results of our study. Only anoxic waters of Gotland Deep profile (where high resolution sampling was performed) will be further divided into an "oxygen-depleted" layer and a "euxinic" layer (see Section 5.5.3.1 for details).

Hafnium and neodymium concentration data obtained during the cruise in the central Baltic Sea are shown in Table 5.1 and Figure 5.3. Overall, Nd concentrations in surface water (upper 5 m water depth) of stations 1 - 4 are slightly lower than those of stations 5-9, Table 5.1), with a total range from 14.6 - 34.6 pmol/kg. The maximum surface concentration is observed at Aland Deep (station 7), and the minimum is found at Gdansk Deep (station 1). Except the Aland Deep (station 7) and Arkona-E (station 2), the other 5 depth profiles (Figure 5.3) reveal a general increase of Nd concentrations with depth. In particular, Nd concentrations reach a maximum value of 150 pmol/kg in Gotland Deep bottom waters, while the bottom water sample of the Landsort Deep is only moderately enriched in Nd (48.6 pmol/kg). Neodymium enrichments are also observed in bottom waters of the Gulf of Finland (station 8) and the Gdansk Deep (station 1) at a shallower depth (~90-100 m). Moreover, surface Hf concentrations at station 5, 7, and 8 are distinctively higher than the other stations, while the Hf concentrations in the halocline layer are generally lower than the corresponding surface water. In contrast to a total range of Nd concentrations between 14.6 and 150.5 pmol/kg in the central Baltic Sea, Hf concentrations show a significantly smaller variability (0.6 – 1.7 pmol/kg). While a slight increase in Hf concentration is observed in the Gotland Deep profile (from 1.0 pmol/kg at

the surface to 1.5 pmol/kg at 160 m depth), Hf concentrations slightly decreased in bottom waters of Gulf of Finland (from 1.6 at the surface to 1.3 pmol/kg) and of the Landsort Deep (from 1.8 at the surface to 0.9 poml/kg).

5.4.2 Distribution of Hf and Nd isotope compositions

Both Nd and Hf show large isotopic variability in surface waters (Figure 5.3). The Nd isotope compositions become systematically less radiogenic from the Gdansk Deep (ε_{Nd}= -14.4) to the Aland Deep (ε_{Nd}= -17.1) along the counterclockwise pathway of the surface currents. The return flow along the southeastern coast of Sweden becomes more radiogenic towards the south (ε_{Nd}= -16.0, -15.6) but remains less radiogenic than the eastern part of the central Baltic Sea. In contrast, the Hf isotope compositions of the surface waters display a large range, from ε_{Hf} = -5.2 to +4.2 and do not exhibit any clear systematic variations.

In most water column profiles the Nd isotope compositions become progressively more radiogenic with depth (Figure 5.3a). The only exception is the Aland Deep station, which shows invariant Nd isotope signatures. No abrupt changes in Nd isotope compositions are observed at the oxic-anoxic interfaces at the sampled depth resolutions (Figure 5.2, Figure 5.3a). In contrast to the Nd isotope distributions, there are less consistent trends in the Hf isotope profiles (Figure 5.3b). In the Aland Deep, Hf isotope composition becomes less radiogenic with depth (ε_{Hf} +1.2 to -6.9 between 5 and 260 m depth), while Nd isotope compositions are homogeneous (ε_{Nd} around -17.0). Except for the stations at Gdansk Deep and in the Gulf of Finland which remain constant with depth in ε_{Hf}, all other stations show a shift to less radiogenic ε_{Hf} signatures in the same depth range between 5 and 80 m. Unlike the profiles in the Aland and Landsort Deeps, which document a continuous trend to less radiogenic ε_{Hf} signatures towards the bottom of the profiles, the high resolution profile of Gotland Deep reveals an abrupt shift in Hf isotope compositions back to a more radiogenic ε_{Hf} signatures of +1.3 at 110 m depth followed by a sharp negative shift to -2.7 at 130 m. Below 130 m, the Hf isotope compositions stays invariant.

Table 5.1 Hf and Nd concentrations and isotope compositions of samples from the central Baltic Sea and rivers

station No.[a]	Latitude (N)	Longitude (E)	depth (m)	T (°C)	S (psu)	Hf (pmol/kg)	Nd (pmol/kg)	ε_{Nd}[b]	Int. (± 1 SEM)	ε_{Hf}[c]	Int. (± 1 SEM)
central Baltic Sea											
1	54°55'	18°59'	5	11.44	7.04	0.9	14.6	-14.4	±0.08	-3.0	±0.35
1	55°01'	18°59'	90	5.09	10.79	1.4	69.5	-13.5	±0.08	-3.3	±0.35
2	55°19'	18°25'	5	10.75	7.03	1.0	18.5	-15.4	±0.06	3.9	±0.46
2	55°22'	18°22'	80	5.03	9.81	0.6	19.4	-14.3	±0.08	-2.0	±0.42
							19.4[d]				
3	56°06'	16°19'	5			1.0	20.8	-15.6	±0.08	0.8	±0.39
4	57°11'	19°47'	5	10.51	6.91	1.0	23.1	-15.2	±0.10	-0.3	±0.46
4	57°14'	19°59'	80	5.29	9.99	0.9	21.1	-14.3	±0.12	-6.4	±0.74
							21.0[d]				
4	57°14'	19°59'	110	5.68	11.09	0.8	11.9	-13.9	±0.12	1.0	±0.35
							11.9[d]				
4	57°15'	19°55'	130	6.28	11.64	0.9	31.2	-14.1	±0.10	-3.0	±0.35
							31.3[d]				
4	57°15'	19°54'	160	6.43	12.04	1.5	102.0	-13.6	±0.16	-2.5	±0.32
							102.5[d]				
4	57°15'	19°57'	220	6.43	12.28	1.4	150.5	-13.1	±0.35	-2.2	±0.42
							151.0[d]				
5	58°39'	18°24'	60	3.38	8.11	1.2	22.7	-15.3	±0.08	-6.5	±0.28
							22.7[d]				
5	58°40'	18°23'	344	5.88	10.66	0.8	48.6	-14.5	±0.12	-9.1	±0.46
							48.9[d]				
5	58°33'	18°33'	5	9.44	6.79	1.6	23.5	-16.0	±0.12	-4.2	±0.32

6	58°16'	19°46'	5	10.06	6.79	1.1	21.8	-15.3	±0.10	-2.4	±0.35
7	60°05'	19°17'	5	7.99	5.64	1.7	34.6	-17.1	±0.10	0.9	±0.21
7	60°06'	19°21'	60	5.22	6.95	1.3	29.0	-16.8	±0.10	-4.7	±0.28
7	60°08'	19°16'	260	3.37	7.11	1.5	28.1	-16.9	±0.10	-7.2	±0.32
							28.1[d]				
8	59°22'	21°56'	5	10.48	6.75	1.7	21.7	-16.3	±0.12	-5.6	±0.28
8	59°22'	21°59'	98	5.67	10.48	1.3	60.7	-14.7	±0.12	-5.7	±0.28
							60.6[d]				
9	57°24'	17°43'	5			1.1	26.6			-1.1	±0.35
							26.6[d]				
river water											
Kalix	1					12.9	575.5	-25.1	±0.08	16.6	±0.18
Kalix-duplicate sample	1							-25.4	±0.08	15.0	±0.18
Schwentine	1					6.4	17.8	-13.8	±0.10	-10.7	±0.35

a. Referring to Figure 5.1.

b. $\varepsilon_{Nd} = [(^{143}Nd/^{144}Nd)_{sample}/(^{143}Nd/^{144}Nd)_{CHUR} -1]*10^4$; where $(^{143}Nd/^{144}Nd)_{CHUR} = 0.512638$ (Jacobsen and Wasserburg, 1980).

c. $\varepsilon_{Hf} = [(^{176}Hf/^{177}Hf)_{sample}/(^{176}Hf/^{177}Hf_{CHUR})-1]*10^4$; where $(^{176}Hf/^{177}Hf)_{CHUR}=0.282769$ (Nowell et al., 1998).

d. Duplicate sample for Nd concentration measurement.
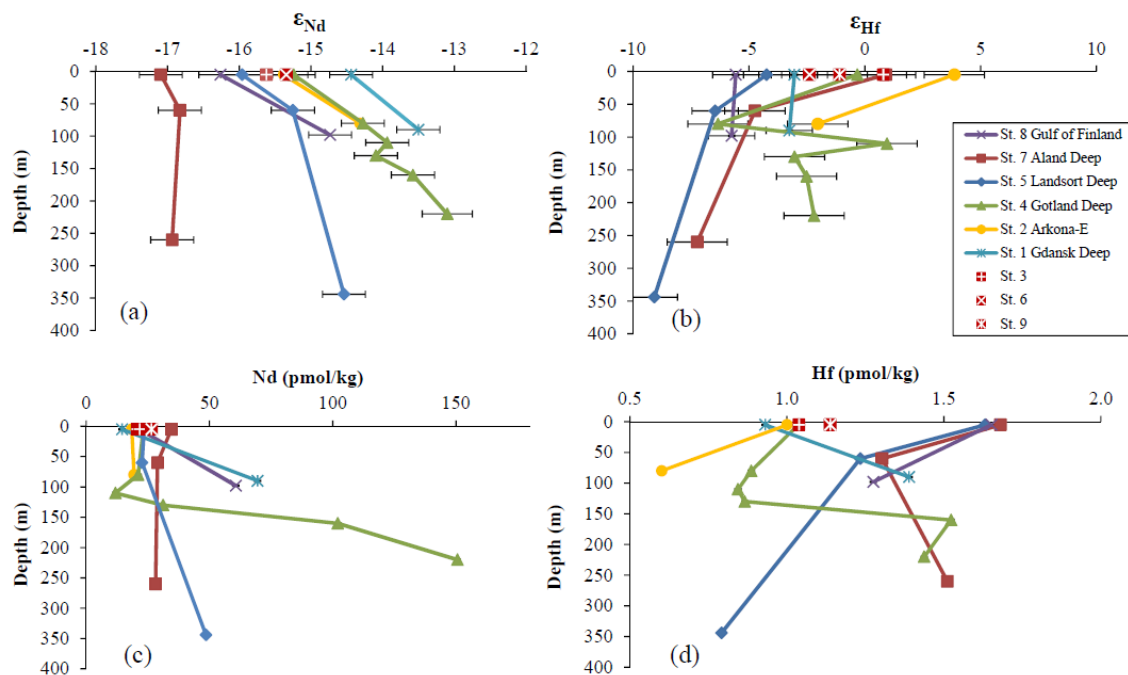
Figure 5.3 Neodymium and hafnium isotope compositions (a, b) and concentrations (c, d), respectively, as a function of water depth in the central Baltic Sea.

5.4.3 Kalix and Schwentine river

Hafnium concentrations in river waters (Kalix: 12.9 pmol/kg, Schwentine: 6.4 pmol/kg) are notably higher than those of Baltic seawater (0.6 to 1.7 pmol/kg) and are in the same range as previously reported concentrations in Arctic rivers (7.6 to 29.6 pmol/kg, Zimmermann et al., 2009a), but are higher than those reported for Alpine rivers (0.05 to 5.3 pmol/kg, Rickli et al., 2013). The ε_{Hf} (+15.0)/ε_{Nd} (-25.4) signatures of the Kalix river sample are exceptionally radiogenic/unradiogenic compared to the Baltic seawater samples, while its Nd isotope composition agrees well with earlier observations during summer months (-24.8 to -26.5 from May to June, Andersson et al., 2001). In contrast, the Hf isotope composition of the Schwentine river is particularly unradiogenic (ε_{Hf}= -10.7), while its Nd isotope composition ($\varepsilon_{Nd=}$ -13.8) is close to that of the southern Baltic surface waters (e.g., Gdansk Deep, -14.4).
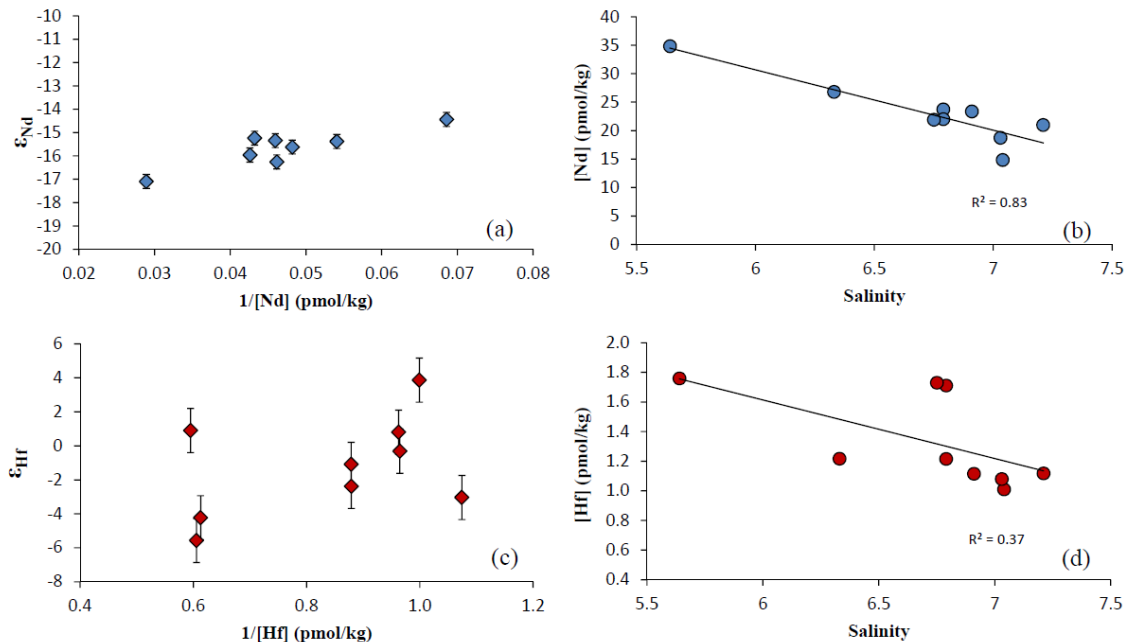
Figure 5.4 Neodymium and hafnium relationships of surface waters. (a) ε_{Nd} versus reciprocal Nd concentrations, (b) Nd concentrations versus salinity, (c) ε_{Hf} versus reciprocal Hf concentrations, (d) Hf concentrations versus salinity. Solid lines represent linear regressions of the concentration data.

5.5 Discussion

5.5.1 Processes controlling Hf and Nd isotope compositions of surface waters

Freshwater inputs to the Baltic Sea are dominated by river discharge. About 80% of the continental runoff originates from catchment areas around the Gulf of Bothnia, the Gulf of Finland, and the Gulf of Riga (Figure 5.1, Graham, 2000), thus controlling the north-south surface water salinity gradient of the central Baltic Sea. Correspondingly, the surface waters at the location of the Aland Deep are the freshest of our dataset (5.64) and show the highest Nd and Hf concentrations (Figures 5.3b and 5.3d), which is consistent with the high Hf and Nd concentrations observed in the Kalix River. The unradiogenic Nd isotope signature at this location is due to weathering inputs from the Precambrian basement rocks of the northern terrains, which is supported by the low ε_{Nd} of the Kalix

river sample. Towards the south, Nd concentrations linearly decrease with increasing salinity, accompanied by more radiogenic Nd isotope signatures. The processes controlling the Nd isotope compositions in the surface ocean of the southern Baltic Sea are complicated by strong vertical mixing (e.g., at Arkona Basin, Meier, 2007; Reissmann et al. 2009) and weathering contributions supplied from different southern source terrains (e.g., Cenozoic-Mesozoic sedimentary or volcanic rocks). Nevertheless, the central Baltic surface Nd concentration and isotope data are well explained by quasi-conservative mixing between southern and northern source waters, as demonstrated by the correlations between ε_{Nd} and 1/[Nd], as well as of Nd concentration and salinity (Figure 5.4a, b). This implies that the Nd inputs to the central Baltic surface waters can be grouped into two distinct sources: the old and unradiogenic source rocks in the north and the young and radiogenic ones in the south (including both local weathering inputs and supply of Atlantic water), consistent with the geological framework presented in Figure 5.1. In addition, considering the close association of surface water Nd isotope variations with the natural source inputs, anthropogenic contamination should have negligible influence on the geochemical cycling of Nd in the central Baltic Sea.

In contrast to Nd, the scatter of the Hf concentrations and isotopic compositions compared to salinity (Figures 5.3c, d) confirms the heterogeneous distribution of Hf isotope compositions in central Baltic Sea surface waters, excluding a simple binary mixing system comparable to the one observed for Nd. In view of the very large difference in the Hf isotope composition of the Kalix and Schwentine rivers, we suggest that the behavior of Hf in surface waters is most likely caused by highly variable Hf isotope signatures (e.g., due to incongruent weathering) supplied by different rivers, combined with a shorter residence time of Hf than of Nd.

If we extrapolate the Nd concentrations to a salinity of zero (Figure 5.4b), a fresh water endmember with a Nd concentration of about 94 pmol/kg is obtained which is significantly lower than that of the Kalix river water sample (576 pmol/kg). This implies that a large fraction of the fresh water Nd (85% of the Kalix river Nd) is lost in the estuarine system, which is in good agreement with previous observations (e.g., Lawrence and Kamber, 2006). A similar extrapolation in Figure 5.4d results in a fresh water

endmember Hf concentration of about 4 pmol/kg (30% of the Kalix river Hf concentration). In comparison, Godfrey et al., 2008 reported a ~50% of dissolved Hf removal during mixing in the Hudson river estuary. It appears that there is less Hf loss from fresh water during the estuarine mixing and/or more reworking and release of Hf from the shelf sediments, and thus a more efficient transfer of local signatures to the Baltic compared with Nd. Nevertheless, we are aware that one single data point from Kalix River and the poor correlation in Figure 5.4d essentially prevent a confident extrapolation of the Hf concentrations. More studies on Hf behavior in estuarine systems are needed before robust conclusions can be drawn.
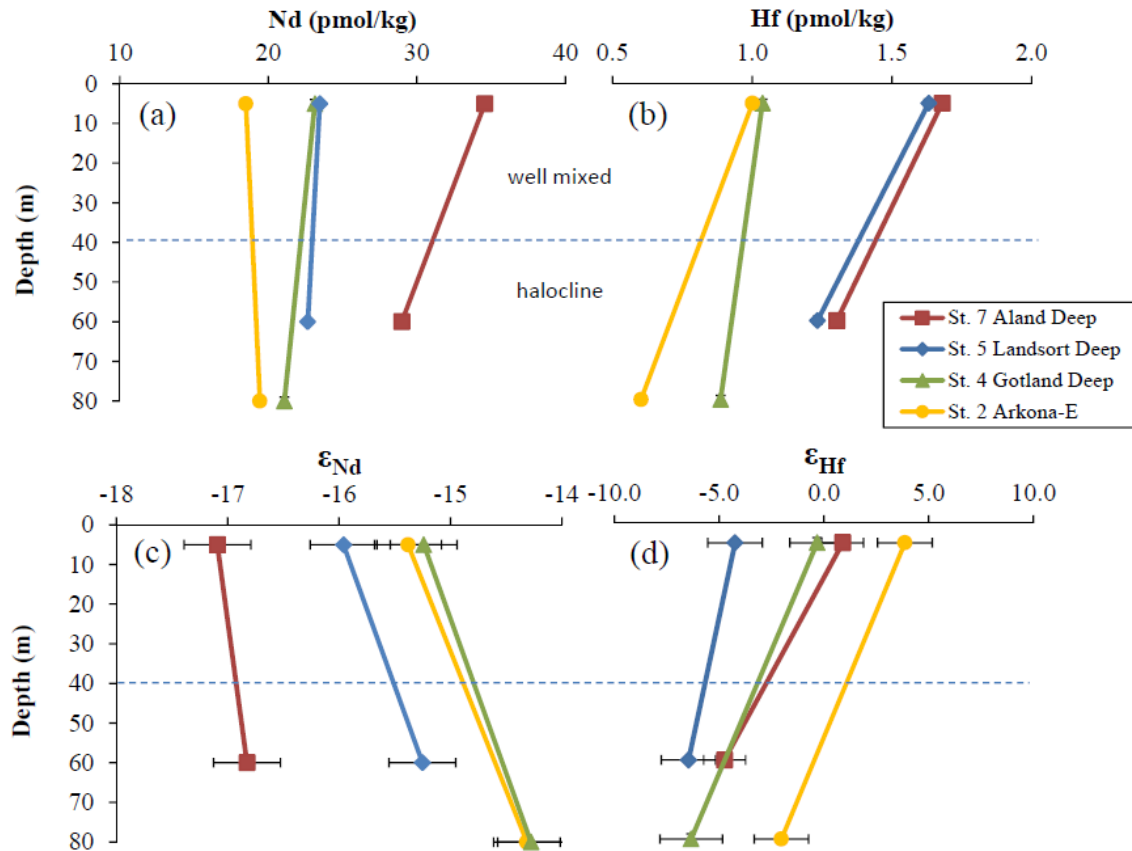
Figure 5.5 Comparison between Nd and Hf concentrations (a, b) and isotope compositions (c, d) in surface and subsurface oxygenated waters.

5.5.2 Hf and Nd isotope compositions in the halocline layer

At the upper boundary of the halocline layer, oxygen contents start to decrease rapidly but the waters do not become anoxic (Figure 5.2). Hafnium concentrations (and to a lesser extent also the Nd concentrations) exhibit a small decrease from the oxygenated surface layer into the halocline layer (Figure 5.5a, b, 40 to 80 m water depth). Given that the magnitude of concentration decrease has no apparent relationship with the salinity changes from the surface to the halocline (Figure 5.2b), it is likely that this decrease is regulated by the local scavenging effects besides mixing of the advected water masses.

We assume that the surface water Nd isotope compositions reflect the potential isotopic range of local weathering sources ultimately supplied to the subsurface waters. At the four stations where samples of the halocline layer are available (Figure 5.5), Nd isotope compositions of the halocline are all more radiogenic, thus indicating that advective supply of Nd must contribute to the observed variability. In this respect, the Nd isotope compositions and hydrographic properties of the halocline layer are consistent with the contribution of more saline and radiogenic Atlantic waters entering the southern Baltic Sea. However, the same scenario does not explain the distribution of Hf isotope compositions because the Atlantic seawater Hf source of the halocline should be characterized by ε_{Hf} signatures near 0 (if the Bay of Biscay data can be considered representative, Rickli et al., 2009; 2010). Despite that the subsurface E-Arkona sample can be explained by advective contributions of Atlantic waters, the other halocline samples are too unradiogenic in ε_{Hf} to be consistent with mixing with Atlantic source waters. We thus infer that the halocline decrease in ε_{Hf} represents mixing of Hf from local advective sources, which is not observed for Nd. This supports a shorter residence time for Hf in the water column than Nd (Rickli et al., 2009), which is also in agreement with the heterogeneous distribution of the surface water Hf isotope compositions (Figure 5.4c).
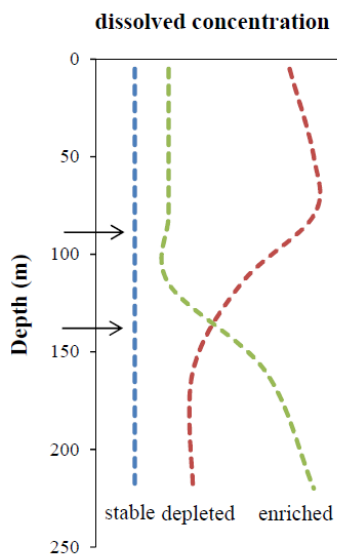
Figure 5.6 Schematic illustration of three typical profiles of trace metal concentration variations (stable, depleted and enriched) in the Gotland Deep station (e.g., Pohl and Hennings 2005). The two black arrows indicate the upper and lower boundaries of the oxygen-depleted layer.

5.5.3 Comparison of Hf and Nd cycling across the redox interface

To better understand the factors controlling Nd and Hf geochemical cycling across the redox transitions, we identify three typical metal concentration profiles observed at the Gotland Deep station (stable, depleted, and enriched; Figure 5.6). Firstly, the stable profile represents trace metal concentrations with little variations (i.e., less than a factor of 2). This normally includes the conservative trace elements such as Sr (Andersson et al., 1992), and highly particle reactive elements such as Pb (e.g., Pohl and Hennings 2005). Secondly, many elements exhibit depleted concentrations in euxinic waters, such as Cd, Zn, and Cu, which is caused by the formation of insoluble sulfide precipitates. However, there may nevertheless be a slight increase in concentration from the surface to the halocline layer due to the decomposition of organic particles and associated metal release (Pohl and Hennings 2005). The third type shows enriched concentrations in the euxinic layer, which includes Fe, Mn (Neretin et al., 2003; Pohl et al., 2004; Staubwasser et al., 2013) and closely related elements such as Co. The enrichment is a consequence of redox

cycling with reductive dissolution and accumulation of Mn and Fe oxy-hydroxides (which also carry Co), in the euxinic waters (Pohl and Hennings 2005, 2008; Staubwasser et al., 2013).

5.5.3.1 Nd cycling

Euxinic conditions have always been found in the Gotland Deep basin during prolonged periods of stagnation similar to the situation prior to our cruise in winter 2011 (e.g., Neretin et al., 2003; Pohl et al., 2012; Staubwasser et al., 2013; Dalsgaard et al., 2013). Based on NO_3 concentrations obtained on our cruise, anoxic waters of the Gotland Deep are further divided into an oxygen-depleted layer and a euxinic layer (Figure 5.7). In the lower part of the oxygen-depleted layer, denitrification leads to a rapid decrease of nitrate concentrations to trace levels, which well defines the approximate depth of the onset of euxinic conditions (e.g., Neretin et al., 2003; Yemenicioglu et al., 2006; Yakushev et al., 2007; Dalsgaard et al., 2013). This is supported by an H_2S concentration profile close to our station obtained on a cruise one year before (August 2010, Figure 5.7, Dalsgaard et al., 2013). Neodymium concentrations of the Gotland Deep show a minimum in oxygen-depleted waters followed by a continuous increase with depth in euxinic waters by more than an order of magnitude (Figure 5.7), consistent with the "enriched profile" revealed in Figure 5.6.

Redox cycling of the rare earth elements including Nd was previously studied in detail at other locations (e.g., German et al., 1991; Sholkovitz et al., 1992). It was found that Nd concentration minima generally coincided with maxima of particulate Mn in oxygen-depleted waters, indicating enhanced scavenging of Nd. Below, the reductive dissolution of Mn oxides results in increased concentrations of both dissolved Nd and Mn. Our data are consistent with this observation and support that differences in Nd concentrations between oxygen-depleted and euxinic waters are closely associated with Mn and Fe oxy-hydroxides formation and reductive dissolution.
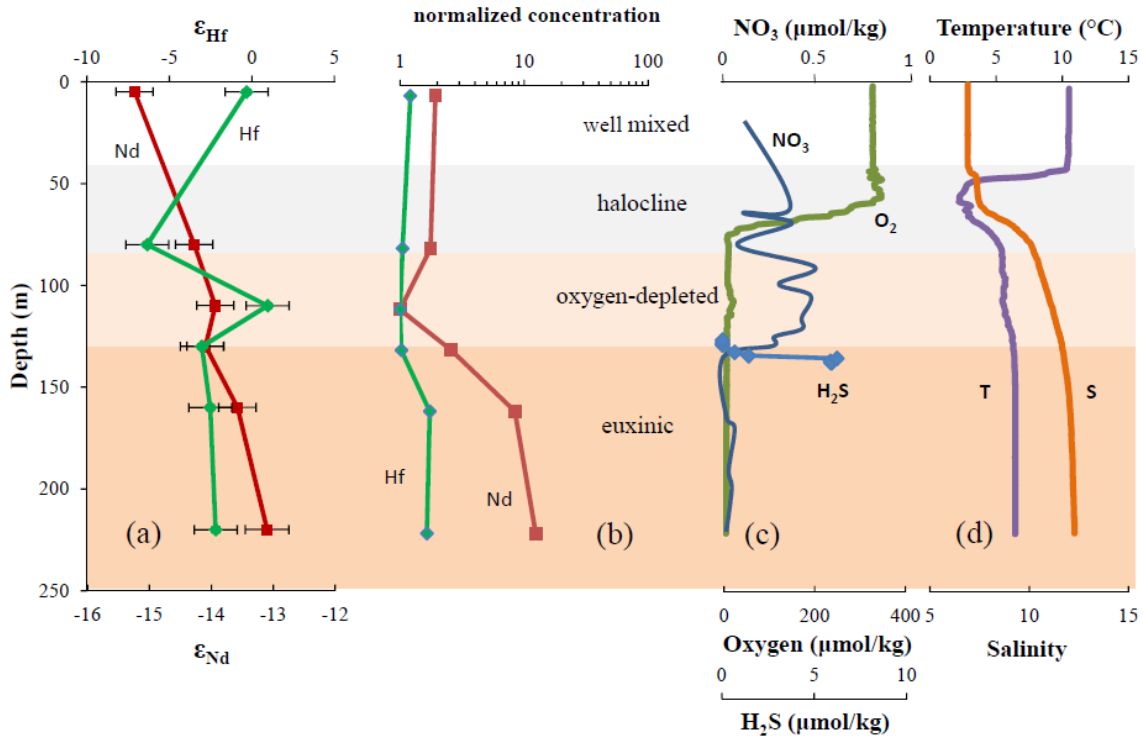
Figure 5.7 Vertical profiles of (a) ε_{Hf} and ε_{Nd}, (b) Hf and Nd concentrations (normalized to concentration at 110 m water depth in order to visualize the variability within the oxygen-depleted layer), (c) nitrate, and oxygen concentrations of our cruise, together with H_2S concentrations obtained in 2010 from a profile close to our station (Dalsgaard et al., 2013), (d) temperature and salinity at the Gotland Deep station.

Throughout the entire water column, Nd isotope compositions become more radiogenic with depth (Figure 5.7a) which requires a radiogenic mixing endmember (e.g., the Atlantic waters or release from surface sediments). It is expected that the average Nd isotope composition released from surface sediments should reflect an integrated signature of the anoxic water body at the end of major oxygenation events. Currently, the depth integrated ε_{Nd} of the euxinic water body is about -13.5, which is essentially identical to the bottom boundary layer (ε_{Nd}= -13.1, Figure 5.2a). Given a longer period of stagnation, average Nd isotope signatures in the euxinic waters should be even less radiogenic due to the continuous addition of Nd with unradiogenic signatures from the surface waters. Consequently, we conclude that the ε_{Nd} signature of the Nd released from bottom sediment in the Gotland Basin will on average be less radiogenic than -13.5. Thus

Atlantic-derived Nd is the most likely candidate for the radiogenic endmember. It is noted that we do not argue against Nd released from dissolution of surface sediments (e.g., Mn-oxides) during anoxia being a potential source to account for the Nd enrichment of the euxinic waters. Rather we suggest that it might not be the radiogenic endmember. For example, if (i) Nd from 110 m to 220 m water depth at the Gotland Deep had initial concentrations as low as at the surface (e.g., 21.1 pmol/kg) and initial ε_{Nd} similar to the inflowing signature of the North Sea (ε_{Nd}= ~-10, Andersson et al. 1992); and (ii) Nd was accumulating in the euxinic water column without being exported to the sediment, mass balance (by summing the Nd concentration $\times$ isotope composition for 110 m to 220 m water depth) requires an external Nd flux approximately 3 times as high as the initial deep water inventory with an average ε_{Nd} of about -14.6. This estimated isotope composition is consistent with the subsurface Nd isotope signatures of the Gotland Deep (-14.3). Our result therefore implies that Nd isotope signatures advected with major Atlantic inflow events can still be distinguished after several years of stagnation (i.e., about 8 years).

For a first order approximation, allowing a continuous stagnation (assuming persistent accumulation of Nd in euxinic waters without any removal) in the Gotland Deep and applying the above calculated external flux and ε_{Nd} signature (-14.6), it will require another 8 years for the euxinic waters to reach an ε_{Nd} of about -14.0. Any further decrease of ε_{Nd} will be very slow given that the Nd inventory becomes larger. If the current inventory of Nd has already stabilized in the Gotland Deep euxinic layer (i.e, the sinking flux equals the external inputs), it will only take another 15 years to essentially homogenize the Nd isotopes in the Gotland Deep (i.e., ε_{Nd} < -14.3).

In addition, more than half of the surface water dissolved Nd (< 0.45 μm) is probably represented by the fraction bound to colloids in the Baltic (Dahlqvist et al., 2005). Coagulation of these colloids could contribute to the downward flux of Nd to the deep waters. However, this process is most likely of minor importance for the deep enrichment of Nd compared to redox cycling. For example, the Aland Deep shows no enrichment of Nd in the deep water (Figure 5.3c), probably due to the lack of redox related Nd cycling.

5.5.3.2 Hf cycling

The distribution of Hf concentrations and isotope compositions shows no consistent patterns between the different depth profiles. At the Gotland Deep, Hf concentration variations are significantly different from those of Nd (Figure 5.7b). A slight increase in Hf concentration only occurs within the euxinic layer. Moreover, the increase of Hf concentrations is not continuous in the euxinic waters. Rather, the concentration at 220 m (1.4 pmol/kg) is essentially the same as at 160 m (1.5 pmol/kg). In the Landsort Deep, we see no enrichment but rather a slight decrease of Hf concentrations in anoxic waters. It is clear, however, that the Hf concentration variability is rather small among all the depth profiles, implying that Hf cycling is not strongly regulated by redox changes.

At the Gotland Deep, the pH is about 8.3 in surface water and decreases to about 7.3 in the euxinic waters (Ulfsbo et al., 2011). In such a pH range, $Hf(OH)_5^{-1}$ is expected to always be the dominant species of "truly dissolved" Hf (Byrne, 2002). On the other hand, given that Hf has very low reduction potential (Plieth 2008), redox related Hf concentration variations can also be excluded. In fact, the negatively charged $Hf(OH)_5^{-1}$ favors association with slightly positively charged Fe oxyhydroxides (Byrne, 2002; Bau and Koschinsky, 2006). Therefore, Hf concentrations in the water column might be closely associated with Fe cycling. Previous sequential leaching of hydrogenetic Fe–Mn crusts demonstrated that Hf is almost exclusively associated with the hydrous Fe oxide component (Bau and Koschinsky, 2006). However, it is intriguing that the Hf concentrations increase by a factor of only 1.7 from oxygen-depleted to euxinic waters, while dissolved Fe concentrations increase by up to an order of magnitude in euxinic waters (Turnewitsch and Pohl 2010). In addition, the Landsort Deep even shows decrease in Hf concentration of bottom waters. From our data we cannot make a clear judgment whether Hf is exclusively associated with Fe cycling. Other positively charged colloids and particles may also be important but could not be clearly understood in this study. Unlike Nd, it is clear that Hf is not strongly affected by Mn redox cycling and is actually close to a "stable concentration profile" introduced above (Figure 5.6), thus indicating fast, irreversible removal by particles similar to Pb (Pohl and Hennings 2005). Schneider et al. (2000) reported a residence time of Pb of only about 0.29 yr which may be comparable to the residence time of Hf in the Baltic Sea.

Hf isotope compositions are decoupled from Nd isotope compositions in the Gotland Deep (Figure 5.7a). As discussed above, the subsurface minimum in ε_{Hf} (-5.1) probably reflects local lateral supplies rather than Atlantic waters. The shift of the Hf isotope signature to a value similar to that of the surface layer at 110 m depth is possibly due to the release of surface-derived Hf from dissolution of sinking particles. Alternatively, it may indicate the presence of yet another lateral source. The other depth profiles also do not show clear Hf isotope variations associated with water mass mixing, probably due to the large variability of Hf isotope signatures of the weathering inputs from different sources and the short residence time in the water column mentioned above.

5.5.4 Implications for marine Nd and Hf geochemistry
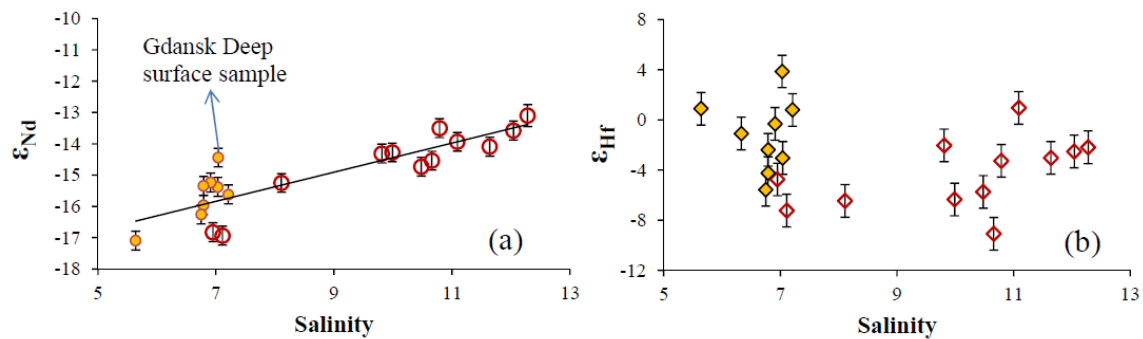
Figure 5.8 Neodymium (a) and hafnium (b) isotope compositions versus salinity for all central Baltic Sea water samples. Surface waters are denoted by filled symbols and deep samples are denoted by open symbols.

5.5.4.1 Nd isotopes versus Hf isotopes: the efficiency as water mass tracers in the central Baltic Sea

As shown in Figure 5.8, surface water Nd isotope compositions in the central Baltic Sea are in general less radiogenic than the subsurface waters. Thus it may be concluded that more saline subsurface waters reflects larger contribution from the more radiogenic Atlantic waters, as discussed above. Despite that major intrusions of Atlantic waters ($\varepsilon_{Nd}= \sim$ -10) only occur sporadically (the last one in 2003), their radiogenic isotope

fingerprint is still preserved in the present day anoxic bottom waters of the central Baltic Sea.

Note that the Nd isotopic deviation of Gdansk Deep surface water sample (southern Baltic) from the overall mixing trend in Figure 5.8a still supports the contribution of coastal Southern Baltic Nd input to the surface waters. One interesting question is why the coastal input from the southern Baltic Sea does not appear to be an important mixing endmember for deep waters. Besides the possibility that the sediments from Gulf of Bothnia or Gulf of Finland release Nd more efficiently than the southern Baltic sediments (i.e., supply limitation), we suggest that limitation of the transport of Nd of coastal origin may be important to explain the apparently conservative nature of Nd isotopes (Figure 5.8a). On the one hand, inflow from the Atlantic mainly occurs as intrusion events which may experience limited exchange of Nd with the southern Baltic sediments due to the rapidity of the events. On the other hand, abundant fresh water supply from the north and intense vertical mixing (e.g., in the Aland Deep, Figure 5.2) could more effectively transport/entrain the unradiogenic Nd into the central Baltic deep waters. In contrast, Hf isotope compositions show a heterogeneous behavior and cannot be explained by water mass mixing, i.e. admixture of Atlantic waters (Figure 5.8b).

5.5.4.2 Seawater Nd-Hf isotope array and the impact of weathering on the Hf isotope signatures

Unlike Sm/Nd ratios in different minerals which are generally similar to each other, Lu/Hf ratios vary considerably among different minerals. For example zircon, as a heavy and refractory mineral, hosts much of the Hf of bulk magmatic rocks, resulting in its very low Lu/Hf ratios and unradiogenic Hf isotope composition (e.g., Patchett et al. 1984; Chen et al., 2011). On the other hand, apatite is highly enriched in rare earth elements (e.g., Lu) but depleted in Hf, and has thus highly radiogenic Hf isotope compositions (e.g., Bayon et al., 2006). It is well known that hydrothermal input is negligible to the seawater Nd budget, while recent studies have also argued against a significant contribution of hydrothermal Hf to seawater (Rickli et al., 2009; Firdaus et al., 2011; Stichel et al., 2012a; Chen et al., 2013).
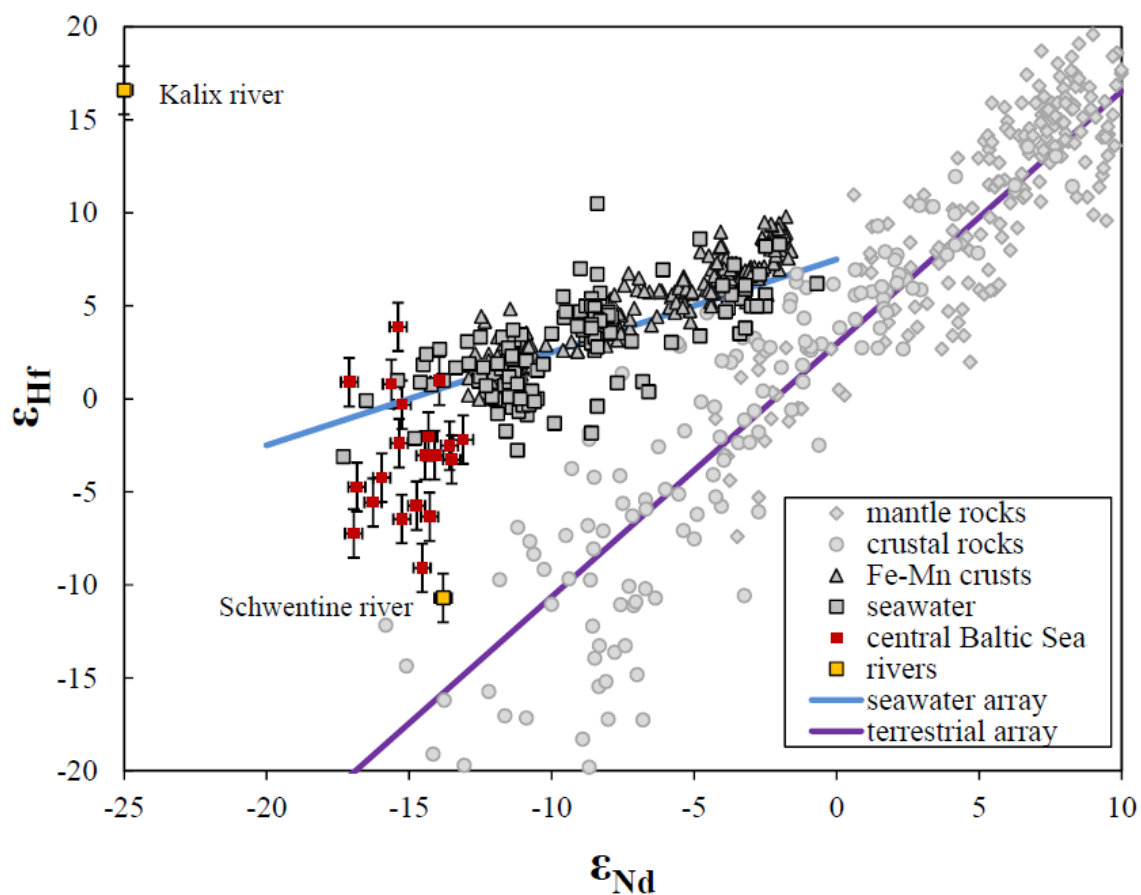
Figure 5.9 Neodymium-hafnium isotope systematics of the central Baltic Sea, in comparison with published ε_{Nd}-ε_{Hf} data of terrestrial rocks (terrestrial array, Vervoort et al., 1999), seawater (<0.45 µm, Rickli et al., 2009, 2010; Zimmermann et al., 2009a, b; Stichel et al., 2012a, b) and Fe-Mn crusts (Lee et al., 1999; Piotrowski et al., 2000; David et al., 2001; van de Flierdt et al., 2004; seawater array, Albarède et al., 1998).

The data obtained in our study (Figure 5.9), although with a large scatter, are significantly more radiogenic in Hf isotopes for a given Nd isotope composition compared to terrestrial rocks and are generally consistent with the global seawater Nd-Hf isotope trend. Note that central Baltic Sea is essentially dominated by continental inputs without hydrothermal influence. Our data thus provide additional support that hydrothermal influence is probably not a significant source for the seawater Hf budget.

During the very initial stage of glacial weathering, trace minerals such as apatite and allanite, which are easily alterable and contain highly radiogenic Hf compositions, are suggested to be preferentially weathered (Bayon et al., 2006). This seems to be supported by Nd-Hf isotope data for the Kalix river (Table 5.1), which is dominated by input from very recently exposed granitic tills. In fact, because the source rocks of the till are of Archean age (1.8-1.9 Ga, Öhlander et al., 2000), even the Nd isotope compositions have been shown to experience notable incongruent weathering after the early Holocene retreat of the glaciers. For example, the modern ε_{Nd} of the Kalix river (-25.1) is significantly lower than its bulk source materials (-22 ~ -23, Andersson et al., 2001; Öhlander et al., 2000). REE-rich minerals such as allanite and monazite (which are characterized by high Lu/Hf) might be the dominant phases releasing unradiogenic Nd (Andersson et al., 2001; Öhlander et al., 2000) and probably also radiogenic Hf signatures. The Schwentine river, however, shows unexpectedly unradiogenic Hf isotope compositions (ε_{Hf} = -10.7). Rather than an active glacially denuded area like the Kalix river watershed, the Schwentine basin has received sediment deposition from previous glacial cycles, which includes complex sources of different ages with averaged ε_{Nd} around -14 (i.e., the riverine dissolved isotope composition). It is likely that the Hf supply to the Schwentine river is dominated by weathering sources which have gone through relatively late magmatic activities and the associated isotope equilibrium between different minerals and thus more similar Hf isotope compositions among different minerals (Chen et al., 2011). Furthermore, the unradiogenic Hf isotope signature of the Schwentine river may also reflect a more congruent weathering signature following the initial radiogenic pulse of Hf. In fact, a radiogenic pulse of Pb and Sr isotope release has been observed during incipient moraine weathering in the field (Blum and Erel, 1997; Harlavan et al., 1998) and for leachates of crushed granitoid samples in lab experiments (Harlavan and Erel, 2002; Erel et al., 2004). These radiogenic isotope signatures are all closely linked with dissolution of easily alterable minerals at the very initial stage of weathering, which may not be the case for the Schwentine catchment.

5.5.4.3 Oceanic residence time of Hf compared to Nd

Final conclusions on the seawater residence time of Hf and its comparison to that of Nd have not yet been reached (Godfrey et al., 1996; Godfrey et al., 2008, 2009; Rickli et al., 2009, 2010; Zimmermann et al., 2009a, b; Firdaus et al., 2011; Stichel et al., 2012a). In the present day global open ocean, deep water Hf concentrations are not enriched along the deep oceanic conveyor belt, indicating higher particle reactivity of Hf compared to Nd. However, given that the overall global range of seawater Hf concentrations is small, this may also be in agreement with a longer residence time of Hf than that of Nd (Godfrey et al., 2009; Stichel et al., 2012a). The results of our study suggest that Hf is more susceptible to the influence of local sources in the central Baltic Sea. In particular, Hf is not enriched in the bottom anoxic waters, indicating fast irreversible particulate removal similar to Pb (Pohl and Hennings 2005). These two observations strongly suggest that the oceanic residence time of Hf is likely to be much shorter than that of Nd.

The heterogeneously distributed signatures of dissolved Hf isotope signatures in the Baltic Sea seem to contradict the homogeneity of Hf isotope compositions in the open ocean (Rickli et al., 2009; Zimmermann et al., 2009b; Stichel et al., 2012a). Our preferred interpretation is that: (1) the continental Baltic drainage systems have been under the influence of glacial weathering regimes of very different time scales and lithology (e.g., Lundqvist, 1986), which may result in highly variable degrees of incongruent weathering. Therefore, the central Baltic region is not representative of the global continental source heterogeneity in terms of Hf isotope compositions. (2) Mixing within the source areas, such as reflected by large rivers and eolian dust effectively erase the large local Hf isotopic variability before entering the open ocean.

5.6 Conclusions

The first combined Nd-Hf isotope compositions and concentrations in a marginal brackish basin with anoxic bottom waters (the central Baltic Sea) are presented in this study. While Nd is distinctly enriched in bottom anoxic waters, the overall variability of Hf concentrations is rather small. In a high resolution profile at the Gotland Deep, the different geochemical behavior between Hf and Nd is revealed. We propose that Hf is

rapidly removed by particles, which prevents Hf accumulation in anoxic waters, while Nd is closely associated with Mn and Fe redox cycling.

In general, Nd isotope compositions can be explained by quasi-conservative mixing between local inputs and Atlantic-derived more radiogenic subsurface source waters, demonstrating the efficiency of Nd isotope compositions as a water mass tracer in the central Baltic Sea. Hafnium isotope compositions, however, show an unexpectedly large variability and the observed patterns are not explainable by water mass mixing. Hafnium is suggested to have a shorter residence time than Nd in seawater, and is more easily influenced by local inputs. Since the central Baltic Sea is a basin without hydrothermal influence, the general consistency of Hf-Nd isotope data with the global seawater trend implies that continental weathering alone is most likely sufficient to produce the oceanic radiogenic Hf isotope signatures, which is in line with previous studies (Bayon et al., 2009; Rickli et al., 2009; Stichel et al., 2012a; Chen et al., 2013).

References

Albarède, F., Simonetti, A., Vervoort, J. D., Blichert-Toft, J., and Abouchami, W. (1998) A Hf-Nd isotopic correlation in ferromanganese nodules. *Geophys. Res. Lett.* **25**, 3895-3898.

Amakawa, H., Alibo, D. S., and Nozaki, Y. (2000) Nd isotopic composition and REE pattern in the surface waters of the eastern Indian Ocean and its adjacent seas. *Geochim. Cosmochim. Acta* **64**, 1715-1727.

Andersson, P. S., Dahlqvist, R., Ingri, J., and Gustafsson, O. (2001) The isotopic composition of Nd in a boreal river: A reflection of selective weathering and colloidal transport. *Geochim. Cosmochim. Acta* **65**, 521-527.

Andersson, P. S., Wasserburg, G. J., and Ingri, J. (1992) The Sources and Transport of Sr and Nd Isotopes in the Baltic Sea. *Earth Planet. Sci. Lett.* **113**, 459-472.

Arsouze, T., Dutay, J. C., Lacan, F., and Jeandel, C. (2009) Reconstructing the Nd oceanic cycle using a coupled dynamical - biogeochemical model. *Biogeosciences* **6**, 2829-2846.

Bau, M. and Koschinsky, A. (2006) Hafnium and neodymium isotopes in seawater and in ferromanganese crusts: The "element perspective". *Earth Planet. Sci. Lett.* **241**, 952-961.

Bayon, G., Burton, K. W., Soulet, G., Vigier, N., Dennielou, B., Etoubleau, J., Ponzevera, E., German, C. R., and Nesbitt, R. W. (2009) Hf and Nd isotopes in marine sediments: Constraints on global silicate weathering. *Earth Planet. Sci. Lett.* **277**, 318-326.

Bayon, G., Vigier, N., Burton, K. W., Brenot, A., Carignan, J., Etoubleau, J., and Chu, N. C. (2006) The control of weathering processes on riverine and seawater hafnium isotope ratios. *Geology* **34**, 433-436.

Bertram, C. J. and Elderfield, H. (1993) The Geochemical Balance of the Rare-Earth Elements and Neodymium Isotopes in the Oceans. *Geochim. Cosmochim. Acta* **57**, 1957-1986.

Blum, J. D. and Erel, Y. (1997) Rb-Sr isotope systematics of a granitic soil chronosequence: The importance of biotite weathering. *Geochim. Cosmochim. Acta* **61**, 3193-3204.

Bock, B., Liebetrau, V., Eisenhauer, A., Frei, R., and Leipe, T. (2005) Nd isotope signature of Holocene Baltic Mn/Fe precipitates as monitor of climate change during the Little Ice Age. *Geochim. Cosmochim. Acta* **69**, 2253-2263.

Byrne, R. H. (2002) Inorganic speciation of dissolved elements in seawater: the influence of pH on concentration ratios. *Geochem. Trans.* **3**, 11-16.

Chen, T.-Y., Ling, H.-F., Frank, M., Zhao, K.-D., and Jiang, S.-Y. (2011) Zircon effect alone insufficient to generate seawater Nd-Hf isotope relationships. *Geochem. Geophys. Geosyst.* **12**, Q05003. doi: 10.1029/2010gc003363.

Chen, T.-Y., Li, G., Frank, M., and Ling, H.-F. (2013) Hafnium isotope fractionation during continental weathering: implications for the generation of the seawater Nd-Hf isotope relationship. *Geophys. Res. Lett*, **40**, doi: 10.1002/grl.50217.

Chu, N.-C., Taylor, R. N., Chavagnac, V., Nesbitt, R. W., Boella, R. M., Milton, J. A., German, C. R., Bayon, G., and Burton, K. (2002) Hf isotope ratio analysis using multi-collector inductively coupled plasma mass spectrometry: an evaluation of isobaric interference corrections. *J. Anal. Atom. Spectrom.* **17**, 1567-1574.

Dahlqvist, R., Andersson, P. S., and Ingri, J., 2005. The concentration and isotopic composition of diffusible Nd in fresh and marine waters. *Earth and Planetary Science Letters* **233**, 9-16.

Dalsgaard, T., De Brabandere, L., and Hall, P. O. J., 2013. Denitrification in the water column of the central Baltic Sea. *Geochimica et Cosmochimica Acta* **106**, 247-260.

David, K., Frank, M., O'Nions, R. K., Belshaw, N. S., and Arden, J. W. (2001) The Hf isotope composition of global seawater and the evolution of Hf isotopes in the deep Pacific Ocean from Fe-Mn crusts. *Chem. Geol.* **178**, 23-42.

Erel, Y., Blum, J. D., Roueff, E., and Ganor, J. (2004) Lead and strontium isotopes as monitors of experimental granitoid mineral dissolution. *Geochim. Cosmochim. Acta* **68**, 4649-4663.

Feistel, R., Nausch, G., Matthäus, W., and Hagen, E. (2003) Temporal and spatial evolution of the Baltic deep water renewal in spring 2003. *Oceanologia* **45**, 623-642.

Firdaus, M. L., Minami, T., Norisuye, K., and Sohrin, Y. (2011) Strong elemental fractionation of Zr-Hf and Nb-Ta across the Pacific Ocean. *Nat. Geosci.* **4**, 227-230.

Frank, M. (2002) Radiogenic isotopes: Tracers of past ocean circulation and erosional input. *Rev.Geophys.* **40**, doi: 10.1029/2000RG000094.

Gaál, G. and Gorbatschev, R. (1987) An Outline of the precambrian evolution of the baltic shield. *Precambrian Res.* **35**, 15-52.

German, C. R., Holliday, B. P., and Elderfield, H. (1991) Redox Cycling of Rare-Earth Elements in the Suboxic Zone of the Black-Sea. *Geochim. Cosmochim. Acta* **55**, 3553-3558.

German, C. R., Klinkhammer, G. P., Edmond, J. M., Mitra, A., and Elderfield, H. (1990) Hydrothermal Scavenging of Rare-Earth Elements in the Ocean. *Nature* **345**, 516-518.

Godfrey, L. V., Field, M. P., and Sherrell, R. M. (2008) Estuarine distributions of Zr, Hf, and Ag in the Hudson River and the implications for their continental and anthropogenic sources to seawater. *Geochem. Geophys. Geosyst.* **9**, Q12007, doi: 10.1029/2008gc002123.

Godfrey, L. V., White, W. M., and Salters, V. J. M. (1996) Dissolved zirconium and hafnium distributions across a shelf break in the northeastern Atlantic Ocean. *Geochim. Cosmochim. Acta* **60**, 3995-4006.

Godfrey, L. V., Zimmermann, B., Lee, D. C., King, R. L., Vervoort, J. D., Sherrell, R. M., and Halliday, A. N. (2009) Hafnium and neodymium isotope variations in NE Atlantic seawater. *Geochem. Geophys. Geosyst.* **10**, doi: 10.1029/2009GC002508.

Goldstein, S. L., Hemming, S. R., Heinrich, D. H., and Karl, K. T. (2003) Long-lived Isotopic Tracers in Oceanography, Paleoceanography, and Ice-sheet Dynamics, *Treatise on Geochemistry*. Pergamon, Oxford.

Graham, P. L. (2000) Large-scale hydrologic modeling in the Baltic basin, KTH.

Halliday, A. N., Davidson, J. P., Holden, P., Owen, R. M., and Olivarez, A. M. (1992) Metalliferous Sediments and the Scavenging Residence Time of Nd near Hydrothermal Vents. *Geophys. Res. Lett.* **19**, 761-764.

Hansson M., Axe, P., and L. Andersson, 2009, Extent of anoxia and hypoxia in the Baltic Sea, 1960-2009, SMHI Report Mo2009-214, available online at http://www.smhi.se/polopoly_fs/1.10354!Oxygen_timeseries_1960_2009.pdf

Harlavan, Y. and Erel, Y. (2002) The release of Pb and REE from granitoids by the dissolution of accessory phases. *Geochim. Cosmochim. Acta* **66**, 837-848.

Harlavan, Y., Erel, Y., and Blum, J. D. (1998) Systematic changes in lead isotopic composition with soil age in glacial granitic terrains. *Geochim. Cosmochim. Acta* **62**, 33-46.

Ingri, J., Widerlund, A., Land, M., Gustafsson, Ö., Andersson, P., and Öhlander, B. (2000) Temporal variations in the fractionation of the rare earth elements in a boreal river; the role of colloidal particles. *Chem. Geol.* **166**, 23-45.

Jacobsen, S. B. and Wasserburg, G. J. (1980) Sm-Nd Isotopic Evolution of Chondrites. *Earth Planet. Sci. Lett.* **50**, 139-155.

Kuhlmann, G., de Boer, P. L., Pedersen, R. B., and Wong, T. E. (2004) Provenance of Pliocene sediments and paleoenvironmental changes in the southern North Sea region using Samarium-Neodymium (Sm/Nd) provenance ages and clay mineralogy. *Sediment. Geol.* **171**, 205-226.

Lacan, F. and Jeandel, C. (2001) Tracing Papua New Guinea imprint on the central Equatorial Pacific Ocean using neodymium isotopic compositions and Rare Earth Element patterns. *Earth Planet. Sci. Lett.* **186**, 497-512.

Lacan, F. and Jeandel, C. (2005) Neodymium isotopes as a new tool for quantifying exchange fluxes at the continent-ocean interface. *Earth Planet. Sci. Lett.* **232**, 245-257.

Lawrence, M. G. and Kamber, B. S., 2006. The behaviour of the rare earth elements during estuarine mixing—revisited. *Mar. Chem.* **100**, 147-161.Lee, D. C., Halliday, A. N., Hein, J. R., Burton, K. W., Christensen, J. N., and Gunther, D. (1999) Hafnium isotope stratigraphy of ferromanganese crusts. *Science* **285**, 1052-1054.

Lundqvist, J. (1986) Late Weichselian glaciation and deglaciation in Scandinavia. *Quaternary Sci. Rev.* **5**, 269-292.

Mansfeld, J. (2001) Age and epsilon(Nd) constraints on the Palaeoproterozoic tectonic evolution in the Baltic-Sea region. *Tectonophysics* **339**, 135-151.

Matthäus, W., D. Nehring, R. Feistel, G. Nausch, V. Mohrholz, and H.-U. Lass (2008) The Inflow of Highly Saline Water into the Baltic Sea, in *State and Evolution of the Baltic Sea, 1952–2005*, edited, pp. 265-309, John Wiley & Sons, Inc.

Meier, H. E. M. (2007) Modeling the pathways and ages of inflowing salt- and freshwater in the Baltic Sea. *Estuar. Coast. Shelf S* **74**, 610-627.

Neretin, L. N., Pohl, C., Jost, G., Leipe, T., and Pollehne, F. (2003) Manganese cycling in the Gotland Deep, Baltic Sea. *Mar. Chem.* **82**, 125-143.

Nowell, G. M., Kempton, P. D., Noble, S. R., Fitton, J. G., Saunders, A. D., Mahoney, J. J., and Taylor, R. N. (1998) High precision Hf isotope measurements of MORB and OIB by thermal ionisation mass spectrometry: insights into the depleted mantle. *Chem. Geol.* **149**, 211-233.

Nozaki, Y. and Alibo, D. S. (2003) Importance of vertical geochemical processes in controlling the oceanic profiles of dissolved rare earth elements in the northeastern Indian Ocean. *Earth Planet. Sci. Lett.* **205**, 155-172.

Ohlander, B., Ingri, J., Land, M., and Schoberg, H. (2000) Change of Sm-Nd isotope composition during weathering of till. *Geochim. Cosmochim. Acta* **64**, 813-820.

Oka, A., Hasumi, H., Obata, H., Gamo, T., and Yamanaka, Y. (2009) Study on vertical profiles of rare earth elements by using an ocean general circulation model. *Global Biogeochem. Cy.* **23**, -.

Patchett, P. J., White, W. M., Feldmann, H., Kielinczuk, S., and Hofmann, A. W. (1984) Hafnium Rare-Earth Element Fractionation in the Sedimentary System and Crustal Recycling into the Earths Mantle. *Earth Planet. Sci. Lett.* **69**, 365-378.

Piotrowski, A. M., Lee, D. C., Christensen, J. N., Burton, K. W., Halliday, A. N., Hein, J. R., and Gunther, D. (2000) Changes in erosion and ocean circulation recorded in the Hf isotopic compositions of North Atlantic and Indian Ocean ferromanganese crusts. *Earth Planet. Sci. Lett.* **181**, 315-325.

Piotrowski, J. A. (1997) Subglacial hydrology in north-western Germany during the last glaciation: Groundwater flow, tunnel valleys and hydrological cycles. *Quaternary Sci. Rev.* **16**, 169-185.

Plieth, W. (2008) 3 - Electrode Potentials, *Electrochemistry for Materials Science*. Elsevier, Amsterdam.

Pohl, C. and Fernández-Otero, E., 2012. Iron distribution and speciation in oxic and anoxic waters of the Baltic Sea. *Marine Chemistry* **145–147**, 1-15.

Pohl, C. and Hennings, U. (2005) The coupling of long-term trace metal trends to internal trace metal fluxes at the oxic-anoxic interface in the Gotland Basin (57°19,20' N; 20°03,00' E) Baltic Sea. *J. Mar. Syst.* **56**, 207-225.

Pohl, C., and Hennings U. (2008) Trace Metals in Baltic Seawater, in *State and Evolution of the Baltic Sea, 1952–2005*, edited, pp. 367-393, John Wiley & Sons, Inc.

Pohl, C., Loffler, A., and Hennings, U. (2004) A sediment trap flux study for trace metals under seasonal aspects in the stratified Baltic Sea (Gotland Basin; 57°19.20' N; 20°03.00' E). *Mar. Chem.* **84**, 143-160.

Reissmann, J. H., Burchard, H., Feistel, R., Hagen, E., Lass, H. U., Mohrholz, V., Nausch, G., Umlauf, L., and Wieczorek, G. (2009) Vertical mixing in the Baltic Sea and consequences for eutrophication - A review. *Prog. Oceanogr.* **82**, 47-80.

Rempfer, J., Stocker, T. F., Joos, F., Dutay, J. C., and Siddall, M. (2011) Modelling Nd-isotopes with a coarse resolution ocean circulation model: Sensitivities to model parameters and source/sink distributions. *Geochim. Cosmochim. Acta* **75**, 5927-5950.

Rickli, J., Frank, M., and Halliday, A. N. (2009) The hafnium-neodymium isotopic composition of Atlantic seawater. *Earth Planet. Sci. Lett.* **280**, 118-127.

Rickli, J., Frank, M., Baker, A. R., Aciego, S., de Souza, G., Georg, R. B., and Halliday, A. N. (2010) Hafnium and neodymium isotopes in surface waters of the eastern Atlantic Ocean: Implications for sources and inputs of trace metals to the ocean. *Geochim. Cosmochim. Acta* **74**, 540-557.

Rickli, J., Frank, M., Stichel, T., Georg, R. B., Vance, D., and Halliday, A. N. (2013) Controls on the incongruent release of hafnium during weathering of metamorphic and sedimentary catchments. *Geochim. Cosmochim. Acta* **101**, 263-284.

Schlitzer, R. (2012) Ocean Data View, http://odv.awi.de.

Schneider, B., Ceburnis, D., Marks, R., Munthe, J., Petersen, G., and Sofiev, M., 2000. Atmospheric Pb and Cd input into the Baltic Sea: a new estimate based on measurements. *Marine Chemistry* **71**, 297-307.

Sholkovitz, E. R., Landing, W. M., and Lewis, B. L. (1994) Ocean particle chemistry: The fractionation of rare earth elements between suspended particles and seawater. *Geochim. Cosmochim. Acta* **58**, 1567-1579.

Sholkovitz, E. R., Shaw, T. J., and Schneider, D. L. (1992) The Geochemistry of Rare-Earth Elements in the Seasonally Anoxic Water Column and Porewaters of Chesapeake Bay. *Geochim. Cosmochim. Acta* **56**, 3389-3402.

Siddall, M., Khatiwala, S., van de Flierdt, T., Jones, K., Goldstein, S. L., Hemming, S., and Anderson, R. F. (2008) Towards explaining the Nd paradox using reversible scavenging in an ocean general circulation model. *Earth Planet. Sci. Lett.* **274**, 448-461.

Staubwasser, M., Schoenberg, R., von Blanckenburg, F., Krüger, S., and Pohl, C. (2013) Isotope fractionation between dissolved and suspended particulate Fe in the oxic and anoxic water column of the Baltic Sea. *Biogeosciences* **10**, 233-245.

Stichel, T., Frank, M., Rickli, J., and Haley, B. A. (2012a) The hafnium and neodymium isotope composition of seawater in the Atlantic sector of the Southern Ocean. *Earth Planet. Sci. Lett.* **317–318**, 282-294.

Stichel, T., Frank, M., Rickli, J., Hathorne, E. C., Haley, B. A., Jeandel, C., and Pradoux, C. (2012b) Sources and input mechanisms of hafnium and neodymium in surface waters of the Atlantic sector of the Southern Ocean. *Geochim. Cosmochim. Acta* **94**, 22-37.

Tachikawa, K., Athias, V., and Jeandel, C. (2003) Neodymium budget in the modern ocean and paleo-oceanographic implications. *J. Geophys. Res.* **108**, doi: 10.1029/1999jc000285.

Tanaka, T., Togashi, S., Kamioka, H., Amakawa, H., Kagami, H., Hamamoto, T., Yuhara, M., Orihashi, Y., Yoneda, S., Shimizu, H., Kunimaru, T., Takahashi, K., Yanagi, T., Nakano, T., Fujimaki, H., Shinjo, R., Asahara, Y., Tanimizu, M., and Dragusanu, C. (2000) JNdi-1: a neodymium isotopic reference in consistency with LaJolla neodymium. *Chem. Geol.* **168**, 279-281.

Turnewitsch, R. and Pohl, C. (2010) An estimate of the efficiency of the iron- and manganese-driven dissolved inorganic phosphorus trap at an oxic/euxinic water column redoxcline. *Global Biogeochem. Cy.* **24**, doi: 10.1029/2010GB003820.

Ulfsbo, A., Hulth, S., and Anderson, L. G. (2011) pH and biogeochemical processes in the Gotland Basin of the Baltic Sea. *Mar. Chem.* **127**, 20-30.

van de Flierdt, T., Frank, M., Lee, D. C., and Halliday, A. N. (2002) Glacial weathering and the hafnium isotope composition of seawater. *Earth Planet. Sci. Lett.* **198**, 167-175.

van de Flierdt, T., Frank, M., Lee, D. C., Halliday, A. N., Reynolds, B. C., and Hein, J. R. (2004) New constraints on the sources and behavior of neodymium and hafnium in seawater from Pacific Ocean ferromanganese crusts. *Geochim. Cosmochim. Acta* **68**, 3827-3843.

Vervoort, J. D., Patchett, P. J., Blichert-Toft, J., and Albarede, F. (1999) Relationships between Lu-Hf and Sm-Nd isotopic systems in the global sedimentary system. *Earth Planet. Sci. Lett.* **168**, 79-99.

von Blanckenburg, F. (1999) Perspectives: Paleoceanography - Tracing past ocean circulation? *Science* **286**, 1862-1863.

Yakushev, E. V., Pollehne, F., Jost, G., Kuznetso, I., Schneider, B., and Urnlauf, L. (2007) Analysis of the water column oxic/anoxic interface in the Black and Baltic seas with a numerical model. *Mar. Chem.* **107**, 388-410.

Yemenicioglu, S., Erdogan, S., and Tugrul, S. (2006) Distribution of dissolved forms of iron and manganese in the Black Sea. *Deep-Sea Res. Pt. II* **53**, 1842-1855.

Zimmermann, B., Porcelli, D., Frank, M., Andersson, P. S., Baskaran, M., Lee, D. C., and Halliday, A. N. (2009a) Hafnium isotopes in Arctic Ocean water. *Geochim. Cosmochim. Acta* **73**, 3218-3233.

Zimmermann, B., Porcelli, D., Frank, M., Rickli, J., Lee, D. C., and Halliday, A. N. (2009b) The hafnium isotope composition of Pacific Ocean water. *Geochim. Cosmochim. Acta* **73**, 91-101.

Chapter 6

Variations of North Atlantic inflow to the central Arctic Ocean over the last 14 million years inferred from hafnium and neodymium isotopes

Abstract

The warm and saline North Atlantic inflow to the Arctic Ocean is a major component of high northern latitude circulation and the main mechanism of deep water renewal in the Arctic Ocean. Knowledge of its past variability is critical for understanding the high latitude feedback mechanisms of the climate system. Here we present the first combined seawater Hf and Nd isotope compositions of past Arctic Intermediate Water extracted from the authigenic Fe-Mn oxyhydroxide fraction of two sediment cores recovered near the North Pole, to reconstruct changes in contributions from glacial brines of the Eurasian shelf and past inflow of Atlantic waters. The Hf and Nd isotopic compositions obtained from leachates of the authigenic fraction show closely coupled and environmentally controlled variations over the past 14 million years. An observed offset of these data from seawater ε_{Hf} and ε_{Nd} compositions from other ocean basins (seawater array) is interpreted as the result of continuously prevailing glacial weathering conditions on the high latitude Eurasian continent. In the late Quaternary, large amplitude Hf and Nd isotopic variations of Arctic Intermediate Water (AIW) was characterized by more radiogenic isotope signatures generally prevailing under glacial conditions and less radiogenic values during interglacial periods. On the basis of the close coupling between Nd and Hf isotopes, we suggest that the evolution of Hf isotope compositions of central Arctic AIW has primarily been controlled by changes in ocean circulation and provenance of weathering inputs, rather than changes in weathering regime.

6.1 Introduction

Water mass exchange between the North Atlantic and the Arctic Ocean strongly affects heat and salinity distribution in the Arctic Ocean and thus the climate of the circum-Arctic continental regions (e.g., Aagaard et al., 1985; Rudels et al., 1994; Zhang et al., 1998). It has been demonstrated that modern heat transfer to the Arctic through Atlantic water inflow is significantly enhanced, which is most likely related to the Arctic amplification of global warming (Spielhagen et al., 2011). Therefore, knowledge of past variability of North Atlantic inflow to the Arctic is important for understanding the

feedback mechanisms with the local and global climate system, as well as for predicting future changes. Until now, studies on the history of North Atlantic inflow are still rare and have focused on sediment records covering the last two glacial cycles at best (e.g., Spielhagen et al., 2004), whereas information on the evolution of the central Arctic basin and further back in time is still limited. Presently, inflowing North Atlantic water is transformed into Arctic intermediate waters, which remain largely decoupled from the atmosphere after entering the Arctic Ocean through Fram Strait and the Barents Sea (Figure 6.1, Rudels et al., 1994; Karcher and Oberhuber, 2002). The central Arctic Intermediate Water (AIW) occupies water depths between 200 and 1,500 m and predominantly consists of these waters of North Atlantic origin. Major present-day modifications of AIW include interactions with brine water ejected by seasonal sea-ice production on the shallow Barents and Kara Sea shelves (e.g., Andersson et al., 2008). In the Eurasian Basin (Amundsen Basin and Nansen Basin), the topographically constrained cyclonic circulation brings the intermediate water back towards the Fram Strait along the Lomonosov Ridge (Figure 6.1). A change of the inflow of Atlantic water will thus be directly reflected by corresponding changes of the chemical composition of AIW. In turn, the study of past compositions of AIW in the central Arctic basin will provide essential information about the temporal variability of the Atlantic inflow.

Combined radiogenic Hf-Nd isotope compositions of seawater were suggested as a proxy for changes in water mass provenance and mixing (Zimmermann et al., 2009a; b; Godfrey et al., 2009; Rickli et al., 2009; 2010; Stichel et al., 2012), as well as intensity and regime of past continental weathering, a signature produced by weathering-induced fractionation processes of Hf isotopes (van de Flierdt et al., 2002; 2007; Bayon et al., 2006; 2009). Past variations of the combined Hf-Nd isotope compositions of seawater have so far only been reconstructed from coarse resolution long term records obtained from ferromanganese crusts (Lee et al., 1999; Piotrowski et al. 2000; David et al., 2001; van de Flierdt et al., 2002; 2004a; b; Frank et al., 2006). Millennial scale resolution reconstructions of weathering regimes and water mass mixing applying past Hf-Nd isotope variations have so far been hampered by the lack of suitable analytical methods to extract seawater Hf isotope compositions from marine sediments. The leaching methods

routinely applied for extracting seawater Nd and Pb isotope compositions (e.g. Bayon et al., 2002; Haley et al., 2008a) do not work for Hf isotopes due to the re-adsorption of the seawater-derived Hf to the detrital phase during leaching (Gutjahr, 2006).
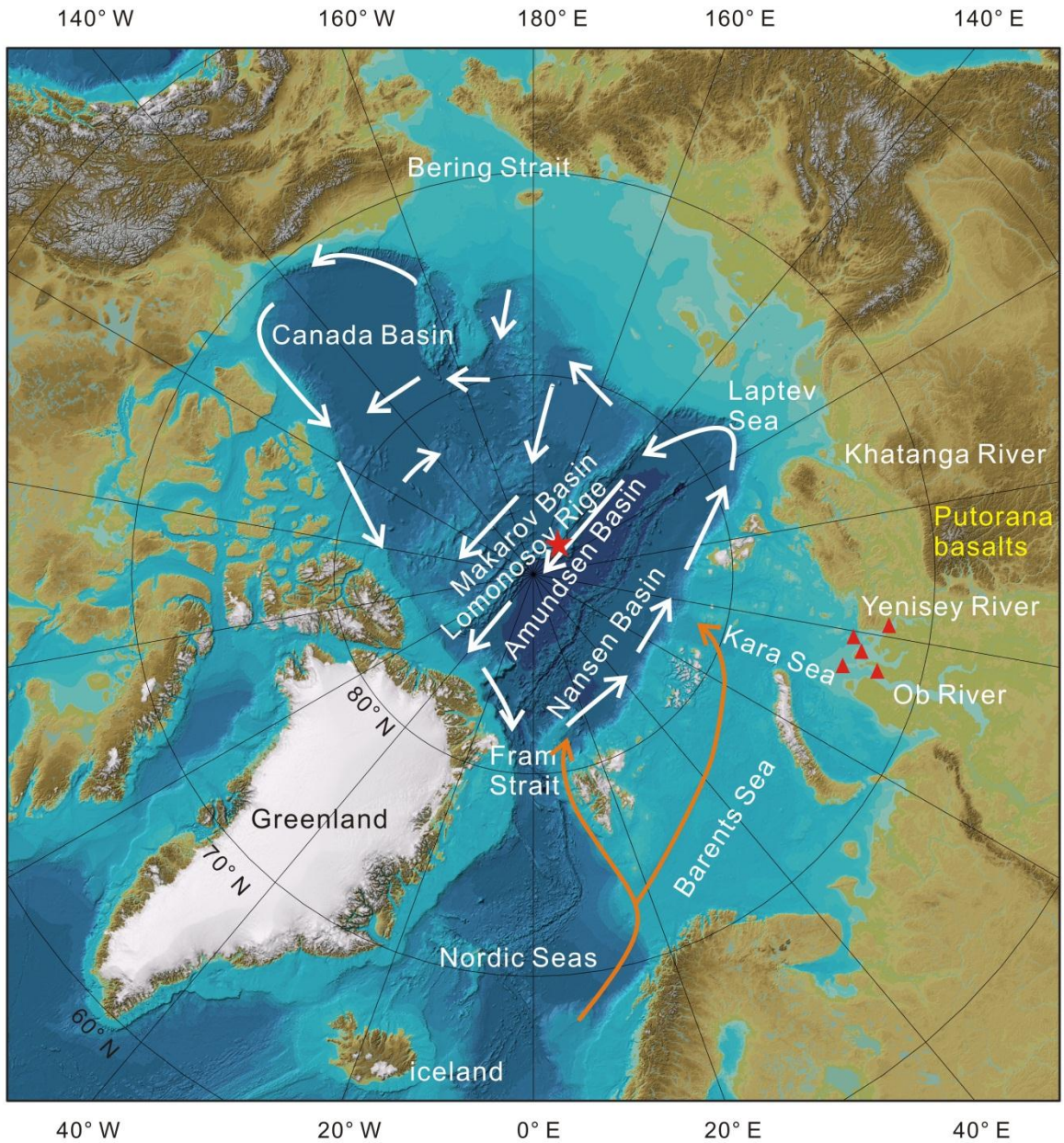
Figure 6.1 Map of the high northern latitude seas and schematic modern ocean circulation patterns. PS2185 and the IODP Leg 302 cores are marked with a star on the Lomonosov Ridge. Kara Sea samples are represented by the triangles. The dashed arrows indicate the inflow of Atlantic near surface and intermediate waters from the Nordic Seas. An eastern branch flows across the Barents Sea, while a western

branch flows along the western Svalbard margin. The solid arrows indicate the general circulation of the Arctic Intermediate Water (Rudels et al., 2004). This map is drawn based on the International Bathymetric Chart of the Arctic Ocean (IBCAO).

Previous work (Haley et al., 2008a) investigating past Nd isotope signatures of AIW revealed much more radiogenic values during glacial time (ε_{Nd} >-7) than today (ε_{Nd}: about -10.8). In fact, Icelandic basalts (located near the site of "headwaters" of North Atlantic inflow) and the Putorana flood basalts of Siberia are the only two possible sources to release radiogenic Nd and Hf to the central Arctic (Figure 6.1). For various reasons including distance and general flow patterns, the Icelandic basalts were previously suggested a highly unlikely source for more radiogenic glacial Nd isotope compositions of AIW (Haley et al., 2008a). The Putorana flood basalts of Siberia remain the only major source able to supply radiogenic Nd isotope signatures to AIW. Therefore, radiogenic Nd isotope signatures of AIW in glacial times was interpreted as intrusion of significant amounts of dense brines carrying radiogenic Nd isotope compositions especially in the Kara Sea region during periods of extensive continental glaciation on Siberia. The early shift of the Nd isotopes of AIW towards less radiogenic signatures at about 50 ka was then explained by the absence of a land based ice cover in the Kara Sea region after 50 ka including the LGM (cf. Svendsen et al., 2004). While a viable mechanism for the transfer of radiogenic shelf Nd isotope signatures to water masses around 1000 m deep where AIW prevailed has been provided by Haley et al. (2008a), there were no Nd isotope signatures from the Kara Sea shelf available. Therefore, the relative contribution between North Atlantic inflow and Kara Sea shelf input could not be well constrained.

A combined reconstruction of Hf-Nd isotope compositions of past central Arctic Intermediate Water (AIW) from authigenic, early diagenetic Fe-Mn oxyhydroxide of marine sediment is presented in this study. The investigations were carried out applying a modified leaching method of Gutjahr et al. (2007) and Haley et al. (2008a) to high-resolution central Arctic combined box/kastenlot core PS2185 (87° 31.9' N; 144° 22.9' E; 1,051 m water depth) and to Integrated Ocean Drilling Program (IODP) Leg 302 (a

composite record of cores M0002 and M0004, 87°5 N, 137° E; 1,250 m water depth, Expedition "ACEX", thereafter referred to as Leg 302 core). Both PS2185 and Leg 302 cores were recovered on the Lomonosov Ridge (Figure 6.1), for which well-developed age models are available (Spielhagen et al., 2004; Backman et al., 2008). Moreover, in order to better constrain the radiogenic isotope endmember signatures of the Siberian Arctic, five core-top samples from the Kara Sea were also analyzed for Nd and Hf isotope compositions (Figure 6.1).

6.2 Materials and Methods

Detailed published information about the stratigraphy and composition of the sediments of core PS2185 can be found in Spielhagen et al., (2004). The location, sedimentary features, and age model of Leg 302 core have been presented in Moran et al. (2006) and Backman et al. (2008). The sedimentation rates of the upper part of the Leg 302 core were constrained using cosmogenic ^{10}Be. Due to a recent revision of the half-life of ^{10}Be from 1.51 Myr to 1.387 Myr (Chmeleff et al., 2010; Korschinek et al., 2010), the age model for the uppermost 151 m of the Leg 302 core previously dated to cover the past 12.3 million years (Frank et al., 2008) had to be revised and is applied here for all data. The revised sedimentation rate for the upper 151 m is now 15.75 m/Myr resulting in an age of only 11.3 Ma at 151 m core depth, including a hiatus of 2 Myr duration between 135 and 140 m core depth. Within uncertainties this revised chronological information is still consistent with the few other independent biostratigraphic age constraints available (Backman et al., 2008). Two core-top sediment samples from the Lomonosov Ridge were measured to prove the seawater origin of the extracted Hf isotope compositons.

Approximately one gram of bulk sediment per sample is needed to guarantee the extraction of sufficient amounts of seawater-derived Hf (>50 ng) for high precision isotope measurements. After washing samples three times with Milli-Q water, Nd and Hf contained in the sedimentary oxyhydroxide fraction were leached for about one hour in a single step using a dilute reducing and complexing solution consisting of 0.005 M hydroxylamine hydrochloride, 1.5% acetic acid, and 0.03 M EDTA-2Na, buffered to pH = 4 with suprapur® NaOH. A buffered acetic acid leach step was omitted since these

sediments are essentially devoid of carbonates. The hydroxylamine hydrochloride and acetic acid mixture was 10-fold diluted compared with the method of Gutjahr et al. (2007) in order to avoid any potential contamination caused by leaching of clay minerals. To keep the extracted Hf in solution, we added 0.03M EDTA-2Na to the leaching solution for complexing the Hf following Gutjahr (2006), which yielded 50-100 ng authigenic Hf per gram of bulk sediment. After centrifugation, the leach solution was decanted, evaporated, and processed through a cation exchange resin AG 50WX8 to separate and purify Nd and Hf. The Nd and Hf cuts were further separated from the other REEs, ytterbium and lutetium, respectively, with Ln-spec resin (Pin and Zalduegui, 1997; Münker et al., 2001). In order to constrain the origin of the detrital particles, prior to total dissolution of the detrital fraction, the previously leached sediments were leached again for about 24 hours with a stronger leaching solution (0.05 M hydroxylamine hydrochloride) to ensure complete removal of residual Fe-Mn oxyhydroxides following the method applied in Gutjahr et al. (2007) and Haley et al. (2008a). Then the detrital samples were treated in aqua regia mixed with concentrated HF on a hotplate before complete dissolution in concentrated HNO_3 and HF in steel jacketed autoclaves at ~180-200°C for 3-4 days. Subsequent separation and purification of the Nd and Hf followed the same procedures as described above.

The procedural blank for both elements was negligible (less than 1% and 0.2% contribution for Hf and Nd, respectively). Hafnium and Nd isotope ratios were measured on a Nu instruments MC-ICP-MS at GEOMAR. Instrumental bias was corrected applying an exponential mass fractionation law using $^{146}Nd/^{144}Nd$ of 0.7219 and $^{179}Hf/^{177}Hf$ of 0.7325, respectively. To monitor the external reproducibility and system drift, generally four to six samples were bracketed by analyses of the standard JMC 475 and an internal laboratory standard solution (CertiPUR) for Hf isotopes, and of standard JNdi-1 and an internal laboratory standard (SPEX) for Nd isotopes. $^{176}Hf/^{177}Hf$ results were normalized to JMC475 = 0.282160 (Nowell et al., 1998) while $^{143}Nd/^{144}Nd$ results were normalized to JNdi-1 = 0.512115 (Tanaka et al., 2000). The 2σ external reproducibility of repeated standard measurements was 0.21 (n=28) and 0.30 (n=28) epsilon units for Hf and Nd isotopes, respectively.
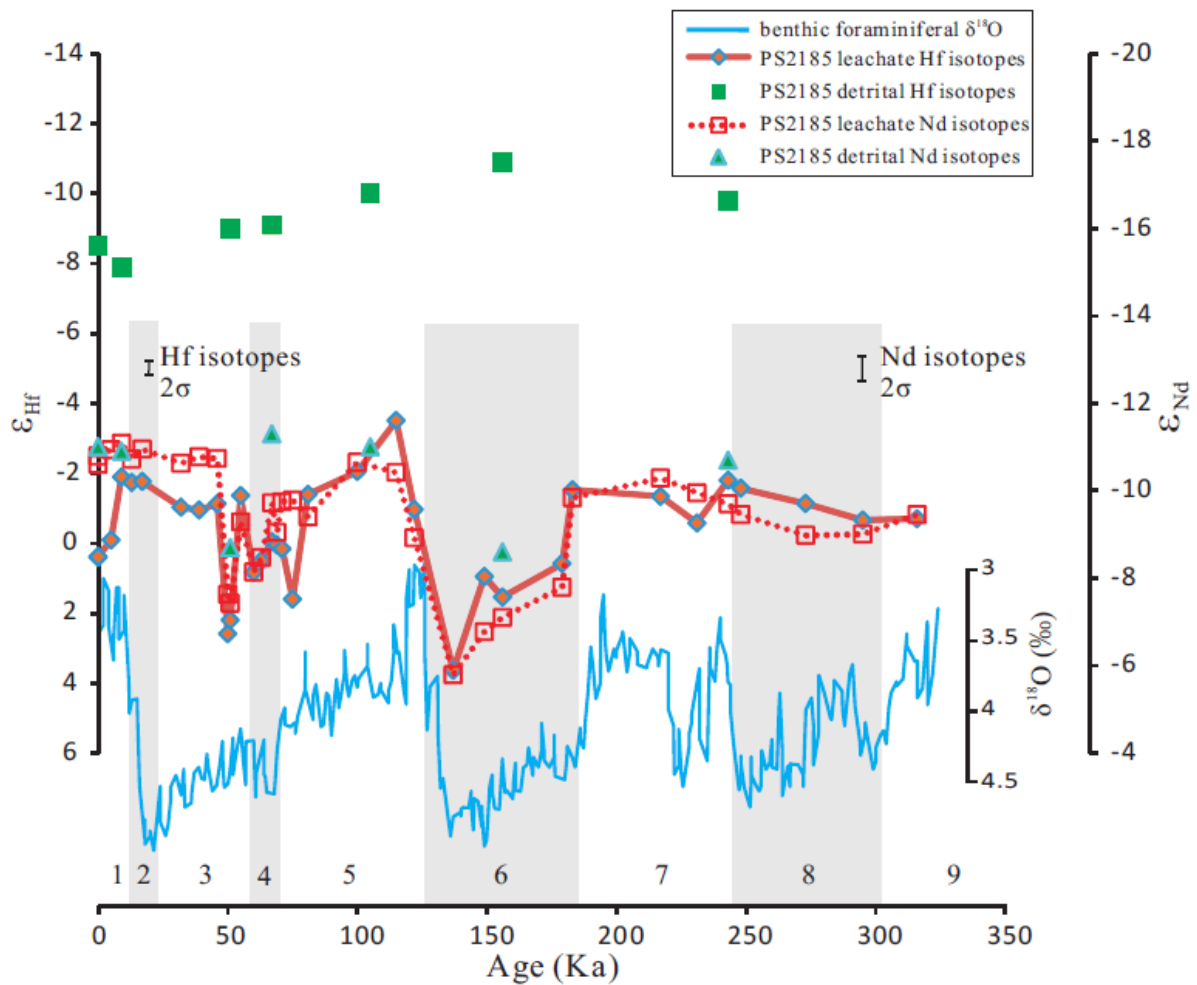
Figure 6.2 Late Quaternary Nd (dashed line and open squares) – Hf (solid line and full diamonds) isotopic evolution of Arctic Intermediate Water obtained from core PS2185. Glacial–interglacial cycles of Nd and Hf isotopes are compared with the globally stacked benthic foraminiferal $\delta^{18}O$ data (Zachos et al., 2001). Gray bands correspond to the glacial isotope stages. Also shown are Hf-Nd isotope compositions of the detrital fraction in this core. The axis dimensions for Nd and Hf isotopes are adjusted in order to demonstrate the close co-evolution of leachate Nd-Hf isotope signatures with the global benthic foraminiferal $\delta^{18}O$ evolution.

Table 6.1 Nd-Hf isotopes from leachates and detrital materials of the Arctic sediments.

Sample[a]	Depth (m)	Age (Ma)	Leachate ^{143}Nd/^{144}Nd (2σ)	ε_{Nd}[b]	Haley et al.[c]	Leachate ^{176}Hf/^{177}Hf (2σ)	ε_{Hf}[d]	Detrital ^{143}Nd/^{144}Nd (2σ)	ε_{Nd}[b]	Detrital ^{176}Hf/^{177}Hf (2σ)	ε_{Hf}[d]
PS2179-1	coretop	0.000	0.512093±4	-10.6	-10.5	0.282780±3	0.4	0.512073±4	-11.0	0.282529±4	-8.5
PS70\316	coretop	0.000	0.512085±4	-10.8		0.282780±3	0.4				
duplicate run			0.512094±4	-10.6							
PS2185-3	0.03	0.005	0.512077±4	-10.9	-10.8	0.282766±3	-0.1				
duplicate run			0.512089±5	-10.7							
PS2185-3	0.08	0.009	0.512070±5	-11.1	-10.8	0.282715±3	-1.9	0.512082±4	-10.9	0.282547±3	-7.9
duplicate run			0.512070±4	-11.1							
PS2185-3	0.10	0.013	0.512088±7	-10.7	-10.5	0.282720±3	-1.7				
PS2185-3	0.12	0.017	0.512077±5	-10.9	-11.0	0.282719±5	-1.8				
PS2185-3	0.16	0.032	0.512093±5	-10.6	-10.7	0.282740±2	-1				
PS2185-3	0.21	0.039	0.512086±4	-10.8	-10.7	0.282742±3	-1				
PS2185-3	0.26	0.046	0.512088±5	-10.7	-10.6	0.282737±3	-1.1				
PS2185-3	0.31	0.050	0.512247±5	-7.6	-7.8	0.282842±3	2.6				
PS2185-3	0.36	0.051	0.512257±4	-7.4	-7.4	0.282831±2	2.2	0.512193±4	-8.7	0.282514±2	-9
PS2185-6	0.69	0.055	0.512162±4	-9.3		0.282731±3	-1.4				
PS2185-6	0.95	0.060	0.512221±4	-8.1	-7.3	0.282793±3	0.8				
PS2185-6	1.13	0.063	0.512204±5	-8.5		0.282783±4	0.5				
PS2185-6	1.25	0.067	0.512140±5	-9.7		0.282768±3	0	0.512061±5	-11.3	0.282513±3	-9.1
PS2185-6	1.35	0.069	0.512174±3	-9.0		0.282770±3	0.1				
PS2185-6	1.45	0.071	0.512138±3	-9.7		0.282774±3	0.2				
PS2185-6	1.61	0.075	0.512136±3	-9.8		0.282814±3	1.6				
duplicate run			0.512134±3	-9.8							
PS2185-6	1.81	0.081	0.512156±3	-9.4		0.282730±2	-1.4				
duplicate run			0.512159±4	-9.3							
PS2185-6	2.05	0.093	0.512092±3	-10.7		0.282711±3	-2				
duplicate run			0.512098±4	-10.5							
PS2185-6	2.21	0.105	0.512104±3	-10.4		0.282670±2	-3.5	0.512074±4	-11.0	0.282486±3	-10
PS2185-6	2.41	0.122	0.512180±4	-8.9	-10.3	0.282742±3	-1				
PS2185-6	2.56	0.137	0.512341±4	-5.8		0.282872±3	3.6				
PS2185-6	2.7	0.149	0.512291±4	-6.8		0.282796±3	1				
PS2185-6	2.78	0.156	0.512274±3	-7.1	-6.5	0.282813±3	1.5	0.512195±4	-8.6	0.282462±3	-11
PS2185-6	3.01	0.179	0.512239±4	-7.8		0.282785±3	0.6				
PS2185-6	3.15	0.183	0.512134±4	-9.8		0.282726±3	-1.5				
PS2185-6	3.41	0.217	0.512111±4	-10.3		0.282731±2	-1.3				
PS2185-6	3.51	0.231	0.512128±4	-10.0		0.282753±3	-0.6				
PS2185-6	3.59	0.243	0.512138±5	-9.7	-10.0	0.282718±3	-1.8	0.512091±4	-10.7	0.282492±4	-9.8
PS2185-6	3.61	0.250	0.512153±4	-9.5		0.282725±3	-1.6				

Sample			^{143}Nd/^{144}Nd	ε_{Nd}	ε_{Nd}	^{176}Hf/^{177}Hf	ε_{Hf}	^{143}Nd/^{144}Nd	ε_{Nd}	^{176}Hf/^{177}Hf	ε_{Hf}
PS2185-6	3.67	0.273	0.512178±4	-9.0	-9.8	0.282737±2	-1.1				
PS2185-6	3.73	0.295	0.512176±4	-9.0	-7.8	0.282750±3	-0.7				
PS2185-6	3.83	0.316	0.512153±4	-9.5		0.282749±3	-0.7				
duplicate run			0.512150±4	-9.5							
4/3/2/143-145	10.81	0.686	0.512152±4	-9.5	-10.3	0.282735±3	-1.2	0.512034±6	-11.8	0.282489±4	-9.9
duplicate run			0.512144±3	-9.6							
4/4/1/110-112	13.69	0.869	0.512192±4	-8.7	-8.0	0.282755±3	-0.5				
duplicate run			0.512196±4	-8.6							
2/5/1/100-102	21.42	1.360	0.512252±5	-7.5	-9.3	0.282776±3	0.2				
2/5/2/50-52	22.43	1.424	0.512268±4	-7.2	-6.3	0.282790±3	0.7	0.512043±5	-11.6	0.282424±2	-12
2/7/2/52-54	31.14	1.977	0.512174±4	-9.1	-8.2	0.282717±2	-1.8				
2/10/2/70-72	43.76	2.778	0.512193±4	-8.7	-8.0	0.282720±2	-1.7	0.512024±7	-12.0	0.282420±4	-12
2/11/3/70-72	49.70	3.156	0.512163±3	-9.3	-8.3	0.282739±3	-1.1	0.512022±4	-12.0	0.282445±3	-12
2/14/1/80-82	60.80	3.860	0.512232±3	-7.9	-7.5	0.282768±2	0				
2/19/1/25-27	81.45	5.171	0.512215±4	-8.2	-7.6	0.282767±3	-0.1				
2/20/2/70-72	88.41	5.613	0.512219±3	-8.2	-7.2	0.282773±2	0.2				
2/25/1/78-80	110.99	7.047	0.512239±4	-7.8	-6.9	0.282790±3	0.8	0.512086±6	-10.8	0.282455±3	-11
2/29/2/70-72	130.40	8.279	0.512207±3	-8.4	-8.2	0.282757±2	-0.4	0.512089±7	-10.7	0.282497±2	-9.6
2/35/2/78-80	155.05	11.527	0.512224±3	-8.1	-7.6	0.282767±2	-0.1			0.282511±5	-9.1
2/40/2/80-82	175.38	12.818	0.512176±4	-9.0	-8.7	0.282792±3	0.8				
2/43/2/70-72	189.68	13.726	0.512202±4	-8.5	-9.4	0.282758±2	-0.4				
BP97-12	coretop	0.000	0.512338±5	-5.9		0.282845±3	2.7	0.512236±4	-7.8	0.282667±3	-3.6
BP97-32	coretop	0.000	0.512357±5	-5.5		0.282916±3	5.2	0.512237±6	-7.8	0.282653±3	-4.1
BP97-46	coretop	0.000	0.512337±5	-5.9		0.282879±4	3.9	0.512222±4	-8.1	0.282546±3	-7.9
BP97-52	coretop	0.000	0.512325±4	-6.1		0.282856±5	3.1	0.512219±4	-8.2	0.282367±3	-14.2
BP97-56	coretop	0.000	0.512333±5	-6.0		0.282869±4	3.5	0.512201±5	-8.5	0.282374±3	-14.0

a.   PS2185 and the nearby core-top samples PS2179-1, PS70\316 were from combined box/kastenlot cores taken in the central Arctic (Spielhagen et al., 2004). IODP Leg 302 samples in this study were recovered from drill cores M0002A and M0004C (Expedition 302 Scientists, 2005). The BP97 sediment samples were taken by Bettina Finkenberger (GEOMAR) in 1997 during an expedition with RV Akademik Boris Petrov to the Kara Sea.

b. $\varepsilon_{Nd} = [(^{143}Nd/^{144}Nd)_{sample}/(^{143}Nd/^{144}Nd)_{CHUR} -1]*10^4$; where $(^{143}Nd/^{144}Nd)_{CHUR} = 0.512638$ (Jacobsen and Wasserburg, 1980).

c.   comparison with previously published neodymium isotope data from Haley et al. (2008a).

d. $\varepsilon_{Hf} = [(^{176}Hf/^{177}Hf)_{sample}/(^{176}Hf/^{177}Hf_{CHUR})-1]*10^4$; where $(^{176}Hf/^{177}Hf)_{CHUR}=0.282769$ (Nowell et al., 1998).

6.3 Results

The Hf and Nd isotope data obtained from leachates and detrital fractions are provided in Table 6.1. The Fe-Mn oxyhydroxide based ε_{Nd} (-10.6, -10.8) and ε_{Hf} (+0.4, +0.4) reproduced present day AIW (ε_{Nd}: about -10.8, ε_{Hf}: about +0.6, Andersson et al. 2008; Porcelli et al., 2009; Zimmermann et al., 2009a) as shown by leaching of two core-top

samples on the Lomonosov Ridge (PS2185 and PS70/316, which is a location close to core PS2185). Three water samples at the core of AIW around 1000 m seem to have lower ε_{Hf} (+0.3, -0.4, and -1.4, Zimmermann et al., 2009a). Given that the analytical uncertainties of the Hf isotope data in their study were very high ($\pm$ 2 to 3 epsilon units), an unambiguous comparison of the Hf isotope signatures between core-top leachates and modern AIW remains difficult. It is however noted that the modern ε_{Hf} of AIW of about +0.6 is suggested to be the likely present day Atlantic inflow signature (Zimmermann et al., 2009a) which dominates the modern AIW. Without better constraints, modern AIW ε_{Hf} of about +0.6 is thus used here. The Kara Sea sediment leachates have isotope signatures similar to the Ob and Yenisei rivers (ε_{Nd}: -6.1 $\pm$ 0.3, -5.2 $\pm$ 0.3 and ε_{Hf}: +1.5 $\pm$ 1.3, +3.0 $\pm$ 1.3, respectively), whereas the detrital fractions from Kara Sea sediments are clearly less radiogenic (ε_{Nd}: -7.8 to -8.5; ε_{Hf}: -3.6 to -14.2). The down core Nd-Hf isotope records from the Lomonosov Ridge show remarkably closely coupled trends. Two sets of isotopic records on millennial (Fig. 2, the Late Quaternary record) and million year (Fig. 3, the Neogene record) time scales were obtained.
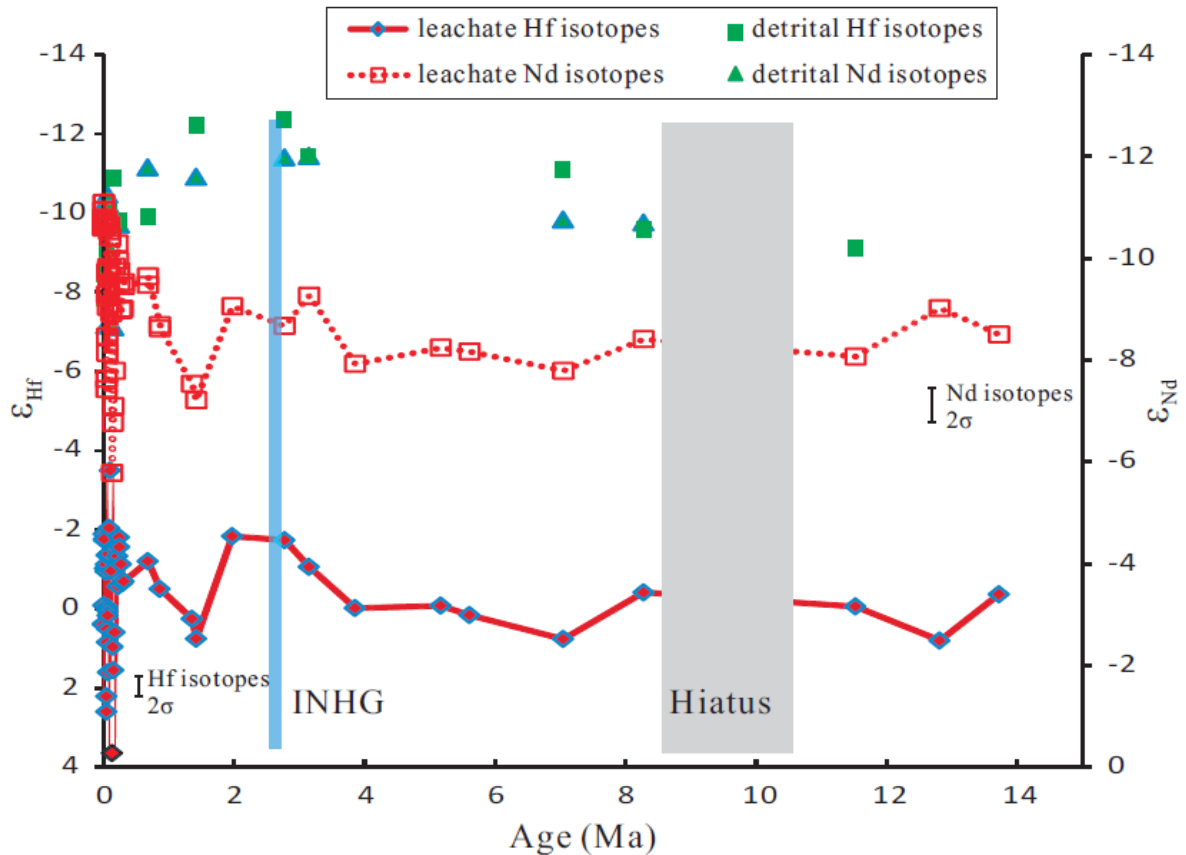
Figure 6.3 Nd–Hf isotopic evolution of the Arctic Intermediate Water from the Middle Miocene to the present. Also shown are total dissolution data of the detrital fraction (triangles). The data are from both PS2185 (0 to 300,000 years) and IODP Leg 302 (0.7 to 13.7 million years). Note that the axis dimensions for Nd and Hf isotopes are different from Figure 6.2. INHG denotes the time of major intensification of Northern Hemisphere Glaciation.

In the Late Quaternary record, more radiogenic ε_{Hf} signatures are observed during glacial MIS 4, 6, but no resolvable change in MIS 8 which may be due to the lower time resolution for this part of the record (Figure 6.2). While the ε_{Nd} signature of AIW remained virtually unchanged over the past 50 kyr, the ε_{Hf} signature of AIW decreased from -1.0 at 30 ka to -1.9 until the early Holocene and then became more radiogenic to reach the ε_{Hf} signature of +0.4 at the present day. The most significant excursion on the order of seven ε_{Hf} units from +4.0 to -3.1 occurred at the end of MIS 6. The ε_{Nd} evolution of AIW resembles the pattern of ε_{Hf} very closely albeit at smaller amplitude. No

noticeable phase lag has been found between the two isotope systems at the studied time resolution. This similarity also holds for the Neogene (14 to 2 Myr, Figure 6.3), during which ε_{Nd} and ε_{Hf} varied between -11.1 and -5.8 and between -3.5 and +3.6, respectively. Both the Nd and Hf isotopic records displayed only relatively small variations prior to 4 Ma and thereafter became overall less radiogenic and more variable. During the early Pleistocene, the ε_{Hf} signal shifted back to +0.7 at 1.7 Ma before decreasing again to -1.2 at 0.8 Ma. It is likely that further high-resolution variations occurred and have been missed in the early Pleistocene record because of the lower time resolution in this part of our record. Overall, the Nd isotopes showed a smaller range of variability than the Hf isotopes on the Myr timescale. These leachate data are within the range of data defined by Arctic seawater samples in ε_{Nd} versus ε_{Hf} space (Figure 6.4), but are below the seawater array (Albarède et al., 1998) defined by global seawater and slow-growing Fe-Mn nodule and crust data.

For comparison, the Hf and Nd isotope compositions of the detrital fractions in several sediment samples were measured to investigate the detrital provenance and the leaching efficiency in terms of selectively dissolving the authigenic, seawater-derived phase only. The detrital fractions have significantly less radiogenic isotope signatures than those of the Fe-Mn oxyhydroxide phase (Figure 6.2, 6.3, 6.4). The detrital ε_{Hf} signature in central Arctic sediments ranges from -7.9 to -12.3 and the average ε_{Hf} difference between the leached and detrital fraction is about 10 ε_{Hf} units. In fact, the ε_{Hf}-ε_{Nd} signatures of the bulk sediments from the central Arctic as well as from the Kara Sea are indistinguishable from the terrestrial array (Figure 6.4).
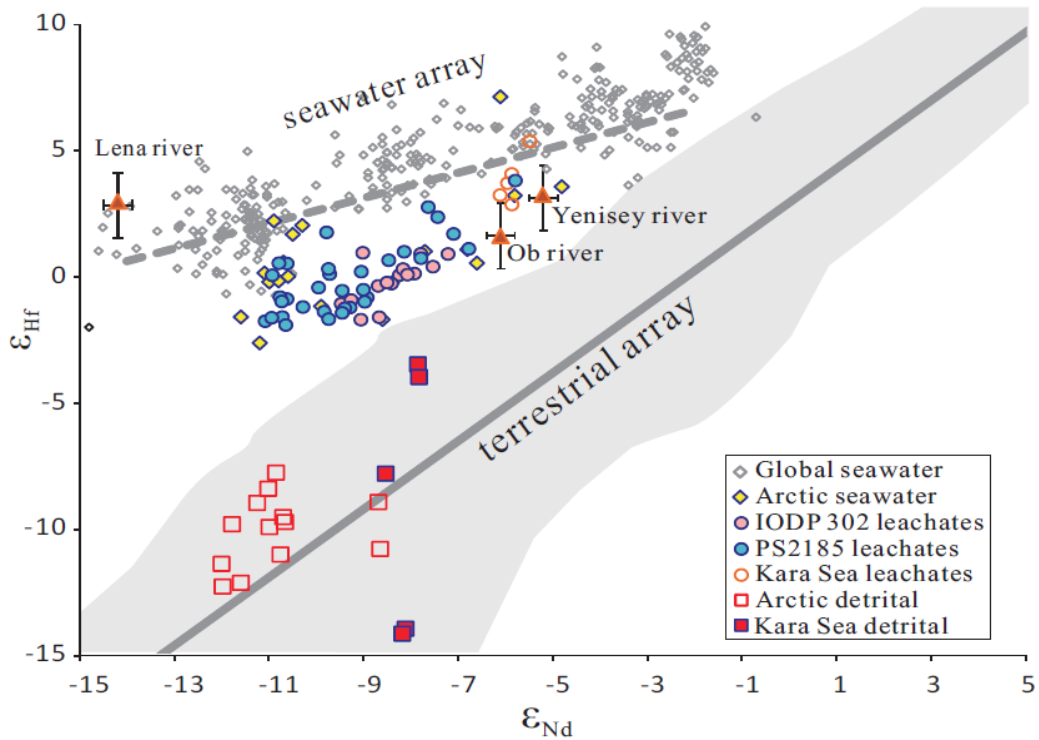
Figure 6.4 Hafnium–neodymium isotope systematics of the leachates and detrital materials in this study together with previously published data and ε_{Nd}-ε_{Hf} correlation lines from the literature. The gray shaded area denotes the terrestrial igneous rocks (van de Flierdt et al., 2004a). The data from leachates and Arctic seawater (Zimmermann et al., 2009a) are significantly above the terrestrial array (Vervoort et al., 1999), but still somewhat below the seawater array (Albarède et al., 1998). Global seawater Nd-Hf isotope data were obtained from hydrogenetic Fe-Mn crusts/nodules (Lee et al., 1999; Piotrowski et al., 2000; van de Flierdt et al., 2004a, b) and seawater dissolved component (<0.45 μm, Rickli et al., 2009, 2010 Zimmermann et al., 2009a, b; Stichel et al., 2012). Data of the Arctic rivers are from Zimmermann et al., 2009a.

6.4 Discussion

6.4.1 The leached Hf isotope compositions: reliable record of past bottom water signatures?

It has been demonstrated that the Nd isotope compositions of bulk sediment leachates in various abyssal marine settings represent a seawater signal, except for locations with a

presence of volcanic ash (e.g. Piotrowski et al., 2005; Gutjahr et al., 2008; Haley et al., 2008a, Elmore et al., 2011). However, it has yet to be demonstrated that this is also the case for the extracted Hf isotope compositions. Using a similar method as described above, Gutjahr (2006) presented Hf isotope records obtained from the authigenic Fe-Mn oxyxyhdroxide fraction of Blake Ridge sediments, and suggested that seawater-derived Hf can be extracted from marine sediments. However, the Hf concentration in the leachates was generally very low, and although systematically higher than the detrital fraction, Hf/Al were not as clearly distinguishable from the detrital fraction as in the case of Nd/Al or Pb/Al (Gutjahr, 2006). Due to the low concentration of Hf in the authigenic fraction, the mass balance approach taken in Gutjahr et al. (2007) cannot be reliably applied to assess potential offsets of authigenic ε_{Hf} signatures by contributions from partial dissolution of detrital material. Nevertheless, several lines of evidences presented below corroborate that our leached Hf isotope compositions represent a bottom water signature.

First, the two core top samples yield Hf-Nd isotope signatures (Table 6.1) that are within error identical to previously determined signatures in the Nansen, Amundsen, and Makarov Basins (ε_{Nd}= -10.8, ε_{Hf}= +0.6 albeit with large uncertainty, Andersson et al., 2008; Porcelli et al., 2009; Zimmermann et al., 2009a), which have been suggested to represent the isotopic compositions of the North Atlantic inflow (Zimmermann et al., 2009a). In addition, the Hf isotopic signatures of the downcore leachates are significantly more radiogenic than their corresponding detrital Hf isotope compositions. Moreover, the late Quaternary detrital Hf isotope signal fluctuated much less and did not vary in a fashion similar to the leached ε_{Hf} signatures (Figure 6.2). Rather, the evolution of leached Hf isotope signatures was very similar to that of Nd isotopes. In Nd-Hf isotope space (Figure 6.4), the leachates and detrital fractions fall into completely different areas. Finally, all the leachate data vary within the range of the modern Nd-Hf isotopic composition of Arctic seawater (Figure 6.4). Together, these arguments lend strong support to our suggestion that the leached Hf isotope records shown here reliably represent a past seawater signal.

6.4.2 Consistency of detrital Nd-Hf isotope compositions of the Lomonosov Ridge sediments with the terrestrial array

While detrital ε_{Nd} signatures of present day Kara Sea sediments show very similar signatures ($\Delta\varepsilon_{Nd} \leq 0.6$), their ε_{Hf} signal varies widely ($\Delta\varepsilon_{Hf}$ reaches 10.6) (Figure 6.4). This is explained by different portions of zircon in the sediment at different locations on the shelf as a consequence of some mineral and grain size sorting effects (Patchett et al., 1984; Carpentier et al., 2009; Bayon et al., 2009; Vervoort et al., 2011). The inhomogenous zircon distribution in these sediments is probably caused by the currents of the Kara Sea and the supply of material from different rock types in the hinterland. However, the detrital Hf-Nd isotope compositions from the more remote Lomonosov Ridge are close to the terrestrial array and display smaller Hf isotopic variations (Figure 6.4). Therefore, their Hf-Nd isotope distribution likely reflected poor sorting of sediments during shelf sea ice or iceberg transport over the last 14 million years (Haley 2008b), which is expected not to fractionate zircons significantly from the other minerals. Our interpretation is supported by the perennial sea ice conditions over the last 14 Myr in the Arctic Ocean (Darby et al., 2008; Frank et al., 2008; St. John, 2008; Polyak et al., 2010).
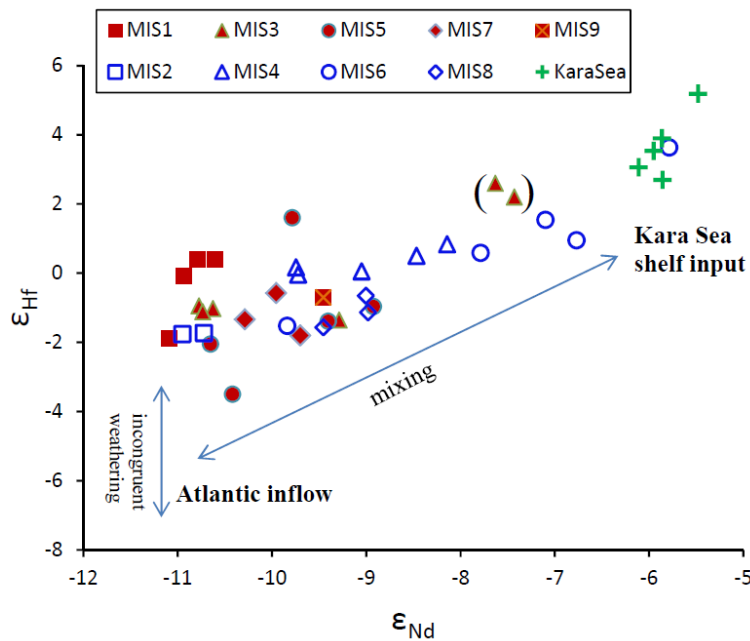
Figure 6.5 Hafnium–neodymium isotope systematics of the leachates obtained from core PS2185 at different marine isotope stages. Also shown are the data of Kara Sea surface sediment leachates. The

isotopic variation of PS2185 can be interpreted as mainly reflecting a two-component mixing between the Atlantic inflow and radiogenic input from the Kara Sea shelf (oblique arrow), while incongruent weathering (vertical arrow) seems to only play a subordinate role.

6.4.3 Subordinate role of weathering regime changes in driving the Hf isotopic evolution of AIW

Similar to Nd isotopes, the Hf isotope composition of AIW has been controlled by weathering contributions from different sources, distributed and mixed in dissolved form by the deep circulation. However, the release of Hf from these sources may also have depended on changes of the weathering regime. Zircon, as the main host mineral of Hf, is very resistant to weathering and contains highly unradiogenic Hf because of its very low Lu/Hf ratios. As a result, isotope compositions of Hf dissolved during weathering processes are generally more radiogenic than those of the bulk rocks (the "zircon effect", White et al., 1986; Albarède et al., 1998; van de Flierdt et al., 2002), although the zircon effect alone is probably not enough to produce the seawater trend in ε_{Nd} versus ε_{Hf} space (Chen et al., 2011). During glacial weathering, enhanced breakdown and dissolution of zircons may in turn potentially drive the dissolved Hf isotope signatures in seawater towards less radiogenic bulk rock isotope compositions (i.e., more congruent weathering), while Nd isotopes are not influenced significantly by these processes (van de Flierdt et al., 2002). The AIW record shows a very closely coupled evolution of Hf and Nd isotope compositions of AIW on both glacial-interglacial (Figure 6.2), as well as on longer time scales (Figure 6.3). For example, the late Quaternary changes can be related to processes mostly following glacial-interglacial time scales (except the data younger than 50 ka). Figure 6.5 shows the late Quaternary variability of the Nd and Hf isotope data of AIW obtained from the PS2815 leachates for different marine isotopes stages. The interglacial stages are generally characterized by less radiogenic isotope compositions. MIS6 contains the most radiogenic isotope compositions that even approached the likely Kara Sea endmember of weathering inputs (Figure 6.4, 6.5) whereas the penultimate deglaciation witnessed the most abrupt drop both in Nd (5 ε units) and Hf isotope compositions (7 ε units) to less radiogenic values. Given the synchronous variations of

Nd and Hf isotopes, changes in weathering regime have obviously only played a subordinate role in driving the Hf isotopic evolution of AIW.

6.4.4 Variations of North Atlantic inflow to AIW over the past 14 Myr

6.4.4.1 Constraints on the sources of Nd and Hf in AIW

North Atlantic inflow today shows a relatively homogeneous and unradiogenic signature throughout the water column in its Nd isotope composition (ε_{Nd} ~-10.7 to -10.8, Piepgras and Wasserburg, 1987; Lacan and Jeandel, 2004; Andersson et al., 2008), which precludes contributions from weathering or exchange with sediments near Iceland as a significant source of Nd. Reportedly, present day exchange with Iceland derived basaltic material does not affect the deep water ε_{Nd} signature of the main path of North Atlantic inflow but rather mainly influences the signature of southward flowing currents such as the East Greenland Current (Lacan and Jeandel, 2004). The same situation probably also holds for Hf, given that the average Hf isotope composition of Arctic deep water (ε_{Hf} ~0.6, Zimmermann et al., 2009a) is similar to the marginal North Atlantic surface water (-1 to 1.4, Rickli et al., 2009; 2010; Godfrey et al., 2009). Riverine inflow and shelf sediment-seawater exchange processes also contribute Nd and Hf to Arctic seawater (Andersson et al., 2008; Porcelli et al., 2009; Zimmermann et al., 2009a). As a consequence of these inputs into the semi-enclosed Arctic basin, the concentrations of Hf and Nd in the Arctic deep water are slightly elevated compared with the Atlantic inflow. Nevertheless, most of the deep and intermediate waters in the Nansen, Amundsen, and Makarov Basins have Nd-Hf isotope compositions very close to the Atlantic inflow, supporting the dominant source from the Atlantic waters. In the Canada Basin, where more radiogenic waters of Pacific origin (for both Nd and Hf, Porcelli et al., 2009; Zimmermann et al., 2009b) exert an influence via the Bering Strait, Nd and Hf isotopes are generally more radiogenic than in the other basins of Arctic Ocean. Thus, at first glance, it may seem reasonable to interpret the more radiogenic isotope signatures found in glacial times (Figure 6.2) to reflect enhanced input from the Pacific. However, this possibility can be excluded given that the Bering Strait inflow was already closed during incipient glaciation at a sea level about 50 m lower than today.

As mentioned in the introduction, the only major source for supplying radiogenic Nd (and probably also Hf) isotope compositions were the Putorana flood basalts of Siberia. All Nd-Hf leachate data obtained here fit within a mixing envelope between Kara Sea shelf input and North Atlantic waters (Figure 6.4, 6.5), supporting the assertion that both Nd and Hf isotopic variations can be explained by changing mixing proportions of the above two endmembers. The other potential sources around the Arctic, such as the Eastern Laptev Sea, North America and Greenland unlikely dominated the AIW signatures at the Lomonosov Ridge sampling site, mainly because of the lack of suitable transport mechanisms of water masses and detrital material from these sources to the studied area (Haley et al., 2008b). In addition, Nd-Hf isotopic compositions of these sources are not consistent with mixing relationships in Figure 6.4 (for example the Eastern Laptev Sea shelf input, as represented by the Lena river signature, Zimmermann et al., 2009a).

6.4.4.2 Glacial reduction of North Atlantic inflow into the Arctic

The newly obtained record of Hf isotopic AIW records, as well as our constraints on the isotope compositions of inputs from the Kara Sea, allows a close look at the characteristics of changes in contributions between the two potential endmembers: Atlantic inflow and brines formed on the more radiogenic Eurasian shelf.

During the penultimate glacial period, the very radiogenic values both in ε_{Hf} (+3.6) and ε_{Nd} (-5.8) are essentially indistinguishable from the Kara Sea endmember values (Figure 6.4, 6.5). This suggests that the Atlantic inflow has almost completely lost its influence on the Nd-Hf isotope signature of AIW at the Lomonosov Ridge sampling site during this interval. We thus propose that at least during the penultimate glacial period, North Atlantic water inflow was significantly reduced compared to the modern situation.

One may argue that much more radiogenic isotope signatures of the brines could have formed on the Kara sea shelf during glacial times. Consequently, high ε_{Hf} and ε_{Nd} of AIW in glacial times approaching the modern Kara sea endmember may not necessarily reflect changes in inflow flux of the North Atlantic. However, this is unlikely given the ε_{Nd} signatures of Kara Sea/Laptev Sea shelf sediments were inferred to have been similar between modern time and glacial maxima (Tütken et al., 2002). In addition, Pb isotopic

compositions of AIW imply that the late Quaternary Eurasian sediment weathering around the Arctic was generally more "congruent" than around the North Atlantic at least in terms of its Pb-specific chemical weathering behaviour (Haley et al., 2008b; Kurzweil et al., 2010). Thus the isotopic composition of Kara Sea input most likely did not change significantly over glacial-interglacial periods. In fact, reduced glacial North Atlantic inflow (and its unradiogenic Nd and Hf isotopes) to the Arctic Ocean is consistent with previous studies from the Arctic Ocean. From stable isotopes and microfossil abundances in a number of Arctic Ocean deep-sea cores, it was shown that strong Atlantic Water advection was restricted to interglacials and interstadials of the last 200 ky (Spielhagen et al. 2004). Moreover, cyclic variations in color and manganese content in sediments from the central Arctic Ocean also imply decreased ventilation of the Arctic Ocean during glacial times (Jakobsson et al., 2000; März et al., 2011).

However, the actual glaciation history on the Eurasian continent through time has been variable (Svendsen et al., 2004) and has not been directly coupled with global ice sheet volume inferred from benthic foraminifera (Figure 6.2). In this regard, the global benthic oxygen isotope variations in Figure 6.2 rather serve as a global climatic reference frame for the data presented in our study. From about 30 ka to the LGM, the Fennoscandian ice sheet expanded towards the shelf edge in the Nordic Seas (Ottesen et al., 2008; Mangerud et al., 2011), thereby transporting glacially eroded material to the continental margin off Northwest Europe. The Hf isotope composition of the North Atlantic inflow may potentially have been modified along the pathway of the inflow by exchange processes between these glacial sediments and seawater and/or by brine injection from sea ice formation at the ice sheet margin. As Nd isotope compositions through this period were virtually invariable, the Hf isotope variability was most likely controlled by incongruent weathering. This is demonstrated by the increasingly congruent weathering signature carried by the North Atlantic inflow from about 30 ka to the early Holocene, i.e., ε_{Hf} signature of AIW decreased from -1.0 at 30 ka to -1.9 at 9 ka. During the Holocene, the North Atlantic inflow was enhanced (e.g., Slubowska et al., 2005), whereas the weathering regime of the sediments along the inflow path became more incongruent (i.e., release of more radiogenic Hf). This inference is consistent with our record, in which the

ε_{Hf} signature of AIW became more radiogenic in the Holocene while the ε_{Nd} signature remained stable. Nevertheless, because of the complex erosional and glaciation history of the high latitude Eurasian continent, it is worthy to note that Hf isotope fractionation induced by incongruent weathering might not always have responded linearly to the orbital scale glacial-interglacial cycles. In other words, interglacial marine isotope stages may not always correspond to more incongruent weathering than glacial isotope stages around the Arctic.

6.4.5 The Neogene leachate record and weathering regime of the high latitude Eurasian continent

We suggest that the intermediate and comparatively stable Hf isotope signatures during most of the Neogene period (Figure 6.3) reflect relatively steady contributions from North Atlantic inflow and brine formation in the Kara sea region. Since around 4 Ma, the Hf and Nd isotope signatures have varied at higher amplitude (Figure 6.3), probably as a consequence of more pronounced glacial/interglacial cycles.

Water mass exchange between the North Atlantic and the Arctic may already have occurred as early as the Eocene (Gleason et al., 2009; Poirier et al., 2011) and should not have been tectonically restricted any more since the full opening of the Fram Strait for deep water exchange 17.5 million years ago (Jakobsson et al., 2007). However, the inflow of Atlantic water volumetrically similar to the present day situation, which was likely linked to the development of a far north-reaching Norwegian Current, may only have started as late as the mid Pleistocene (1.1-1.0 Ma, Thiede et al., 1998). This early suggestion is consistent with the Nd-Hf isotope data presented here, given that ε_{Nd} signatures essentially identical to the Atlantic endmember were only observed during the interglacials of the late Quaternary. Therefore, the dominant role of Atlantic inflow for the deep and intermediate Arctic Ocean may only be a relatively recent phenomenon.

Similar to modern Arctic seawater, most of the leachate data are plotted significantly above the terrestrial array (Vervoort et al., 1999) but still below the seawater array as defined by the data from other ocean basins (Figure 6.4, Albarède et al., 1998).

According to Piotrowski et al. (2000) and van de Flierdt et al. (2002), glacial weathering regimes on the continents are needed to explain such an offset. Thus these data suggest that glacial climatic conditions linked to preferentially physical weathering regimes dominated the past 14 Myr. IRD (ice rafted debris) records and surface morphology of sand-sized quartz from Leg 302 core sediments also indicated that the ice-house conditions, probably initiated as early as the mid-Eocene, were able to support growth of land-based ice sheets around the Arctic margin throughout our studied period of time (St. John, 2008). Due to the restricted connection of the Arctic "Mediterranean" ocean basin and the relatively short residence time of Hf in seawater on the order of a few hundred years (Rickli et al. 2009), the remaining global ocean was not affected by these weathering regimes and the global seawater data were characterized by less congruent weathering (van de Flierdt et al., 2002). Consequently, according to our data, the intensification of Northern Hemisphere glaciation at about 2.7 Ma (e.g. Raymo, 1994) did not result in significant changes of weathering inputs around the Arctic Ocean. In this respect, weathering regime changes after the onset of NHG that led to more radiogenic Pb isotope and a deviation of Hf isotope compositions toward the "terrestrial Nd-Hf isotope array (see Figure 6.4)" of the North Atlantic were most likely dominated by inputs from Greenland and Canada (von Blanckenburg and Nägler, 2001; van de Flierdt et al., 2002), rather than the Eurasian continental margin.

6.5 Conclusions

A first combined Nd-Hf isotopic record has been obtained from the authigenic Fe-Mn oxyhydroxide fraction of two sediment cores recovered in the central Arctic. The remarkably close coupling of the evolution of the two radiogenic isotope records, the overall systematic variations, and the agreement between core top data with modern seawater suggest that seawater-derived Hf isotope compositions can be reliably extracted from marine sediments. An observed offset of Nd and Hf isotopic compositions from the seawater array, which has also been observed from previous Arctic seawater analyses, is probably the result of a prevailing glacial weathering regime around the Arctic Ocean since at least 14 Myr ago. The data obtained in this study are explained by radiogenic Hf

and Nd inputs originating mainly from the Kara Sea shelf area and a severely restricted inflow of waters from the North Atlantic in glacial time. During MIS6, the most radiogenic isotope compositions of both Nd and Hf essentially approached the Kara sea shelf endmember compositions, indicating an essentially ceased Atlantic inflow to the central Arctic. However, the intensity of North Atlantic inflow has been weaker during most of the Neogene than during late Quaternary interglacial times. This study demonstrates that authigenic Hf isotopes extracted from marine sediments are a potentially powerful proxy for continental weathering inputs, as well as for water mass mixing in high resolution paleoceanographic studies.

References

Andersson, P. S., Porcelli, D., Frank, M., Bjork, G., Dahlqvist, R., and Gustafsson, O., 2008. Neodymium isotopes in seawater from the Barents Sea and Fram Strait Arctic-Atlantic gateways. Geochimica et Cosmochimica Acta 72, 2854-2867.

Aagaard, K., Swift, J. H., and Carmack, E.C., 1985. Thermohaline circulation in the Arctic mediterranean seas. Journal of Geophysical Research 90, 4833–4846.

Albarède, F., Simonetti, A., Vervoort, J. D., Blichert-Toft, J., and Abouchami, W., 1998. A Hf-Nd isotopic correlation in ferromanganese nodules. Geophysical Research Letters 25, 3895-3898.

Backman, J., Jakobsson, M., Frank, M., Sangiorgi, F., Brinkhuis, H., Stickley, C., O'Regan, M., Lovlie, R., Palike, H., Spofforth, D., Gattacecca, J., Moran, K., King, J., and Heil, C., 2008. Age model and core-seismic integration for the Cenozoic Arctic Coring Expedition sediments from the Lomonosov Ridge. Paleoceanography 23(1); doi:10.1029/2007PA001476.

Bayon, G., German, C. R., Boella, R. M., Milton, J. A., Taylor, R. N., and Nesbitt, R. W., 2002. An improved method for extracting marine sediment fractions and its application to Sr and Nd isotopic analysis. Chemical Geology 187, 179-199.

Bayon, G., Burton, K. W., Soulet, G., Vigier, N., Dennielou, B., Etoubleau, J., Ponzevera, E., German, C. R., and Nesbitt, R. W., 2009. Hf and Nd isotopes in marine sediments: Constraints on global silicate weathering. Earth and Planetary Science Letters 277, 318-326.

Bayon, G., Vigier, N., Burton, K. W., Brenot, A., Carignan, J., Etoubleau, J., and Chu, N. C., 2006. The control of weathering processes on riverine and seawater hafnium isotope ratios. Geology 34, 433-436.

Carpentier, M., Chauvel, C., Maury, R. C., and Mattielli, N., 2009. The "zircon effect" as recorded by the chemical and Hf isotopic compositions of Lesser Antilles forearc sediments. Earth and Planetary Science Letters 287, 86-99.

Chen, T.-Y., Ling, H.-F., Frank, M., Zhao, K.-D., and Jiang, S.-Y., 2011. Zircon effect alone insufficient to generate seawater Nd-Hf isotope relationships. Geochemistry, Geophysics, Geosystems 12, Q05003, doi:10.1029/2010GC003363.

Chmeleff, J., von Blanckenburg, F., Kossert, K., and Jakob, D., 2010. Determination of the (10)Be half-life by multicollector ICP-MS and liquid scintillation counting. Nuclear Instruments & Methods in Physics Research Section B-Beam Interactions with Materials and Atoms 268, 192-199.

Darby, D. A., 2008. Arctic perennial ice cover over the last 14 million years. Paleoceanography 23, PA1S07, doi:10.1029/2007PA001479.

David, K., Frank, M., O'Nions, R. K., Belshaw, N. S., and Arden, J. W., 2001. The Hf isotope composition of global seawater and the evolution of Hf isotopes in the deep Pacific Ocean from Fe-Mn crusts. Chemical Geology 178, 23-42.

Elmore, A. C., Piotrowski, A. M., Wright, J. D., and Scrivner, A. E., 2011. Testing the extraction of past seawater Nd isotopic composition from North Atlantic deep sea sediments and foraminifera. Geochemistry, Geophysics, Geosystems 12 Q09008, doi: 10.1029/2011gc003741.

Expedition 302 Scientists, 2005. Arctic Coring Expedition (ACEX): paleoceanographic and tectonic evolution of the central Arctic Ocean. IODP Preliminary Report., 302. doi:10.2204/iodp.pr.302.2005

Frank, M., Marbler, H., Koschinsky, A., de Flierdt, T. V., Klemm, V., Gutjahr, M., Halliday, A. N., Kubik, P. W., and Halbach, P., 2006. Submarine hydrothermal venting related to volcanism in the Lesser Antilles: Evidence from ferromanganese precipitates. Geochemistry Geophysics Geosystems 7, Q04010; doi 10.1029/2005gc001140.

Frank, M., Backman, J., Jakobsson, M., Moran, K., O'Regan, M., King, J., Haley, B. A., Kubik, P. W., and Garbe-Schönberg, D., 2008. Beryllium isotopes in central Arctic Ocean sediments over the past 12.3 million years: Stratigraphic and paleoclimatic implications. Paleoceanography 23, PA1S02, doi: 10.1029/2007PA001478

Gleason, J. D., Thomas, D. J., Moore, T. C., Blum, J. D., Owen, R. M., and Haley, B. A., 2009. Early to middle Eocene history of the Arctic Ocean from Nd-Sr isotopes in

fossil fish debris, Lomonosov Ridge. Paleoceanography 24, PA2215, doi: 10.1029/2008pa001685.

Godfrey, L. V., Zimmermann, B., Lee, D. C., King, R. L., Vervoort, J. D., Sherrell, R. M., and Halliday, A. N., 2009. Hafnium and neodymium isotope variations in NE Atlantic seawater. Geochemistry Geophysics Geosystems 10, Q08015, doi: 10.1029/2009GC002508.

Gutjahr, M., 2006. Reconstruction of changes in ocean circulation and continental weathering using radiogenic isotopes in marine sediments, Swiss Federal Institute of Technology Zürich.

Gutjahr, M., Frank, M., Stirling, C. H., Keigwin, L. D., and Halliday, A. N., 2008. Tracing the Nd isotope evolution of North Atlantic deep and intermediate waters in the Western North Atlantic since the Last Glacial Maximum from Blake Ridge sediments. Earth and Planetary Science Letters 266, 61-77.

Gutjahr, M., Frank, M., Stirling, C. H., Klemm, V., van de Flierdt, T., and Halliday, A. N., 2007. Reliable extraction of a deepwater trace metal isotope signal from Fe-Mn oxyhydroxide coatings of marine sediments. Chemical Geology 242, 351-370.

Haley, B. A., Frank, M., Spielhagen, R. F., and Eisenhauer, A., 2008a. Influence of brine formation on Arctic Ocean circulation over the past 15 million years. Nature Geoscience 1, 68-72.

Haley, B. A., Frank, M., Spielhagen, R. F., and Fietzke, J., 2008b. Radiogenic isotope record of Arctic Ocean circulation and weathering inputs of the past 15 million years. Paleoceanography 23, PA1S13, doi: 10.1029/2007PA001486.

Jacobsen, S. B. and Wasserburg, G. J., 1980. Sm-Nd Isotopic Evolution of Chondrites. Earth and Planetary Science Letters 50, 139-155.

Jakobsson, M., Lovlie, R., Al-Hanbali, H., Arnold, E., Backman, J., and Morth, M., 2000. Manganese and color cycles in Arctic Ocean sediments constrain Pleistocene chronology. Geology 28, 23-26.

Jakobsson, M., Backman, J., Rudels, B., Nycander, J., Frank, M., Mayer, L., Jokat, W., Sangiorgi, F., O'Regan, M., Brinkhuis, H., King, J., and Moran, K., 2007. The Early Miocene onset of a ventilated circulation regime in the Arctic Ocean. Nature 447, 986-990.

Karcher, M. J. and Oberhuber, J. M., 2002. Pathways and modification of the upper and intermediate waters of the Arctic Ocean. Journal of Geophysical Research-Oceans 107.

Knies, J. and C. Gaina, 2008. Middle Miocene ice sheet expansion in the Arctic: Views from the Barents Sea. Geochemistry Geophysics Geosystems 9, Q02015, doi:10.1029/2007GC001824.

Korschinek, G., Bergmaier, A., Faestermann, T., Gerstmann, U. C., Knie, K., Rugel, G., Wallner, A., Dillmann, I., Dollinger, G., von Gostomski, C. L., Kossert, K., Maiti, M., Poutivtsev, M., and Remmert, A., 2010. A new value for the half-life of (10)Be by Heavy-Ion Elastic Recoil Detection and liquid scintillation counting. Nuclear Instruments & Methods in Physics Research Section B-Beam Interactions with Materials and Atoms 268, 187-191.

Kurzweil, F., Gutjahr, M., Vance, D., and Keigwin, L., 2010. Authigenic Pb isotopes from the Laurentian Fan: Changes in chemical weathering and patterns of North American freshwater runoff during the last deglaciation. Earth and Planetary Science Letters 299, 458-465.

Lacan, F. and Jeandel, C., 2004. Neodymium isotopic composition and rare earth element concentrations in the deep and intermediate Nordic Seas: Constraints on the Iceland Scotland Overflow Water signature. Geochemistry Geophysics Geosystems 5, Q11006, 10.1029/2004GC000742.

Lee, D. C., Halliday, A. N., Hein, J. R., Burton, K. W., Christensen, J. N., and Gunther, D., 1999. Hafnium isotope stratigraphy of ferromanganese crusts. Science 285, 1052-1054.

Mangerud, J., Gyllencreutz, R., Lohne, Ø and Svendsen, J. I., 2011. Glacial History of Norway. In: J. Ehlers, P.L. Gibbard and P.D. Hughes (eds), Developments in Quaternary Science, Vol. 15, Amsterdam, The Netherlands, pp. 279-298.

März, C., Stratmann, A., Matthiessen, J., Meinhardt, A. K., Eckert, S., Schnetger, B., Vogt, C., Stein, R., and Brumsack, H. J., 2011. Manganese-rich brown layers in Arctic Ocean sediments: Composition, formation mechanisms, and diagenetic overprint. Geochimica et Cosmochimica Acta 75, 7668-7687.

Moran, K., Backman, J., Brinkhuis, H., Clemens, S.C., Cronin, T., Dickens, G.R., Eynaud, F., Gattacceca, J., Jakobsson, M., Jordan, R.W., Kaminski, M., King, J., Koc, N., Krylov, A., Martinez, N., Matthiessen, J., McInroy, D., Moore, T.C., Onodera, J., O'Regan, M., Paelike, H., Rea, B., Rio, D., Sakamoto, T., Smith, D.C., Stein, R., John, K.S., Suto, I., Suzuki, N., Takahashi, K., Watanabe, M., Yamamoto, M., Farrell, J., Frank, M., Kubik, P., Jokat, W., Kristoffersen, Y., 2006. The Cenozoic palaeoenvironment of the Arctic Ocean. Nature 441, 601–605.

Münker, C., Weyer, S., Scherer, E., and Mezger, K., 2001. Separation of high field strength elements (Nb, Ta, Zr, Hf) and Lu from rock samples for MC-ICPMS measurements. Geochemistry Geophysics Geosystems 2, 1064, doi:10.1029/2001GC000183.

Nørgaard-Pedersen, N., Spielhagen, R. F., Erlenkeuser, H., Grootes, P. M., Heinemeier, J., and Knies, J., 2003. Arctic Ocean during the Last Glacial Maximum: Atlantic and polar domains of surface water mass distribution and ice cover. Paleoceanography 18, 1063, doi: 10.1029/2002PA000781

Nowell, G. M., Kempton, P. D., Noble, S. R., Fitton, J. G., Saunders, A. D., Mahoney, J. J., and Taylor, R. N., 1998. High precision Hf isotope measurements of MORB and OIB by thermal ionisation mass spectrometry: insights into the depleted mantle. Chemical Geology 149, 211-233.

Ottesen, D., Stokes, C.R., Rise, L., Olsen, L., 2008. Ice-sheet dynamics and ice streaming along the coastal parts of northern Norway. Quaternary Science Reviews 27, 922–940.

Patchett, P. J., White, W. M., Feldmann, H., Kielinczuk, S., and Hofmann, A. W., 1984. Hafnium Rare-Earth Element Fractionation in the Sedimentary System and Crustal Recycling into the Earths Mantle. Earth and Planetary Science Letters 69, 365-378.

Piepgras, D. J. and Wasserburg, G. J., 1987. Rare-Earth Element Transport in the Western North-Atlantic Inferred from Nd Isotopic Observations. Geochimica et Cosmochimica Acta 51, 1257-1271.

Pin, C. and Zalduegui, J. F. S., 1997. Sequential separation of light rare-earth elements, thorium and uranium by miniaturized extraction chromatography: Application to isotopic analyses of silicate rocks. Analytica Chimica Acta 339, 79-89.

Piotrowski, A. M., Goldstein, S. L., Hemming, S. R., and Fairbanks, R. G., 2005. Temporal Relationships of Carbon Cycling and Ocean Circulation at Glacial Boundaries. Science 307, 1933-1938.

Piotrowski, A. M., Lee, D. C., Christensen, J. N., Burton, K. W., Halliday, A. N., Hein, J. R., and Günther, D., 2000. Changes in erosion and ocean circulation recorded in the Hf isotopic compositions of North Atlantic and Indian Ocean ferromanganese crusts. Earth and Planetary Science Letters 181, 315-325.

Poirier, A., and Hillaire-Marcel, C., 2011. Improved Os-isotope stratigraphy of the Arctic Ocean. Geophysical Research Letters 38, L14607, doi:10.1029/2011GL047953.

Polyak, L., Alley, R. B., Andrews, J. T., Brigham-Grette, J., Cronin, T. M., Darby, D. A., Dyke, A. S., Fitzpatrick, J. J., Funder, S., Holland, M., Jennings, A. E., Miller, G. H., O'Regan, M., Savelle, J., Serreze, M., St. John, K., White, J. W. C., Wolff, E., 2010. History of sea ice in the Arctic. Quaternary Science Reviews 29, 1757-1778.

Porcelli, D., Andersson, P. S., Baskaran, M., Frank, M., Björk, G., and Semiletov, I., 2009. The distribution of neodymium isotopes in Arctic Ocean basins. Geochimica et Cosmochimica Acta 73, 2645-2659.

Raymo, M. E., 1994. The Initiation of Northern-Hemisphere Glaciation. Annual Review of Earth and Planetary Sciences 22, 353-383.

Rickli, J., Frank, M., and Halliday, A. N., 2009. The hafnium-neodymium isotopic composition of Atlantic seawater. Earth and Planetary Science Letters 280, 118-127.

Rickli, J., Frank, M., Baker, A. R., Aciego, S., de Souza, G., Georg, R. B., and Halliday, A. N., 2010. Hafnium and neodymium isotopes in surface waters of the eastern Atlantic Ocean: Implications for sources and inputs of trace metals to the ocean. Geochimica et Cosmochimica Acta 74, 540-557.

Rudels, B., Jones, E. P., Anderson, L. G. and Kattner G., 1994. On the intermediate depth waters of the Arctic Ocean. In: The Polar Oceans and Their Role in Shaping the

Global Environment, O. M. Johannessen, R. D. Muench, J. E. Overland, Eds. (American Geophysical Union, Washington, DC), pp. 33–46.

Rudels, B., Jones, E. P., Schauer, U., and Eriksson, P., 2004. Atlantic sources of the Arctic Ocean surface and halocline waters. Polar Research 23, 181-208.

Slubowska, M. A., Koc, N., Rasmussen, T. L., and Klitgaard-Kristensen, D., 2005. Changes in the flow of Atlantic water into the Arctic Ocean since the last deglaciation: Evidence from the northern Svalbard continental margin, 80 degrees N. Paleoceanography 20, PA4014, doi:10.1029/2005PA001141.

Spielhagen, R. F., Baumann, K. H., Erlenkeuser, H., Nowaczyk, N. R., Nørgaard-Pedersen, N., Vogt, C., and Weiel, D., 2004. Arctic Ocean deep-sea record of northern Eurasian ice sheet history. Quaternary Science Reviews 23, 1455-1483.

Spielhagen, R. F., Werner, K., Sorensen, S. A., Zamelczyk, K., Kandiano, E., Budeus, G., Husum, K., Marchitto, T. M., and Hald, M., 2011. Enhanced Modern Heat Transfer to the Arctic by Warm Atlantic Water. Science 331, 450-453.

Stichel, T., Frank, M., Rickli, J., and Haley, B. A., 2012. The hafnium and neodymium isotope composition of seawater in the Atlantic sector of the Southern Ocean. Earth and Planetary Science Letters 317–318, 282-294.

St. John, K., 2008. Cenozoic ice-rafting history of the central Arctic Ocean: Terrigenous sands on the Lomonosov Ridge. Paleoceanography 23, PA1S05, doi:10.1029/2007PA001483.

Svendsen, J. I., Alexanderson, H., Astakhov, V. I., Demidov, I., Dowdeswell, J. A., Funder, S., Gataullin, V., Henriksen, M., Hjort, C., Houmark-Nielsen, M., Hubberten, H. W., Ingolfsson, O., Jakobsson, M., Kjaer, K. H., Larsen, E., Lokrantz, H., Lunkka, J. P., Lysa, A., Mangerud, J., Matiouchkov, A., Murray, A., Moller, P., Niessen, F., Nikolskaya, O., Polyak, L., Saarnisto, M., Siegert, C., Siegert, M. J., Spielhagen, R. F., and Stein, R., 2004. Late quaternary ice sheet history of northern Eurasia. Quaternary Science Reviews 23, 1229-1271.

Tanaka, T., Togashi, S., Kamioka, H., Amakawa, H., Kagami, H., Hamamoto, T., Yuhara, M., Orihashi, Y., Yoneda, S., Shimizu, H., Kunimaru, T., Takahashi, K., Yanagi, T., Nakano, T., Fujimaki, H., Shinjo, R., Asahara, Y., Tanimizu, M., and

Dragusanu, C., 2000. JNdi-1: a neodymium isotopic reference in consistency with LaJolla neodymium. Chemical Geology 168, 279-281.

Thiede, J., Winkler, A., Wolf-Welling, T., Eldholm, O., Myhre, A. M., Baumann, K. H., Henrich, R., and Stein, R., 1998. Late Cenozoic history of the Polar North Atlantic: Results from ocean drilling. Quaternary Science Reviews 17, 185-208.

Tütken, T., Eisenhauer, A., Wiegand, B., and Hansen, B. T., 2002. Glacial-interglacial cycles in Sr and Nd isotopic composition of Arctic marine sediments triggered by the Svalbard/Barents Sea ice sheet. Marine Geology 182, 351-372.

van de Flierdt, T., Frank, M., Lee, D. C., and Halliday, A. N., 2002. Glacial weathering and the hafnium isotope composition of seawater. Earth and Planetary Science Letters 198, 167-175.

van de Flierdt, T., Frank, M., Lee, D. C., Halliday, A. N., Reynolds, B. C., and Hein, J. R., 2004a. New constraints on the sources and behavior of neodymium and hafnium in seawater from Pacific Ocean ferromanganese crusts. Geochimica et Cosmochimica Acta 68, 3827-3843.

van de Flierdt, T., Frank, M., Halliday, A. N., Hein, J. R., Hattendorf, B., Gunther, D., and Kubik, P. W., 2004b. Tracing the history of submarine hydrothermal inputs and the significance of hydrothermal hafnium for the seawater budget-a combined Pb-Hf-Nd isotope approach. Earth and Planetary Science Letters 222, 259-273.

van de Flierdt, T., Goldstein, S. L., Hemming, S. R., Roy, M., Frank, M., and Halliday, A. N., 2007. Global neodymium-hafnium isotope systematics - revisited. Earth and Planetary Science Letters 259, 432-441.

Vervoort, J. D., Patchett, P. J., Blichert-Toft, J., and Albarède, F., 1999. Relationships between Lu-Hf and Sm-Nd isotopic systems in the global sedimentary system. Earth and Planetary Science Letters 168, 79-99.

Vervoort, J. D., Plank, T., and Prytulak, J., 2011. The Hf-Nd isotopic composition of marine sediments. Geochimica et Cosmochimica Acta 75, 5903-5926.

von Blanckenburg, F. and Nägler, T. F., 2001. Weathering versus circulation-controlled changes in radiogenic isotope tracer composition of the Labrador Sea and North Atlantic Deep Water. Paleoceanography 16, 424-434.

White, W. M., Patchett, J., and Benothman, D., 1986. Hf Isotope Ratios of Marine-Sediments and Mn Nodules - Evidence for a Mantle Source of Hf in Seawater. Earth and Planetary Science Letters 79, 46-54.

Zachos, J., Pagani, M., Sloan, L., Thomas, E., and Billups, K., 2001. Trends, rhythms, and aberrations in global climate 65 Ma to present. Science 292, 686-693.

Zhang, J., Rothrock, D. A., and Steele, M., 1998. Warming of the Arctic Ocean by a strengthened Atlantic Inflow: Model results. Geophysical Research Letters 25, 1745-1748.

Zimmermann, B., Porcelli, D., Frank, M., Andersson, P. S., Baskaran, M., Lee, D. C., and Halliday, A. N., 2009a. Hafnium isotopes in Arctic Ocean water. Geochimica et Cosmochimica Acta 73, 3218-3233.

Zimmermann, B., Porcelli, D., Frank, M., Rickli, J., Lee, D. C., and Halliday, A. N., 2009b. The hafnium isotope composition of Pacific Ocean water. Geochimica et Cosmochimica Acta 73, 91-101.

Chapter 7

Late Quaternary Nd-Hf isotope evolution of seawater at the Weddell Sea margin and in the abyssal Southern Ocean

Abstract

The Southern Ocean deep circulation has played a critical role in regulating the atmospheric CO_2 concentration over glacial-interglacial time scales. It has been suggested that the Southern Ocean deep water was dominated by a significant expansion of Antarctic Bottom Water during glacial times, which acted as a more effective carbon trap than during modern times. While Nd and Hf isotopes have been demonstrated to be effective tracers of deep ocean circulation and continental weathering inputs at many locations of the global ocean, relatively little is known about the Nd and in particular the Hf isotope evolution of the Southern Ocean on orbital time scales. This study reconstructs the Nd-Hf isotope evolution of deep waters at the Weddell Sea margin (sediment core PS1388-3, water depth 2526 m) and in the deep Agulhas Basin (Core PS2082-1, water depth 4610 m) over the last 250 kyr from bulk sediment and planktic foraminiferal leachates in order to better understand the history of changes of the deep circulation and of weathering inputs.

The deep Southern Ocean had a less radiogenic Nd isotope signature during interglacials similar to today (ε_{Nd}: ~ -9) and a more radiogenic signature during glacials (ε_{Nd}: ~ -6). Since the variability of the endmember Nd isotope composition of Northern Component Water exported to the Southern Ocean remains inconclusive, it is currently difficult to unambiguously interpret the reason for the glacial radiogenic Nd isotope signatures. Nevertheless, the changes in abyssal Southern Ocean Nd isotope signatures most likely reflect a reorganization of the deep circulation in the Atlantic. Unlike atmospheric CO_2 concentration or temperature recorded in Antarctic ice cores, there is no early interglacial peak of unradiogenic Nd isotope signatures (MIS 5e or 7e) which most likely reflects the decoupling of sea surface gas exchange and deep circulation during glacial to interglacial transitions. In contrast, the Hf isotope signatures extracted from core PS2082-1 show very limited variations around ε_{Hf} of +4, implying only small changes in chemical weathering intensity on the surrounding continental landmasses over the last two glacial-interglacial cycles as recorded by the Southern Ocean deep water.

In contrast, the Nd isotope compositions extracted from PS1388-3 do not show systematic glacial-interglacial variations and are much less radiogenic (ε_{Nd} around ~ -12)

than the abyssal Southern Ocean at nearby locations, while the Hf isotopes show peak radiogenic values ($\varepsilon_{Hf} > +8$) at the very beginning of the interglacial periods. The results thus indicate that these signatures have been controlled by Antarctic weathering inputs. Preferential release of Hf from fresh surfaces of minerals with high Lu/Hf is the most likely explanation for these extremely radiogenic Hf isotope signatures.

7.1. Introduction

The Southern Ocean air–sea exchange of CO_2 has been increasingly recognized to have played a major role in controlling glacial-interglacial (G-I) variability of atmospheric CO_2 concentrations (Anderson et al., 2009; Sigman, et al., 2010; Jaccard et al., 2013; Ziegler et al., 2013). This is mainly involves two processes: (a) biological activity that strips CO_2 out of the surface ocean and atmosphere; (b) physical processes such as ocean stratification, deep water mass formation and upwelling, which have determined the rate of physical communication between the surface and the deep waters. It has, however, proven difficult to deconvolve these two processes for the past ocean based on nutrient proxies, such as carbon isotopes. One major problem of the nutrient proxies is that they are sensitive to (local) nutrient cycling (c.f. Piotrowski et al., 2005; 2008). Therefore, the interpretation of ocean circulation changes based on variability nutrient proxies may not be reliable. Despite a good global ocean data coverage of nutrient proxy data, which makes the interpretation of past oceanic processes more robust (Curry and Oppo, 2005), other proxies less prone to changes by (local) nutrient cycling are preferable to provide independent constraints on the deep oceanic processes. One such proxy is radiogenic Nd isotopes, which have a residence time of several hundred years in the deep ocean allowing long distance transport but preventing complete homogenization of deep water mass Nd isotope signatures (c.f. Frank, 2002). Moreover, as Nd has been shown to be a reversible scavenging type element (c.f., Siddall et al., 2008) and open ocean surface Nd isotope compositions and concentrations are not expected to be considerably influenced by local coastal inputs especially in the Southern Ocean (Chen et al., 2013b), Nd isotopes

in Southern Ocean deep water thus essentially reflect water mass mixing rather than local inputs (Carter et al., 2012; Stichel et al., 2012).
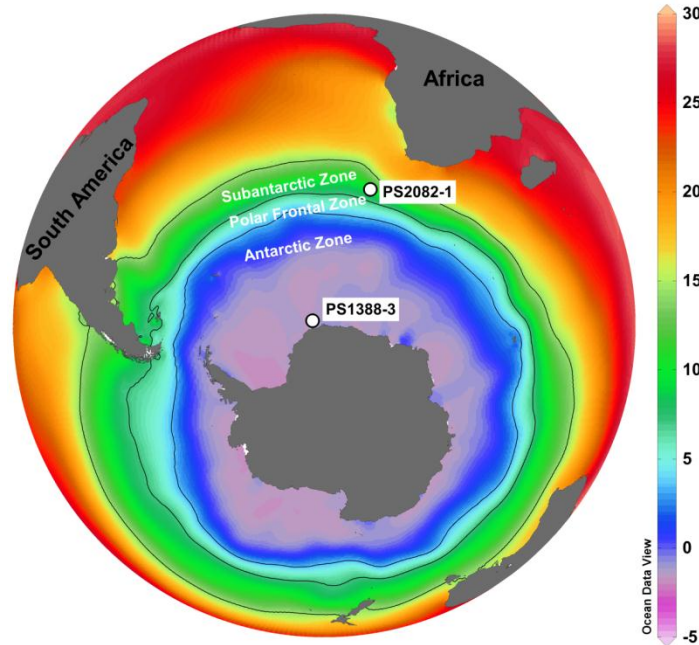
Figure 7.1 Sample locations and the Southern Ocean surface water frontal zones. Colors show austral summer surface water temperatures. The location of core PS2082-1 is currently underneath the Subantarctic zone while PS1388-3 is located at the margin of Weddell Sea below the Antarctic zone. The approximate locations of the ocean fronts are denoted by the black lines (Orsi et al., 1995).

Previous studies in the Southern Ocean have focused on the relationships between Nd isotopes, benthic carbon and oxygen isotopes and deep circulation on millennial time scales (Piotrowski et al., 2005; 2008). It has been inferred that more radiogenic Nd isotope signatures in the deep Southern Ocean during the Last Glacial Maximum (LGM) or during stadial periods reflect diminished contributions of Northern Component Water (NCW). However, the variability of Southern Ocean Nd isotopes during previous G-I cycles remains unclear. Besides, given that Southern Ocean deep water is a mixture of Pacific water, Antarctic Bottom Water (AABW), and NADW, it is also important to know the past Nd isotope composition of AABW. Moreover, combined Nd and Hf isotope compositions have been demonstrated to trace past continental weathering inputs, weathering regime, as well as deep ocean circulation (David et al., 2001; van de Flierdt et

al., 2004; Chen et al., 2012). Compared with other weathering intensity proxies, such as Li and Sr isotopes, Hf has a relatively short oceanic residence time (e.g., most likely shorter than that of Nd and the global ocean mixing time, Rickli et al., 2009; Chen et al., 2013c). This makes it suitable to study continental weathering changes over G-I time scales as recorded by seawater.

In the last 5 years there has been significant progress in producing a global modern seawater dataset for both radiogenic isotope systems (e.g., Rickli et al., 2009; Zimmermann et al., 2009; Stichel et al., 2012) now allowing a detailed calibration of the paleo-records. Nevertheless, almost our entire knowledge of the past oceanic variability of Hf isotopes is based on coarse resolution ferromanganese crust time series (e.g., van de Flierdt et al., 2004) and very little is known about glacial-interglacial or shorter term Hf isotope variability.

In this study, we reconstruct the Nd-Hf isotope evolution of past seawater and the detrital fraction in the abyssal Southern Ocean (gravity core PS2082-1, 43°13.21' S, 11° 44.30' E, water depth 4610 m, Figure 7.1) and the Weddell Sea margin (gravity core PS1388-3, 69°2.0' S, 5° 55.0' W, water depth 2526 m) to better understand deep circulation and weathering inputs over the last 250 kyr.

7.2. Material and Methods

Sediment core PS2082-1 was recovered from in the Agulhas Basin in the subantarctic zone of the Southern Ocean during RV Polarstern Cruise ANT IX-4. Sediment core PS1388-3 was recovered on the mid-slope of the Antarctic continent of the eastern Weddell Sea during RV Polarstern Cruise ANT-IV/3. The age models of Core PS2082-1 and PS1388-3 were obtained by tuning the benthic (PS2082-1, *Cibicidoides spp.*, PS1388-3, *E. exigua*) and planktonic (PS1388-3, *N. pachyderma*) δ^{18}O records to the SPECMAP stacked record (Mackensen et al., 1989; Grobe and Mackensen, 1992; Mackensen et al., 1994; Frank and Mackensen, 2002). For reference, Figure 7.2 shows a comparison of foraminiferal δ^{18}O records of PS2082-1 and PS1388-3 with the LR04 stacked benthic δ^{18}O record (Lisiecki and Raymo, 2005).

We mainly obtained the past seawater Nd-Hf isotope compositions by bulk sediment leaching using a reductive leaching solution (Gutjahr et al., 2007). Consistent with Chen et al. (2012) and Haley et al. (2008), as well as recently recommended leaching protocols (Wilson et al., 2013), we did not apply a de-carbonation step. Approximately two grams of freeze-dried and homogenized bulk sediment per sample were leached with a mixture of 30 ml of 0.005 M hydroxylamine hydrochloride, 1.5% acetic acid, and 0.03 M Na-EDTA, buffered to pH = 4 with suprapure NaOH for one hour at room temperature. Subsequently, the samples were centrifuged and the supernatants were dried for column chemistry. In order to evaluate the reliability of the leaching procedure, test experiments were carried out with different sample/leaching solution ratios. The test results (Table 7.1) has shown that leachate isotope compositions were not sensitive to the different sample/leaching solution ratios, therefore the composition and amount of the leaching solution was kept the same as above for all samples.

Several mixed planktonic and benthic foraminifera samples were picked from the bulk sediments in order to compare the Nd isotope compositions of the foraminiferal coatings with those of the leachates. From these samples the clay fraction was removed (non-clean) and some of the samples were further cleaned applying oxidative–reductive cleaning solutions following the method of Vance and Burton (1999) (redox-cleaned).

A number of samples were selected for measurement of the detrital Nd-Hf isotope compositions. The residues of the leached samples were leached again with a stronger leaching solution for one day to remove all remaining Fe-Mn oxyhydroxides. Afterwards, these samples were dried, ground, and added 5% H_2O_2 to remove organics over the weekend. Then the samples were further dissolved using aqua regia on hotplate at 140°C before they were dissolved in the mixture of concentrated HNO_3 and HF in steel jacketed autoclaves at ~180-200°C for 3-4 days.

A cation exchange resin (AG 50WX8) was used to first separate HFSEs and REEs. Then the HFSE and REE cuts were further purified with Ln-spec resin following (Pin and Zalduegui, 1997) and (Münker et al., 2001), respectively. Hf and Nd isotope compositions were measured on a Nu instruments MC-ICP-MS at GEOMAR. Instrumental mass bias was calculated applying an exponential mass fractionation law

with a natural ^{179}Hf/^{177}Hf ratio of 0.7325 and ^{146}Nd/^{144}Nd of 0.7219, respectively. Blanks of Nd and Hf are always less than 0.2 % and 2 % of the sample concentrations, respectively, and are thus negligible. In order to obtain reliable external reproducibilities, the cconcentrations of the standards were adjusted to be similar to those of the samples during each measurement session. The external reproducibility for Nd and Hf isotopes is reported in Table 7.1, 7.2, 7.3. The ^{176}Hf/^{177}Hf ratios of all samples were normalized to JMC475 = 0.282160 (Nowell et al., 1998) while their ^{143}Nd/^{144}Nd ratios were normalized to JNdi-1 = 0.512115 (Tanaka et al., 2000).

The presence of high amounts of carbonates in some of the samples resulted in the less efficient removal of Yb during the column chemistry procedure described above. Given that ^{176}Yb interferes with ^{176}Hf during mass spectrometric measurement, a Yb standard doping calibration (e.g., Stichel et al., 2012) was carried out to quantify the influence of present Yb on the measured Hf isotope ratios. An additional correction of Yb interference (after the internal standard mass fractionation correction) was found to be necessary (e.g., the deviations of some samples with high ^{176}Yb contribution were larger than the external reproducibility) and was applied based on the above doping calibration in order to obtain accurate Hf isotope compositions (e.g., similar to Stichel et al., 2012).
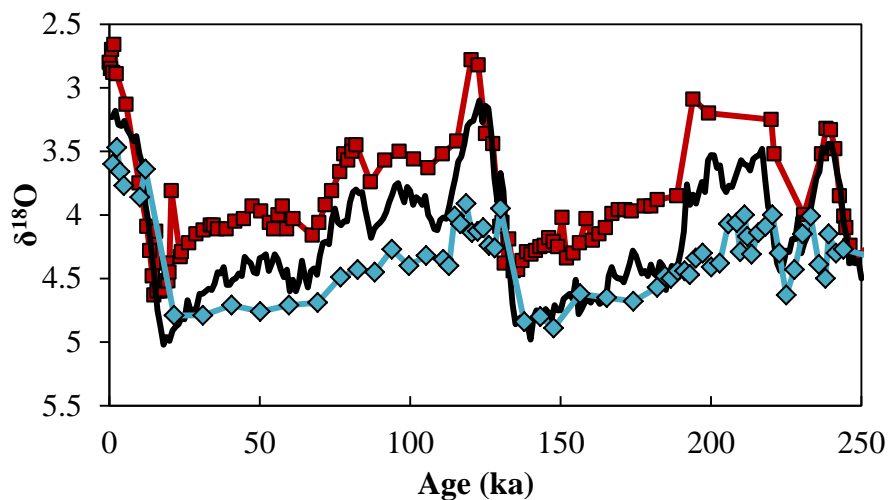
Figure 7.2 Benthic (PS2082-1, *Cibicidoides spp.*, squares, Mackensen et al., 1994) and planktonic (PS1388-3, *N. pachyderma*, diamonds, Mackensen et al., 1989;) δ^{18}O records of the investigated cores over

the last 250 kyr, compared with the LR04 stacked benthic δ^{18}O record black line (Lisiecki and Raymo, 2005).

Table 7.1 Nd-Hf isotopes from leachates of the sediment core PS2082-1 and PS1388-3

Core	Depth interval (cm)	Age	leachate ε_{Nd}[e]	ext. repro. (2 S.D.)	leachate ε_{Hf}[f]	ext. repro. (2 S.D.)
PS2082-1SL	9-10	4.2	-8.9	0.26		
PS2082-1SL	16-19	8.5	-8.7	0.25	3.7	0.88
PS2082-1SL	36-37	13.4	-6.8	0.26		
duplicate run[a]			-6.9	0.26		
PS2082-1SL	58-59	15.7	-6.0	0.20	3.8	0.40
PS2082-1SL			-5.8	0.20		
PS2082-1SL	92-93	18.5	-6.2	0.26	4.2	0.66
PS2082-1SL	101-102	18.8	-5.7	0.25	3.3	0.85
l/v-0.5[b]	101-102	18.8	-5.9	0.25	3.4	0.85
l/v-2[c]	101-102	18.8	-6.0	0.25	3.5	0.85
duplicate run[a]			-6.1	0.25		
PS2082-1SL	140	20.3	-5.5	0.25	4.3	0.85
duplicate sample[d]	140	20.3			4.7	0.66
PS2082-1SL	221.5-222.5	23.3	-5.9	0.20	4.9	0.40
duplicate sample[d]	222	23.3			4.8	0.66
PS2082-1SL	271.5-272.5	31.7	-7.3	0.20	3.2	1.08
PS2082-1SL	301-302	39.3	-7.1	0.20	3.8	0.40
duplicate sample[d]	301-302	39.3			3.6	0.66
PS2082-1SL	322-323	45.3	-7.5	0.26		
PS2082-1SL	341-342	50.8	-7.6	0.20	3.7	0.40
PS2082-1SL	371-372	59.3	-6.8	0.26	3.9	0.66
duplicate run[a]			-7.0	0.26	4.5	0.66
PS2082-1SL	391-392	63.6	-6.3	0.20	4.1	0.40
duplicate sample[d]	391-392	63.6			4.3	0.40
PS2082-1SL	421.5-422.5	70.1	-7.3	0.20	3.8	0.40
duplicate sample[d]	421.5-422.5	70.1			4.1	0.66
duplicate run[a]			-7.4	0.20		
PS2082-1SL	435-436	72.9	-8.0	0.26	4.3	0.66
PS2082-1SL	451-452	77.0	-8.2	0.20	4.5	0.82
PS2082-1SL	481-482	87.5	-8.3	0.26		
PS2082-1SL	502-503	97.5	-8.0	0.25	3.7	0.60

duplicate sample[d]	502-503	97.5			3.5	0.86
PS2082-1SL	535-536	113.3	-8.3	0.26		
PS2082-1SL	542-543	116.7	-8.2	0.25	3.6	0.60
duplicate sample[d]	542-543	116.7			3.4	0.66
PS2082-1SL	562-563	126.3	-7.6	0.26		
PS2082-1SL	581.5-582.5	131.6	-6.6	0.25		
PS2082-1SL	615-616	136.6	-6.1	0.26		
PS2082-1SL	681-682	146.3	-5.7	0.26		
PS2082-1SL	702-703	149.4	-5.6	0.20	4.6	0.40
PS2082-1SL	791-792	167.4	-6.3	0.40	4.1	0.20
PS2082-1SL	861-862	182.5	-6.5	0.20	4.8	0.40
PS2082-1SL	895-896	189.8	-7.7	0.40	4.7	0.20
duplicate run[a]					4.7	0.20
PS2082-1SL	922-923	201.8	-8.3	0.20	4.4	0.40
PS2082-1SL	942-943	220.49	-7.7	0.40	5.0	0.44
PS2082-1SL	961-962	224.21	-6.1	0.40	4.9	0.20
PS2082-1SL	1000	235.3	-8.0	0.20	4.1	0.40
PS2082-1SL	1016-1017	240.17	-8.2	0.40		
PS2082-1SL	1051-1052	247.12	-6.8	0.4	3.8	0.27
PS1388-3SL	0-2	1.1833	-11.0	0.40	3.4	0.20
PS1388-3SL	5	1.9	-12.3	0.25	4.5	0.85
l/v-0.5[b]	5	1.9	-12.2	0.25	3.6	0.85
l/v-2[c]	5	1.9	-12.3	0.25	3.4	0.85
PS1388-3SL	15	3.8	-12.9	0.20	8.7	0.40
PS1388-3SL	18-19	4.4	-12.3	0.25	8.6	0.85
PS1388-3SL	30-31	6.6	-11.1	0.25	10.2	0.85
duplicate run[a]			-11.1	0.25		
PS1388-3SL	60	12.0	-12.2	0.25	5.5	0.85
PS1388-3SL	80	31.1	-12.0	0.25	4.2	0.85
duplicate sample[d]	80	31.1			2.9	0.66
PS1388-3SL	110	59.7	-12.5	0.25	2.7	0.60
PS1388-3SL	251	122.6	-12.5	0.20	9.2	0.40
duplicate run[a]			-12.2	0.20		
PS1388-3SL	281	128.3	-12.1	0.20	7.8	0.40
PS1388-3SL	310-311	148.1	-12.0	0.20	2.6	0.40
PS1388-3SL	330-331	165.78	-12.7	0.40	-0.2	0.24
PS1388-3SL	350-351	183.1	-12.3	0.20	1.7	0.40
PS1388-3SL	430-431	205.9	-11.8	0.25	1.1	0.60
PS1388-3	431-432	206.16	-12.1	0.40	1.0	0.20
PS1388-3SL	571-572	241.7	-10.4	0.20	13.4	0.40

a. duplicate run of the same sample solution

b. leaching solution to sample weight ratio is half of the original one

c. leaching solution to sample weight ratio is twice of the original one

d. duplicate samples were processed separately from weighting

e. $\varepsilon_{Nd} = [(^{143}Nd/^{144}Nd)_{sample}/(^{143}Nd/^{144}Nd)_{CHUR} -1]*10^4$; where $(^{143}Nd/^{144}Nd)_{CHUR} = 0.512638$ (Jacobsen and Wasserburg, 1980)

f. $\varepsilon_{Hf} = [(^{176}Hf/^{177}Hf)_{sample}/(^{176}Hf/^{177}Hf_{CHUR})-1]*10^4$; where $(^{176}Hf/^{177}Hf)_{CHUR}=0.282769$ (Nowell et al., 1998).

Table 7.2 Nd-Hf isotopes from the detrital fractions of the sediment core PS2082-1 and PS1388-3

Core	Depth interval (cm)	Age	detrital ε_{Nd}[a]	ext. repro. (2 S.D.)	detrital ε_{Hf}[b]	ext. repro. (2 S.D.)
PS2082-1SL	16-19	8.5	-6.5	0.26	0.1	0.28
PS2082-1SL	58-59	15.7	-5.2	0.26	1.1	0.28
PS2082-1SL	101-102	18.8	-5.1	0.26	0.6	0.28
duplicate run		18.8	-5.1	0.26		
duplicate sample		18.8	-5.0	0.26	0.9	0.20
PS2082-1SL	221.5-222.5	23.3	-5.7	0.26	-0.1	0.28
PS2082-1SL	271.5-272.5	31.7	-6.1	0.26	-2.3	0.28
PS2082-1SL	341-342	50.8	-6.6	0.26	-1.9	0.28
duplicate run		50.8			-1.7	0.28
PS2082-1SL	421.5-422.5	70.1	-6.8	0.26	-0.9	0.28
PS2082-1SL	502-503	97.5	-7.7	0.26	-2.4	0.28
PS2082-1SL	581.5-582.5	131.6	-6.5	0.26	-1.7	0.28
PS2082-1SL	702-703	149.4	-4.7	0.26	0.8	0.28
PS2082-1SL	922-923	201.8	-8.4	0.26	-2.5	0.28
PS1388-3SL	15	3.8	-14.9	0.26	-15.4	0.20
PS1388-3SL	60	12.0	-14.8	0.26	-14.7	0.20
PS1388-3SL	80	31.1	-14.4	0.26	-13.6	0.20
duplicate run		31.1			-13.7	0.20
PS1388-3SL	110	59.7	-12.7	0.26	-14.0	0.20
PS1388-3SL	281	128.3	-12.7	0.26	-13.4	0.20
PS1388-3SL	310-311	148.11	-12.7	0.26	-12.4	0.28
duplicate run		148.11	-12.3	0.26		
PS1388-3SL	350-351	183.1	-12.6	0.26	-14.9	0.20

PS1388-3SL	430-431	205.9	-12.2	0.26	-14.3	0.20
PS1388-3SL	571-572	241.7	-11.1	0.26	-11.2	0.20

a. $\varepsilon_{Nd} = [(^{143}Nd/^{144}Nd)_{sample}/(^{143}Nd/^{144}Nd)_{CHUR} -1]*10^4$; where $(^{143}Nd/^{144}Nd)_{CHUR} = 0.512638$ (Jacobsen and Wasserburg, 1980)

b. $\varepsilon_{Hf} = [(^{176}Hf/^{177}Hf)_{sample}/(^{176}Hf/^{177}Hf_{CHUR})-1]*10^4$; where $(^{176}Hf/^{177}Hf)_{CHUR}=0.282769$ (Nowell et al., 1998).

Table 7.3 Nd isotopes from the mixed planktic-benthic foraminifera of the sediment core PS1388-3

Core	Depth interval (cm)	Age	Method	foram ε_{Nd}[a]	ext. repro. (2 S.D.)	weight (mg)
PS1388-3SL	215.5	115.9	UNCLEAN	-12.3	0.88	57
PS1388-3SL	215.5	115.9	REDOX	-11.5	0.88	137
PS1388-3SL	330.5	165.8	UNCLEAN	-12.1	0.88	63
PS1388-3SL	330.5	165.8	REDOX	-12.6	0.88	115
PS1388-3SL	431.5	206.2	UNCLEAN	-11.7	0.88	62
PS1388-3SL	531.5	230.8	UNCLEAN	-11.6	0.88	76
PS1388-3SL	209	114.6	UNCLEAN	-12.3	0.88	43

a. $\varepsilon_{Nd} = [(^{143}Nd/^{144}Nd)_{sample}/(^{143}Nd/^{144}Nd)_{CHUR} -1]*10^4$; where $(^{143}Nd/^{144}Nd)_{CHUR} = 0.512638$ (Jacobsen and Wasserburg, 1980)

7.3. Results

7.3.1 Nd-Hf isotopic evolution of deep waters in the deep Agulhas Basin

The results of the leachate and detrital Nd-Hf isotopic signatures of PS2082-1 are presented in Table 7.1, 7.2 and in Figure 7.3 (applying the age model mentioned above). The Holocene ε_{Nd} signature of the leachates is -8.7 while that of the detrital fraction is -6.5 (8.5 ka). Both seawater and detrital Nd isotope signatures were more radiogenic during cold marine isotope stages (e.g., MIS 2, 4, and 6), while the seawater Nd isotope compositions were generally less radiogenic than or similar to the detrital Nd isotope

ratios. The most radiogenic signatures are found for MIS 2 and 6 (ε_{Nd} of about -5.0 ~ -6.0).
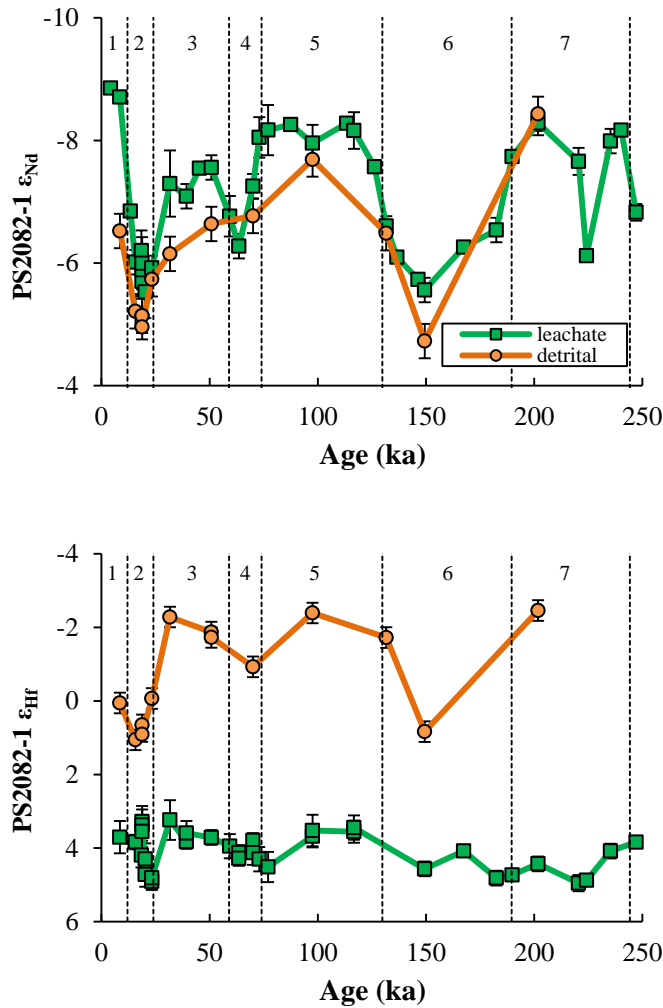
Figure 7.3 Comparison between leachate and detrital Nd (upper plot) and Hf isotope (lower plot) signatures of Core PS2082-1. Error bars (± 1 S. D.) smaller than the symbols are not shown.

Comparison with previously published records of past seawater ε_{Nd} from the Cape Basin (Piotrowski et al., 2005; 2008; Skinner et al., 2013, Figure 7.4) reveals that the patterns of the PS2082-1 record are consistent with previous records, however, with slightly different absolute values. For example, the ε_{Nd} signatures of the PS2082-1 leachates ranged between -5 and -6 during MIS2, which is similar to the record obtained from

benthic foraminiferal coatings of nearby Core MD07-3076 from the Southern Ocean (Skinner et al., 2013) but distinctively more radiogenic than the Cape Basin records (ε_{Nd} of about -6.5, RC11-83, TNO57-21) (Piotrowski et al., 2005; 2008). Moreover, our record shows no high frequency ε_{Nd} changes during MIS 3 as was revealed by the Cape Basin records, most likely due to the lower sampling resolution and/or the lower sedimentation rate of PS2082-1. Interestingly, there was no significant variability of ε_{Nd} both in the Southern Ocean deep water (PS2082-1) and in the equatorial Indian Ocean deep water during MIS 5, although the ε_{Nd} values of the former were about 1 unit higher than the latter during this period (Figure 7.4).
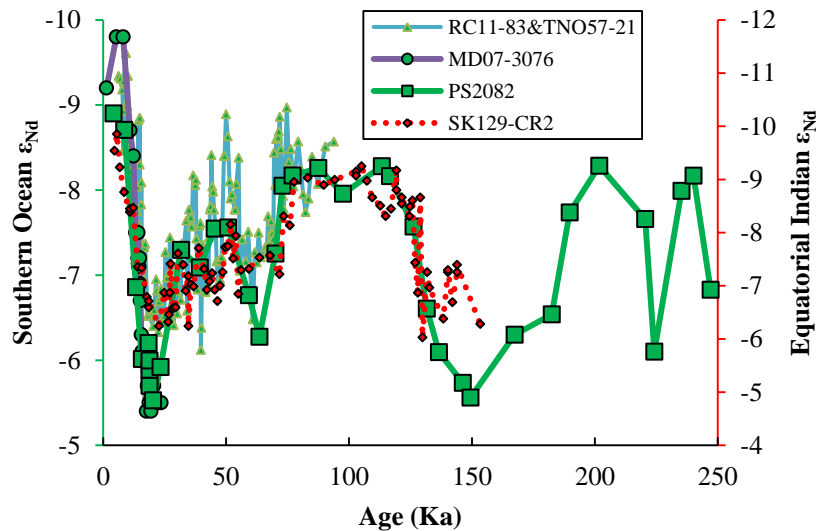
Figure 7.4 Seawater Nd isotope record of PS2082-1 obtained from leachates of abyssal Southern Ocean sediments (PS2082-1) compared with published records from the Cape Basin in the deep Southern Ocean (RC11-83&TNO57-21, Piotrowski et al., 2008; MD07-3076, Skinner et al., 2013) and the deep equatorial Indian Ocean (SK129-CR2, Piotrowski et al., 2009).

The detrital Hf record shows an evolution pattern similar to the detrital and leachate Nd records (Figure 7.3). During glacial stages (MIS 2, 4, and 6) the detrital Hf isotope compositions were significantly more radiogenic (ε_{Hf} up to +1.1) than during interglacials (ε_{Hf} as low as ~ -2.5). From late MIS 6 to MIS1, the leachate record appears to correlate

with the evolution of the detrital fractions. For example, there is a continuous decrease of ε_{Hf} (note the y-axis is reversed) in both the leachates and the detrital fractions from the early MIS 4 to late MIS 3, whereas later in the record they show an increase in ε_{Hf} at the MIS 3-2 transition. Overall, the leachate Hf isotope signatures show much less variability with an average ε_{Hf} value of $+4.4\pm0.5$ (1 S. D.) throughout the record.
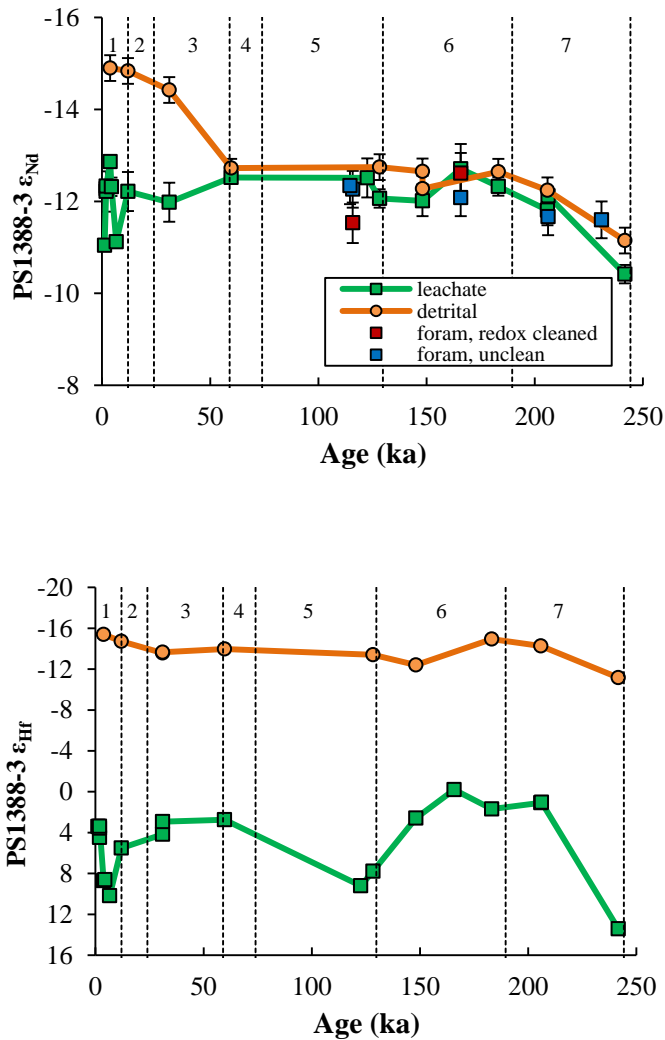
Figure 7.5 Comparison between Nd (upper plot) and Hf isotope (lower plot) signatures of Core PS1388. Error bars ($\pm$ 1 S. D.) smaller than the symbols are not shown.

7.3.2 Nd-Hf isotopic evolution of seawater at the Weddell Sea margin

The results of the leachate and detrital Nd-Hf isotopic signatures of Core PS1388-3, as well as those of the seawater Nd isotope compositions extracted from the coatings of the foraminifera are presented in Tables 7.1, 7.2, 7.3 and in Figure 7.5. In contrast to the records of Core PS2082-1, there was a stepwise decrease (mainly during MIS 3 and 7) of the detrital ε_{Nd} signatures from -11.1 to -14.9 over the last 2 G-I cycles. The seawater Nd isotopic evolution pattern obtained from the leachates closely followed that of the detrital fraction prior to MIS 3. The beginning of MIS 7 was marked by more radiogenic Nd isotope signatures in both the leachate and detrital records (ε_{Nd} of -10.4 ~ -11.1). From late MIS 7 to early MIS 3, the seawater and detrital Nd isotope signatures only show a small variability near ε_{Nd} of -12. Thereafter a clear decoupling between detrital and seawater signatures occurred as consequence of a shift to less radiogenic signatures of the detrital fraction (e.g., ε_{Nd} of -14.9 in the late Holocene). Throughout the record, three were no distinct cyclic changes of the seawater or detrital Nd isotope compositions over G-I time scales. In addition, seawater Nd isotope results obtained from non-reductively cleaned and reductively cleaned foraminiferal samples are indistinguishable and confirm the validity of the leachate data.

The detrital Hf isotope record is similar to that of the detrital Nd isotopes in that it decreased from -11.2 to -14.9 across MIS 7 and from -13.6 to -15.4 throughout MIS1-3. In marked contrast to Core PS2082-1, the leachate Hf isotope signatures show a very large variability with a range of 13.6 ε_{Hf} units. Highly radiogenic leachate Hf isotope signatures (ε_{Hf} up to +10.2, +9.2, +13.4 in MIS 1, 5, 7, respectively) are observed during the early interglacial periods. During other periods, the ε_{Hf} of the leachates had a range of -0.2 to +5.5.
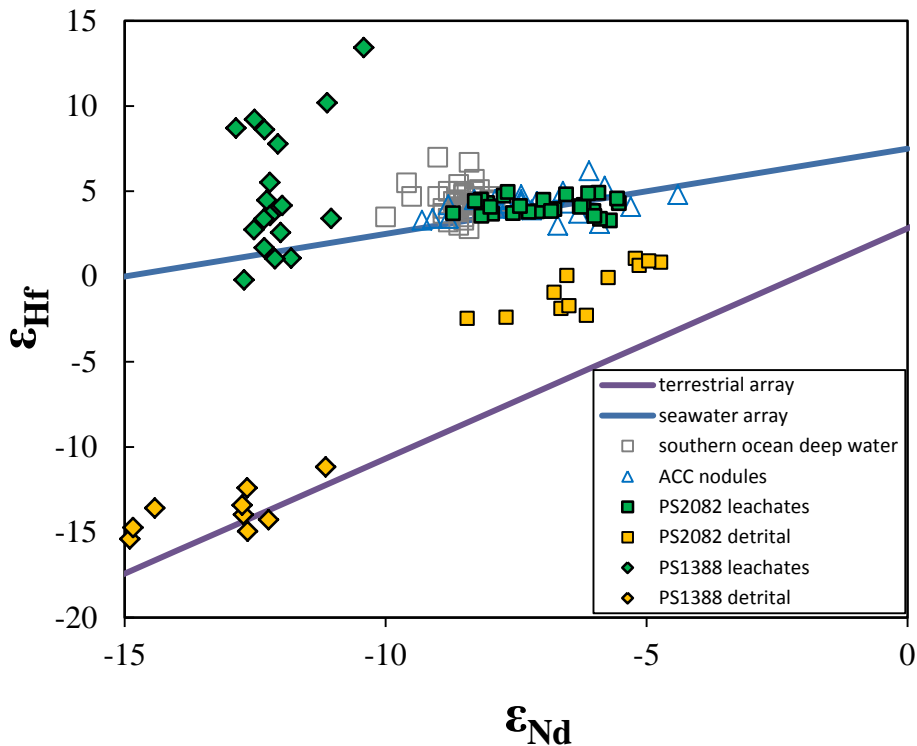
Figure 7.6 The Nd-Hf isotope systematics of the leachate and detrital data of PS2082-1 and PS1388-3 compared with the terrestrial array and the seawater array (Data sources: terrestrial array, Vervoort et al., 1999; seawater array, Albarède et al., 1998; Surface scrapings of ACC Fe-Mn nodules: van de Flierdt et al., 2006a; Southern Ocean deep water, Stichel et al., 2012).

7.4. Discussion

7.4.1 Reliability of the seawater signatures obtained from leachates of PS2082-1 and PS1388-3

At the present day, strong horizontal and vertical mixing within the Atlantic sector of the Antarctic Circumpolar Current (ACC) system results in the efficient homogenization of Nd isotopes in Circumpolar Deep Water (CDW) and thus a very small range of ε_{Nd} signatures between -8.4 and -8.6 (Stichel et al., 2011). Average AABW has a ε_{Nd} of -9.0, which is only slightly less radiogenic than the Nd isotope signature of CDW due to

unradiogenic inputs from the Antarctic continent. The unradiogenic ε_{Nd} signature of NADW is clearly distinguishable to about 47° S in Southern Ocean deep water between 2000 and 3000 meters water depth (ε_{Nd} = ~-10.0, Stichel et al., 2011). Overall, the ε_{Nd} of modern CDW is expected to be recorded by the surface sediments of Core PS2082-1 (e.g., -8.7 ~ -8.9) and of AABW for Core PS1388-3 (e.g., -9.0 to -10.0). In contrast, the modern Hf isotope composition of Southern Ocean deep water is very homogeneous and identical at ε_{Hf} of +4.6 within current analytical precision (e.g., 2σ external reproducibility of 0.9 ε_{Hf} units (Stichel et al., 2011)). Therefore, Hf isotopes cannot be used as a water mass tracer in the present day Southern Ocean. Rather, they may provide information on how the signatures of large scale continental inputs varied over G-I cycles.

In our study we did not include core-top sediment samples, but the Holocene ε_{Nd} and ε_{Hf} signatures of PS2082-1 are fully consistent with modern day seawater signatures. In ε_{Nd}-ε_{Hf} space, the leachate data of PS2082-1 are in the range of modern seawater and surface scrapings of Fe-Mn nodules (Figure 7.6). Together with the consistency with previously published Nd isotope time series from the deep Atlantic sector of the Southern Ocean (Figure 7.4), we suggest that the leachate data of PS2082-1 faithfully recorded past Southern Ocean deep water signatures.

In contrast, similar arguments are not applicable to PS1388-3 which has recorded much less radiogenic Nd isotope compositions in the surface sediments that clearly differ from the expected seawater range (Figure 7.6). This suggests that PS1388-3 mainly recorded local weathering inputs and exchange of the deep water with the Antarctic continent rather than the well homogenized open ocean AABW signatures.

7.4.2 The detrital Hf-Nd isotope record of PS2082-1 and PS1388-3 and implications for source provenance changes over the last two G-I cycles

A better understanding of the sources and transport of terrestrial material supplying the Southern Ocean will help to reconstruct ocean current patterns as well as the role of different terrestrial inputs that potentially fueled the biological pump in the past through micronutrient release (e.g., Jaccard et al., 2013).

The radiogenic isotopes of Nd and Hf are particularly useful proxies to trace terrestrial sources and transport mechanisms. Due to the similarity of the fractionation behavior between the Sm-Nd and Lu-Hf element pairs during the Earth's magmatic processes, Hf and Nd isotopic compositions of most terrestrial rocks display a strong positive correlation, which has previously been defined as the terrestrial array (Vervoort et al., 1999; Figure 7.6). However, Lu/Hf ratios vary significantly among different minerals which contrast with their similar Sm/Nd ratios (Bayon et al., 2006). Nd isotopes are generally not sensitive to mineral sorting, while Hf isotope signatures are considerably more radiogenic in the fine size fractions than in bulk sediments, probably mainly due to zircon loss during sediment transport (e.g., Vervoort et al., 1999; Carpentier et al., 2009; Chen et al., 2013a). Thus detrital Hf isotope signatures can be used as a proxy to assess mineral sorting associated with eolian, ocean current, or ice transport (e.g., Chen et al., 2012).

In fact, there are a number of studies applying radiogenic isotopes in combination with other proxies (e.g., clay minerals, particle fluxes) and have been dedicated to investigate the sources and transport pathways of Southern Ocean sediments (e.g., Walter et al., 2000; Roy et al., 2007; Hegner et al., 2007; Noble et al., 2012). A latitudinal gradient in radiogenic isotope signatures in the Atlantic sector Southern Ocean was found both for the Holocene and for the last glacial maximum (LGM). In general, the unradiogenic Nd isotope endmember represents inputs from South Africa and eastern Antarctica, while the radiogenic endmember mainly originates from South America and western Antarctica. However, continuous radiogenic isotope records of the detrital material of the Weddell Sea or the southeast Atlantic are still lacking and are subject of this study.

The detrital Nd isotope signatures of PS2082-1 show clear G-I oscillations similar to previous findings from the Scotia Sea (both in magnitude and isotope signatures) over the last two G-I cycles (Walter et al., 2000) (Figure 7.4). We thus suggest that the mechanisms controlling the transport of detrital materials to both the southern Scotia Sea (south of Polar Front) and site of Core PS2082-1 in the Southeast Atlantic (located in Subantarctic Zone) have been similar. However, the location of Core PS2082-1 is more distant from the radiogenic western Antarctic sources than the South Scotia Sea sites.

This supports the notion that, during glacial times, there was a significantly increased supply of radiogenic material originating from South America and subsequent transport by the ACC (Noble et al., 2012). Detrital Hf isotope signatures were also more radiogenic during glacial times, implying that changes in sediment sources have been the main drivers of Hf isotope variability. Moreover, the Nd-Hf isotope data of PS2082-1 deviate considerably from the terrestrial array (Figure 7.6), which is attributed to mineral sorting by current transport in the ACC.
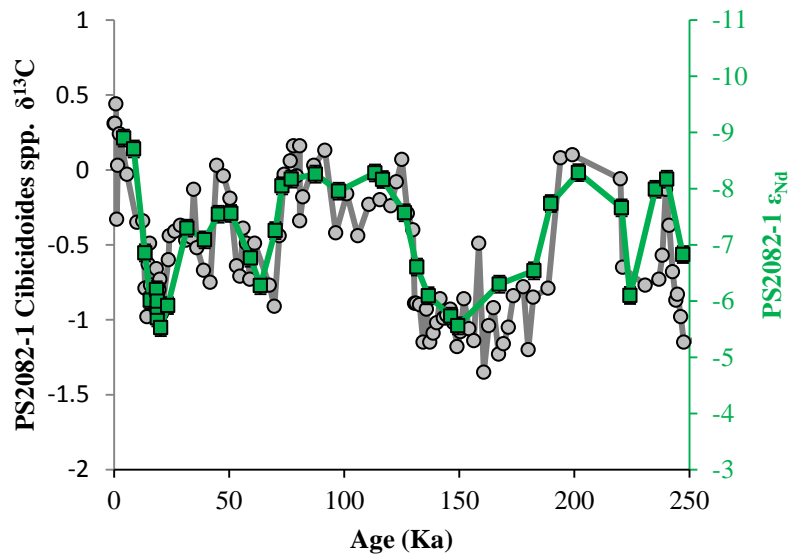
Figure 7.7 A comparison between leachate Nd isotopes of PS202 and previously published benthic carbon isotope data of *Cibicidoides spp* (Mackensen et al., 1994).

Since the mechanism of sediment input to the Weddell Sea margin has mainly been glacial erosion of the Antarctic continent (e.g., Grobe et al., 1992), the stepwise trend to less radiogenic Nd isotope signatures recorded over time by Core PS1388-3 implies changes in ice-sheet dynamics between eastern and western Antarctica and/or simply changes in the locations of basal erosion (Flowerdew et al., 2013) over the last 250 kyr. Given that the Nd isotope change has been a long term trend, it would be interesting to obtain isotope data further back in time in the future and to compare these data to the variability of the Antarctic ice sheets (e.g. Cook et al., 2013), in order to better understand the response of Antarctic ice sheets to climatic changes. Moreover, our detrital Nd-Hf isotope compositions of Core PS1388-3 plot fully on the terrestrial array

(Figure 7.6), consistent with its detrital sources being the Antarctic continent with poor mineral sorting of glacial sediments and transport by ice.

7.4.3 Factors controlling the seawater Nd isotope signatures of the Southern Ocean over the last 250 kyr

One important feature of the seawater Nd isotope signatures recorded By Core PS2082-1 over the past 250 kyr is that they correlate very well with the benthic carbon isotope record of the same core (Figure 7.7), without clear evidence for phase lags between the two parameters at the low sampling resolution of our study. Such a coupling between Nd isotopes and benthic carbon isotopes was also observed from previous high resolution studies of Southern Ocean deep water variability on orbital time scales (the last 90 kyr), although millennial scale phase lags between these two proxies during MIS 3 were observed (Piotrowski et al., 2005; 2008). Therefore, ocean circulation has been one of the main drivers of the abyssal carbon isotope evolution in this region on orbital scales.

At present, the Nd isotope signature of CDW reflects nearly conservative mixing between Atlantic and Pacific deep waters with negligible contributions from exchange with the Antarctic continent (Carter et al., 2012; Stichel et al., 2012). Therefore, the Nd isotope record of Core PS2082-1 (which reflects changes of CDW signatures) has essentially only been sensitive to changes in mixing proportion of the two endmembers (i.e., changes in the Atlantic Meridional Overturning Circulation (AMOC)) or to changes in the isotope compositions of the endmembers themselves. If CDW has remained well mixed in the past, Nd isotopes would not be sensitive to Southern Ocean surface water stratification. With the endmember isotope composition unchanged over G-I cycles, a more radiogenic glacial Nd isotope signature of CDW will thus most likely reflect diminished contributions from NCW. However, whether Nd isotope compositions or even the Nd concentration of the NCW endmember remained unchanged on G-I timescales is not fully clarified. van de Flierdt et al. (2006b) and Foster et al. (2007) suggested essentially invariant NCW Nd isotope compositions between the last glacial and the Holocene. However, the LGM was not covered by the coral data of van de Flierdt et al. (2006b), and the time resolution and age control of the laser ablation data on the ferromanganese crusts in Foster et al. (2007) was still very coarse and integrated over almost 10,000 years, so

that a reliable signature could not be obtained for the LGM in both studies. In contrast, Gutjahr et al. (2008) proposed that the ε_{Nd} signature of LGM NCW endmember that was flowing south at shallower depth than today may have been up to 3.8 ε_{Nd} units more radiogenic during LGM than at present. However, the locations of the Gutjahr et al. (2008) study were strongly affected by sediment redistribution which may also have biased their LGM records. Indeed, if the Nd concentration and isotope composition of NCW depended on where the different components of this deep water mass formed, it is not unlikely that the NCW endmember composition changed over G-I time scales. For example, modeling studies have predicted a southward shift of the main sites of deep water mass formation in the North Atlantic during the LGM (e.g., Ganopolski et al., 1998). Besides, changes in the formation rate of Labrador Sea deep water, which has the least radiogenic Nd isotope composition of the water masses contributing to NCW, may also have affected its Nd isotope composition (e.g., Roberts et al., 2010).

Compared with the modern situation, the PMIP (Paleoclimate Modeling Intercomparison Project) coupled model simulations produced vastly different Atlantic AMOC responses to glacial conditions (from reduction to strengthening in overturning, Weber et al., 2007), thus currently limiting the understanding of this issue based on models. Results from LGM-Holocene $^{231}Pa/^{230}Th$ variation suggest that the strength of glacial AMOC may have been as strong as the modern one but that the southward transport mainly occurred at intermediate depth (e.g., Lippold et al., 2012), similar to the results of Gutjahr et al. (2008). Enhanced ventilation of intermediate Atlantic waters during the LGM is also supported by reconstructions based on nutrient proxies, such as $\delta^{13}C$ (Curry and Oppo, 2005) or Cd/Ca (Marchitto and Broecker, 2006). However, whether the overall southward advection of NCW was reduced during the LGM or not is less clear. From the Nd isotope evolution of Southern Ocean deep water, simple mass balance calculations (c.f., Stichel et al., 2011) require a significant reduction of the NCW contribution to CDW during LGM, unless the endmember ε_{Nd} of NCW was as radiogenic as at least -7.5, which is very unlikely (e.g., Flierdt et al., 2006b; Foster et al., 2007; Gutjahr et al., 2008). Another possibility is that CDW was strongly stratified in terms of Nd isotope compositions. In order to investigate this possibility, more Nd isotope time series from shallower depths of the Southern Ocean are necessary.
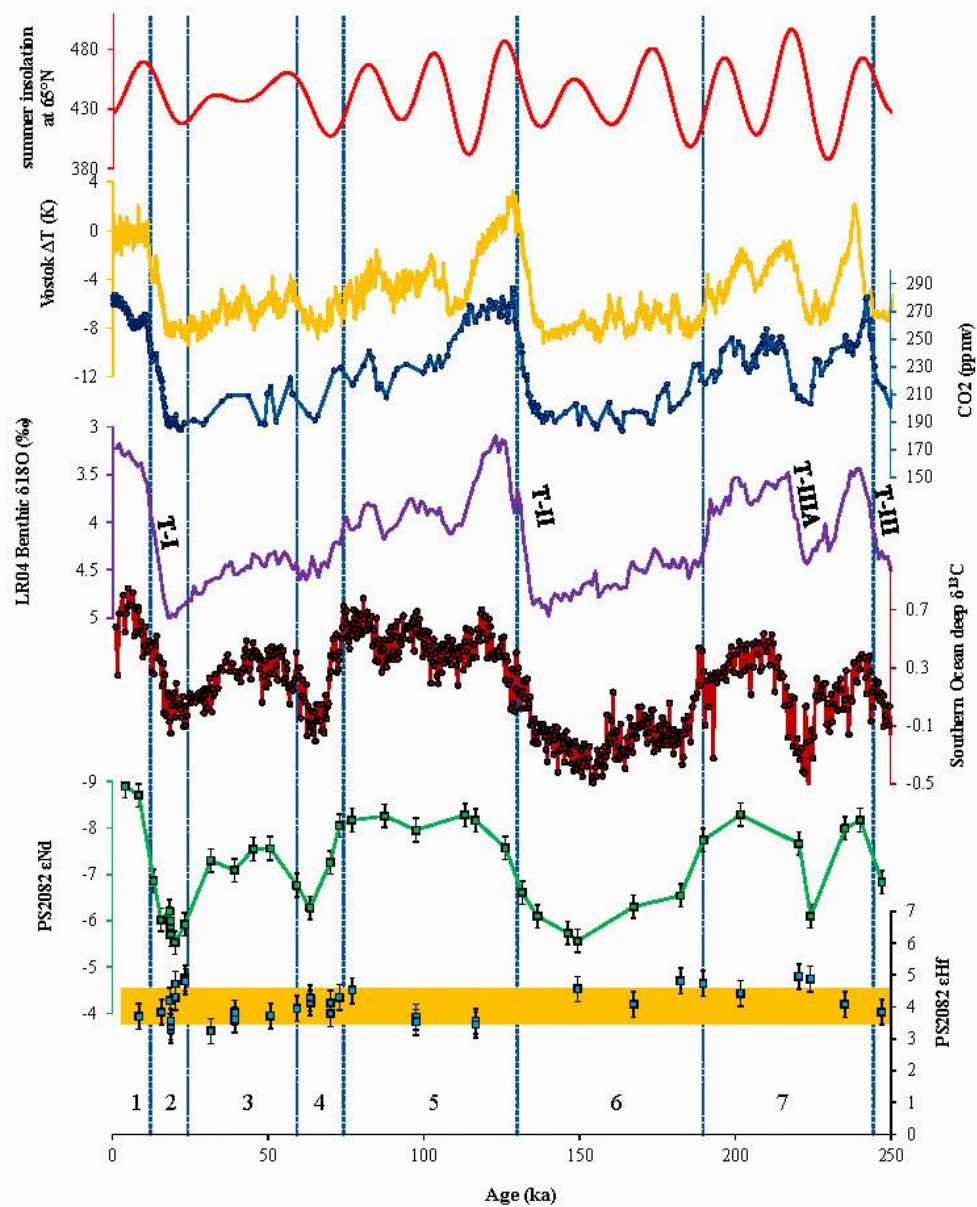
Figure 7.8 Southern Ocean deep water Nd and Hf isotope evolution of the past 250 kyr reconstructed from Core PS2082-1, in comparison with other published climate records (numbers at the bottom denote marine isotope stages). From top to bottom,: summer insolation at 65°N (Berger and Loutre, 1991); Vostok ice-core temperatures; atmospheric CO_2 concentrations (Petit et al., 1999); LR04 benthic oxygen isotope stack (Lisiecki and Raymo, 2005), where T denotes termination events; a high resolution benthic carbon isotope record from the deep Southern Ocean (~2900 m; MD02-2588, Ziegler et al., 2013); seawater Nd isotopes of PS2082-1; and seawater Hf isotopes of PS2082-1.

Interestingly, our new ε_{Nd} values of LGM deep waters in the Agulhas Basin (and also a nearby core MD07-3076 from the deep Southern Ocean, Skinner et al., 2013) were systematically more radiogenic by about ~0.7 ε_{Nd} units than the Cape Basin records (Piotrowski et al., 2008), which may indicate a higher glacial contribution of Pacific waters to the deep Agulhas Basin. If this difference is not an artifact of the leaching procedures applied, the glacial Southern Ocean deep water was less well mixed horizontally than at present.

7.4.4 Responses of Nd and C isotope signatures of Southern Ocean deep water to orbital forcing

It has been found that the amplitude of the precessional forcing of the Earth's orbit was larger during interglacials than during glacials (Hays et al., 1976). During MIS5 and 7, the amplitude of variations in summer insolation at 65°N was larger than those of the following glacial periods (Figure 7.8). Interestingly, the Nd isotope signatures of the Southern Ocean deep waters remained nearly constant throughout MIS 5 (Figure 7.8), which is also supported by leachate data from the equatorial Indian Ocean (Figure 7.4, Piotrowski et al.., 2009). Similarly, benthic carbon isotopes in this region do not indicate the same "overshooting" behavior as other climatic parameters (such as the global temperature, atmospheric pCO_2 (Figure 7.8), and ice volume/sea level (e.g., Siddall et al., 2003; Bintanja et al., 2005) after major terminations, for example during MIS 5e. A global carbon isotope data synthesis of the last 150 kyr also indicates that basin-scale carbon isotope records do not show any pronounced increase during MIS 5e similar to ice volume and atmospheric pCO_2 (Oliver et al., 2010). At the beginning of MIS 7 when summer insolation at 65°N decreased to a low value, both deep water Nd and carbon isotopes went through a major shift in their signatures (Figure 7.8). Nevertheless, there was no significant difference of the isotope signatures between the beginning and the end of MIS 7, which is also different from the global temperature and atmospheric pCO_2 records. It appears that the deep Southern Ocean did not respond sensitively to these shifts when atmospheric CO_2 concentrations were higher than ~230 ppmv throughout the last two G-I cycles. Overall, if the peaks of the atmospheric CO_2 concentrations or

surface temperature records after major termination events are cut off, the residual records are strikingly similar to the C or Nd isotope records (Figure 7.8).

The invariable Nd isotope signatures throughout MIS 5, as well as between the beginning and the end of MIS 7 most likely reflect similar deep circulation patterns, from which the question arises: what was the mechanism of interglacial atmospheric pCO_2 decrease after MIS5e and 7e, when both C and Nd isotopes of the Southern Ocean deep water did not change much? This question is directly related to the role/response of the deep ocean in controlling glacial inceptions.

During the last interglacial (MIS5), deep ocean circulation did not change much as denoted by Nd isotopes. Invariant benthic $\delta^{13}C$ signatures of CDW consequently have 3 possible origins: (1) the decrease of atmospheric CO_2 was **not** associated with carbon storage in the abyssal Southern ocean during MIS 5; (2) a northward expansion of southern component water (i.e., AABW, Govin et al., 2009); (3) the decrease of atmospheric CO_2 was associated with a whole ocean alkalinity increase (e.g., a decrease in neritic $CaCO_3$ production associated with sea-level drop, (c.f., Berger, 1982; Yu et al., 2013). Based on Atlantic $^{231}Pa/^{230}Th$ changes it has been suggested that the transition from MIS 5e (the last interglacial or "peaks" in the CO_2 and temperature records) to 5d was associated with an increase in overturning of intermediate waters (Guihou et al, 2011). This means that intermediate depths were well ventilated and were not likely the reservoir to store carbon from the atmosphere during MIS 5a-d, which makes scenario (1) unlikely. Since a clearly distinguishable MIS5e peak of $\delta^{13}C$ has only been observed in two cores of the deep Indian sector of the Southern Ocean (Govin et al., 2009), more studies from the Southern Ocean are necessary to investigate the importance of this scenario. Our current preferred scenario is thus (3): A CO_2 decrease during glacial inception associated with a whole ocean alkalinity increase in response to the preceding overshoot of CO_2 and alkalinity minimum (e.g., Toggweiler, 2008; Omta et al., 2013; Yu et al., 2013). The gradual change in CO_2 storage in the deep ocean may thus reflect internal oceanic carbon system feedbacks, rather than changes in deep circulation.

7.4.5 Negligible changes in chemical weathering intensity recorded by Southern Ocean deep water over G-I transitions?

Bayon et al. (2009) have shown that Hf isotope signatures of secondary clays in Congo fan sediments varied significantly and systematically as a function of chemical weathering intensity. Interestingly, our study indicates that the Hf isotope signatures of the open Southern Ocean deep water have no distinct variations over G-I cycles. It is thus possible that chemical weathering intensity of the surrounding continents recorded by Southern Ocean deep water did not change significantly over G-I cycles or the changes were too small to be detected by Hf isotopes distal from the continental source areas in the deep open Southern Ocean. On one hand, the intensity of kinetically limited continental silicate weathering must have changed as a function of temperature, precipitation, atmospheric pCO_2, etc. (e.g., West et al., 2005). On the other hand, the transport-limited weathering is usually characterized by complete leaching of cations from fresh regolith and its flux is directly proportional to the supply of material by physical erosion (West et al., 2005). Since the chemical flux from the continent is suggested to be dominated by weathering of the continental low sloping areas which are transport-limited (Willenbring et al., 2013), it may not be surprising to see that continental weathering intensity as recorded by the Southern Ocean deep water overall did not change much over the late Quaternary G-I cycles, though for specific locations (e.g., the mountainous region) this might not be true. Nevertheless, more weathering processes studies on Hf isotope geochemistry (e.g., Rickli et al., 2013), are necessary to define the sensitivity of Hf isotopes to weathering.

7.4.6 The dominance of local continental inputs on leachate Nd-Hf isotope signatures in the Weddell Sea margin (Core PS1388-3)

As discussed in section 7.4.1, the leachate Nd-Hf isotope signatures obtained from Core PS1388-3 clearly recorded a local weathering signal. The leachate Nd isotope signatures remained stable despite that the detrital signatures shifted to less radiogenic signatures over the past 250 kyr. We suggest that the seawater Nd isotopes have integrated local Nd isotope signatures of different shelf waters from a larger area. It thus appears that the sources from the Antarctic continent supplying their unradiogenic signatures to AABW

have been fairly stable over this period of time. Moreover, the radiogenic peaks during the beginning of every interglacial period suggest that easily alterable minerals with highly radiogenic Hf isotope compositions were preferentially released documenting a significant change in the weathering regime on the Antarctic continent most likely linked to retreat of the ice sheets in particular areas (e.g. Cook et al., 2013). As it was not possible to extract enough authigenic Hf from foraminifera for measurements and Fe-Mn nodule data are also lacking, it is difficult to distinguish if the Hf isotopes (especially during the periods when the sediment was barren of carbonates) reflect the signatures of the authigenic seawater-derived phase or some contamination during leaching originating from partial dissolution of the detrital phases. Therefore, more experimental work on the Antarctic shelf sediments is needed before robust conclusions can be drawn. Nevertheless, the data suggest, that any release of less radiogenic Hf isotope signatures as a consequence of more congruent glacial weathering (van de Flierdt et al., 2002), either caused by enhanced dissolution of zircons or through incongruent weathering of other minerals, was at least preceded by a radiogenic pulse. Similar highly radiogenic signatures have also been observed in field studies of river waters draining glacially eroded continental areas (Chen et al., 2013c) or in leaching experiments of granitic rocks (Bayon et al., 2006).

7.5. Summary

This study presents detrital and leachate Nd-Hf isotope data obtained from two marine sediment cores recovered from the deep open Southern Ocean (PS2082-1) and the Weddell Sea margin (PS1388-3). Leachate Nd isotope signatures of PS2082-1 are consistent with previously published records from the neighboring Cape Basin, however, revealing more radiogenic signatures than in the Cape Basin during glacials. In contrast, leachate Hf isotope signatures show a much smaller variability over the last two glacial-interglacial cycles. Nd-Hf isotope signatures of the PS2082-1 leachates are entirely within the range of seawater data constrained by surface scrapings of Fe-Mn nodules and modern seawater from the Southern Ocean, supporting that the leachate Nd and Hf isotope signatures have a pure seawater origin. We suggest that the radiogenic Nd isotope

signatures observed in the glacial Southern Ocean deep water most likely reflected a reduction of the contribution of Northern Component Waters (NCW) to the ACC system, provided that glacial endmember ε_{Nd} of the NCW was less radiogenic than -7.5 and the overturning rate of Pacific deep water did not change significantly. Based on the invariant Nd and stable benthic C isotope signatures throughout MIS 5 (as well as at the beginning and end of MIS 7), it is likely that the gradual CO_2 storage in the deep ocean after the peak interglacials (MIS 5e and 7e) reflects internal oceanic carbon system feedbacks, rather than changes in deep ocean circulation. Based on the invariant Hf isotope signatures of PS2082-1, it is likely that changes in chemical weathering intensity recorded by the open Southern Ocean deep water were small over the last two G-I cycles. The seawater record of PS1388-3 has been strongly affected by local weathering inputs from the Antarctic continent, whereby preferential release of Hf from fresh surfaces of minerals with high Lu/Hf most likely explains the highly radiogenic Hf isotope signatures at the very beginning of interglacials, which implies some change in ice sheet extent and weathering regime. At the same time, the boundary source contribution from the Antarctic continent to AABW has overall been relatively stable over the last 2 G-I cycles.

References

Albarede, F., Simonetti, A., Vervoort, J. D., Blichert-Toft, J., and Abouchami, W. (1998) A Hf-Nd isotopic correlation in ferromanganese nodules. *Geophysical Research Letters* **25**, 3895-3898.

Anderson, R. F., Ali, S., Bradtmiller, L. I., Nielsen, S. H. H., Fleisher, M. Q., Anderson, B. E., and Burckle, L. H. (2009) Wind-Driven Upwelling in the Southern Ocean and the Deglacial Rise in Atmospheric CO2. *Science* **323**, 1443-1448.

Bayon, G., Burton, K. W., Soulet, G., Vigier, N., Dennielou, B., Etoubleau, J., Ponzevera, E., German, C. R., and Nesbitt, R. W. (2009) Hf and Nd isotopes in marine sediments: Constraints on global silicate weathering. *Earth and Planetary Science Letters* **277**, 318-326.

Bayon, G., German, C. R., Boella, R. M., Milton, J. A., Taylor, R. N., and Nesbitt, R. W. (2002) An improved method for extracting marine sediment fractions and its application to Sr and Nd isotopic analysis. *Chemical Geology* **187**, 179-199.

Bayon, G., Vigier, N., Burton, K. W., Brenot, A., Carignan, J., Etoubleau, J., and Chu, N. C. (2006) The control of weathering processes on riverine and seawater hafnium isotope ratios. *Geology* **34**, 433-436.

Berger, A. and Loutre, M. F. (1991) Insolation Values for the Climate of the Last 10000000 Years. *Quaternary Science Reviews* **10**, 297-317.

Berger, W. H. (1982) Increase of carbon dioxide in the atmosphere during deglaciation: the coral reef hypothesis. *Naturwissenschaften* **69**, 87-88.

Bintanja, R., van de Wal, R. S., and Oerlemans, J. (2005) Modelled atmospheric temperatures and global sea levels over the past million years. *Nature* **437**, 125-128.

Carpentier, M., Chauvel, C., Maury, R. C., and Mattielli, N. (2009) The "zircon effect" as recorded by the chemical and Hf isotopic compositions of Lesser Antilles forearc sediments. *Earth and Planetary Science Letters* **287**, 86-99.

Carter, P., Vance, D., Hillenbrand, C. D., Smith, J. A., and Shoosmith, D. R. (2012) The neodymium isotopic composition of waters masses in the eastern Pacific sector of the Southern Ocean. *Geochimica et Cosmochimica Acta* **79**, 41-59.

Chen, T.-Y., Frank, M., Haley, B. A., Gutjahr, M., and Spielhagen, R. F. (2012) Variations of North Atlantic inflow to the central Arctic Ocean over the last 14 million years inferred from hafnium and neodymium isotopes. *Earth and Planetary Science Letters* **353–354**, 82-92.

Chen, T.-Y., Li, G., Frank, M., and Ling, H.-F. (2013a) Hafnium isotope fractionation during continental weathering: Implications for the generation of the seawater Nd-Hf isotope relationships. *Geophys Res Lett* **40**, 916-920.

Chen, T.-Y., Rempfer, J., Frank, M., Stumpf, R., and Molina-Kescher, M. (2013b) Upper ocean vertical supply: A neglected primary factor controlling the distribution of neodymium concentrations of open ocean surface waters? *Journal of Geophysical Research: Oceans*, doi: 10.1002/jgrc.20288.

Chen, T.-Y., Stumpf, R., Frank, M., Bełdowski J., and Staubwasser M. (2013c). Contrasting geochemical cycling of hafnium and neodymium in the central Baltic Sea. *Geochimica et Cosmochimica Acta*, in press, doi:10.1016/j.gca.2013.09.011.

Cook, C. P., van de Flierdt, T., Williams, T., Hemming, S. R., Iwai, M., Kobayashi, M., Jimenez-Espejo, F. J., Escutia, C., Gonzalez, J. J., Khim, B. K., McKay, R. M., Passchier, S., Bohaty, S. M., Riesselman, C. R., Tauxe, L., Sugisaki, S., Galindo, A. L., Patterson, M. O., Sangiorgi, F., Pierce, E. L., Brinkhuis, H., and Scientists, I. E. (2013) Dynamic behaviour of the East Antarctic ice sheet during Pliocene warmth. *Nature Geoscience* **6**, 765-769.

Curry, W. B. and Oppo, D. W. (2005) Glacial water mass geometry and the distribution of delta C-13 of Sigma CO2 in the western Atlantic Ocean. *Paleoceanography* **20**.

David, K., Frank, M., O'Nions, R. K., Belshaw, N. S., and Arden, J. W. (2001) The Hf isotope composition of global seawater and the evolution of Hf isotopes in the deep Pacific Ocean from Fe-Mn crusts. *Chemical Geology* **178**, 23-42.

Flowerdew, M. J., Tyrrell, S., and Peck, V. L. (2013) Inferring sites of subglacial erosion using the Pb isotopic composition of ice-rafted feldspar: Examples from the Weddell Sea, Antarctica. *Geology* **41**, 147-150.

Foster, G. L., Vance, D., and Prytulak, J. (2007) No change in the neodymium isotope composition of deep water exported from the North Atlantic on glacial-interglacial time scales. *Geology* **35**, 37-40.

Frank, M. (2002) Radiogenic isotopes: Tracers of past ocean circulation and erosional input. *Review of Geophysics* **40**, doi: 10.1029/2000RG000094.

Frank, Martin; Mackensen, Andreas (2002): Age model of sediment core PS2082-1. doi:10.1594/PANGAEA.81103

Ganopolski, A., Rahmstorf, S., Petoukhov, V., and Claussen, M. (1998) Simulation of modern and glacial climates with a coupled global model of intermediate complexity. *Nature* **391**, 351-356.

Godfrey, L. V., Zimmermann, B., Lee, D. C., King, R. L., Vervoort, J. D., Sherrell, R. M., and Halliday, A. N. (2009) Hafnium and neodymium isotope variations in NE Atlantic seawater. *Geochemistry Geophysics Geosystems* **10**.

Govin, A., Michel, E., Labeyrie, L., Waelbroeck, C., Dewilde, F., and Jansen, E. (2009) Evidence for northward expansion of Antarctic Bottom Water mass in the Southern Ocean during the last glacial inception. *Paleoceanography* **24**, doi: 10.1029/2008pa001603.

Grobe, H. and Mackensen, A. (1992) Late Quaternary climatic cycles as recorded in sediments from the Antarctic continental margin. *The Antarctic Paleoenvironment: A Perspective on Global Change: Part One*, 349-376.

Guihou, A., Pichat, S., Govin, A., Nave, S., Michel, E., Duplessy, J.-C., Telouk, P., and Labeyrie, L. (2011) Enhanced Atlantic Meridional Overturning Circulation supports the Last Glacial Inception. *Quaternary Science Reviews* **30**, 1576-1582.

Gutjahr, M., Frank, M., Stirling, C. H., Klemm, V., van de Flierdt, T., and Halliday, A. N. (2007) Reliable extraction of a deepwater trace metal isotope signal from Fe-Mn oxyhydroxide coatings of marine sediments. *Chemical Geology* **242**, 351-370.

Haley, B. A., Frank, M., Spielhagen, R. F., and Eisenhauer, A. (2008) Influence of brine formation on Arctic Ocean circulation over the past 15 million years. *Nature Geoscience* **1**, 68-72.

Hays, J. D., Imbrie, J., and Shackleton, N. J. (1976) Variations in the Earth's Orbit: Pacemaker of the Ice Ages. *Science* **194**, 1121-1132.

Hegner, E., Dauelsberg, H. J., van der Loeff, M. M. R., Jeandel, C., and de Baar, H. J. W. (2007) Nd isotopic constraints on the origin of suspended particles in the Atlantic sector of the Southern Ocean. *Geochemistry Geophysics Geosystems* **8**, doi: 10.1029/2007gc001666.

Jaccard, S. L., Hayes, C. T., Martinez-Garcia, A., Hodell, D. A., Anderson, R. F., Sigman, D. M., and Haug, G. H. (2013) Two Modes of Change in Southern Ocean Productivity Over the Past Million Years. *Science* **339**, 1419-1423.

Jacobsen, S. B. and Wasserburg, G. J., 1980. Sm-Nd Isotopic Evolution of Chondrites. Earth and Planetary Science Letters 50, 139-155.

Lippold, J., Luo, Y., Francois, R., Allen, S. E., Gherardi, J., Pichat, S., Hickey, B., and Schulz, H. (2012) Strength and geometry of the glacial Atlantic Meridional Overturning Circulation. *Nature Geosciences* **5**, 813-816.

Lisiecki, L. E. and Raymo, M. E. (2005) A Pliocene-Pleistocene stack of 57 globally distributed benthic delta O-18 records. *Paleoceanography* **20**, doi: 10.1029/2004pa001071.

Mackensen, A., Grobe, H., Hubberten, H. W., Spiess, V., and Futterer, D. K. (1989) Stable Isotope Stratigraphy from the Antarctic Continental-Margin during the Last One Million Years. *Marine Geology* **87**, 315-321.

Mackensen, A., Grobe, H., Hubberten, H. W., Kuhn, G. (1994) Table 2. Sediment core PS2082: benthic and planktic foraminiferal d18O and d13C, benthic census and primary productivity. doi:10.1594/PANGAEA.50113

Marchitto, T. M. and Broecker, W. S. (2006) Deep water mass geometry in the glacial Atlantic Ocean: A review of constraints from the paleonutrient proxy Cd/Ca. *Geochemistry Geophysics Geosystems* **7**, doi: 10.1029/2006gc001323.

Münker, C., Weyer, S., Scherer, E., and Mezger, K. (2001) Separation of high field strength elements (Nb, Ta, Zr, Hf) and Lu from rock samples for MC-ICPMS measurements. *Geochemistry Geophysics Geosystems* **2**, doi: 10.1029/2001GC000183.

Noble, T. L., Piotrowski, A. M., Robinson, L. F., McManus, J. F., Hillenbrand, C. D., and Bory, A. J. M. (2012) Greater supply of Patagonian-sourced detritus and transport by the ACC to the Atlantic sector of the Southern Ocean during the last glacial period. *Earth and Planetary Science Letters* **317**, 374-385.

Nowell, G. M., Kempton, P. D., Noble, S. R., Fitton, J. G., Saunders, A. D., Mahoney, J. J., and Taylor, R. N. (1998) High precision Hf isotope measurements of MORB and OIB by thermal ionisation mass spectrometry: insights into the depleted mantle. *Chemical Geology* **149**, 211-233.

Oliver, K. I. C., Hoogakker, B. A. A., Crowhurst, S., Henderson, G. M., Rickaby, R. E. M., Edwards, N. R., and Elderfield, H. (2010) A synthesis of marine sediment core delta C-13 data over the last 150 000 years. *Climate of the Past* **6**, 645-673.

Omta, A. W., K. van Voorn, G. A., M. Rickaby, R. E., and Follows, M. J. (2013) On the potential role of marine calcifiers in glacial-interglacial dynamics. *Global Biogeochemical Cycles*, doi: 10.1002/gbc.20060.

Orsi, A. H., Whitworth, T., and Nowlin, W. D. (1995) On the Meridional Extent and Fronts of the Antarctic Circumpolar Current. *Deep-Sea Research Part I-Oceanographic Research Papers* **42**, 641-673.

Petit, J. R., Jouzel, J., Raynaud, D., Barkov, N. I., Barnola, J. M., Basile, I., Bender, M., Chappellaz, J., Davis, M., Delaygue, G., Delmotte, M., Kotlyakov, V. M., Legrand, M., Lipenkov, V. Y., Lorius, C., Pepin, L., Ritz, C., Saltzman, E., and Stievenard, M. (1999) Climate and atmospheric history of the past 420,000 years from the Vostok ice core, Antarctica. *Nature* **399**, 429-436.

Pin, C. and Zalduegui, J. F. S. (1997) Sequential separation of light rare-earth elements, thorium and uranium by miniaturized extraction chromatography: Application to isotopic analyses of silicate rocks. *Anal Chim Acta* **339**, 79-89.

Piotrowski, A. M., Banakar, V. K., Scrivner, A. E., Elderfield, H., Galy, A., and Dennis, A. (2009) Indian Ocean circulation and productivity during the last glacial cycle. *Earth and Planetary Science Letters* **285**, 179-189.

Piotrowski, A. M., Goldstein, S. L., Hemming, S. R., and Fairbanks, R. G. (2005) Temporal Relationships of Carbon Cycling and Ocean Circulation at Glacial Boundaries. *Science* **307**, 1933-1938.

Piotrowski, A. M., Goldstein, S. L., R, H. S., Fairbanks, R. G., and Zylberberg, D. R. (2008) Oscillating glacial northern and southern deep water formation from combined neodymium and carbon isotopes. *Earth and Planetary Science Letters* **272**, 394-405.

Rickli, J., Frank, M., and Halliday, A. N. (2009) The hafnium-neodymium isotopic composition of Atlantic seawater. *Earth and Planetary Science Letters* **280**, 118-127.

Rickli, J., Frank, M., Stichel, T., Georg, R. B., Vance, D., and Halliday, A. N. (2013) Controls on the incongruent release of hafnium during weathering of metamorphic and sedimentary catchments. *Geochimica et Cosmochimica Acta* **101**, 263-284.

Roberts, N. L., Piotrowski, A. M., McManus, J. F., and Keigwin, L. D. (2010) Synchronous Deglacial Overturning and Water Mass Source Changes. *Science* **327**, 75-78.

Roy, M., van de Flierdt, T. V., Hemming, S. R., and Goldstein, S. L. (2007) Ar-40/Ar-39 ages of hornblende grains and bulk Sm/Nd isotopes of circum-Antarctic glacio-marine sediments: Implications for sediment provenance in the Southern Ocean. *Chemical Geology* **244**, 507-519.

Siddall, M., Khatiwala, S., van de Flierdt, T., Jones, K., Goldstein, S. L., Hemming, S., and Anderson, R. F. (2008) Towards explaining the Nd paradox using reversible scavenging in an ocean general circulation model. *Earth and Planetary Science Letters* **274**, 448-461.

Siddall, M., Rohling, E. J., Almogi-Labin, A., Hemleben, C., Meischner, D., Schmelzer, I., and Smeed, D. (2003) Sea-level fluctuations during the last glacial cycle. *Nature* **423**, 853-858.

Sigman, D. M., Hain, M. P., and Haug, G. H. (2010) The polar ocean and glacial cycles in atmospheric CO2 concentration. *Nature* **466**, 47-55.

Skinner, L. C., Scrivner, A. E., Vance, D., Barker, S., Fallon, S., and Waelbroeck, C. (2013) North Atlantic versus Southern Ocean contributions to a deglacial surge in deep ocean ventilation. *Geology* doi: 10.1130/g34133.1.

Stichel, T., Frank, M., Rickli, J., and Haley, B. A. (2012) The hafnium and neodymium isotope composition of seawater in the Atlantic sector of the Southern Ocean. *Earth and Planetary Science Letters* **317–318**, 282-294.

Tanaka, T., Togashi, S., Kamioka, H., Amakawa, H., Kagami, H., Hamamoto, T., Yuhara, M., Orihashi, Y., Yoneda, S., Shimizu, H., Kunimaru, T., Takahashi, K., Yanagi, T., Nakano, T., Fujimaki, H., Shinjo, R., Asahara, Y., Tanimizu, M., and Dragusanu, C. (2000) JNdi-1: a neodymium isotopic reference in consistency with LaJolla neodymium. *Chemical Geology* **168**, 279-281.

Toggweiler, J. R. (2008) Origin of the 100,000-year timescale in Antarctic temperatures and atmospheric CO(2). *Paleoceanography* **23** doi: 10.1029/2006pa001405.

van de Flierdt, T., Frank, M., Halliday, A. N., Hein, J. R., Hattendorf, B., Gunther, D., and Kubik, P. W. (2004) Tracing the history of submarine hydrothermal inputs and the significance of hydrothermal hafnium for the seawater budget-a combined Pb-Hf-Nd isotope approach. *Earth and Planetary Science Letters* **222**, 259-273.

van de Flierdt, T., Hemming, S. R., Goldstein, S. L., and Abouchami, W. (2006a) Radiogenic isotope fingerprint of Wilkes Land–Adélie Coast Bottom Water in the circum-Antarctic Ocean. *Geophysical Research Letters* **33,** L12606, doi:10.1029/2006GL026020.

van de Flierdt, T., Robinson, L. F., Adkins, J. F., Hemming, S. R., and Goldstein, S. L. (2006b) Temporal stability of the neodymium isotope signature of the Holocene to glacial North Atlantic. *Paleoceanography* **21,** PA4102, doi:10.1029/2006PA001294.

Vance, D. and Burton, K. (1999) Neodymium isotopes in planktonic foraminifera: a record of the response of continental weathering and ocean circulation rates to climate change. *Earth and Planetary Science Letters* **173**, 365-379.

Vervoort, J. D., Patchett, P. J., Blichert-Toft, J., and Albarede, F. (1999) Relationships between Lu-Hf and Sm-Nd isotopic systems in the global sedimentary system. *Earth and Planetary Science Letters* **168**, 79-99.

Walter, H. J., Hegner, E., Diekmann, B., Kuhn, G., and van der Loeff, M. M. R. (2000) Provenance and transport of terrigenous sediment in the South Atlantic Ocean and their relations to glacial and interglacial cycles: Nd and Sr isotopic evidence. *Geochimica et Cosmochimica Acta* **64**, 3813-3827.

Weber, S. L., Drijfhout, S. S., Abe-Ouchi, A., Crucifix, M., Eby, M., Ganopolski, A., Murakami, S., Otto-Bliesner, B., and Peltier, W. R. (2007) The modern and glacial overturning circulation in the Atlantic Ocean in PMIP coupled model simulations. *Climate of the Past* **3**, 51-64.

West, A. J., Galy, A., and Bickle, M. (2005) Tectonic and climatic controls on silicate weathering. *Earth and Planetary Science Letters* **235**, 211-228.

Willenbring, J. K., Codilean, A. T., and McElroy, B. (2013) Earth is (mostly) flat: Apportionment of the flux of continental sediment over millennial time scales. *Geology* **41**, 343-346.

Wilson, D. J., Piotrowski, A. M., Galy, A., and Clegg, J. A. (2013) Reactivity of neodymium carriers in deep sea sediments: Implications for boundary exchange and paleoceanography. *Geochimica et Cosmochimica Acta* **109**, 197-221.

Yu, J., Anderson, R. F., Jin, Z., Rae, J. W. B., Opdyke, B. N., and Eggins, S. M. (2013) Responses of the deep ocean carbonate system to carbon reorganization during the Last Glacial–interglacial cycle. *Quaternary Science Reviews* **76**, 39-52.

Zimmermann, B., Porcelli, D., Frank, M., Rickli, J., Lee, D. C., and Halliday, A. N. (2009) The hafnium isotope composition of Pacific Ocean water. *Geochimica et Cosmochimica Acta* **73**, 91-101.

Chapter 8

Summary and Outlook

8.1 Summary

Combined oceanic Hf and Nd isotope compositions are a novel geochemical tool developed over a bit more than the past decade to study changes in ocean circulation and continental weathering regimes. Since Hf isotopes are a relatively new proxy, a number of questions regarding the geochemistry of oceanic Hf have previously not been investigated or are controversial. The overall goal of my PhD study is to provide insights into the sources and biogeochemical cycling of oceanic Hf isotopes, as well as to apply it in paleoclimate studies combined with the much better understood oceanic Nd isotopes.

The major findings of this thesis are summarized as follows:

(1) Leaching experiments carried out on Asian dust samples provided clear and direct evidence to the long-standing issue of whether incongruent continental weathering can directly produce the seawater Nd-Hf isotope array. Overall, the leaching data either plot along or slightly above the Nd-Hf seawater array, providing strong direct support that the seawater Nd-Hf isotope relationship is predominantly generated by weathering of UCC. The data also revealed a small but systematic difference of Nd isotope compositions between leachates and detrital silicates of the continental particles, which will help to constrain Nd isotope signatures of weathering into the ocean.

(2) A global compilation of available Nd concentrations from open ocean surface water reveals that upper ocean stratification may be a previously neglected primary factor in determining the basin scale variability of surface water Nd concentrations. Similar to the mechanisms of nutrient supply, this study suggests that stratification inhibits vertical supply of Nd from the subsurface thermocline waters and thus the magnitude of the Nd flux to the surface layer, which is corroborated by modeling results of the Bern3D ocean model of intermediate complexity.

(3) The first combined direct seawater Nd and Hf isotope and concentration measurements from the central Baltic Sea demonstrate markedly different geochemical behavior of the two element and isotope systems. While Nd isotopes indicate a clear trend form less radiogenic values in the northern part of the Baltic Sea to more radiogenic compositions closer to the Atlantic inflow, the distribution of Hf isotopes is significantly

more heterogenous and the variations are less systematic. Nd isotopes essentially trace the mixing between more radiogenic saline waters from the Atlantic in the south and unradiogenic fresh waters from the north, which helps to understand Nd isotopes as water mass tracer in the open ocean. The results obtained from the Kalix river waters support previous assumptions that the Hf isotope signature released during incipient weathering of glacial tills is highly radiogenic due to the dissolution of easily alterable accessory minerals.

Since the central Baltic Sea is a basin without hydrothermal influence, the general consistency of Hf-Nd isotope data with the global seawater trend implies that continental weathering alone is most likely sufficient to produce the oceanic radiogenic Hf isotope signatures.

At the Gotland Deep station, the Nd concentrations in the euxinic waters are higher by a factor >10 than in the overlying oxygen-depleted waters, whereas Hf only shows small concentration variations, which indicates faster removal of Hf from the water column than of Nd. It is thus inferred that Hf has a much shorter residence time than Nd in the Baltic Sea (and most likely also in the global ocean) and is not notably affected by redox cycling.

 (4) Pioneering work on the high resolution seawater Hf isotope evolution from the late Cenozoic to the present has been carried out applying the findings of the previous chapters above. The data show that both Nd and Hf isotope compositions of central Arctic intermediate water and open Southern Ocean deep water can be reliably reconstructed from marine sediments by reductive leaching, while Nd-Hf isotope compositions extracted from Core PS1388 from the Weddell Sea margin represents significant contributions of local inputs and incongruent release of Hf isotopes from the Antarctic continent. The similarity of the Nd and Hf isotope evolution of central Arctic intermediate water is well explained by the mixing between unradiogenic watersfrom the Atlantic/Barents Sea and radiogenic inputs originating from the Kara Sea shelf. In the open Southern Ocean deep water where local weathering inputs such as through dust are negligible, essentially constant Hf isotope signatures are observed, while the Nd isotope signatures closely correlate with benthic carbon isotopes and reflect changes in mixing

between North Atlantic Deep Water and Pacific waters which is similar to previous findings. Thus Hf isotopes have been insensitive to the large scale circulation changes in the Southern Ocean. However, whether this also reflects negligible changes in continental chemical weathering intensity over glacial/interglacial cycles needs to be explored in the future.

8.2 Outlook

This study leaves important questions and raises new issues which need to be answered in the future:

Have endmember Nd isotope compositions and possibly the Nd concentrations of North Atlanic Deep Water really been constant on glacial/interglacial time scales? Since the water mass transit might be much slower in LGM than the present, did Nd isotopes still behave quasi-conservatively in the glacial deep Atlantic? How did changes in deep and intermediate Pacific circulation and overturning contribute to the Nd isotope signatures of CDW over G-I cycles? The null hypothesis is that the contribution remained unchanged. Lisiecki (2010) proposed that carbon isotope signature of Pacific deep water can be well described by a constant mixture of 60% NCW and 40% SCW plus a constant Pacific remineralization offset of -0.5‰. However, glacial carbon isotopes in the Pacific were far from homogenously distributed (e.g, Matsumoto et al., 2002; Mccave et al., 2008) and it is likely that the status of the glacial deep Pacific is not that simple. The solution of these questions is fundamentally important for a reliable application of Nd isotopes in paleoceanography and for understanding the relationships between present/past changes in oceanic circulation and global/local climate.

Initiated by this study, deep ocean Nd isotope signatures generally have three types of origin: "advection" (e.g., Southern Ocean), "advection-local input" (e.g., the central Arctic, the central Baltic), "local/boundary input": Nd influx from regional shelf inputs or partial dissolution ofeolain dust to bottom water, which is not "transport-limited" (e.g., The Weddell Sea margin). It is currently not clear how the boundary sources contribute to the conservative/non-conservative behavior of Nd isotopes and what the exact pathways and transport processes are.

Finally, more studies on continental weathering process and transport of Hf and its isotopic compositions are necessary. How do the weathered Hf isotope signatures reflect changes in weathering environment and different prevailing rock types? What is the influence of estuarine mixing and scavenging and how can the inputs of Hf into the ocean be better constrained? An improved understanding of these issues will help to use Hf more reliably as a proxy for weathering intensity and continental inputs.

References

Matsumoto, K., Oba, T., Lynch-Stieglitz, J., and Yamamoto, H. (2002) Interior hydrography and circulation of the glacial Pacific Ocean. *Quaternary Science Reviews* **21**, 1693-1704.

McCave, I. N., Carter, L., and Hall, I. R. (2008) Glacial-interglacial changes in water mass structure and flow in the SW Pacific Ocean. *Quaternary Science Reviews* **27**, 1886-1908.

Lisiecki, L. E. (2010) A simple mixing explanation for late Pleistocene changes in the Pacific-South Atlantic benthic δ13C gradient. *Climate of the Past* **6**, 305-314.

Appendix

Table A1 Reagents used in this study

	product grade	purification in lab	company	remark
Milli-Q water	> 18 MΩ		Merck Millipore	
H_2O_2	for analysis		Roth	redox cleaning of forams
H_2O_2	super pure		Merck	oxidizing organics before isotope measurement
Citric acid	for analysis		Roth	
Ascorbic acid	for analysis		Roth	
Acetic acid	for analysis		Merck	decarbonation
Acetic acid	super pure		Merck	leaching
hydroxylammonium chloride	for analysis		Merck	
HCl	for analysis	Savillex distill	Roth	
HNO_3	for analysis	Savillex distill	Roth	
HF	super pure		Merck	
$HClO_4$	super pure		Roth	
Ammonia solution	for analysis		Roth	redox cleaning of forams
Ammonia solution	super pure		Merck	co-precipitation
NaOH solution	for analysis		Roth	
NaOH solution	super pure		Merck	
Natriumacetat	for analysis		Roth	
hydrazinium hydroxide	for synthesis		Merck	
Methanol	for analysis		Roth	
Titriplex III	for analysis		Merck	
Diethylether	for analysis	Back-extraction	Roth	
$FeCl_3$ x 6 H_2O		Back-extraction		

Figure A1
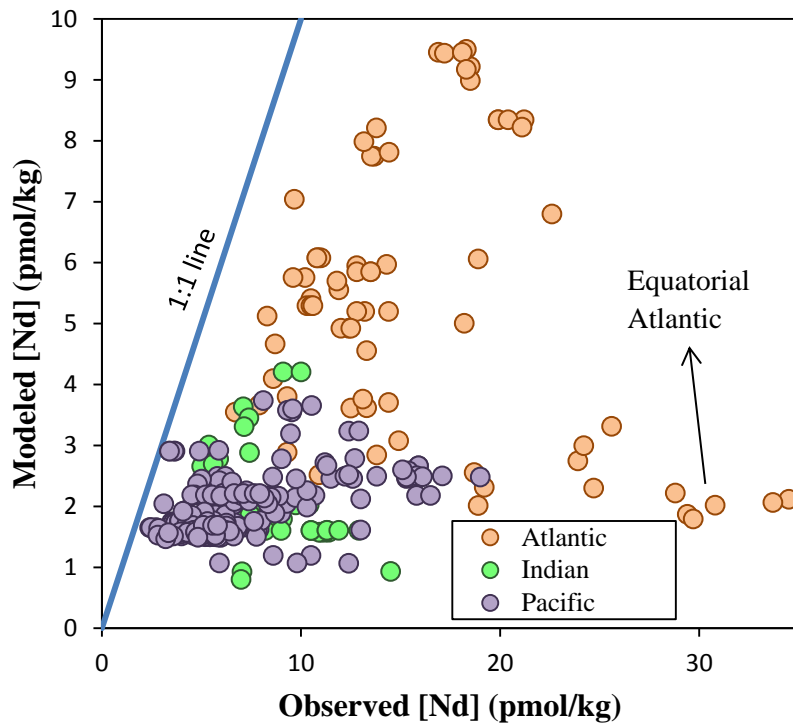
Figure A1. A comparison between observed and modeled data from the control run. For clarity, a few data points from the subpolar North Atlantic with significantly higher modeled concentrations (e.g., see Figure 5a) are not shown.

Model Description for Chapter 4

For the simulations as presented in Figure 5, we use the Bern3D ocean model of intermediate complexity [Müeller et al., 2006], coupled to an energy-moisture balance model [Ritz et al., 2011a, b]. The resolution in the horizontal is 36 x 36 grid cells, equidistant in longitude and in the sine of latitude. Spacing of the 32 depth layers is logarithmic, i.e., the thickness of the depth layers increases with depth from 39 m in the uppermost to 397 m in the bottom layer.

A comprehensive approach for the simulation of neodymium isotopes ([143]Nd and [144]Nd) has been included into the Bern3D model (see Rempfer et al. [2011, 2012] for a detailed description of the approach). Three different sources of Nd to the oceans are taken into

account; the sediment-water interface (the boundary source), release from dust, and river discharge. The boundary source is represented by a globally uniform flux of Nd across the sediment-water interface at depths between 0 and 3000 m. The isotopic composition of the boundary source is based on a global map of ε_{Nd} [Jeandel et al., 2007]. A global map of atmospheric dust flux [Luo et al., 2003] is prescribed at the sea surface. The concentration of Nd in dust (20 μg/g) is assumed to be globally constant. 2% of the Nd in dust is released to seawater in the shallowest depth layer. ε_{Nd} in dust varies between different regions (see Rempfer et al. [2011] for further details). Values for discharge and dissolved Nd concentration in major rivers [Goldstein et al., 1987] are prescribed at the seasurface. Estuarine removal of Nd is taken into account by releasing only 30% of the riverine Nd to the ocean.

Within the water column Nd isotopes are subject to internal cycling, i.e. adsorption onto and desorption from surfaces of opal, calcite, particulate organic carbon and aeolian dust (no desorption occurs from the latter). This internal cycling is parameterized by a reversible scavenging approach [Rempfer et al., 2011, 2012]. Particle export fluxes of calcite, particulate organic carbon, and opal are calculated from prognostic equations (see Tschumi et al. [2008] for a detailed description of the approach).

Table A2 Data compilation on Nd concentrations of open ocean surface waters

Source	Station	Longitude (°E)	Latitude (°N)	Depth (m)	estimated σ_{200m}	estimated σ_{1000m}	$\Delta(\sigma_{1000m}-\sigma_{-200m})$	Nd (pmol/kg) < 100 m
this study[1]	SO213-50-1	-114.4	-40.3	2	26.43	27.23	0.80	5.87
this study	SO213-54-2	-120.5	-43.7	2	26.79	27.23	0.44	10.53
this study	SO213-66-1	-151.7	-45.4	2	26.85	27.19	0.34	9.53
this study	SO-SS-1	-178.0	-46.2	2	26.74	27.19	0.45	8.10
this study	SO-SS-2	179.6	-45.9	2	26.72	27.20	0.48	9.32
this study	SO-SS-3	178.0	-46.0	2	26.71	27.20	0.49	9.58
[Vance et al., 2004]	TPS47 39-1	161.1	47.0	3	26.86	27.46	0.60	15.90
[Vance et al., 2004]	TPS24 271-1	150.5	24.3	0	25.25	27.30	2.05	5.40
[Vance et al., 2004]	HOT-115-2 (4.73)	-158.0	22.8	50	25.35	27.37	2.02	5.36
[Vance et al., 2004]	HOT-115-2 (4.73)	-158.0	22.8	50	25.35	27.37	2.02	5.56
[Vance et al., 2004]	MW98-13-118 (1.12)	-156.1	20.2	50	25.45	27.40	1.95	5.30
[Hongo et al., 2006]	SAP ssw-1	155.1	44.0	5	26.81	27.45	0.64	12.20
[Hongo et al., 2006]	SAP ssw-2	165.1	50.0	5	26.89	27.46	0.57	12.70
[Hongo et al., 2006]	SAP ssw-8	-163.0	52.3	5	26.82	27.44	0.62	9.47
[Hongo et al., 2006]	SAP ssw-9	-160.0	53.4	5	26.80	27.44	0.64	12.40
[Hongo et al., 2006]	SAP ssw-10	-154.4	55.4	5	26.81	27.44	0.63	12.90
[Hongo et al., 2006]	SAP ssw-11	-149.6	55.0	5	26.84	27.43	0.59	9.02
[Hongo et al., 2006]	SAP ssw-12	-144.6	55.0	5	26.73	27.41	0.68	8.58
[Hongo et al., 2006]	SAP ssw-13	-145.0	49.6	5	26.73	27.41	0.68	6.52
[Hongo et al., 2006]	SAP ssw-14	-134.6	48.6	5	26.62	27.39	0.77	7.25
[Hongo et al., 2006]	YS ssw-2	163.3	47.5	5	26.86	27.47	0.61	11.20
[Hongo et al., 2006]	YS ssw-3	161.1	47.1	5	26.86	27.46	0.60	11.30
[Hongo et al., 2006]	YS ssw-4	157.6	46.1	5	26.85	27.46	0.61	15.40
[Hongo et al., 2006]	YS ssw-5	155.2	45.3	5	26.82	27.45	0.63	12.40
[Hongo et al., 2006]	YS ssw-6	152.4	44.4	5	26.79	27.44	0.65	15.80
[Hongo et al., 2006]	YS ssw-7	150.1	43.5	5	26.74	27.42	0.68	17.10
[Hongo et al., 2006]	SO ssw-3	153.2	30.2	5	25.22	27.23	2.01	5.59
[Hongo et al., 2006]	BO ssw-5	148.4	37.1	5	26.02	27.34	1.32	9.28
[Hongo et al., 2006]	BO ssw-6	152.6	38.1	5	26.30	27.36	1.06	6.66
[Hongo et al., 2006]	BO ssw-7	156.1	39.0	5	26.43	27.37	0.94	9.72
[Hongo et al., 2006]	BO ssw-9	164.6	40.0	5	26.43	27.38	0.95	7.01
[Hongo et al., 2006]	BO ssw-10	168.3	40.0	5	26.40	27.37	0.97	10.70
[Hongo et al., 2006]	BO ssw-11	173.5	40.0	5	26.35	27.36	1.01	8.88
[Hongo et al., 2006]	BO ssw-12	177.1	40.0	5	26.34	27.35	1.01	8.31
[Hongo et al., 2006]	BO ssw-13	-179.6	39.2	5	26.30	27.34	1.04	8.50
[Hongo et al., 2006]	BO ssw-14	-178.3	39.6	5	26.31	27.35	1.04	5.97
[Hongo et al., 2006]	BO ssw-15	-175.5	38.0	5	26.18	27.33	1.15	7.38

[Hongo et al., 2006]	BO ssw-16	-170.6	35.4	5	26.05	27.31	1.26	5.15
[Hongo et al., 2006]	BO ssw-17	-168.4	34.3	5	26.00	27.31	1.31	4.52
[Hongo et al., 2006]	BO ssw-18	-164.4	32.3	5	25.92	27.32	1.40	6.04
[Hongo et al., 2006]	BO ssw-19	-162.4	31.2	5	25.88	27.33	1.45	5.06
[Hongo et al., 2006]	BO ssw-20	-159.2	28.2	5	25.73	27.34	1.61	5.60
[Hongo et al., 2006]	BO ssw-21	-158.2	24.5	5	25.34	27.37	2.03	5.53
[Hongo et al., 2006]	BO ssw-23	-159.4	18.3	5	25.51	27.40	1.89	5.30
[Hongo et al., 2006]	BO ssw-24	-159.1	20.3	5	25.42	27.39	1.97	6.82
[Hongo et al., 2006]	BO ssw-26	-166.6	19.6	5	25.32	27.38	2.06	6.25
[Hongo et al., 2006]	BO ssw-27	-170.1	19.6	5	25.26	27.37	2.11	4.27
[Hongo et al., 2006]	BO ssw-28	-178.4	20.0	5	25.18	27.37	2.19	4.58
[Hongo et al., 2006]	BO ssw-29	177.5	19.6	5	25.13	27.37	2.24	6.25
[Hongo et al., 2006]	BO ssw-32	165.2	20.2	5	25.20	27.37	2.17	6.21
[Hongo et al., 2006]	BO ssw-33	162.1	20.5	5	25.16	27.36	2.20	5.09
[Hongo et al., 2006]	BO ssw-37	148.3	23.4	5	25.20	27.30	2.10	7.76
[Hongo et al., 2006]	BO ssw-38	145.1	25.6	5	25.17	27.28	2.11	5.97
[Greaves et al., 1999, 2001]	349	128.4	24.3	5	24.95	27.29	2.34	6.61
[Greaves et al., 1999, 2001]	333	132.8	24.3	5	25.03	27.29	2.26	4.84
[Greaves et al., 1999, 2001]	275	150.5	24.3	5	25.25	27.30	2.05	5.41
[Greaves et al., 1999, 2001]	227	168.0	24.3	5	25.29	27.32	2.03	4.56
[Greaves et al., 1999, 2001]	189	-176.8	24.2	5	25.32	27.34	2.02	4.42
[Greaves et al., 1999, 2001]	181	-173.6	24.2	5	25.32	27.34	2.02	4.64
[Greaves et al., 1999, 2001]	173	-170.7	23.4	5	25.26	27.35	2.09	4.61
[Greaves et al., 1999, 2001]	157	-167.2	24.1	5	25.42	27.35	1.93	4.15
[Greaves et al., 1999, 2001]	150	-166.7	24.5	5	25.45	27.35	1.90	3.94
[Greaves et al., 1999, 2001]	140	-165.7	25.5	5	25.50	27.35	1.85	4.29
[Greaves et al., 1999, 2001]	128	-161.3	24.9	5	25.43	27.36	1.93	5.02
[Greaves et al., 1999, 2001]	116	-156.7	24.2	5	25.34	27.37	2.03	4.71
[Greaves et al., 1999, 2001]	100	-151.3	24.3	5	25.33	27.38	2.05	4.87
[Greaves et al., 1999, 2001]	88	-146.9	24.2	5	25.27	27.38	2.11	4.71
[Greaves et al., 1999, 2001]	81	144.0	24.2	5	25.17	27.29	2.12	5.82
[Greaves et al., 1999, 2001]	62	-135.6	24.3	5	25.40	27.40	2.00	5.24
[Greaves et al., 1999, 2001]	56	-133.2	24.3	5	25.46	27.40	1.94	6.41
[Greaves et al., 1999, 2001]	46	-128.8	25.2	5	25.59	27.40	1.81	7.63
[Greaves et al., 1999, 2001]	31	-123.9	29.1	5	25.96	27.39	1.43	8.69
[Greaves et al., 1999, 2001]	28	-122.6	30.0	5	26.06	27.39	1.33	10.30
[Greaves et al., 1999, 2001]	26	-122.0	30.5	5	26.13	27.39	1.26	8.34
[Greaves et al., 1999, 2001]	24	-121.2	30.9	5	26.21	27.40	1.19	8.16
[Greaves et al., 1999, 2001]	22	-120.6	31.2	5	26.27	27.40	1.13	10.30
[Greaves et al., 1999, 2001]	18	-119.7	31.7	5	26.31	27.39	1.08	9.75
[Greaves et al., 1999, 2001]	16	-119.5	31.8	5	26.31	27.39	1.08	13.80
[Amakawa et al., 2004]	CM SSW-1	142.5	37.1	5	26.05	27.35	1.30	13.00

[Amakawa et al., 2004]	CM SSW-3	145.8	42.4	5	26.67	27.40	0.73	16.10
[Amakawa et al., 2004]	CM SSW-4	151.3	43.4	5	26.76	27.43	0.67	19.00
[Amakawa et al., 2004]	CM SSW-5	153.0	43.6	5	26.79	27.44	0.65	15.30
[Amakawa et al., 2004]	CM SSW-6	152.1	46.2	5	26.78	27.43	0.65	15.10
[Klinkhammer et al., 1983]	RAMA	145.0	18.0	0	24.81	27.38	2.57	5.10
[Debaar et al., 1985]	VERTEX II	-108.0	18.0	0	26.35	27.40	1.05	13.00
[Amakawa et al., 2009]	BO-1	160.0	40.0	0	26.47	27.39	0.92	15.80
[Amakawa et al., 2009]	BO-1	160.0	40.0	100	26.47	27.39	0.92	16.50
[Amakawa et al., 2009]	BO-3	160.0	30.0	11	25.31	27.25	1.94	5.50
[Amakawa et al., 2009]	BO-3	160.0	30.0	51	25.31	27.25	1.94	5.70
[Amakawa et al., 2009]	BO-3	160.0	30.0	75	25.31	27.25	1.94	5.02
[Amakawa et al., 2009]	BO-3	160.0	30.0	100	25.31	27.25	1.94	5.70
[Amakawa et al., 2009]	BO-5	-175.0	20.0	9	25.19	27.36	2.17	5.09
[Amakawa et al., 2009]	BO-5	-175.0	20.0	50	25.19	27.36	2.17	5.56
[Amakawa et al., 2009]	BO-5	-175.0	20.0	99	25.19	27.36	2.17	5.81
[Alibo and Nozaki, 1999]	-	139.9	34.7	5	25.68	27.31	1.63	6.64
[Alibo and Nozaki, 1999]	-	139.9	34.7	49	25.68	27.31	1.63	7.12
[Alibo and Nozaki, 1999]	-	139.9	34.7	99	25.68	27.31	1.63	7.65
[Alibo and Nozaki, 1999]	-	139.9	34.7	150	25.68	27.31	1.63	7.93
[Amakawa et al., 2000]	SSW 1	138.1	31.5	5	25.15	27.26	2.11	4.07
[Amakawa et al., 2000]	SSW 2	134.3	25.3	5	25.06	27.27	2.21	4.82
[Amakawa et al., 2000]	SSW 3	130.9	19.3	5	24.83	27.36	2.53	3.11
[Amakawa et al., 2000]	SSW 4	128.1	14.3	5	25.02	27.39	2.37	2.85
[Amakawa et al., 2000]	SSW 36	120.9	21.5	5	25.02	27.35	2.33	2.81
[Amakawa et al., 2000]	SSW 37	123.5	24.5	5	24.94	27.30	2.36	3.60
[Amakawa et al., 2000]	SSW 38	126.7	27.3	5	25.01	27.27	2.26	3.20
[Amakawa et al., 2000]	SSW 39	128.2	28.7	5	25.09	27.28	2.19	3.34
[Amakawa et al., 2000]	SSW 40	131.7	31.6	5	25.27	27.30	2.03	3.11
[Lacan and Jeandel, 2001]	EqPac 12°S	-135.0	-12.0	20	25.27	27.38	2.11	5.70
[Lacan and Jeandel, 2001]	EqPac 12°S	-135.0	-12.0	60	25.27	27.38	2.11	6.20
[Lacan and Jeandel, 2001]	EqPac 0°	-140.0	0.0	40	26.40	27.39	0.99	5.20
[Lacan and Jeandel, 2001]	N Pac EqPac 2°N	-140.0	2.0	15	26.41	27.39	0.98	8.00
[Lacan and Jeandel, 2001]	N Pac EqPac 2°N	-140.0	2.0	40	26.41	27.39	0.98	5.60
[Grenier et al., 2013]	EUC-Fe 26	145.0	2.0	25.0	25.76	27.39	1.63	6.60
[Grenier et al., 2013]	EUC-Fe 25	149.5	0.0	25.0	25.72	27.39	1.67	6.10
[Grenier et al., 2013]	EUC-Fe 23	156.0	-1.4	50.0	25.76	27.39	1.63	4.20
[Grenier et al., 2013]	EUC-Fe 22	156.0	0.4	20.0	25.79	27.39	1.60	6.70
[Grenier et al., 2013]	EUC-Fe 21	156.0	2.0	25.0	25.84	27.39	1.55	4.90
[Grenier et al., 2013]	EUC-Fe 15	180.0	-2.0	15.0	25.90	27.38	1.48	4.00
[Grenier et al., 2013]	EUC-Fe 15	180.0	-2.0	75.0	25.90	27.38	1.48	3.50
[Grenier et al., 2013]	EUC-Fe 14	180.0	0.0	15.0	25.88	27.38	1.50	4.00
[Grenier et al., 2013]	EUC-Fe 14	180.0	0.0	97.0	25.88	27.38	1.50	4.50

[Grenier et al., 2013]	EUC-Fe 13	180.0	2.0	15.0	25.97	27.38	1.41	3.70
[Grenier et al., 2013]	EUC-Fe 13	180.0	2.0	80.0	25.97	27.38	1.41	3.40
[Grenier et al., 2013]	EUC-Fe 3	-140.0	-2.0	15.0	26.35	27.39	1.04	3.50
[Grenier et al., 2013]	EUC-Fe 3	-140.0	-2.0	60.0	26.35	27.39	1.04	3.60
[Grenier et al., 2013]	EUC-Fe 2	-140.0	0.0	15.0	26.37	27.39	1.02	3.70
[Grenier et al., 2013]	EUC-Fe 2	-140.0	0.0	50.0	26.37	27.39	1.02	3.70
[Grenier et al., 2013]	EUC-Fe 2	-140.0	0.0	90.0	26.37	27.39	1.02	3.90
[Grenier et al., 2013]	EUC-Fe 1	-140.0	2.0	15.0	26.40	27.39	0.98	3.90
[Grenier et al., 2013]	EUC-Fe 1	-140.0	2.0	50.0	26.40	27.39	0.98	3.90
[Wang and Yamada, 2007]	St. 6	160.0	0.0	0	25.80	27.39	1.59	6.93
[Wang and Yamada, 2007]	St. 6	160.0	0.0	50	25.80	27.39	1.59	6.88
[Wang and Yamada, 2007]	St. 6	160.0	0.0	101	25.80	27.39	1.59	7.16
[Wang and Yamada, 2007]	St. 9	175.0	0.0	0	25.86	27.38	1.52	5.45
[Wang and Yamada, 2007]	St. 10	175.0	0.0	25	25.86	27.38	1.52	5.18
[Wang and Yamada, 2007]	St. 11	175.0	0.0	50	25.86	27.38	1.52	5.88
[Wang and Yamada, 2007]	St. 12	175.0	0.0	70	25.86	27.38	1.52	5.45
[Wang and Yamada, 2007]	St. 13	175.0	0.0	100	25.86	27.38	1.52	5.65
[Wang and Yamada, 2007]	St. 12	-170.0	0.0	0	25.94	27.39	1.45	6.82
[Wang and Yamada, 2007]	St. 13	-170.0	0.0	50	25.94	27.39	1.45	4.87
[Wang and Yamada, 2007]	St. 14	-170.0	0.0	100	25.94	27.39	1.45	5.09
[Wang and Yamada, 2007]	St. 14	-160.0	0.0	0	26.19	27.38	1.19	5.09
[Wang and Yamada, 2007]	St. 15	-160.0	0.0	50	26.19	27.38	1.19	4.96
[Wang and Yamada, 2007]	St. 16	-160.0	0.0	99	26.19	27.38	1.19	6.00
[Zhang and Nozaki, 1996]	sta SA5	149.9	-0.1	0	25.68	27.39	1.71	4.67
[Zhang and Nozaki, 1996]	sta SA5	149.9	-0.1	9	25.68	27.39	1.71	4.51
[Zhang and Nozaki, 1996]	sta SA5	149.9	-0.1	30	25.68	27.39	1.71	5.44
[Zhang and Nozaki, 1996]	sta SA5	149.9	-0.1	74	25.68	27.39	1.71	5.20
[Zhang and Nozaki, 1996]	sta SA5	149.9	-0.1	97	25.68	27.39	1.71	5.53
[Piepgras and Wasserburg, 1982]	Station 31	-160.0	-20.0	30	25.11	27.39	2.28	2.90
[Piepgras and Jacobsen, 1992]	TPS27 39-1	161.1	47.0	3	26.86	27.46	0.60	15.90
[Piepgras and Jacobsen, 1992]	TPS24 271-1	150.5	24.3	0	25.25	27.30	2.05	5.41
[Shimizu et al., 1994]	DE4	-177.0	44.7	0	26.69	27.43	0.74	11.50
[Shimizu et al., 1994]	DE4	-177.0	44.7	50	26.69	27.43	0.74	12.60
[Shimizu et al., 1994]	DE4	-177.0	44.7	100	26.69	27.43	0.74	15.30
[Zhang and Nozaki, 1996]	sta SA7	154.3	-14.3	0	25.39	27.38	1.99	3.40
[Zhang and Nozaki, 1996]	sta SA7	154.3	-14.3	2	25.39	27.38	1.99	4.89
[Zhang and Nozaki, 1996]	sta SA7	154.3	-14.3	30	25.39	27.38	1.99	3.67
[Zhang and Nozaki, 1996]	sta SA7	154.3	-14.3	50	25.39	27.38	1.99	3.62
[Zhang and Nozaki, 1996]	sta SA7	154.3	-14.3	99	25.39	27.38	1.99	3.40
[Zhang and Nozaki, 1996]	sta SA12	175.4	-27.3	0	25.91	27.21	1.30	2.72
[Zhang and Nozaki, 1996]	sta SA12	175.4	-27.3	2	25.91	27.21	1.30	2.40
[Zhang and Nozaki, 1996]	sta SA12	175.4	-27.3	46	25.91	27.21	1.30	2.46

[Zhang and Nozaki, 1996]	sta SA12	175.4	-27.3	74	25.91	27.21	1.30	3.80
[Grasse et al., 2012]	St. 2	-80.0	-10.0	2	26.38	27.39	1.01	5.80
[Grasse et al., 2012]	St. 2	-80.0	-10.0	101	26.38	27.39	1.01	6.20
[Grasse et al., 2012]	St. 30	-75.5	-16.0	3	26.47	27.40	0.92	5.60
[Grasse et al., 2012]	St. 78	-77.1	-14.0	2	26.44	27.39	0.96	5.90
[Grasse et al., 2012]	St. 93	-85.8	-14.0	3	26.32	27.39	1.06	5.00
[Grasse et al., 2012]	St. 103	-85.8	-9.0	2	26.37	27.39	1.02	4.80
[Grasse et al., 2012]	St. 109	-85.8	-3.6	2	26.25	27.41	1.16	7.90
[Grasse et al., 2012]	St. 117	-82.0	-3.6	2	26.22	27.41	1.19	7.80
[Grasse et al., 2012]	St. 134	-85.8	-6.0	2	26.31	27.41	1.09	9.00
[Grasse et al., 2012]	St. 134	-85.8	-6.0	99	26.31	27.41	1.09	6.30
[Grasse et al., 2012]	St. 152	-85.8	0.0	3	26.39	27.40	1.00	8.60
[Grasse et al., 2012]	St. 152	-85.8	0.0	90	26.39	27.40	1.00	10.50
[Grasse et al., 2012]	St. 159	-85.8	1.3	1	26.38	27.40	1.02	9.80
[Grasse et al., 2012]	St. 159	-85.8	1.3	52	26.38	27.40	1.02	5.90
[Grasse et al., 2012]	St. 159	-85.8	1.3	99	26.38	27.40	1.02	19.60
[Grasse et al., 2012]	St. 160	-85.8	1.6	4	26.37	27.40	1.03	12.40
[Jeandel et al., 1998]	Ind Stn10	117.4	-16.3	104	25.61	27.38	1.77	7.10
[Jeandel et al., 1998]	Ind Stn20	116.0	-11.5	59	25.75	27.39	1.64	9.10
[Jeandel et al., 1998]	Ind Stn20	116.0	-11.5	99	25.75	27.39	1.64	10.00
[Bertram and Elderfield, 1993]	CD1502	53.6	-12.3	10	26.14	27.42	1.28	6.93
[Bertram and Elderfield, 1993]	CD1502	53.6	-12.3	25	26.14	27.42	1.28	6.97
[Bertram and Elderfield, 1993]	CD1502	53.6	-12.3	49	26.14	27.42	1.28	6.91
[Bertram and Elderfield, 1993]	CD1503	55.6	-18.6	6	25.40	27.37	1.97	8.43
[Bertram and Elderfield, 1993]	CD1503	55.6	-18.6	50	25.40	27.37	1.97	7.48
[Bertram and Elderfield, 1993]	CD1503	55.6	-18.6	90	25.40	27.37	1.97	8.32
[Bertram and Elderfield, 1993]	CD1504	57.0	-27.0	11	26.20	27.18	0.98	8.23
[Bertram and Elderfield, 1993]	CD1504	57.0	-27.0	25	26.20	27.18	0.98	7.91
[Bertram and Elderfield, 1993]	CD1504	57.0	-27.0	101	26.20	27.18	0.98	7.90
[Bertram and Elderfield, 1993]	CD1505	57.0	-24.6	10	25.92	27.23	1.31	7.67
[Bertram and Elderfield, 1993]	CD1505	57.0	-24.6	60	25.92	27.23	1.31	9.07
[Bertram and Elderfield, 1993]	CD1505	57.0	-24.6	90	25.92	27.23	1.31	7.75
[Bertram and Elderfield, 1993]	CD1506	52.8	-8.5	93	26.41	27.43	1.02	9.74
[Bertram and Elderfield, 1993]	CD1506	52.8	-8.5	100	26.41	27.43	1.02	10.41
[Bertram and Elderfield, 1993]	CD1507	59.8	-6.1	10	26.46	27.43	0.97	6.90
[Bertram and Elderfield, 1993]	CD1507	59.8	-6.1	25	26.46	27.43	0.97	7.32
[Bertram and Elderfield, 1993]	CD1507	59.8	-6.1	50	26.46	27.43	0.97	7.25
[Bertram and Elderfield, 1993]	CD1507	59.8	-6.1	75	26.46	27.43	0.97	7.44
[Bertram and Elderfield, 1993]	CD1605	66.9	14.4	4	26.07	27.49	1.42	11.40
[Bertram and Elderfield, 1993]	CD1605	66.9	14.4	20	26.07	27.49	1.42	11.20
[Bertram and Elderfield, 1993]	CD1605	66.9	14.4	40	26.07	27.49	1.42	11.00
[Bertram and Elderfield, 1993]	CD1605	66.9	14.4	60	26.07	27.49	1.42	10.90

[Bertram and Elderfield, 1993]	CD1608	60.7	22.5	3	26.25	27.49	1.24	10.50
[Bertram and Elderfield, 1993]	CD1608	60.7	22.5	15	26.25	27.49	1.24	10.50
[Bertram and Elderfield, 1993]	CD1608	60.7	22.5	50	26.25	27.49	1.24	8.20
[Bertram and Elderfield, 1993]	CD1608	60.7	22.5	75	26.25	27.49	1.24	9.00
[Bertram and Elderfield, 1993]	CD1609	59.0	23.6	4	26.40	27.50	1.10	12.90
[Bertram and Elderfield, 1993]	CD1609	59.0	23.6	15	26.40	27.50	1.10	11.30
[Bertram and Elderfield, 1993]	CD1609	59.0	23.6	23	26.40	27.50	1.10	11.30
[Bertram and Elderfield, 1993]	CD1609	59.0	23.6	30	26.40	27.50	1.10	11.90
[Amakawa et al., 2000]	SSW 10	114.3	-18.7	5	25.67	27.39	1.72	7.38
[Amakawa et al., 2000]	SSW 11	112.5	-25.3	5	25.92	27.37	1.45	5.86
[Amakawa et al., 2000]	SSW 12	114.1	-30.0	5	26.33	27.32	0.99	5.01
[Amakawa et al., 2000]	SSW 13	115.5	-31.9	5	26.42	27.31	0.89	5.59
[Amakawa et al., 2000]	SSW 17	107.8	-23.0	5	25.84	27.38	1.54	5.37
[Amakawa et al., 2000]	SSW 18	104.5	-17.0	5	25.67	27.39	1.72	7.14
[Amakawa et al., 2000]	PA-7	102.0	-10.0	5	26.08	27.39	1.31	7.41
[Amakawa et al., 2000]	SSW 19	97.4	-4.9	5	26.40	27.41	1.01	7.04
[Amakawa et al., 2000]	SSW 20	92.3	0.8	5	26.39	27.44	1.05	6.99
[Amakawa et al., 2000]	SSW 21	90.2	3.8	5	26.31	27.44	1.13	14.50
[Amakawa et al., 2000]	SSW 14	113.6	-37.3	5	26.65	27.23	0.58	3.78
[Amakawa et al., 2000]	SSW 15	112.0	-42.5	5	26.79	27.20	0.41	4.78
[Amakawa et al., 2000]	PA-4	110.0	-40.0	5	26.74	27.19	0.45	4.06
[Amakawa et al., 2000]	SSW 16	110.0	-36.8	5	26.62	27.25	0.63	2.95
[Lacan and Jeandel, 2004a]	station 7	-44.0	55.6	40	27.62	27.76	0.14	21.40
[Lacan and Jeandel, 2004a]	station 9	-37.6	62.7	25	27.57	27.76	0.19	18.60
[Lacan and Jeandel, 2004a]	station 9	-37.6	62.7	101	27.57	27.76	0.19	18.80
[Lacan and Jeandel, 2004a]	station 12	-27.8	56.4	20	27.41	27.72	0.31	17.40
[Lacan and Jeandel, 2004a]	station 12	-27.8	56.4	74	27.41	27.72	0.31	19.50
[Lacan and Jeandel, 2004a]	station 14	-30.2	65.0	31	27.59	27.76	0.17	14.90
[Lacan and Jeandel, 2004a]	station 15	-30.9	65.3	20	27.59	27.76	0.17	16.60
[Lacan and Jeandel, 2004a]	station 1	-52.1	55.0	21	27.63	27.77	0.14	17.20
[Lacan and Jeandel, 2004a]	station 2	-47.1	58.9	30	27.66	27.77	0.11	17.90
[Lacan and Jeandel, 2004a]	station 2	-47.1	58.9	101	27.66	27.77	0.11	19.10
[Lacan and Jeandel, 2004b]	station 21	-10.1	66.6	20	27.50	27.73	0.23	14.80
[Lacan and Jeandel, 2004b]	station 21	-10.1	66.6	101	27.50	27.73	0.23	15.60
[Lacan and Jeandel, 2004b]	station 22	-9.0	62.8	20	27.46	27.69	0.23	12.70
[Lacan and Jeandel, 2004b]	station 22	-9.0	62.8	50	27.46	27.69	0.23	17.50
[Lacan and Jeandel, 2004b]	station 23	-5.0	60.5	51	27.38	27.63	0.25	16.90
[Lacan and Jeandel, 2004b]	station 23	-5.0	60.5	99	27.38	27.63	0.25	18.30
[Piepgras and Wasserburg, 1987]	Stn144	-3.3	67.7	65	27.65	27.83	0.18	14.30
[Piepgras and Wasserburg, 1987]	Hu83-036 Stn9	-52.1	54.3	5	27.59	27.77	0.18	25.00
[Piepgras and Wasserburg, 1987]	Hu83-036 Stn11	-47.0	52.1	5	27.56	27.76	0.20	21.10
[Piepgras and Wasserburg, 1987]	Stn39	-52.1	36.2	5	26.44	27.57	1.13	7.90

[Piepgras and Wasserburg, 1987]	Stn79	-20.0	36.3	5	26.88	27.65	0.77	9.30
[Piepgras and Wasserburg, 1987]	Stn63 (Chelex)	-40.7	7.7	0	26.84	27.48	0.64	18.20
[Piepgras and Wasserburg, 1987]	Stn30	-62.0	36.3	5	26.48	27.56	1.08	14.40
[Lacan and Jeandel, 2005]	station 3	-53.9	62.7	16	27.67	27.77	0.10	23.70
[Lacan and Jeandel, 2005]	station 4, salinometer	-57.4	58.0	7	27.66	27.77	0.11	27.30
[Lacan and Jeandel, 2005]	station 4, salinometer	-57.4	58.0	7	27.66	27.77	0.11	26.70
[Piepgras and Wasserburg, 1983]	NE Atl A-II 109-1 stn 95	-10.0	36.3	0	26.96	27.69	0.73	12.50
[Spivack and Wasserburg, 1988]	NE Atl TTO-TAS 80	-30.5	27.8	0	26.52	27.56	1.04	13.80
[Rickli et al., 2010]	sw 1	-7.7	44.6	5	27.11	27.63	0.52	10.50
[Rickli et al., 2010]	sw 2	-9.0	44.0	5	27.11	27.64	0.53	11.90
[Rickli et al., 2010]	snorkel 1	-10.3	40.3	5	27.06	27.67	0.61	13.30
[Rickli et al., 2010]	snorkel 4	-14.1	34.2	5	26.87	27.65	0.78	13.30
[Rickli et al., 2010]	snorkel 6	-16.5	30.3	5	26.67	27.59	0.92	25.60
[Rickli et al., 2010]	fish 8	-19.0	24.6	5	26.59	27.55	0.96	23.90
[Rickli et al., 2010]	fish 9	-20.2	22.9	5	26.57	27.55	0.98	18.70
[Rickli et al., 2010]	fish 12	-20.9	19.2	5	26.58	27.54	0.95	24.70
[Rickli et al., 2010]	fish 14	-20.9	17.5	5	26.61	27.53	0.91	28.80
[Rickli et al., 2010]	fish 16	-21.0	14.7	5	26.68	27.50	0.82	34.50
[Rickli et al., 2010]	fish 18	-20.5	12.6	5	26.70	27.49	0.79	33.70
[Rickli et al., 2010]	fish 20	-20.1	10.6	5	26.68	27.48	0.80	30.80
[Rickli et al., 2010]	fish 23	-18.0	7.6	5	26.62	27.47	0.85	29.40
[Rickli et al., 2010]	fish 27	-15.2	4.3	5	26.61	27.48	0.87	29.70
[Rickli et al., 2010]	fish 30	-9.3	-3.2	5	26.69	27.49	0.80	14.90
[Rickli et al., 2010]	fish 23	-12.4	0.8	5	26.63	27.51	0.88	18.90
[Rickli et al., 2010]	fish 27	-11.3	-0.7	5	26.65	27.51	0.86	19.20
[Rickli et al., 2010]	sw 4	-8.1	-4.8	5	26.71	27.47	0.76	13.10
[Rickli et al., 2010]	fish 33	-2.8	-11.5	5	26.75	27.44	0.69	17.80
[Rickli et al., 2010]	fish 34	1.8	-17.2	5	26.63	27.45	0.82	11.30
[Rickli et al., 2010]	fish 38	4.5	-20.6	5	26.60	27.45	0.85	10.30
[Rickli et al., 2010]	fish 44	7.4	-24.0	5	26.58	27.45	0.87	10.90
[Rickli et al., 2010]	Antarc Stn315	-62.3	-61.0	50	27.46	27.72	0.26	12.80
[Rickli et al., 2010]	Antarc Stn 327	-66.6	-56.5	50	27.08	27.50	0.42	8.30
[Jeandel, 1993]	S Atl 217	-1.4	-30.0	108	26.24	27.32	1.08	8.50
[Jeandel, 1993]	S ATl 302	-41.8	-33.3	49	26.39	27.25	0.86	9.30
[Jeandel, 1993]	S Atl 271	-33.4	-49.7	48	27.26	27.67	0.41	8.70
[German et al., 1995]	AJAX Station 47	1.0	-39.0	3	26.67	27.32	0.65	7.92
[German et al., 1995]	AJAX Station 47	1.0	-39.0	40	26.67	27.32	0.65	7.74
[German et al., 1995]	AJAX Station 47	1.0	-39.0	78	26.67	27.32	0.65	7.97
[Stichel et al., 2012]	S2	11.6	-38.8	5	26.55	27.31	0.76	6.70
[Stichel et al., 2012]	101	9.0	-42.4	75	26.76	27.35	0.59	8.60
[Stichel et al., 2012]	104	4.3	-47.7	75	27.11	27.58	0.47	8.20

[Stichel et al., 2012]	105	4.3	-47.7	5	27.10	27.58	0.48	7.40
[Stichel et al., 2012]	113	0.0	-53.0	75	27.56	27.79	0.23	16.10
[Stichel et al., 2012]	116	0.0	-54.3	5	27.62	27.81	0.19	15.80
[Stichel et al., 2012]	133	0.0	-59.3	5	27.80	27.84	0.04	18.20
[Stichel et al., 2012]	142	0.0	-62.3	5	27.81	27.84	0.03	17.30
[Stichel et al., 2012]	153	0.0	-65.3	5	27.79	27.84	0.05	17.30
[Stichel et al., 2012]	156	0.4	-67.1	5	27.78	27.84	0.06	19.50
[Stichel et al., 2012]	161	0.0	-66.5	100	27.79	27.84	0.05	17.90
[Stichel et al., 2012]	GvN	-4.8	-68.5	5	27.75	27.84	0.09	16.80
[Stichel et al., 2012]	S3	-15.7	-69.0	5	27.78	27.84	0.06	16.90
[Stichel et al., 2012]	186	-17.4	-69.0	25	27.79	27.84	0.05	17.20
[Stichel et al., 2012]	191	-23.7	-67.3	25	27.82	27.84	0.02	18.50
[Stichel et al., 2012]	S4	-36.8	-65.5	5	27.82	27.85	0.03	18.50
[Stichel et al., 2012]	S5	-42.0	-65.0	5	27.81	27.84	0.03	18.30
[Stichel et al., 2012]	S6	-46.1	-64.3	5	27.80	27.84	0.04	18.10
[Stichel et al., 2012]	210	-48.3	-64.0	25	27.78	27.84	0.06	18.30
[Stichel et al., 2012]	222	-52.8	-63.3	25	27.74	27.82	0.08	19.90
[Stichel et al., 2012]	222	-52.8	-63.3	50	27.74	27.82	0.08	21.20
[Stichel et al., 2012]	222	-52.8	-63.3	100	27.74	27.82	0.08	19.90
[Stichel et al., 2012]	222	-52.8	-63.3	180	27.74	27.82	0.08	20.40
[Stichel et al., 2012]	223	-52.8	-63.2	25	27.74	27.82	0.08	21.10
[Stichel et al., 2012]	S7	-52.8	-62.1	5	27.71	27.81	0.10	22.60
[Stichel et al., 2012]	S8	-60.0	-60.0	5	27.47	27.72	0.25	14.30
[Stichel et al., 2012]	230	-55.3	-60.1	50	27.58	27.77	0.19	18.90
[Stichel et al., 2012]	241	-60.9	-57.6	50	27.27	27.61	0.34	11.80
[Stichel et al., 2012]	244	-62.5	-57.9	25	27.26	27.61	0.35	10.20
[Stichel et al., 2012]	244	-62.5	-57.9	50	27.26	27.61	0.35	9.60
[Carter et al., 2012]	station 008	-76.8	-68.3	10	27.57	27.78	0.21	13.68
[Carter et al., 2012]	station 008	-76.8	-68.3	79	27.57	27.78	0.21	13.54
[Carter et al., 2012]	Station 010	-91.1	-70.8	10	27.55	27.77	0.22	13.16
[Carter et al., 2012]	Station 021	-106.7	-69.2	18	27.41	27.75	0.34	13.79
[Carter et al., 2012]	Station 022	-108.3	-60.5	16	27.16	27.57	0.41	9.66
[Carter et al., 2012]	Station 024	-83.3	-67.8	15	27.52	27.77	0.25	14.42
[Zhang et al., 2008]	C5	75.6	-52.4	0	27.30	27.70	0.40	10.90
[Zhang et al., 2008]	C5	75.6	-52.4	30	27.30	27.70	0.40	10.80
[Zhang et al., 2008]	C5	75.6	-52.4	50	27.30	27.70	0.40	11.00
[Zhang et al., 2008]	C5	75.6	-52.4	100	27.30	27.70	0.40	10.80
[Zhang et al., 2008]	C11	78.0	-51.7	0	27.24	27.68	0.44	13.50
[Zhang et al., 2008]	C11	78.0	-51.7	50	27.24	27.68	0.44	12.80
[Zhang et al., 2008]	C11	78.0	-51.7	150	27.24	27.68	0.44	13.50
[Zhang et al., 2008]	B11	77.0	-50.5	0	27.13	27.61	0.48	14.40
[Zhang et al., 2008]	B12	77.0	-50.5	50	27.13	27.61	0.48	13.20

[Zhang et al., 2008]	B13	77.0	-50.5	100	27.13	27.61	0.48	12.80
[Zhang et al., 2008]	A11	74.0	-49.1	20	27.05	27.53	0.48	12.40
[Zhang et al., 2008]	A11	74.0	-49.1	60	27.05	27.53	0.48	12.00
[Zhang et al., 2008]	A11	74.0	-49.1	100	27.05	27.53	0.48	12.50
[Zhang et al., 2008]	KERFIX	68.4	-50.7	0	27.08	27.59	0.51	10.30
[Zhang et al., 2008]	KERFIX	68.4	-50.7	50	27.08	27.59	0.51	10.50
[Zhang et al., 2008]	KERFIX	68.4	-50.7	100	27.08	27.59	0.51	10.60

1. These new results were obtained on surface samples taken by M. M.-K. during cruise SO213 in austral summer 2010/11. The samples were obtained using the ship's seawater intake system while the ship was moving in order to avoid contamination. All samples were filtered through 0.45μm cellulose acetate filters and acidified immediately after collection. Nd concentration data were obtained by isotope dilution following the method and carried out in the same laboratory as described in detail in Stichel et al. [2012]. The procedure involves isotope spiking with a pre-concentration by FeOOH co-precipitation, and further purification of Nd using 1.4 ml resin of BIORAD® AG50W-X8, 200–400 μm mesh-size. The Nd concentration measurements were performed on a Nu instruments MC-ICP-MS at GEOMAR with an external reproducibility of 2%. The analytical blank was negligible (see Stichel et al. [2012] for further details).

Supplementary References

Alibo, D. S., and Y. Nozaki (1999), Rare earth elements in seawater: Particle association, shale-normalization, and Ce oxidation, *Geochim. Cosmochim. Acta*, *63*(3-4), 363-372.

Amakawa, H., D. S. Alibo, and Y. Nozaki (2000), Nd isotopic composition and REE pattern in the surface waters of the eastern Indian Ocean and its adjacent seas, *Geochim. Cosmochim. Acta.*, *64*(10), 1715-1727.

Amakawa, H., K. Sasaki, and M. Ebihara (2009), Nd isotopic composition in the central North Pacific, *Geochim. Cosmochim. Acta*, *73*(16), 4705-4719.

Amakawa, H., Y. Nozaki, D. S. Alibo, J. Zhang, K. Fukugawa, and H. Nagai (2004), Neodymium isotopic variations in Northwest Pacific waters, *Geochim. Cosmochim. Acta*, *68*(4), 715-727.

Bertram, C. J., and H. Elderfield (1993), The Geochemical Balance of the Rare-Earth Elements and Neodymium Isotopes in the Oceans, *Geochim. Cosmochim. Acta*, *57*(9), 1957-1986.

Carter, P., D. Vance, C. D. Hillenbrand, J. A. Smith, and D. R. Shoosmith (2012), The neodymium isotopic composition of waters masses in the eastern Pacific sector of the Southern Ocean, *Geochim. Cosmochim. Acta*, *79*, 41-59.

Debaar, H. J. W., M. P. Bacon, P. G. Brewer, and K. W. Bruland (1985), Rare-Earth Elements in the Pacific and Atlantic Oceans, *Geochim. Cosmochim. Acta*, *49*(9), 1943-1959.

German, C. R., T. Masuzawa, M. J. Greaves, H. Elderfield, and J. M. Edmond (1995), Dissolved Rare-Earth Elements in the Southern-Ocean - Cerium Oxidation and the Influence of Hydrography, *Geochim. Cosmochim. Acta*, *59*(8), 1551-1558.

Goldstein, S. J., and S. B. Jacobsen (1987), The Nd and Sr Isotopic Systematics of River-Water Dissolved Material - Implications for the Sources of Nd and Sr in Seawater, *Chem. Geol.*, *66*(3-4), 245-272.

Grasse, P., T. Stichel, R. Stumpf, L. Stramma, and M. Frank (2012), The distribution of neodymium isotopes and concentrations in the Eastern Equatorial Pacific: Water mass advection versus particle exchange, *Earth Planet. Sci. Lett.*, *353–354*(0), 198-207.

Greaves, M. J., H. Elderfield, and E. R. Sholkovitz (1999), Aeolian sources of rare earth elements to the Western Pacific Ocean, *Mar. Chem.*, *68*(1-2), 31-38.

Greaves, M. J., H. Elderfield, and E. R. Sholkovitz (2001), Aeolian sources of rare earth elements to the Western Pacific Ocean, *Mar. Chem.*, *74*(4), 319-319.

Grenier, M., C. Jeandel, F. Lacan, D. Vance, C. Venchiarutti, A. Cros, and S. Cravatte (2013), From the subtropics to the central equatorial Pacific Ocean: Neodymium isotopic composition and rare earth element concentration variations, *J. Geophys. Res. 118*, doi: 10.1029/2012JC008239.

Hongo, Y., H. Obata, D. S. Alibo, and Y. Nozaki (2006), Spatial variations of rare earth elements in North Pacific surface water, *J. Oceanogr.*, *62*(4), 441-455.

Jeandel, C. (1993), Concentration and Isotopic Composition of Nd in the South-Atlantic Ocean, *Earth Planet. Sci. Lett.*, *117*(3-4), 581-591.

Jeandel, C., D. Thouron, and M. Fieux (1998), Concentrations and isotopic compositions of neodymium in the eastern Indian Ocean and Indonesian straits, *Geochim. Cosmochim. Acta*, *62*(15), 2597-2607.

Jeandel, C., T. Arsouze, F. Lacan, P. Techine, and J. C. Dutay (2007), Isotopic Nd compositions and concentrations of the lithogenic inputs into the ocean: A compilation, with an emphasis on the margins, *Chem. Geol.*, *239*(1-2), 156-164.

Kawakami, H., and M. Kusakabe (2008), Surface water mixing estimated from Ra-228 and Ra-226 in the northwestern North Pacific, *J. Environ. Radioactiv.*, *99*(8), 1335-1340.

Klinkhammer, G., H. Elderfield, and A. Hudson (1983), Rare-Earth Elements in Seawater near Hydrothermal Vents, *Nature*, *305*(5931), 185-188.

Lacan, F., and C. Jeandel (2001), Tracing Papua New Guinea imprint on the central Equatorial Pacific Ocean using neodymium isotopic compositions and Rare Earth Element patterns, *Earth Planet. Sci. Lett.*, *186*(3-4), 497-512.

Lacan, F., and C. Jeandel (2004a), Neodymium isotopic composition and rare earth element concentrations in the deep and intermediate Nordic Seas: Constraints on the Iceland Scotland Overflow Water signature, *Geochem. Geophys. Geosyst.*, *5*, Q11006, doi:10.1029/2004GC000742.

Lacan, F., and C. Jeandel (2004b), Subpolar Mode Water formation traced by neodymium isotopic composition, *Geophys. Res. Lett.*, 31, L14306, doi:10.1029/2004GL019747.

Lacan, F., and C. Jeandel (2005), Acquisition of the neodymium isotopic composition of the North Atlantic Deep Water, *Geochem. Geophys. Geosyst.*, 6, Q12008, doi:10.1029/2005GC000956.

Luo, C., N. M. Mahowald, and J. del Corral (2003), Sensitivity study of meteorological parameters on mineral aerosol mobilization, transport, and distribution, *J. Geophys. Res.*, 108, doi: 10.1029/2003jd003483.

Müller, S. A., F. Joos, N. R. Edwards, and T. F. Stocker (2006), Water mass distribution and ventilation time scales in a cost-efficient, three-dimensional ocean model, *J. Climate*, *19*(21), 5479-5499.

Piepgras, D. J., and G. J. Wasserburg (1982), Isotopic Composition of Neodymium in Waters from the Drake Passage, *Science*, *217*(4556), 207-214.

Piepgras, D. J., and G. J. Wasserburg (1983), Influence of the Mediterranean Outflow on the Isotopic Composition of Neodymium in Waters of the North-Atlantic, *J. Geophys. Res.*, *88*(10), 5997-6006.

Piepgras, D. J., and G. J. Wasserburg (1987), Rare-Earth Element Transport in the Western North-Atlantic Inferred from Nd Isotopic Observations, *Geochim. Cosmochim. Acta*, *51*(5), 1257-1271.

Piepgras, D. J., and S. B. Jacobsen (1988), The Isotopic Composition of Neodymium in the North Pacific, *Geochim. Cosmochim. Acta*, *52*(6), 1373-1381.

Piepgras, D. J., and S. B. Jacobsen (1992), The Behavior of Rare-Earth Elements in Seawater - Precise Determination of Variations in the North Pacific Water Column, *Geochim. Cosmochim. Acta*, *56*(5), 1851-1862.

Rempfer, J., T. F. Stocker, F. Joos, and J. C. Dutay (2012), On the relationship between Nd isotopic composition and ocean overturning circulation in idealized freshwater discharge events, *Paleoceanography*, *27*, Pa3211, doi 10.1029/2012pa002312.

Rempfer, J., T. F. Stocker, F. Joos, J. C. Dutay, and M. Siddall (2011), Modelling Nd-isotopes with a coarse resolution ocean circulation model: Sensitivities to model parameters and source/sink distributions, *Geochim. Cosmochim. Acta*, *75*(20), 5927-5950.

Rickli, J., M. Frank, A. R. Baker, S. Aciego, G. de Souza, R. B. Georg, and A. N. Halliday (2010), Hafnium and neodymium isotopes in surface waters of the eastern Atlantic Ocean: Implications for sources and inputs of trace metals to the ocean, *Geochim. Cosmochim. Acta*, *74*(2), 540-557.

Ritz, S. P., T. F. Stocker, and F. Joos (2011a), A Coupled Dynamical Ocean-Energy Balance Atmosphere Model for Paleoclimate Studies, *J. Climate*, *24*(2), 349-375.

Ritz, S. P., T. F. Stocker, and J. P. Severinghaus (2011b), Noble gases as proxies of mean ocean temperature: sensitivity studies using a climate model of reduced complexity, *Quaternary Sci. Rev.*, *30*(25-26), 3728-3741.

Shimizu, H., K. Tachikawa, A. Masuda, and Y. Nozaki (1994), Cerium and Neodymium Isotope Ratios and Ree Patterns in Seawater from the North Pacific-Ocean, *Geochim. Cosmochim. Acta*, *58*(1), 323-333.

Spivack, A. J., and G. J. Wasserburg (1988), Neodymium Isotopic Composition of the Mediterranean Outflow and the Eastern North-Atlantic, *Geochim. Cosmochim. Acta*, *52*(12), 2767-2773.

Stichel, T., M. Frank, J. Rickli, E. C. Hathorne, B. A. Haley, C. Jeandel, and C. Pradoux (2012), Sources and input mechanisms of hafnium and neodymium in surface waters of the Atlantic sector of the Southern Ocean, *Geochim. Cosmochim. Acta*, *94*(0), 22-37.

Tschumi, T., F. Joos, and P. Parekh (2008), How important are Southern Hemisphere wind changes for low glacial carbon dioxide? A model study, *Paleoceanography*, *23*(4), doi: 10.1029/2008pa001592.

Vance, D., A. E. Scrivner, P. Beney, M. Staubwasser, G. M. Henderson, and N. C. Slowey (2004), The use of foraminifera as a record of the past neodymium isotope composition of seawater, *Paleoceanography*, *19*(2), doi: 10.1029/2003pa000957.

Wang, Z. L., and M. Yamada (2007), Geochemistry of dissolved rare earth elements in the Equatorial Pacific Ocean, *Environ. Geol.*, *52*(4), 779-787.

Zhang, J., and Y. Nozaki (1996), Rare earth elements and yttrium in seawater: ICP-MS determinations in the East Caroline, Coral Sea, and South Fiji basins of the western South Pacific Ocean, *Geochim. Cosmochim. Acta*, *60*(23), 4631-4644.

Zhang, Y., F. Lacan, and C. Jeandel (2008), Dissolved rare earth elements tracing lithogenic inputs over the Kerguelen Plateau (Southern Ocean), *Deep Sea Res., Part II*, *55*(5-7), 638-652.

Acknowledgements

Tian-Yu Chen

Gender: Male; Nationality: China
Born: Dec. 1986; Place of Birth: Hubei, China

Education

Oct. 2010 - Nov. 2013, PhD study in Paleoceanography, GEOMAR, Germany
                    Advisor: Prof. Dr. Martin Frank
Sept. 2007 - Oct. 2010, Graduate study in Isotope Geochemistry, Nanjing University, China
                    Advisor: Prof. Dr. Hong-Fei Ling
Sept. 2003 - Jun. 2007, Undergraduate study in Geochemistry, Nanjing University, China

Honors and Awards

European Consortium of Ocean Research Drilling (ECORD) Scholarship (2013)
Chinese Government Scholarship for doctoral study abroad (2010-2013)
Traffic Holding Company Scholarship: Top Grade Award (2011)
Outstanding graduate student, Nanjing University (2011)
National Scholarship of China (three times, 2004; 2005; 2006)

Selected Publications

Chen, T.-Y., Stumpf, R., Frank, M., Bełdowski J., and Staubwasser M., 2013. Contrasting geochemical cycling of hafnium and neodymium in the central Baltic Sea. *Geochimica et Cosmochimica Acta*, 123, 166-180, doi: 10.1016/j.gca.2013.09.011.

Chen, T.-Y., Rempfer J., Frank, M., Stumpf R., and Molina-Kescher M., 2013. Upper ocean vertical supply: a neglected primary factor controlling the distribution of neodymium concentrations of open ocean surface waters? *Journal of Geophysical Research-oceans*, 118, 3887-3894, doi: 10.1002/jgrc.20288.

Chen, T.-Y., Li G., Frank, M., and Ling, H.-F., 2013. Hafnium isotope fractionation during continental weathering: implications for the generation of seawater Nd-Hf isotope relationships. *Geophysical Research Letters*, 40, 916-920, doi: 10.1002/grl.50217.

Chen, T.-Y., Ling, H.-F., Hu, R., Frank, M., and Jiang, S.-Y., 2013. Lead isotope provinciality of central North Pacific Deep Water over the Cenozoic. *Geochemistry Geophysics Geosystems*, 14, 1523-1537, doi: 10.1002/ggge.20114.

Chen, T.-Y., Frank, M., Haley, B. A., Gutjahr, M., and Spielhagen, R. F., 2012. Variations of North Atlantic inflow to the central Arctic Ocean over the last 14 million years inferred from hafnium and neodymium isotopes. *Earth and Planetary Science Letters* 353–354, 82-92.

Chen, T.-Y., Ling, H.-F., Frank, M., Zhao, K.-D., and Jiang, S.-Y., 2011. Zircon effect alone insufficient to generate seawater Nd-Hf isotope relationships. *Geochemistry Geophysics Geosystems* 12, Q05003, doi: 10.1029/2010gc003363.